Electricity markets, network and generation evolution towards the decarbonization process of the power systems

Department of Electrical and Information Engineering
ELECTRICAL AND INFORMATION ENGINEERING
Ph.D. Program
SSD: ING-IND/33–ELECTRICAL POWER SYSTEMS

Final Dissertation

Electricity Markets, Network and Generation Evolution Towards the Decarbonization Process of the Power Systems

by
Gioacchino Tricarico

Supervisors:

Prof. Maria Dicorato

Eng. Michele Principato

Coordinator of Ph.D. Program:
Prof. Mario Carpentieri

Course n° 35 01/11/2019–31/01/2023

Politecnico di Bari

LIBERATORIA PER L'ARCHIVIAZIONE DELLA TESI DI DOTTORATO

Al Magnifico Rettore
del Politecnico di Bari

Il sottoscritto Gioacchino Tricarico nato a Terlizzi il 16/01/1993 residente a Terlizzi in Contrada Piscina degli Zingari, 15 e-mail gioacchino.tricarico@poliba.it iscritto al 3° anno di Corso di Dottorato di Ricerca in Ingegneria Elettrica e dell'Informazione ciclo XXXV ed essendo stato ammesso a sostenere l'esame finale con la prevista discussione della tesi dal titolo:

Electricity Markets, Network and Generation Evolution Towards the Decarbonization Process of the Power Systems

DICHIARA

1) di essere consapevole che, ai sensi del D.P.R. n. 445 del 28.12.2000, le dichiarazioni mendaci, la falsità negli atti e l'uso di atti falsi sono puniti ai sensi del codice penale e delle Leggi speciali in materia, e che nel caso ricorressero dette ipotesi, decade fin dall'inizio e senza necessità di nessuna formalità dai benefici conseguenti al provvedimento emanato sulla base di tali dichiarazioni;
2) di essere iscritto al Corso di Dottorato di ricerca in Ingegneria Elettrica e dell'Informazione ciclo XXXV, corso attivato ai sensi del "*Regolamento dei Corsi di Dottorato di ricerca del Politecnico di Bari*", emanato con D.R. n.286 del 01.07.2013;
3) di essere pienamente a conoscenza delle disposizioni contenute nel predetto Regolamento in merito alla procedura di deposito, pubblicazione e autoarchiviazione della tesi di dottorato nell'Archivio Istituzionale ad accesso aperto alla letteratura scientifica;
4) di essere consapevole che attraverso l'autoarchiviazione delle tesi nell'Archivio Istituzionale ad accesso aperto alla letteratura scientifica del Politecnico di Bari (IRIS-POLIBA), l'Ateneo archivierà e renderà consultabile in rete (nel rispetto della Policy di Ateneo di cui al D.R. 642 del 13.11.2015) il testo completo della tesi di dottorato, fatta salva la possibilità di sottoscrizione di apposite licenze per le relative condizioni di utilizzo (di cui al sito http://www.creativecommons.it/Licenze), e fatte salve, altresì, le eventuali esigenze di "embargo", legate a strette considerazioni sulla tutelabilità e sfruttamento industriale/commerciale dei contenuti della tesi, da rappresentarsi mediante compilazione e sottoscrizione del modulo in calce (Richiesta di embargo);
5) che la tesi da depositare in IRIS-POLIBA, in formato digitale (PDF/A) sarà del tutto identica a quelle **consegnate**/inviate/da inviarsi ai componenti della commissione per l'esame finale e a qualsiasi altra copia depositata presso gli Uffici del Politecnico di Bari in forma cartacea o digitale, ovvero a quella da discutere in sede di esame finale, a quella da depositare, a cura dell'Ateneo, presso le Biblioteche Nazionali Centrali di Roma e Firenze e presso tutti gli Uffici competenti per legge al momento del deposito stesso, e che di conseguenza va esclusa qualsiasi responsabilità del Politecnico di Bari per quanto riguarda eventuali errori, imprecisioni o omissioni nei contenuti della tesi;
6) che il contenuto e l'organizzazione della tesi è opera originale realizzata dal sottoscritto e non compromette in alcun modo i diritti di terzi, ivi compresi quelli relativi alla sicurezza dei dati personali; che pertanto il Politecnico di Bari ed i suoi funzionari sono in ogni caso esenti da responsabilità di qualsivoglia natura: civile, amministrativa e penale e saranno dal sottoscritto tenuti indenni da qualsiasi richiesta o rivendicazione da parte di terzi;
7) che il contenuto della tesi non infrange in alcun modo il diritto d'Autore né gli obblighi connessi alla salvaguardia di diritti morali od economici di altri autori o di altri aventi diritto, sia per testi, immagini, foto, tabelle, o altre parti di cui la tesi è composta.

Luogo e data BARI, 24/03/2023 Firma Gioacchino Tricarico

Il sottoscritto, con l'autoarchiviazione della propria tesi di dottorato nell'Archivio Istituzionale ad accesso aperto del Politecnico di Bari (POLIBA-IRIS), pur mantenendo su di essa tutti i diritti d'autore, morali ed economici, ai sensi della normativa vigente (Legge 633/1941 e ss.mm.ii.),

CONCEDE

- al Politecnico di Bari il permesso di trasferire l'opera su qualsiasi supporto e di convertirla in qualsiasi formato al fine di una corretta conservazione nel tempo. Il Politecnico di Bari garantisce che non verrà effettuata alcuna modifica al contenuto e alla struttura dell'opera.
- al Politecnico di Bari la possibilità di riprodurre l'opera in più di una copia per fini di sicurezza, back-up e conservazione.

Luogo e data BARI, 24/03/2023 Firma Gioacchino Tricarico

Politecnico di Bari

Department of Electrical and Information Engineering
ELECTRICAL AND INFORMATION ENGINEERING
Ph.D. Program
SSD: ING-IND/33–ELECTRICAL POWER SYSTEMS

Final Dissertation

Electricity Markets, Network and Generation Evolution Towards the Decarbonization Process of the Power Systems

by
Gioacchino Tricarico

Referees:
Prof. Alberto Berizzi
Dr. Benedetto Aluisio

Supervisors:
Prof. Maria Dicorato
Eng. Michele Principato

Coordinator of Ph.D. Program
Prof. Mario Carpentieri

Course n° 35 01/11/2019–31/01/2023

Contents

Acknowledgments

A Ph.D. is a long and challenging journey and its successful completion would not come without the support and inspiration from all the people that surround me.

I am deeply grateful to my supervisors Prof. Maria Dicorato and Eng. Michele Principato for their support and guidance, which have been invaluable qualities for the accomplishment of this thesis. I would also like to thank them for promoting an open-minded research environment, based on trust and creative collaboration, which helped me develop my research skills in both academic and industrial perspectives.

I wish to express my gratitude to my co-supervisor, Dr. Giuseppe Forte, for his contributions, remarks and advices on all steps of this research work, as well as for our fruitful collaboration.

During my PhD, I had the honor to work with Prof. Francisco Gonzalez-Longatt in Norway and England. I will be immensely thankful to him for accepting my abroad experience and for sharing his knowledge and experiences, which I extensively used to prepare a portion of my thesis.

I would like to thank my colleagues at Politecnico di Bari, who provided every possible form of support, much friendship and good humor in so many different ways.

I am truly fortunate in knowing so many people in my foreign experience whom I could turn to for information, thoughts and ability to talk things through, as well as support and sympathy.

I cannot forget my family, especially my mother and father, who have always believed in me since the beginning of this journey; they taught me the meaning of hard work by letting an obstacle to appear as a small hill to climb.

Finally, I consider myself fortunate to have Anna by my side, she had been as a shield during difficult times and like a motivator when I doubted my ability to do this work. I will be extremely grateful for her help and support over the last three years.

Abstract

The electricity market and power system frameworks are currently being adjusted to account for both the growing energy consumption and the decarbonization of electrical energy production. This evolution is required to cope with the tightening constraints of the power system operation and the further uncertainties introduced by load and renewable energy sources (RES).

From the network perspective, the development has to consider the load and RES growth in order to avoid technical limitations. However, increased RES production puts a strain on system flexibility, due to uncorrelation with load demand trend, and to installation mostly located on distribution system. This, in turn, causes a change in power flow directions, resulting in unusual transmission network operating conditions with possible current capacity saturation and overvoltage issues.

From the market perspective, the production and consumption schedules, ensuring the minimization of the overall costs as yields of the various market sessions over medium- and short-time horizon, could be subject to further redispatching actions to tackle RES and load forecast errors, and to cope with network constraints and contingencies.

Useful methodologies to overcome the aforementioned issues are based on approaches combining market and network analysis procedures. To these purposes, a complete and detailed concept of the system operation is required from long-term planning to real-time strategies. Therefore, the present doctoral research thesis is concerned with the integrated development, from day-ahead schedule to real-time operations, of electricity markets and transmission systems, as well as the long-term network evolution planning. It is specifically illustrated how market and steady-state simulations can be used to create various methodological frameworks to carry out an appropriate analysis, in accordance with the issues under study. This thesis is divided into six chapters, related to the published or submitted scientific papers on the treated topic.

The first chapter is the dissertation's comprehensive introduction. The fundamentals of modern energy and ancillary service markets as well as of network evolution planning are described. In particular, methods and models to develop the aforementioned studies are presented in this chapter, providing a further literature review to pinpoint the respective state-

of-the-art. The second chapter is focused on the IEEE 39-bus system, that is suitably modified to include solar and wind generation in the traditional generation mix. The third chapter concerns two methodologies for technical and economic benefit evaluation of network development projects. The fourth chapter proposes a generation investment analysis in a deregulated market framework, evaluating the most suitable size and location to maximize the investor economic profit. In the fifth chapter a practical method for calculating operating reserve requirements considering system uncertainties. Furthermore, a procedure for security constrained redispatch optimization problem is proposed. In the last chapter a real case study to evaluate transmission system operator strategies from the energy to the balancing markets is proposed in order to evaluate the secure operation of the transmission system.

The developed research addresses the following issues:

- Assessing network evolution planning under load and RES increase, in order to improve the social welfare and to reduce redispatching actions.
- Accurate reserve requirements sizing, to effectively manage ancillary service provision, fulfilling the network constraints and market mechanisms.
- Considering system operator and market participant viewpoints, to evaluate respective planning and operation strategies and their interactions.
- Real-case applications, to test the method validity for large-scale system issues.

Sommario

Oggigiorno la struttura dei mercati e dei sistemi elettrici di potenza sono sotto continua evoluzione per via della crescita dei consumi energetici e del processo di decarbonizzazione della produzione di energia elettrica. Questa evoluzione è necessaria per far fronte ai vincoli stringenti nel funzionamento delle reti elettriche e alle ulteriori incertezze introdotte dal carico e dalle fonti di energia rinnovabile (FER).

Dal punto di vista della rete il suo sviluppo deve considerare la crescita del carico e delle FER al fine di evitare limitazioni tecniche. Tuttavia, l'aumento di produzione da FER mette a dura prova la flessibilità del sistema, per l'indipendenza con l'andamento della domanda di carico, e per via della sua installazione che è prevalentemente localizzata sul sistema di distribuzione. Questo, a sua volta, causa un cambiamento delle direzioni dei flussi di potenza, risultando in condizioni operative inusuali del sistema di trasmissione con possibili problemi di saturazioni delle portate di corrente e di sovratensione.

Dal punto di vista del mercato, i programmi di produzione e consumo, definiti in esito alle sessioni dei vari mercati che vanno dal medio al breve termine assicurando la minimizzazione di costi complessivi, potrebbero essere soggetti ad ulteriori azioni di ridispacciamento per fronteggiare errori di previsione di carico e FER, vincoli di rete e contingenze.

Per queste ragioni, è necessaria una completa e dettagliata visione del funzionamento del sistema dalla programmazione a lungo termine fino alle strategie in tempo reale. Pertanto, la presente tesi di ricerca di dottorato tratta lo sviluppo integrato dalla programmazione del mercato giorno prima alle operazioni in tempo reale del sistema, così come la programmazione a lungo termine dello sviluppo del sistema elettrico. In particolare, viene mostrato come le simulazioni di mercato e quelle di regime permanente della rete possono essere impiegate per sviluppare diversi contesti metodologici per svolgere specifiche analisi in funzione della problematica trattata. La tesi in esame è composta da sei capitoli, ognuno dei quali è strutturato sulla base della raccolta delle pubblicazioni scientifiche relativi agli argomenti esaminati.

Il primo capitolo di questa dissertazione fornisce un'introduzione degli argomenti trattati, dove vengono introdotti i concetti fondamentali dei moderni mercati elettrici dell'energia e dei servizi di dispacciamento e dei piani di sviluppo dei sistemi di potenza. In particolare,

vengono descritti i metodi ed i modelli implementati per trattare i suddetti studi, fornendo un'ampia esaminazione della ricerca bibliografica per evidenziare i rispettivi stati dell'arte. Il secondo capitolo si focalizza sugli studi condotti sulla rete test IEEE 39 nodi, che è stata opportunamente modificata per introdurre produzione da fonte solare ed eolica nel mix del parco di generazione. Nel terzo capitolo vengono proposte due metodologie per la valutazione tecnico-economica dei benefici introdotti dallo sviluppo della rete di trasmissione installando una nuova linea elettrica. Nel quarto capitolo viene proposta un'analisi di investimento della generazione in un sistema elettrico liberalizzato, al fine di individuare la taglia e il luogo più idonei che fornisca un guadagno economico all'investitore. Nel quinto capitolo viene descritta una metodologia pratica per determinare i fabbisogni di energia elettrica sulla base delle incertezze del sistema. Inoltre, viene proposta una procedura per risolvere un problema di ottimizzazione di security constrained unit commitment and economic redispatch. Nell'ultimo capitolo viene trattato un caso studio reale al fine valutare le strategie dell'operatore del sistema di trasmissione dal mercato dell'energia a quello in tempo reale per garantire il corretto funzionamento del sistema di trasmissione.

La ricerca condotta affronta le seguenti problematiche:

- Valutazione di metodologie tecnico-economiche per valutare la pianificazione dello sviluppo di rete in condizioni di crescita di carico e FER, per poter migliorare il social welfare e per ridurre le azioni di ridispacciamento.
- Dimensionamento dei fabbisogni di riserva di energia per gestire efficacemente l'approvvigionamento nel mercato dei servizi di dispacciamento, soddisfano i vincoli di rete e dei meccanismi di mercato.
- La considerazione delle prospettive dell'operatore del sistema e dei partecipanti del mercato per valutare le rispettive strategie di pianificazione e operazione e le loro interazioni.
- Applicazioni a casi studio reali, per poter testare la validità del modello per problemi su sistemi di larga scala.

Chapter 1. General Context and Background

This first chapter serves as an introduction to the dissertation and provides all of the necessary background information to understand the following chapters. In this context, the paragraph 1.1 provides an overview of the different electricity markets' framework, (i.e., energy and ancillary service markets), through the presentation of the Italian market mechanisms. In particular, a focus on active power reserve requirements to be provided for secure operations of the transmission system is provided. The presented thesis lies on several topics related to transmission system framework and operation. Thus, concept of transmission and generation investments as well as the several involved aspects are given in the paragraph 1.2 throughout this dissertation. This paragraph also conveys a description of the optimal investment evaluation methodologies in the transmission network.

1.1. An overview on Electricity Markets

The development of electricity markets is based on the premise that electrical energy can be treated as a commodity. Commodities are defined as "economic goods or services with no qualitative differentiation across a market". However, there are significant differences between electrical energy and other commodities, and these distinctions have a significant impact on the organization and rules of electricity markets.

The main distinction is that electrical energy is inextricably linked with a physical system that operates much faster than any market. Supply and demand must be balanced on a real-time basis in this physical power system, fulfilling the constraints of the power system's elements at the same time. If this balance is not maintained, the system will collapse with disastrous results. Such a breakdown is intolerable, because it affects not only the trading system but also an entire region or country, which may be without power for several hours. In the short run, balancing supply and demand for electrical energy is a process that simply cannot be left to a relatively slow-moving and unaccountable entity like a simple market. At the contrary, this balance must be maintained at all costs via a mechanism that does not rely on a market to select and dispatch resources.

For the aforementioned reason, electricity was not until recently commercialized as a commodity. Previously, power systems were centralized and managed by state-owned entities. However, so-called economic liberalization has resulted in the global separation of the

various components of electrical power systems, namely generation, consumption and transmission. This liberalization has two goals: on the one hand, to encourage private entity competition in order to reduce energy prices, and on the other, to define several electricity markets regulated by independent counterparts.

The introduced markets are for energy and ancillary services. Energy markets aim to trade the greatest proportion of electrical energy through an unmanaged open market, such a market is unable to maintain the reliability of the power system, in the short-term. The function of ancillary service markets (ASM) is to match residual load and generation by adjusting flexible generator production and curtailing the demand of willing consumers, in the real-time operation. ASM should also be able to respond to major disruptions caused by the unexpected and sudden disconnect of large generating or consuming units due to unavoidable technical problems. Furthermore, in recent years, there has been a growing need for flexibility in power systems as a result of increased exploitation of renewable energy sources (RESs) and distributed resources, encouraging significant reforms in the electricity market, especially for the ancillary service ones. The subsections below provide a detailed overview of the most important features of each spot electricity market based on Italian ones.

1.1.1. Energy Markets

Energy markets are gathered in day-ahead market (DAM) and intraday market (IM) in which the largest energy volume is treaded, for each hour. These markets are overseen by a Market Operator, for the Italian case Gestore dei Mercati Energetici (GME) is the named one, to ensure a competitive and efficient market platform for the exchange of energy. This authority is also in charge of ensuring the market's transparency and neutrality. DAM and IM are hourly economic merit-order market in which selling and buying bids, composed of price and quantity offered, are ordered according ascending and descending prices, respectively. These sorting progressively led to an equilibrium in which the price clears the market, that is, the supply is equal to the demand. The obtained equilibrium price is the market clearing price (MCP) and represents the cost of the energy for that specific hour. All the selling (buying) offers lower (greater) or equal than MCP are accepted, the remaining are rejected.

The goal of DAM is to estimate the programmed power to be supplied and withdrawn for the day ahead, according to the accepted selling and buying bids, and define the cost of the electrical energy, for each hour, aiming at maximizing the social welfare. For the IM, it

is the adjustment of the scheduled DAM program of the required demand and/or generation availability. After the closure of DAM there is the IM in which are presented new offers in order to update previous results. This update could be necessary for two reasons: to the weather prediction, that has a strong influence on both thermal and RES generation, or to adjust the power output to fulfil the thermal unit constraints.

In the Italian context, as well as in the European one, energy markets have a zonal organization. According to transmission system operator (TSO) experience, the transmission system is modelled in macro-zones, the so called "market zones", in which the cross-boundary lines represent the most critical branches. The power flow of these lines have to be constrained in order to avoid unfeasible operating conditions during the real-time physical exchange on the transmission system. Usually, the available transfer capacity (ATC) between two market zones varies according to several factors of technical and economical nature.

NEMO (Named Electricity Market Operator) was established by European market operators in the last decade to perform tasks related to single day-ahead or single intraday market coupling. The goal is to manage European countries' day-ahead and intraday integrated electricity markets. These markets are known as Single Day-Ahead Coupling (SDAC) and Single Intraday Coupling (SIDC), respectively, and a zonal market framework is implemented as well. Actually, sixteen market operators, from over twenty countries, agreed to work on this project to create a fully functional and interconnected European internal energy market, with the following objectives:

- Security of the energy supplied;
- Increase of the competition among suppliers;
- Affordable energy prices for consumers.

SDAC and SIDC implementation requires strong coordination among NEMOs and TSOs to merge energy national, or regional, market operations with ancillary service ones. In particular, NEMOs are in charge of all the necessary tasks to gather the offers from market participants, run a specific algorithm to match the optimal solution and provide the market results with all the participants as well as with the other NEMOs of both SDAC and SIDC [1].

GME is one of NEMO's member and the introduction of SIDC in 2020 has brought radical changes of the Italian electricity markets' configuration to integrate the project Cross Border Intraday (XBID) and Complementary Regional Intraday Auctions (CRIDA) [2], [3]. First of all, XBID is the common platform for the operational management of the SIDC sessions with continuous trading[1] organized and managed by the participating market operators [4]. XBID project went into operation in 2018 involving NEMOs and TSOs of 12 European countries with the aim of creating a European intra-day market based on continuous trading that would allow implicit capacity allocation[2] according to the logic *first come first served* [2]. XBID is composed of three pan-European implicit intraday auctions, that open at hour 15:00 and 22:00 of the day before (D-1) and at hour 10:00 of the day D. At contrary, CRIDA is a complementary Italian intraday market auction that take's place of the previous Italian IM, in which Slovenia and Greece NEMOs are eligible to participate [5]. Therefore, in this scenario, the Italian IM is presented as a hybrid shape, in which the three European continuous treading auctions of XBID, up to the previous hour of delivery (h-1), interrupted by three implicit auctions of CRIDA.

1.1.1. Ancillary Service Markets

This market is split into two stages: Ex-Ante (EA) and Real-Time (RT). The counterpart of this market is the TSO, thus Terna in the Italian case, but, unlike in energy markets, cleared power in ASM is based on keeping the power balance while meeting generator and network constraints. Although the EA and RT markets are hourly and quarter-hourly, respectively, economic merit-order markets with a pay-as-bid remuneration, technical constraints play a significant role in the clearing process. The eligible generators for ASM present several upward and downward offers to participate in the various services, such as secondary reserve, start-up, shut-down, change set-up and other services. Other services, in particular, is so called because gather tertiary reserve, congestion and balancing services [6].

The primary goal of EA market is to minimize the cost of power plant production based on forecasted load, fulfilling generation and network constraints and providing reserve

[1] mechanism of trading based on automatic matching of demand bids with supply offers, with continuous entry of new bids/offers during the trading sessions.

[2] capacity allocation method in which both the transfer capacity and the corresponding energy amount are allocated at the same time.

requirements. This is known as security constrained unit commitment (SCUC), or unit commitment and economic dispatch (UCED) optimization problem. The RT market, on the other hand, aims to minimize the power dispatch costs, of the reserves provided in the previous stage, in order to maintain power balance against load and RES uncertainties, as well as unexpected outages of generating units or large loads, while satisfying network and generation constraints. This problem is defined economic dispatch ED or security constrained ED (SCED) optimization problem.

A crucial date in the development of ASM optimization is the amount of the reserves to be provided for each type of service for a secure operating condition. On the most basic level, security implies that the power system should be maintained in such a way that its operations can continue indefinitely if external conditions do not change. This means that no component should be operated outside of its safe operating range. However, considering the extension and the number of elements in a power system, assuming that external conditions will not change is very optimistic. For this reason, proper reserves are fundamental to be defined to allow the power system to remain stable following any disturbances and to be able to continue operating in this new state long enough to give the operator time to restore the system to the pre-contingency state. These disturbances are mainly due to load and RES error prediction from energy market to RT and unexpected outage of power system elements (e.g., generating unit or power line).

There are several reserves requirements to cope with specific contingency in relation to the required delivery time to provide the service. In general, they are known as primary (PR), secondary (SR) and tertiary reserve (TR) [7]. PR is an instantaneous automatic response of dispatched generators to overcome any mismatch between generation and load, limiting frequency surges within a specific range. SR is also known as frequency restoration reserve because it is used to restore the power balance, bringing the frequency and the generation production to the pre-contingency condition. TR, in turn, is composed of spinning and replacement reserves. If the contingency persists above fifteen minutes, spinning TR is employed to restore the secondary reserve bandwidth. If the contingency is, for example, a generation outage, replacement TR is employed to restore spinning TR and to replace the unavailable generator.

Terna is involved in the TERRE (Trans-European Replacement Requirement Exchange) project [8], in addition to managing the national EA and RT ASM [6]. TERRE is a European Balancing Market (EBM) project that allows TSO members to exchange replacement reserves. TERRE's goal is to create a reserve requirement (RR) platform and an EBM for market participants. TERRE was started as a pilot project, because of the variety of balancing markets among ENTSO-E members[9]. However, the Electricity Balancing Guideline, which defines the timeline and tasks for exchanging RR in the EBM, was defined in 2017 thanks to TERRE, that is the most developed project. The goal of this market is to connect an economically efficient market and the timely activation of cleared bids while also ensuring the financial TSOs' neutrality [8]. TERRE has been operational since 2020, involving six TSOs. Currently, the TSOs are developing an algorithm optimization to develop the EBM by economic merit-order of the offered bids and considering interzonal available transfer capacity among the involved market zones. Since December 2021 TERRE is a half-hour market, but the goal is to implement a quarter-hour market in January 2025 [10].

1.1.2. Electricity Markets Models

The continuous increase of renewable energy resources (RES) penetration puts an additional strain on system operators (SOs) to accomplish the real-time balancing task for their production uncertainty strictly linked to the weather forecast [11], [12]. The non-fulfilment of this constraint will result in the collapse of the whole power system functioning with catastrophic consequences. For this reason, power system operation entails the coordination of multiple generating units used to supply the demand. This coordination necessitates taking into account various technical aspects of generating units and network behavior [13]. To achieve this further task, an efficient economic management has to be taken into account in the coordination of the generation. These techno-economic management problems are called unit commitment (UC) and economic dispatch (ED) problems. In particular, UC problem aims at minimizing day-ahead generation commitment costs to supply the required load, ensuring that technical and security constraints pertaining to the power plants are satisfied [14]. ED problem minimizes the costs of the power output of the committed generators to keep the power balance, complying with the power network constraints [15]. Due to the sequentiality as well as the common behavior of the cost minimization considering technical constraints, the two problems have been combined defining a unique UCED problem, also known as

Network-Constrained UC (NCUC), Security-Constrained UC (SCUC), or Security-Constrained UCED (SCUCED) [16]–[18]. According to ENTSO-E (European Network for Transmission System Operators for Electricity), the SCUCED is defined as "A mathematical optimization problem which determines the commitment schedule of generation units and their level of generation in order to meet demand for every time step of the modelling horizon. The objective of the problem is to minimize operational cost while satisfying the operational constraints of the power system" [19].

Energy markets (i.e., DAM and IM) are modelled in two ways: using a mixed-integer linear programming (MILP) problem to account for UC constraints; or using a simplified linear programming (LP) problem focusing on the ED perspective. The first model is widely used in the United States, whereas the second is commonly used in the European framework. In [20] are explained the main differences between the two approaches. According to IEEE Standards Terms [21] the ED is defined as "The optimization of the incremental cost of delivered power by allocating generating requirements among the on-control units with consideration of such factors as incremental generating costs and incremental transmission losses".

The most widely accepted objective function for energy markets is the maximization of market surplus; that is the sum of all producer and consumer surplus [22]. The producer surplus is the difference between the energy sold at the market clearing price and the energy bid cost. Similarly, the consumer surplus is the difference between its willingness to pay and the cost of the purchased energy [23]. The most common formulation of the bids are represented by piece-wise linear functions of quantity-costs pairs as expressed below:

$$\max_{P^D_{z,j,s}(t_k),\, P^G_{z,i,s}(t_k)} \sum_{z=1}^{N^Z} \left[\sum_{j=1}^{N^D_z} \sum_{s=1}^{N^S} c^D_{z,j,s}(t_k)\, P^D_{z,j,s}(t_k) - \sum_{j=1}^{N^G_z} \sum_{s=1}^{N^S} c^G_{z,i,s}(t_k)\, P^G_{z,i,s}(t_k) \right] \quad (1)$$

in which, supposing N^Z market zones, each of which has N^D_z zonal loads and N^G_z zonal generators providing N^S bid steps, and $c^D_{z,i,s}$ and $c^G_{z,j,s}$ are, respectively, the purchasing and selling energy costs of the s-th bid step of the j-th load or i-th generator of the z-th market zone at the t_k time step. In the European framework, the objective function (1) is usually subject to the zonal balance (2), maximum load (3) and generation bid steps (4), and the interzonal power flow bound (5), formulated as follows:

$$\sum_{j=1}^{N_z^D}\sum_{s=1}^{N^S} P_{z,j,s}^{D}(t_k) - \sum_{i=1}^{N_z^G}\sum_{s=1}^{N^S} P_{z,i,s}^{G}(t_k) + \sum_{l\in N_z^L} P_{z,l}^{tie} = 0 \quad \forall\, z, \forall\, l \in \Omega_L^Z \tag{2}$$

$$0 \le P_{z,j,s}^{D}(t_k) \le P_{z,j,s}^{D,max} \quad \forall\, z, \forall\, j, \forall\, s, \forall\, t_k \tag{3}$$

$$0 \le P_{z,i,s}^{G}(t_k) \le P_{z,i,s}^{G,max} \quad \forall\, z, \forall\, i, \forall\, s, \forall\, t_k \tag{4}$$

$$P_{z,l}^{lb} \le P_{z,l}^{tie}(t_k) \le P_{z,l}^{ub} \quad \forall\, z, \forall\, t_k, \forall\, l \in \Omega_L^Z \tag{5}$$

where $P_{z,l}^{tie}$ is the power flow of the l-th interconnection line to the z-th market zone, gathered in the set $\Omega_L^Z \subset N^L$, $P_{z,j,s}^{D,max}$ and $P_{z,i,s}^{G,max}$ are the load and generation bid steps' maximum power, respectively, and finally $P_{z,l}^{lb}$ and $P_{z,l}^{ub}$ are the lower and upper power flow bound. However, the main features of the DAM of the main countries can be found in [24]. Alternatively, supposing an inelastic load demand, the problem is converted into a generation cost minimization, that is UC or ED problem.

The most recent scientific contributions address UC and ED problems through optimization-based methods of varying nature and complexity. The UC objective function is fundamentally composed of start-up, shut-down, and operating costs. In addition to the power balance and reserve provision constraints, the generator unit constraints include minimum up and down time, active power bounds, and ramping limits. Power units' constraints are related to their status (on or off) assessed by binary variables [25]. In contrast, ED formulation does not include binary variables and the objective function only involves minimizing operating costs, whereas the constraints concern generator power limits, power balance, and active power bounds of transmission lines [13].

Because of its computational tractability, the MILP approach is the current state-of-the-art for UC problems [26]. The number of integer variables per generator depends on the techno-economic aspects embedded in the problem. Since the first works on UC, three binary variables have been defined to determine start-up and shut-down cleared bids, as well as the status of the single power unit [27]. However, the succeeding unit commitment research takes many different paths, mainly focusing on RES integration [28], co-ordination of multi energy system [29]–[33], system uncertainties [34], as well as network constraints [35], that required

the employment of evolutionary optimization techniques [36], to handle models with higher complexity and greater dimension.

A further well-known optimization method for UC problem, exploited in the past decades, is the Lagrangian relaxation (LR). This technique allows the relaxation of the optimization problem by decomposing the problem into as many subproblems as the number generator units in the system and converting the constraints into penalty factors embedded in the objective function [37]. LR method drawback is the ramping constraint, requiring enlarging state spaces to solve each subproblem [38]. To overcome this limit, hybrid methods have been proposed as the LR combined with evolutionary and quadratic programming [39]. or with particle swarm optimization [40]. However, the accuracy of LR methods have been considered adequate for industrial application until the introduction of wholesale energy markets [38].

Priority list (PL) methods, in addition to optimization-based methods, have been used to solve UC problems. The PL is a heuristic algorithm that entails creating a sorted list of power units based on economic or technical criteria. As a result, the generators are either committed or not according to the predefined list and the required load. The primary advantage of PL methods is that they reduce the size of the problem [41]. and they are simple to apply and efficient in calculation [35]. On the other hand, because global optimality cannot be theoretically guaranteed, these algorithms are usually combined with other algorithms to solve UC problems [42].

California independent system operator (CAISO) defines the UC problem as "the process of determining which generating units will be committed to meet demand and provide ancillary services in the near future" [43]. Let us consider a power system network with N^G units, for the generic time step t_k, in a time horizon composed of N^T time steps, the cost minimisation objective function is as follows:

$$\min_{\boldsymbol{P^G}(t_k),\boldsymbol{u}(t_k)} \left[\boldsymbol{C^O}(t_k,\boldsymbol{P^G},\boldsymbol{u}) + \boldsymbol{C^{SU}}(t_k,\boldsymbol{P^G},\boldsymbol{u}) + \boldsymbol{C^{SD}}(t_k,\boldsymbol{P^G},\boldsymbol{u})\right] \tag{6}$$

where $\boldsymbol{C^O}$, $\boldsymbol{C^{SU}}$ and $\boldsymbol{C^{SD}}$ are the vectors of the operating, start-up and shut-down costs, respectively, of dimension N^G and are function of the generator's cleared power vector ($\boldsymbol{P^G}$) and operating state ($\boldsymbol{u}$).

Operating costs can be expressed as quadratic function of the of the cleared power (P_i^G) and operating state (u_i) variables of the i-th generator:

$$C_i^O(t_k) = a_i\, u_i(t_k) + b_i\, P_i^G(t_k) + c_i\, P_i^G(t_k)^2 \tag{7}$$

in which u_i is a binary variable that is 1 when the generator is suppling energy and 0 when it is shut-down, a_i is the no-load or fixed cost and b_i and c_i are the marginal or variable costs of the i-th power plant (i = 1, …, N^G). Operating costs can be also expressed as cubic [15], linear [16] or piece-wise linear [44] function of the cleared power.

Start-up costs (SUCs) are exponential function of the time in which the generator unit is kept turned-off [13]. To linearize this cost, a constant value (c_i^{SU}) is supposed to depend on the generator status between two consecutive time steps:

$$C_i^{SU}(t_k) = c_i^{SU}\big(u_i(t_k) - u_i(t_k - 1)\big) \tag{8}$$

therefore, C_i^{SU} are taken into account if and only if the generator from off status, at t_k-1, has been cleared. In literature start-up costs have been also modelled as linear function of time [37] or defining hot, warm and cold start-up cost according to the down time [45].

On the contrary, shut-down cost (c_i^{SD}) is constant and depends on the generator status between two consecutive time steps as well:

$$C_i^{SD}(t_k) = c_i^{SD}\big(u_i(t_k - 1) - u_i(t_k)\big) \tag{9}$$

hence, C_i^{SD} is considered if and only if the generator from on status, at t_k, has not been cleared. Further costs can be included in the objective function, as emission penalty [15], load shedding penalty[16], reserve provision [27] or fuel with operation and maintenance [46] costs.

The objective function (6) is subject to several constraints to fulfil the security operation of generating units. The cleared power plants are allowed to supply energy within their technical limits; therefore, a constraint is necessary to link active power bounds with the status of each generator:

$$p_i^{G,min} u_i(t_k) \le P_i^G(t_k) \le\ p_i^{G,max} u_i(t_k) \tag{10}$$

where p_i^{min} and p_i^{max} are minimum and maximum power of the i-th power plant, respectively.

Thermal generators are not able to be shut-down and start-up between two consecutive time steps, because they need a minimum time to reach thermal regime. Consequently, minimum up and down time constraints has to be embedded in the optimization:

$$\left(t_i^U - MUT_i\right)\left(u_i(t_k) - u_i(t_k - 1)\right) \leq 0 \tag{11}$$

$$\left(t_i^D - MDT_i\right)\left(u_i(t_k) - u_i(t_k - 1)\right) \geq 0 \tag{12}$$

in which, for each generator i, t_i^U (t_i^D) is the time step number of consecutive activity (inactivity) at time t_k-1, whereas MUT_i (MDT_i) is the minimum up (down) time.

Moreover, dispatchable units' flexibility is limited; the power output variation throughout two-time steps is bounded within a maximum ramp variation. Hence, ramp-up (RU_i) and ramp-down (RU_i) constraints have to be taken into account to model each generator's flexibility:

$$P_i^G(t_k) - P_i^G(t_k - 1) \leq RU_i \, u_i(t_k) \tag{13}$$

$$P_i^G(t_k - 1) - P_i^G(t_k) \leq RD_i \, u_i(t_k) \tag{14}$$

Finally, power balance between the load demand and the cleared power is required:

$$\sum_{i=1}^{N_G} P_i^G(t_k) = P^D(t_k) \tag{15}$$

where P^D is the total demand load of the considered time step.

The problem (6)–(15) is a mixed-integer quadratic programming (MIQP) optimization model, with one real and one binary decision variable per generator and time step. In order to convert the model into a MILP, the quadratic expression of the operating costs can be linearized into linear or piece-wise costs. In literature additional constraints are modelled to include reserve provision [47], load shedding limits [16], or network constraints considering active power injections[18], DC approximation of the network [48], including N-1 condition security [49], or modelling the full AC network by linear-programming approximation [26] or relaxation and decomposition [50]. Although the presented model is suitable to include solar and wind power generators, deterministic formulation represents a limit in presence of system uncertainties [34]. To tackle this problem, in literature have been applied three different optimization methods: stochastic[51], robust [33] and distributionally robust [31]. UC

problems are large-scale, non-convex and MILP, and the review paper [52] shows the various solvers used to solve UC based on the formulation of the mathematical model.

On the contrary of UC, ED formulations are devoid of integer variables and only optimization-based methods have been applied to cope with these problems. The optimization methods are classified as classical, metaheuristic, and hybrid algorithms, and they are employed depending on whether the problem is convex or non-convex, as well as the elements embedded in the power system [53]. The formers are composed of LR, Newton, linear programming, interior point and quadratic programming methods to solve deterministic problems [54]. However, in an era of climate change caused by greenhouse gas emissions, the scientific community's efforts are focused on integrating a high penetration of RES into the operation of power systems [55]. Given the stochastic nature of solar and wind power production, as well as the required load, the use of appropriate optimization methods to integrate system uncertainties is required. The solution to these problems was discovered in metaheuristic algorithms, which have grown in popularity in the last year due to their ability to deal with non-linear constraints as well. Finally, hybrid methods are enhancements to metaheuristic optimization algorithms that increase the feasibility of optimal solutions while decreasing computation time [56], [57].

ED problems seek to minimize operating costs of the committed generators, therefore, considering the set of cleared generators Ω^G, the objective function (6) becomes:

$$\min_{\boldsymbol{P^G}} \boldsymbol{C^O} \tag{16}$$

in which $\boldsymbol{C^O}$ could be express as quadratic function of the active power as well, but no-load cost is devoid of the status binary variable. Hence, for the i'-th generator ($i' = 1, \ldots, N'_G$)., the cost function is:

$$C^O_{i'} = a_{i'} + b_{i'}\, P^G_{i'} + c_{i'}\, {P^G_{i'}}^2 \tag{17}$$

as for UC problems, operating costs in ED formulation can be expressed as a linear function of cleared power [58]. The main difference is that in ED problems the optimization is solved independently between two consecutive time steps, pinpointed by the absence of t_k in the formulation. Although RES costs are zero, because there are no variable costs associated with fuel consumption, the authors of [59] proposed a novel formulation of solar and wind power

costs. In addition to generators costs, the objective function can include costs for valve-point loading [15], load shedding [60], reserves [61], heating [62], or RES curtailment [63].

Consider an ED problem devoid of network model; with this supposition, the generators are dispatched in order to supply the demand load:

$$\sum_{i' \in \Omega^G} P_{i'}^G = P^D \tag{18}$$

within their active power limits:

$$p_{i'}^{min} \leq P_{i'}^G \leq p_{i'}^{max} \tag{19}$$

and the optimization problem (16)–(19) is a QP ED problem neglecting network constraints.

On the contrary, let us consider a system composed of N_B buses, in which Ω_G^B, Ω_D^B and Ω_L^B are respectively the sets of the generating unit, load demand and line connected to the b-th bus ($b = 1, \ldots, N_B$). A simple method to model lines' power flow is the exploitation of DC load flow approximation [64]. As a result, for each bus b, the power flow equation can be written as follows:

$$f_{b,c} = B_{b,c}(\theta_b - \theta_c) \quad \forall\, c \in \Omega_L^B \tag{20}$$

where $f_{b,c}$ is the power flow from the bus b to the bus c, $B_{b,c}$ is the susceptance of the line b-c, and θ_b and θ_c are the angle voltage at bus b and c, respectively.

Power system lines are designed to carry a maximum power amount; to avoid overheating and premature wear and tear of the component, a constraint must be included in the optimization problem to limit the power flow within their physical limits:

$$f_{b,c}^{min} \leq f_{b,c} \leq f_{b,c}^{max} \quad \forall\, c \in \Omega_L^B \tag{21}$$

in which $f_{b,c}^{min}$ and $f_{b,c}^{max}$ are respectively the minimum and maximum power flow limit to the line b-c.

The active power balance must be considered at nodal level, because the difference between the nodal generation and the nodal load must be equal to the power flowing through the connected lines:

$$\sum_{i' \in \Omega_G^B} P_{i'}^G - \sum_{j \in \Omega_D^B} P_j^D = \sum_{c \in \Omega_L^B} f_{b,c} \tag{22}$$

for each bus $b = 1, \ldots, N_B$; whereas (19) is used to bound generators' dispatch as well.

The employment of DC load flow approximation allows to keep the linear formulation of the constraints (19)–(22). Thus, the objective function (16), with quadratic costs(17), and subject to constraints (19)–(22) remains a QP ED problem.

ED problems has several variants in the formulation of constraints embedded in the optimization problem. The active power losses in [15] were calculated as a quadratic function of the power flowing through a branch and linear function of the power injected at each node. The constraints in a smart grid ED with storage system include spinning reserve and storage flexibility, as well as load shedding limits, as proposed in [60]. In contrast, additional constraints must be included in a UCED problem with ancillary service market to provide reserve requirements for each service [61]. To ensure the proper operation of both systems in a combined power-heating system, the heating system model constraints must be included as well [62]. However, given the high penetration of RES in the power system, RES curtailment limits must be embedded in the problem constraints, in addition to the penalty costs in the objective function [63].

Although a detailed formulation of the system's elements will provide a more realistic optimal solution, the method of solving the optimization problem must be considered. In literature, ED problems are represented modelled as LP, MILP, QP, or quadratic constrained QP (QCQP) optimization problems that can be solved using commercial solvers such as Gurobi or CPLEX. These solvers are simple to implement in a variety of environments, including MATLAB [60], Python [49] or C++ [63]. Several libraries have been used in the literature for UC and ED analysis purpose. According to the review paper [52], the most commonly used software or programming languages on which they have been developed, are MATLAB, C++, IBM CPLEX, and FORTRAN. In terms of optimization libraries, MATLAB has the YALMIP toolbox for optimizing modelling [65], which can model stochastic models as well [30], [60]. C++ and FORTRAN are open-source programming languages in which several libraries for building and solving optimization problems have been developed. For the first, there are ROC++ [66], OptimLib [67], Dakota [68], etc., whereas

[69] contains the list of all the Fortran libraries. The review paper [52] lacks in Python-based libraries to develop these optimization problems. The most spread in literature are SciPy [70] and Pyomo [71] able to model and perform UC [47]–[49], [51], [61], [72] and ED [49], [61], [62], [73] problems. IBM CPLEX Optimization Studio, on the other hand, is a commercial software designed solely to model and solve optimization problems [74]. Further commercial software for power system studies developed advanced features for UC and ED problems. The well-known software PowerFactory, provided by DIgSILENT, developed a toolbox called "Unit Commitment and Dispatch Optimization" and the authors of [52] and [53] envisaged doing a SCUCED by means of this toolbox. On the other hand, the novel software SAInt, developed by encoord, is a planning software to model coupled energy networks & markets [75]. SAInt has a feature named "Security Constrained Unit Commitment and Economic Dispatch" to evaluate coordinate electricity-gas optimization problems [76]–[78]. PowerWorld is another well-known commercial software for power system simulation, despite the previous ones this software is avoided of UC package, and ED problems are solved based on "Optimal Power Flow" toolboxes [79].

1.1.3. Reserve Requirements Sizing

In a power system with a high penetration of renewable energy sources (RES), the critical requirement of power balancing during real-time operation is subject to additional uncertainties that could jeopardize system flexibility. Reserve requirements (RRs) are essential for ensuring adequate power margins to overcome these uncertainties without endangering system flexibility. However, achieving a stable and reliable operation of the electrical power system is only possible if the reserves are sized in relation to the potential contingencies. The methods for calculating RRs can be divided into three broad categories: Deterministic methods: RRs are obtained empirically as the maximum cleared power plant [80], as percentage of the demand load [81] or as percentage of RES production forecast [82]; Probabilistic methods: probabilistic reliability criteria are defined, as loss of load probability (LOLP) or expected energy not served (EENS) to determine the reserve requirements [83]; Cost-benefit methods: RRs are optimized based on an economic analysis of the costs and the benefits generated by their provision [84].

As a result, the RRs are determined based on the probability that a contingency will occur, in order to reach a new stable operating condition. Tertiary reserve requirements

(TRRs) are made up of multiple reserves and are defined differently around the world. On the one hand, the North American Electric Reliability Corporation (NERC) defines contingency reserve as the sum of three terms: spinning (SpRR), non-spinning (non-SpRR), and supplementary RRs On the other hand, the European Network of Transmission System Operators of Electricity (ENTSO-E) defines the TRRs as the sum of the manual frequency restoration reserve and the replacement reserve [85].

Considering the impact of RES on system flexibility [86], several scientific works were developed to size the TRRs in power system with high RES penetration. The majority of studies is focused only on the SpRR determination [83], [87]–[92], or alternatively, are aimed to estimate both the SpRR and the non-SpRR [93]–[95]; whereas, further works determine a unique zonal or total TRR [96]–[103]. RES and load uncertainties, as well as the generator outage probability, are the common parameters to size the RRs. Most of the test cases employed to determine the reserves are related to solar power plants [88], [90], [91], [93], [96], [100], [102] and others only account for load uncertainties [87], [89], [98] representing a limit for several real power system applications. However, novel factors are involved to their sizing, as the interzonal lines stress condition [103], the wind-load correlation [100], the expected energy supplied by electrical vehicles [92], system generation margin and injection shift factors [102], or the definition of fast and low load variation [104].

An important aspect of reserve sizing method is the determination of RES and load forecast errors, and this aspect is faced in literature with different approaches [105]. Deviations are frequently modeled using parametric or non-parametric distributions. Load uncertainty is typically assumed to be a normal distribution with a zero mean [83], [88]–[90], whereas in the case of net load estimation, Kernel-based probability density functions have been used to account for the correlation of more uncertainties [99], [106]. Although a Gaussian distribution is assumed to be suitable for wind uncertainty estimation [90], [96], [104], particularly in the case of a wide power system with wind turbines distributed throughout [88], other methods such as beta-distribution [93], Wasserstein metric [107], multivariate time-series [108] or Weibull distribution [109] have been employed. Finally, for the solar uncertainties Kernel-based probability density functions [94], [99] as well as Gaussian distribution [110] have been applied.

Most of these works do not consider the variation of forecast uncertainties since they focus only on short time horizon or few scenarios, particularly for optimization-based methods. For instance, the robust optimization proposed by [82] determines the RRs considering two range intervals of wind forecast error. The authors of [83] developed a multiscenario risk-based optimization, considering a discretized normal distribution to evaluate a daily reserve requirement. The uncertainties in the random day-ahead optimal dispatch of [93] have been estimated via Kernel density estimation for a day supposing four different wind scenarios. A stochastic optimization problem is employed in [98] in which Ornstein-Uhlenbeck process is applied to define only load forecast error. Analogously, in [95] scenarios are generated by ARMA models, supposing normal distribution; subsequently, a technique based on the Kantorovich distance is applied to reduce the scenario number. Only few papers deal with variable uncertainties, as the authors of [94] in which dynamic reserve requirements are assessed in relation to three different distributions depending on the expected required load, and solar and wind penetration. Even the authors of [96] proposed a scenario-based approach for the system uncertainties based on normal distribution; however, the forecast errors of wind a load are time-dependent and correlated each other. A multivariate ARMA process is used in [108] to estimate timeseries of wind and load uncertainties in a stochastic optimization problem. Other studies demonstrated the seasonal influence on RRs [111]–[113], as well as the daily variation [94]. Further works on RRs sizing in relation to the modelled uncertainties are explained in the review paper [114].

1.2. An Overview on Generation and Transmission Investment

The importance of generation and network constraints on electricity markets, as well as how load and RES uncertainties affect the electricity markets, have been discussed previously. In particular, the necessity to define market zones in order to bound the power flowing through critical lines for DAM. Furthermore, the European Commission established a minimum renewable energy target of 32% in order to reduce greenhouse gas (GHG) emissions of 55% by 2030 [115]. In addition, the European Environment Agency predicts a 1% annual increase in energy consumption from 2020 to 2030 [116].

The power system operations are based on reliability, security and adequacy parameters that are all strictly related each other. The term security of a power system has been

already defined in the previous subsection, whereas in the following the definition of the other two terms is provided. According to [21] the reliability of a power system "is the probability that the system will provide electrical power to the final users without failure, within design parameters, under specific operating conditions, and for a specific period of time". On the other hand, according to [117] the adequacy of a power system is "the ability of an electric power system to supply the aggregate electric power and energy required by the customers, under steady-state conditions, with system component ratings not exceeded, bus voltages and system frequency maintained within tolerances, taking into account planned and unplanned system component outages".

The penetration increase of RES and the growth of the required load put a strain on future security, adequacy and reliability of the power system. Therefore, the system topology must evolve to keep the same level of these parameters during its operations. Studies of power system development planning aim to analyze the interaction of grid configuration, generation and demand. Providing demand envisions, the scheduling goal is to deal with generation evolution (e.g., replacing out-to-date technologies with renewables and innovative ones), combined with demand load trend evolution taking into account economical, reliability, continuity and environmental factors. Furthermore, network development analysis represents a crucial issue due to the analytics intricacy and the big data management. These reasons have brought the definition of Transmission Evolution Planning (TEP) and Generation Evolution Planning (GEP) or combined G&TEP. With regard to TEP, the TSOs must consider the uncertainty of future framework of load demand or renewable generation penetration satisfying technical constraints and ensuring reliability and security, by assessing branch doubling or new grid assets.

When the electrical system was vertically integrated, the evolution of generation and transmission was managed by only one entity to obtain the best level of coordination. On the other hand, after the implementation of the deregulation process in the electricity supply, generation and transmission investments are evaluated separately [118]. Transmission investment, in particular, is sustained by the TSO, whereas generation investment is charged to external investor, and both parties are interested in making a profit in relation to the cost of the new equipment.

Generation and transmission investments are costly, and their development should be undertaken only if technical-economic benefits are provided. As a result, determining the best solution in terms of generation and network operating conditions necessitates a methodical approach. In the following subsections are described the costs associated to transmission elements and generators power plant, as well as basic concepts related to these topics, whereas the methodology to develop these studies are presented in the literature review subsection.

1.1. Transmission Investments Theory and Perspectives

Transmission equipment investments can include transmission lines, transformers, or shunts. Even for elements of the same type, the costs vary depending on the parameters (size, extension, rated voltage, type of supply), as well as if they are a new installation or a redundancy equipment. However, the costs associated with a new transmission equipment can be divided into two categories: investment costs and operation and maintenance costs. Users bear the majority of the investment costs [119], and the investment must provide an economic benefit to users; otherwise, it would simply represent an increase in energy costs. For instance, the installation of a new line must be well designed in order to solve the existing problem; if the size is overestimated, users must pay additional costs for a component that is not fully utilized.

There are several methods for the investment cost allocation to users which will be briefly introduced, further information can be found in [118] and [119]. One method is the *Postage Stamp Method*, in which users pay a system charge based on the rated power of a producer's generating unit or the peak demand of a consumer. The investment allocation may also be affected by the rated voltage, but in general, it is determined by the network's average usage. The *Contract Path Method* is derived from traditional or vertically integrated utilities, in which the consumer must pay an additional charge for network usage according to the path on the transmission system between consumer and producer, specified in the contract. The *MW-mile method* is based on power flow simulations to determine the path on the network due to each transaction. This amount is multiplied by an agreed per-unit cost of the transmission capacity.

Transmission system elements are very expensive, but their expected life is above 20 years, and the investments are irreversible because it is not economically profitable. Hence,

the system analyses must take into account current and future operating condition to find suitable investments. In the European contest National TSOs study the evolution of the system up to 2050, setting out a range of possible future scenarios to analyze the potential investments to assess system security, reliability and adequacy [120]. For the first time, a coupled gas-power network has been developed by ENTSO-E and ENTSO-G in which supply and demand data of both the systems are collected in order to define a *National Trend Scenario* for the Ten-Year Network Development Plans (TYNDPs) [121]. This scenario allows to combine Power-to-Gas (P2G) and Power-to-Liquid (P2L) facilities to evaluate the interactions between the two systems, considering a time horizon up to 2040. Further scenarios are the *Global Ambition* and *Distributed Energy Scenarios* for a full-energy perspective to reach the 55% GHG emission reduction by 2030 and net zero by 2050.

1.2. Generation Investment Theory and Perspectives

In a deregulated system, external investors willingness to finance a power plant is strictly related to the potential profit earns over its lifetime. In other words, the revenue generated by power plant energy supply should exceed the installation and operating costs. To achieve this goal, the investor must assess the selling price of the energy. The price is determined by intrinsic factors of the power plant (technology, fuel, lifetime, and so on) as well as the participating markets.

Short run marginal costs (SRMC) and long run marginal costs (LRMC) are two types of costs defined by economists based on the time required to adjust factors influencing production. Some factors in SRMC are assumed to be constants, whereas in LRMC the time period is considered long enough to assume that all factors are adjustable. In the case of power plants' SRMC, an adjustable factor is the fuel used to generate electricity, whereas installation and scheduled maintenance costs are fixed. Therefore, SRMC calculates the energy cost to participate in a perfectly competitive market in which firms can maximize their profits by adjusting their power output [122]. On the contrary, for power plant investment, the selling price of the energy supplied according to LRMC is evaluated. In this step, each decision represents a variation on final investment cost and the uncertainties affecting the LRMC estimation represent the financial risk of the power plant investment. Hence, the assessment of a power plant's profitability is inherently accompanied by risks since it is a long-term investment involving a large number of assumptions about the future, such as fuel

prices, demand, development of new plant technologies, and installation of new power plants by competitors. One example is the current conflict between Ukraine and Russia, which resulted in a massive increase in coal, oil, and gas prices throughout Europe as well as energy prices in only two weeks [123].

The investment in new power plants depends on demand growth, generation decommission and new power plant technologies development. If demand for electricity rises without a corresponding increase in generation capacity, or if available capacity drops due to decommissioned generating units, the market price for electrical energy will rise. This price increase will incentivize power companies to invest in new plants. Moreover, once a power plant is operational, its designed lifetime becomes a theoretical reference point from which the actual lifetime can deviate significantly. Market conditions may indeed change to the point where the plant's revenues no longer cover its operating costs, and the plant must be retired unless there are compelling reasons to believe that market conditions will improve. In particular, if a dispatchable generator is installed, it could participate in ASM to increase its profit. To avoid a lack of generality in this discussion, it is assumed in the following that the installed generator will only participate in energy markets.

To incentivize power plant investments, TSO can provide economic prizes offering the capacity of the power plants to energy and ancillary service markets. This incentive market is known as *Capacity Market* and is applied by several TSO in Europe [124]. It is a long-term (months or years) economic merit-order market in which the TSO forecasts the demand load, and the power plant owner presents their offers considering the minimum selling price. This system allows to evaluate the evolution of energy price, as well as the adequacy of the installed capacity.

1.3. Transmission and Generation Investments Methodologies

TEP mathematical optimization methods can be grouped in two main categories: programming-based and heuristic optimizations. Linear programming (LP) [125]–[129], MILP [130]–[135], robust optimization (RO) [136]–[139] or games theory [140] are the spread methods of the first group. On the contrary, heuristics can include K-medoids [141], Gbest-Guided Artificial Bee Colony [142], Particle Swarm Optimization [143], [144], multi-criteria decision making and differential evolution [145] social spider algorithm [146], evolutionary

algorithms [147], semi-definitive programming and branch and bound [148], symbiotic organism algorithm [149], or combined search space reducer and bat-inspired algorithm [150].

As regards objective functions, in TEP new transmission line investment costs are usually considered, but additional operating costs or penalties could be included, such as generation operating costs [128], [137], [142], [143], matched with unserved energy costs as in [127], [138], [139], [141], [150], or with load shedding as in [129], [132], [133]. Other works consider loss-of-load probability and load curtailment costs [131], renewable curtailment costs [126], load shedding and renewable curtailment costs [134], losses penalty factor [148], or operational costs, generation curtailment and load shedding costs [135]. Few works neglect generation operating costs in objective function but embed new factors as in [144] where weighted vulnerability factors are introduced to optimize the system security, or in [145] whose purpose is to avoid congestions by means of a penalty factor. A novel case of investment costs omission is evaluated in [125], rather the focus is on the generation costs including fuel, O&M and CO2 costs. In multi-level TEP optimization the investment costs are considered in the last level. Detailed market aspects are modeled in [140] where the first-level optimization pursues generation costs minimization and consumer surplus maximization, the second-level aims at maximizing zonal generation and consumer surpluses and congestion rent earned by the TSO, while the third-level goal is to minimize investment costs and maximize global generation and consumer surpluses. The authors of [136] minimize the generation and load shedding costs in the level-I, and investment costs in level-II.

A crucial perspective in the TEP optimization constraints is the network model. The most employed formulation is the DC load flow (LF), [135]–[144], [139]–[141], [145], [146], [149], in few papers the losses have been embedded by means of quadratic expression in the DC formulation [147], [150]. Nevertheless, other approaches exploit power transfer distribution factors (PTDFs) [125], [126], shifting factors [129], [144], economic dispatch [138] or power balance [147] but all the approaches omit the behavior of losses. AC LF formulation is adopted in [143] and [148]: the first one compares the AC optimal power flow (OPF) model with DC-TEP formulation considering piecewise linear losses, while the second represents the losses as difference between generation and load. As reported above, the TEP optimization methods focus on economic terms, with simplified network models to reduce formulation complexity and reduce computational cost. However, as demonstrated in [143] the AC

OPF solution requires higher capacity installation and lower operating costs compared to the DC-TEP ones. Besides, [151] investigates the influence of losses model in the TEP solution, underlining the variation in investment costs proving that in large-scale systems the losses have a relevant impact.

A separate set of approaches, guided by TSO applications, involve solution techniques of TEP problem different from optimization. The combination of DC-OPF and cost-benefit analysis (CBA) is the common framework employed to evaluate the candidate project selection. The CBA is conducted by means of: wind spillage and production costs indices [152]; the comparison with and without weighted environmental aspects indices [153]; present-value, welfare, investment costs indices [154]; investment costs, congestion costs and risk costs minima [155]; reliability indices and investment, operational and risk costs minima. In [156] ENTSO-E CBA is evaluated through a software called SCANNER. In [157] electrical market with Multi-Area Power-Market Simulator software is considered, with detailed model of intermittent and hydro generation, comparing results by CBA based on investment costs, transmission and generation capacity. A flow-based optimization market capacity is proposed in [158] exploiting PTDFs and remaining available margins (RAMs) through the corridors. Moreover, phase shifter transformers (PSTs) are connected over cross-zonal branch to adjust RAMs by means of an optimization.

Nowadays a worldwide green energy generation and consumption transition is developing and TSOs are organizing a long-term TEP forecasting renewable generation and demand growth. In the field of scientific research this issue is tackled by multi-scenario [125], [130], [132], [138], [141], [143], [153], [156], [157], scenario clustering [131], [134], [135] or multi-year approach [127], [136], [137], [139], [154], [155]. In the first, framework generation and load are uncorrelated, in the second the gathering of scenarios is related to cost minima, while in the last the increases are correlated and predefined. The considered network uncertainties are mainly represented by intermittent renewable generation and load demand.

Simulation time reduction also depends on the number of candidate projects to evaluate, and an established technical analysis is helpful to reduce the set dimension embedding the ones with higher benefits. For this purpose, in [125] the set is determined according to RES penetration, in [127] a relaxed version of the TEP problem is solved to quantify the investment pool with most benefits. Moreover, in [128] following the load flow results, the

reinforcement for congested corridors is considered and locational marginal price advantages for new line addition, in [138] a method based on long- and short-terms network uncertainties is developed to pinpoint the candidate investments, and in [141] different typology of candidate projects are determined according to the potential benefits introduced. For candidate selection, in [147] a load and an angle performance index is defined, in [149] a search space reducer algorithm is solved, in [152] cost-benefit incremental relationship and sensitivity factor of branch capacity and admittance are evaluated, in [153] the probability of branch overload is considered. Further methods, applications, and evaluations are reported in the review papers [159], [160].

There are few papers that include N-k security criteria in TEP assessment. In particular, optimization problems are faced including N-1 security constraint in the formulation [147], [158]. The authors of [128], [161], [162] evaluate an N-k security in the second stage of the procedure in order to define the set of candidate projects and/or to obtain optimal solution, whereas in [155] a risk index is defined including the line outage probability.

From literature analysis, the formulation of a TEP problem has several facets that are hardly caught in the presence of a real-size network, where CBA of single development projects is usually carried out [163], [164]. Moreover, different implications of the development projects should be assessed in the form of scenario analysis. In order to perform useful comparison among different projects by accounting non-commensurable quantities, multi-criteria analysis can be adopted, with particular reference to Analytic Hierarchy Process (AHP) due to high flexibility and applicability [165], [166]. This technique has found application in power system problems such as Generation expansion planning, in a multi-objective model with detailed network representation in [167] and encompassing financial, technical, environmental and social aspects in [168], or distribution system planning [169]. However, TEP problems represent a field of application of AHP for multi-criteria analysis. In particular, application of test network involve IEEE 24-bus test system in [170], where a multi-objective optimization involving congestion cost, investment cost, probabilistic reliability, anti-competition and anti-flexibility indices allows to obtain the Pareto front and it is supported by AHP and TOPSIS to determine the best solution, in [171], exploiting a two-stage TEP algorithm where cost minimization results are analyzed with AHP considering congestion cost, consumer cost, power losses and voltage deviations, and in [145], where dynamic evolution

technique is underpinned by AHP for ranking the best compromise solution. Moreover, in [172] indices of economy, safety, flexibility and vulnerability are taken as criteria of fuzzified AHP method with different comprehensive weights for IEEE 6-bus network with different planning schemes, whereas in [173] location marginal prices from AC load flow in IEEE 9-bus system are used for individuating candidates combined with AHP. As regards real network applications, in [174] a combination of AHP and entropy weight is adopted to evaluate three candidate projects by means of indices of safety (including N-1 and N-2 security ones) and reliability, economy and efficiency, coordination and flexibility, social aspects and risk control. Whereas in [175] a Brazilian network is analyzed considering AHP for probabilistic, strategic, financial, externalities and enterprise risk, and in [176] Paraguay transmission system expansions are analyzed with AHP considering operation and inversion cost, power losses, line length and project financing. It can be noted that the analysis of AHP in TEP has seldom accounted for evolution scenarios of load and renewables, and methods are focused on network with limited extension.

GEP's methodological framework state-of-the-art can be identified in four key categories: risk-based, integrated approach, market-based and multi-disciplinary aspects [177]. Although risk is evident in all decisions, including the GEP problem, risk consideration in the GEP has been facilitated rapidly since the late 1960s, owing primarily to energy crises that caused stagnation in all economic sectors, increased consciousness of environmental concerns, and the liberalization of electricity markets. Infrastructure networks for natural gas and electricity are critical to the global economy and quality of life. The retirement of aging coal power plants as the world transitions to a low-carbon economy and the flexibility provided by fast-ramping natural gas-fired power units to back up increasing amounts of intermittent renewable energy sources have all contributed to the power sector's continued use of natural gas [178]. As renewables' share in the power mix grows, so do the requirements for short-term flexibility, because electricity generation from renewable energy sources, like wind and solar, is characterized by variability and uncertainty. The output of these variable renewable energy sources is highly dependent on meteorological conditions, fluctuating quickly and in response to changes in wind speed or solar irradiation. As a result, it necessitates more flexibility in pinpointing models and approaches to address the problem of GEP with generating unit constraints. Policy issues are crucial in determining market structure and design, and

thus in implementing long-term power investment opportunities and determining the power mix, offering the flexibility that is critical as the share of intermittent renewable energy sources such as wind and solar PV keeps increasing. GEP problems are proposed and studies, as thoroughly reviewed in [177], [179], [180], usually having a centralized viewpoint, typical of vertically-integrated electricity industry, where transmission expansion planning could be analyzed along. However, the combined G&TEP is mainly modelled, as mono- or multi-level programming-based optimization methods to minimize costs, and it is formulated as MILP [181]–[184], Mixed Integer Nonlinear Programming (MINP) [185] or Robust Optimization [186]. Generation and transmission investment costs are the essential terms present in the objective function for all the approaches [181]–[186] whereas additional aspects involve operating costs, expected energy not served (EENS), losses cost, load shedding costs.

The analysis of generation company (GenCo) viewpoint in generation expansion plans is analyzed in different ways in literature. In liberalized market framework, the centralized approaches could depict an optimized and efficient evolution (command-and-control approach), although studies should be devoted to the analysis of generation investors with a market-based approach framework assuming the goal of profit maximization [187], [188]. In particular, a multi-agent competitive environment is proposed in [189] considering reserve and revenue adequacy, whereas the interaction of GenCo with the policy maker is analyzed in [190] considering the presence of contracts for difference. The presence of a set of candidate projects is accounted in [191] using a technical selection based on loss of load and an economic competition based on levelized total cost, whereas in [192] stochastic profit evaluation is provided in a system-level procedure with a price-based approach, and in [187] factors of uncertainties are analyzed. Another stochastic investment approach is proposed in [193] applying an option-game-based method and considering the carbon-fired power plant marginal costs as uncertainty, as well as the required load, in a future perspective. A statistical model, so-called emulator, is employed by the authors of [194] to quantify the uncertainties in wholesale electricity prices in generation investment analysis. Investment planning is dealt with in [195] in the presence of market and network structure, whereas in [196] strategic bids for new investments are considered in scenario framework, and in [197] the influence of reserve provision and demand response on investment plans is investigated. Strategic investment strategies are developed in [198] considering both risk-aversion and strategic behavior

in a bi-level optimization problem. Nuclear power generation investment is envisaged doing in [199] based on real option theory. On the contrary, the GEP evaluated in [200] has been taken into account in different competitive market design criterion. In [201] strategic behavior of the investor is represented by a bilevel model that takes into account market clearing, investment decision and production schedule. These problems as for the TEP, either in test systems or in real networks, can be modeled with a static approach, analyzing a single operation mode, or with a dynamic (multi-stage) planning including different points in time over the planning horizon [188]. In each case, the operation could be evaluated in the presence of representative operating conditions, considering continuity and peaking as well [202]–[204], considering a full yearly analysis [197], [205], or considering a stochastic scenario generation [199].

1.3. Contributions of the Work

This PhD dissertation copes with the actual issues on transmission system operation and planning considering both system operators and market operators perspectives. Its main objective is to assess potential solutions for increasing system operation efficiency according to market and steady-state approaches from long- to short-time horizon. In this context, several approaches are developed with the aim to capture the impact of RES penetration increase in real-time operation, day-ahead generation and consumption schedules, transmission evolution planning and generation investment analyses. In order to represent interactions among various topics, the following features are presented throughout the thesis:

- A deep literature review is provided, to better understand the actual state-of-the-art of the methodologies applied to handle the treated topics.
- The definition of a modified version of the IEEE 39-bus system, for the lacking a suitable dataset to validate novel methods in several network conditions with a one-year dataset of loads and RES; the traditional generators are replaced by solar, wind and several thermal power plant technologies, whereas the loads are commercial with three different behaviours.
- The development of two cost-benefit TEP analyses dealing with technical and economic benefits in a full AC network representation involving electricity market and load flow simulations; the first consists in a flow-based methodology in which linear

sensitivity factors are exploited to evaluate the redispatching costs and benefits in the evolution scenario; the second proposes performance analysis of a portfolio of network development projects, in order to evaluate the subset of projects towards which the TSO should focus its efforts according to positive implications on different technical aspects and limited economic effort.

- The presentation of a methodology for generation investment analysis to determine the most suitable size and location of generation initiatives in an existing zonal market. The method provides static evaluation over a full operation year along with investment profitability analysis, and it is applied to the real test case of Sicily.
- The exploitation of a seasonal classification method, allowing to draw out the influence on RRs estimation of system operation factors, such as RES production and load demand. The RRs estimations are supported by a real reference system exploitation to assess their suitability. The adequacy and feasibility of the estimated RRs is evaluated throughout the year by means of operating conditions grouping in appropriate specific classes.
- The definition of an ASM model by a security constrained unit commitment and economic redispatch (SCUCER) optimization problem in which the units are redispatched to fulfil network, bidding and generation constraints as well as the secondary reserve provision.
- The development of a methodological framework to elaborate the Italian zonal market results and to be converted into nodal load and generation data, to carry out AC load flow routines, analyzing the ASM actions to ensure the security of the system operation.

1.4. List of publications

The list of the scientific papers published, accepted or submitted during the Ph.D. program is reported in the following:

{1} M. Dicorato, G. Tricarico, F. Marasciuolo, G. Forte and M. Trovato, “Performance analysis of EV stations optimal operation in DC microgrid configurations,” 2020 IEEE International Conference on Environment and Electrical Engineering and 2020 IEEE Industrial and Commercial Power Systems Europe (EEEIC / I&CPS Europe), Madrid, Spain, 09-12/06/2020, pp. 1-6.

{2} M. Dicorato, G. Tricarico, M. Trovato, G. Forte and M. Bronzini, “Techno-Economic Benefit of Network Developments: a Flow-Based Evaluation,” 2020 55th International Universities Power Engineering Conference (UPEC), Torino, Italy, 01-04/09/2020, pp. 1-6.

{3} D. Calabrese, G. Tricarico, E. Brescia, G. L. Cascella, V. G. Monopoli, F. Cupertino, “Variable Structure Control of a Small Ducted Wind Turbine in the Whole Wind Speed Range Using a Luenberger Observer,” Energies, 2020; 13(18):4647.

{4} M. Dicorato, G. Tricarico, G. Forte, F. Marasciuolo, “Technical Indicators for the Comparison of Power Network Develop-ment in Scenario Evaluations,” Energies, 2021; 14(14):4179.

{5} G. Tricarico R. Wagle, L. S. Azuara-Grande, F. Gonzalez-Longatt, M. Dicorato, G. Forte, J. L. Rueda, “Security Constrained Unit Commitment and Economic Dispatch by AC Sensitivity Factors,” 2022 IEEE Biennial Congress of Argentina (AR-GENCON), 7-9/09/2022 San Juan, Argentina, pp. 1-5.

{6} L. S. Azuara-Grande, F. Gonzalez-Longatt, G. Tricarico, R. Wagle, S. Arnaltes and R. Granizo, “Real-Time Implementation of Two Grid-Forming Power Converter Controls to Emulate Synchronous Generators,” 2022 IEEE Biennial Congress of Ar-gentina (ARGENCON), 7-9/09/2022 San Juan, Argentina, pp. 1-6.

{7} G. Tricarico, M. Dicorato, G. Forte and F. Gonzalez-Longatt, “Contributions to Tertiary Reserve Requirements under Oper-ating Conditions and Uncertainties,” 2022 18th International Conference on the European Energy Market (EEM), Ljubljana, Slovenia, 13-15/09/2022, pp. 1-6.

{8} G. Tricarico, M. Martucci, G. Forte, M. Dicorato and F. Gonzalez-Longatt, “Market-driven sizing and siting of generation in-vestment,” 2022 AEIT International Annual Conference (AEIT), 03-03/10/2022, pp. 1-6.

{9} G. Tricarico, L. S. Azuara-Grande, R. Wagle, F. Gonzalez-Longatt; M. Dicorato, G. Forte; J. L. Rueda, “Security Constrained Unit Commitment and Economic Dispatch applied to the Modified IEEE 39-bus system Case,” IECON 2022 – 48th Annual Conference of the IEEE Industrial Electronics Society, Brussels, Belgium, 17-20/10/2022, pp. 1-5.

{10} R. Wagle, G. Tricarico, P. Sharma, C. Sharma, J. L. Rueda and F. Gonzalez-Lonzatt, “Cyber-Physical Co-Simulation Testbed for Real-Time Reactive Power Control in Smart Distribution Network,” 2022 IEEE PES Innovative Smart Grid Technolo-gies - Asia (ISGT Asia), Singapore, Singapore, 01-05/11/2022, pp. 11-15.

{11} G. Tricarico, R. Wagle, M. Dicorato, G. Forte, F. Gonzalez-Longatt and J. L. Rueda, “Zonal Day-Ahead Energy Market: A Modified Version of the IEEE 39-bus Test System,” 2022

IEEE PES Innovative Smart Grid Technologies - Asia (ISGT Asia), Singapore, Singapore, 01-05/11/2022, pp. 86-90.

{12} R. Wagle, G. Tricarico, P. Sharma, C. Sharma, J.L. Rueda and F. Gonzalez-Longattt "A Testbed for Modelling Active Distri-bution System Using Cyber-Physical Co-Simulation," NPSC 2022 – 22th National Power Systems Conference, Delhi, India, 17-19/12/2022, pp. 1-5.

{13} F. Marasciuolo, M. Dicorato, G. Tricarico, P. Montegiglio, G. Forte and M. Trovato, "The Influence of EV Usage Scenarios on DC Microgrid Techno-Economic Operation," in IEEE Transactions on Industry Applications, vol. 58, no. 3, 2022, pp. 3957-3966.

{14} G. Tricarico, R. Wagle, M. Dicorato, G. Forte, F. Gonzalez-Longatt and J. L. Rueda, "A Modified Version of the IEEE 39-bus Test System for the Day-Ahead Market," accepted paper to 2023 IEEE PES Innovative Smart Grid Technologies - Middle East (ISGT ME) conference, Abu Dhabi, United Arab Emirates, 12-15/03/2023.

{15} R. Wagle, G. Tricarico, P. Sharma, C. Sharma, J. L. Rueda and F. Gonzalez-Lonzatt, "Experiences in a Cyber-Physical Co-Simulation Testbed Development for a Smarter Distribution Network," accepted paper to 2023 IEEE PES Innovative Smart Grid Technologies - Middle East (ISGT ME) conference, Abu Dhabi, United Arab Emirates, 12-15/03/2023.

{16} G. Tricarico, G. Forte, M. Dicorato, F. Gonzalez-Longatt, "Scenario Clustering and Statistical Estimation of Operating Reserve Requirements," submitted to IEEE Transactions on Power Systems the 31/01/2023.

{17} L. N. Hai Pham, R. Wagle, G. Tricarico, F. Gonzalez-Longatt, "Optimum Coordination of Non-directional Overcurrent Protection for CIGRE European Medium Voltage Benchmark Distribution Network," submitted to 2023 IEEE Statistical Signal Processing Workshop (SSP 2023) conference, 02-05/07/2023, Hanoi, Vietnam.

{18} J. Castro Martinez, F. Gonzalez-Longatt, J.L. Rodriguez Amenedo, G. Tricarico, " Cyber-physical Framework for System Frequency Response using Real-time simulation Phasor Measurement Unit based on ANSI C37.118,", accepted paper to the 2023 IEEE Power & Energy Society General Meeting (GM), Orlando, Florida, 16-20/07/2023.

{19} G. Tricarico, R. Wagle, J. Castro Martinez, F. Gonzalez-Longatt, M. Dicorato, G. Forte, J. L. Rueda, "A Co-simulation based Optimisation Solution for Smart Converter Reactive Power Control in Active Distribution Grids," submitted to EEEIC 2023: International Conference on Environment and Electrical Engineering 2023, 06-09/06/2023, Madrid, Spain.

{20} G. Tricarico, G. Forte, M. Dicorato, F. Gonzalez-Longatt, "A Time-series Hosting Capacity Assessment of the Maximum Distributed Energy Resource Production," submitted to EEEIC

2023: International Conference on Environment and Electrical Engineering 2023, 06-09/06/2023, Madrid, Spain.

In addition, two further papers are going to be published in the next months:

{21} R. Cometa, G. Tricarico, G. Forte, M. Dicorato, F. Gonzalez-Longatt, “A MILP approach to solve Security Constrained Unit Commitment and Economic Redispatch,” to be submitted to IEEE Transactions on Energy Markets, Policy and Regulation.

{22} G. Tricarico, L. N. Hai Pham, F. Gonzalez-Longatt, “Differences an Understandings on Unit Commitment and Economic Dispatch Problems,” to be submitted to IEEE Transactions on Education.

Chapter 2. A Modified Version of IEEE 39-Bus Test System

The traditional IEEE test systems were developed several decades ago and represent a fundamental tool to validate research in the power system field because they provide standard public data. However, the progressive penetration increase of RES requires a network updating to cope with the current power system issues. Therefore, in this chapter a modified version of the IEEE 39-bus system is proposed, for the lacking a suitable dataset to validate novel methods in several network conditions (primarily related to electricity markets) for small test system. It includes a one-year dataset of loads, and traditional generators of the original IEEE 39-bus system [206] are replaced by solar, wind and several thermal power plant technologies. To evaluate the feasibility of the proposed version of the IEEE 39-bus system, techno-economic steady-state simulations is developed. For economic purpose, thermal power plant marginal costs are defined, per each technology, to determine the merit order in ZDAM solving. In contrast, solar production and load profile are defined according to the geographical location of the IEEE 39-bus system busbars and the features embedded in DIgSILENT PowerFactory software. Finally, technical simulations are carried out, by means of AC load flow routines, in which the network operating conditions are assessed considering the dispatched power provided by the ZDAM solution over the year. The results shown that the proposed modified version of IEEE 39-bus test system has been suitably designed. In a second stage, the dispatched power of the generators, obtained from the ZDAM, is exploited to solve a security constrained unit commitment and economic dispatch (SCUCED) optimization problem in which the goal is to minimize the redispatching, operating, and start-up costs considering generation and network constraints. In this stage, an AC load flow is carried out to evaluate the overall operating condition of the system. The network constraints are included in the optimization problem by means of linearized sensitivity factors to consider both active and reactive power network model, as well as the network losses. The simulation is carried out on the yearly peak load day of the modified version of the IEEE 39-bus test system, showing the effectiveness of the proposed method.

2.1. Market and Steady-State Analysis Methodology

The modified version of the IEEE 39-bus network has been developed to suit a two-fold analysis concerning the energy market and steady-state studies in N and N-1 topology conditions, explained in the following sub-sections.

2.1.1. Day-Ahead Energy Market Model

Consider an electric power system with N^G generation units, installed inside a total of N^Z bidding zones inside the market, with N^I interzonal connections represented by transmission lines, where generators as dispatched to provide N^S step bids. The day-ahead market is assumed to be evaluated over a specified time horizon which is discretized into N^T time steps (typically 1-hour resolution over a 24-hour horizon). For each time step, t_k (k = 1, 2, …, N^T), the optimization problem of the zonal day-ahead energy market is solved. In this work, a merit order analysis defines the dispatch priority of each generation unit (I = 1, …, N^G) considering piecewise linear generation costs; and the load demand is assumed to be inelastic. With these suppositions, the ZDAM problem is formulated as an optimization problem, where the objective function is designed to minimize the total cost of generation (C^T) at one specific time period (t_k):

$$\min_{\boldsymbol{P^G}(t_k)} \; [C^T(t_k, \boldsymbol{P^G})] \tag{23}$$

where the total active power dispatched at the moment t_k is:

$$\boldsymbol{P^G}(t_k) = \left[P_1^G(t_k), \dots, P_i^G(t_k), \dots, P_{N_G}^G(t_k)\right]^T \tag{24}$$

and the total cost of generation at the moment t_k is:

$$C^T(t_k, \boldsymbol{P^G}) = \sum_{i=1}^{N_G} \sum_{s=1}^{N_S} c_{i,s} P_{i,s}^G(t_k) \tag{25}$$

in which $P_{i,s}^G(t_k)$ represents the cleared active power of the s-th step of the i-th generator at the moment t_k and $c_{i,s}$ is the marginal cost of the s-th step of the i-th generator. The objective function presented in (23) is subject to five constraints: active power balance of the whole market, zonal active power balance, maximum limit of the generation units, clear bounds of the generators and bounds of the zonal power flows, that are explained below.

1) Active power balance of the market

The total power balance in the market is defined as:

$$\sum_{i=1}^{N^G}\sum_{s=1}^{N^S} P_{i,s}^{G}(t_k) - \sum_{l=1}^{N^I} P_{l}^{tie}(t_k) = \sum_{z=1}^{N^Z} P_{z}^{D}(t_k) \tag{26}$$

where P_l^{tie} represents the power flow of the l-th interzonal transmission line, P_z^D is the total active power demand at the z-th zone.

2) Zonal active power balance

The zonal day-ahead market only transmission capacity limitations between the different biding zones are considered in the market-clearing process. Consequently, a constraint must be included to enforce the active power balance at each bidding zone (z = 1, 2…, N_Z):

$$\sum_{i=1}^{N^G}\sum_{s=1}^{N^S} \alpha_{g,z}\, P_{i,s}^{G}(t_k) - \sum_{l=1}^{N^I} \beta_{l,z}\, P_{l}^{tie}(t_k) = P_{z}^{D}(t_k) \quad \forall\, z \in N^Z \tag{27}$$

where $\alpha_{g,z}$ is a binary parameter equal to 1 if the g-th generator belongs to the z-th zone and 0 otherwise. On the other hand, the binary parameter $\beta_{l,z}$ is introduced to add directionally to the inter-tie power flows, and it equals to 1 if the l-th interzonal connection is entering the z-th zone, -1 if it is exiting, and 0 otherwise.

3) Maximum limit of the generation units

The generators are dimensioned to supply a maximum power, and to avoid an overload operating point, the sum of the accepted bid steps must be lower or equal to the rated power of each generator:

$$0 \le \sum_{s=1}^{N^S} P_{i,s}^{G}(t_k) \le P_{i,s}^{G,max} \quad \forall\, i \in N^G \tag{28}$$

4) Bid steps maximum power

The energy supplier is enabled to offer multiple bid steps; each one is composed of a maximum power amount and suitable energy price. Therefore, a proper constraint enforcing the maximum step powers is required:

$$0 \le P_{i,s}^{G}(t_k) \le P_{i,s}^{G,max} \quad \forall\, i \in N^G, \forall\, s \in N^S \tag{29}$$

5) The zonal Available Transfer Capacity (ATC) bounds

The transmission lines interconnecting the bidding zones have physical ATC limits, set considering the classical *N*-1 security criterion, defined by the upper and lower limits (P_l^{lb} and P_l^{ub}, respectively) as:

$$P_l^{lb} \leq P_l^{tie}(t_k) \leq P_l^{ub} \quad \forall\, l \in N^I \tag{30}$$

The solution of the optimization problem (23)–(30) yields the total dispatched power, as well as the cleared generators, the market-clearing price and the zonal power flows.

2.1.2. Steady-State Simulations

Solving the ZDAM, it is obtained the dispatched power of generation units, according to the economic merit order, summing the cleared power over the bid steps:

$$P_i^G(t_k) = \sum_{s=1}^{N^S} P_{i,s}^G(t_k) \quad \forall\, i \in N^G \tag{31}$$

Considering a power system composed of N^B buses, the steady-state condition of the power system for the generic time step t_k can be defined by a set of equations representing the power balance of the system:

$$\begin{cases} P_b(t_k) = Re\left(v_b^*(t_k)\left(v_b(t_k) y_{bb} + \sum_{\substack{c=1 \\ c \neq b}}^{N^B} v_c(t_k) y_{bc} \right) \right) \\ Q_b(t_k) = Im\left(v_b^*(t_k)\left(v_b(t_k) y_{bb} + \sum_{\substack{c=1 \\ c \neq b}}^{N^B} v_c(t_k) y_{bc} \right) \right) \end{cases}, \quad \forall\, b \in N^B \tag{32}$$

Where y_{bb} is the complex nodal self-admittance on the bus b, y_{bc} is complex nodal admittance between the buses b and c, v_b and v_c are the complex values of the voltages at bus b-th and c-th, respectively, and * indicates the complex conjugate value, whereas P_b and Q_b represent the total active and reactive power injection at the b-th bus and they are defined as:

$$\begin{cases} P_b(t_k) = \sum_{m=1}^{N_b^G} P_m^G(t_k) - \sum_{m=1}^{N_b^D} P_m^D(t_k) \\ Q_b(t_k) = \sum_{m=1}^{N_b^G} Q_m^G(t_k) - \sum_{m=1}^{N_b^D} Q_m^D(t_k) \end{cases}, \quad \forall\, b \in N^B \tag{33}$$

Where N_b^G and N_b^D represent the number of generation units and load demand connected to the b-th busbar.

2.1.3. Proposed SCUCED optimization problem

Fig. 1 shows the framework of the proposed SCUCED optimization model. In the first stage, the ZDAM is solved by providing the generation bids, the required load and the inter-zonal flow bounds. It is a merit-order criterium market in which the UC constraints are neglected, and only the unit's rated power is considered. This formulation is based on the Pan European Single DAM, which the cross-border constraints must fulfil [207]. In the second stage, the dispatched power obtained from the ZDAM is used to develop a SCUCED optimization problem in order to fulfil generators and network constraints. The main advantage in subdividing the methodology into two stages is represented by the UC and ED re-dispatch involving the AC network constraints in order to define generation scheduling fulfilling the network requirements. In the European framework, these operations are usually developed in the Intraday-Market keeping a zonal detail of the transmission network [208]. The SCUCED is carried out by solving AC load flow (ACLF) routines, and sensitivity factors are evaluated in order to embed the linearized ACLF constraints in the problem constraints. Then, the re-dispatching cost minimization is solved considering proper UC constraints and the network ones. In the following two subsections, the two-stage of the proposed method are described.

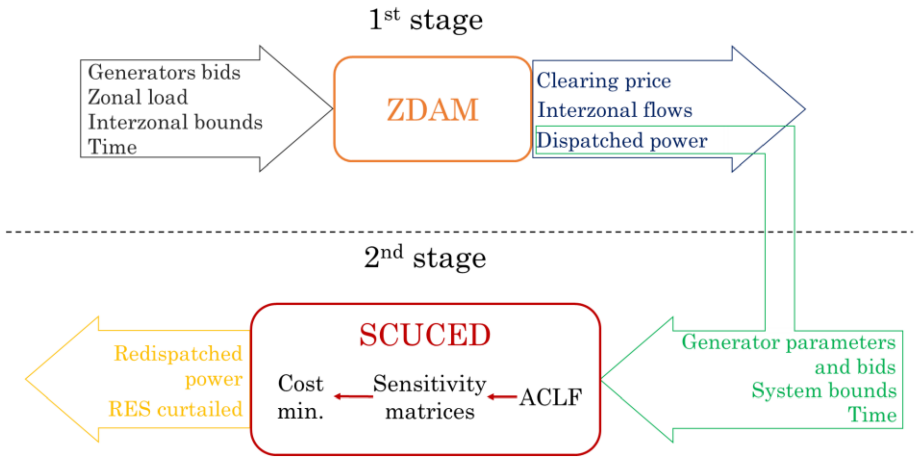

Fig. 1. Flow diagram showing the proposed bi-level optimization method.

The ZDAM optimization problem is the same as proposed by (23)–(30) of the previous paragraph , in which it aims at defining a preliminary generation commitment in relation to the expected RES production, required load and the ATC of the interzonal lines. However, the solution of the proposed problem, with lack of proper UC as well as full network constraints, provides an optimal solution only from the economic perspective, without considering the technical feasibility. Therefore, the SCUCED problem is solved downstream the ZDAM solution in which the goal is to minimize thermal generator re-dispatching, operating, and start-up costs and the cost of the RES curtailment. The optimization problem embeds, therefore: (i) minimum up- (MUT) and down-time (MDT), (ii) generators' active and reactive power limits, (iii) maximum branch power flow, and (iv) bus voltage constraints. The thermal unit operating costs are the unit marginal ones to perform in a perfect competition market hypothesis and from a TSO perspective, a downward re-dispatch is an income, and vice versa for upward re-dispatch. In contrast, a penalty fee is imposed on RES to avoid their curtailment (downward re-dispatch). Generators' limits involve the compliance of the minimum and the maximum power of both active and reactive power and the MUT and MDT. Moreover, these generators' parameters, as well as the marginal costs, depends on the power plant's technology and fuel. The ED is based on stepwise bids, in order to define a merit order criterium as for the ZDAM. The problem is solved considering the generator's active power dispatch and the RES curtailment as control variables.

The proposed SCUCED problem is solved in three consecutive steps, the first is an AC load flow simulation according to the ZDAM results in order to define the initial operating point condition of the system. Downstream, the sensitivity matrices are evaluated in order to

relate the dispatched active power variation to the line power flows, the bus voltages, and system power losses ones. The sensitivity factors, in particular, correlate one unit of redispatched active power of each generator to variations in each branch power flown and loss, as well as voltage of each node. As a result, the sum of the products of the redispatched power of the generators by the sensitivity factors of the respective variable and element yields the total variation on each network element (i.e., branch and node). Finally, the optimization problem is solved exploiting the sensitivity matrix to model the linearized ACLF constraints of the voltages and power flows, as well as the network balance and losses.

2.2. IEEE 39-Bus Modified Version

The proposed test system is based on the classical IEEE 39-bus system; the modified version involves geographical location, load, and generation changes adjusted in order to define one-year dataset do develop market and steady-state simulations. Details of the proposed test system version are shown in the following sub-sections

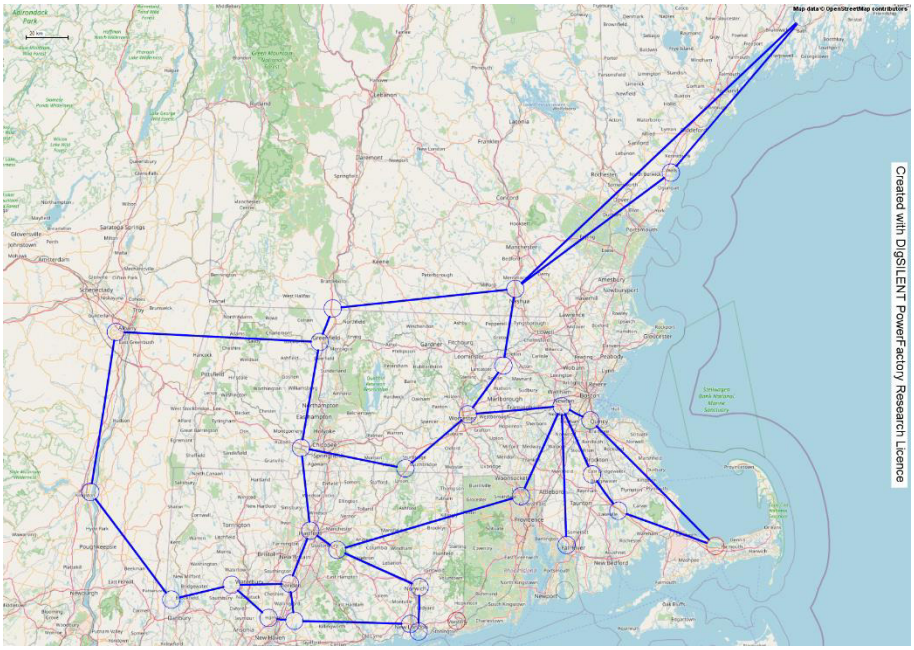

Fig. 2. DIgSILENT PowerFactory geographic diagram of the test system.

A) Geographical location

The IEEE 39-bus system is well known as the ten machines New-England Power System. It represents a simplified transmission network of several Westcoast United States of America. Using publicly available sources of old publication, the geographical coordinates

of the major components of the test system is defined using latitude and longitude. Fig. 2 shows the geo-references of the test system using DIgSILENT PowerFactory.

B) Network market zones

shows the DIgSILENT PowerFactory one-line diagram of the zonal network considering the subdivision provided in [209]. The branch rated powers are set equal to 1000 MVA, according to [210]. The lines of Zone 3 (lines 01-39, 01-02, 39-08 and 08-09) have been doubled because the interconnection of Zone 3 with Zone 1 and Zone 2 are composed of one transmission line (01-02 and 08-09, respectively) and to consider an *N*-1 secure condition it is necessary to consider a doubling of the interconnection between the two zones to avoid the total disconnection. Moreover, line 02-03 interconnects two boundary lines between Zone 1 and Zone 2. Therefore, it is necessary to double this line as well in other to avoid overloads. Thus, the boundary between Zone 1 and Zone 2 (Z1-Z2) has a total rated power of 3000 MVA, the boundaries between Zone 2 and Zone 3 (Z2-Z3) and Zone 3 and Zone 1 (Z3-Z1) of 2000 MVA.

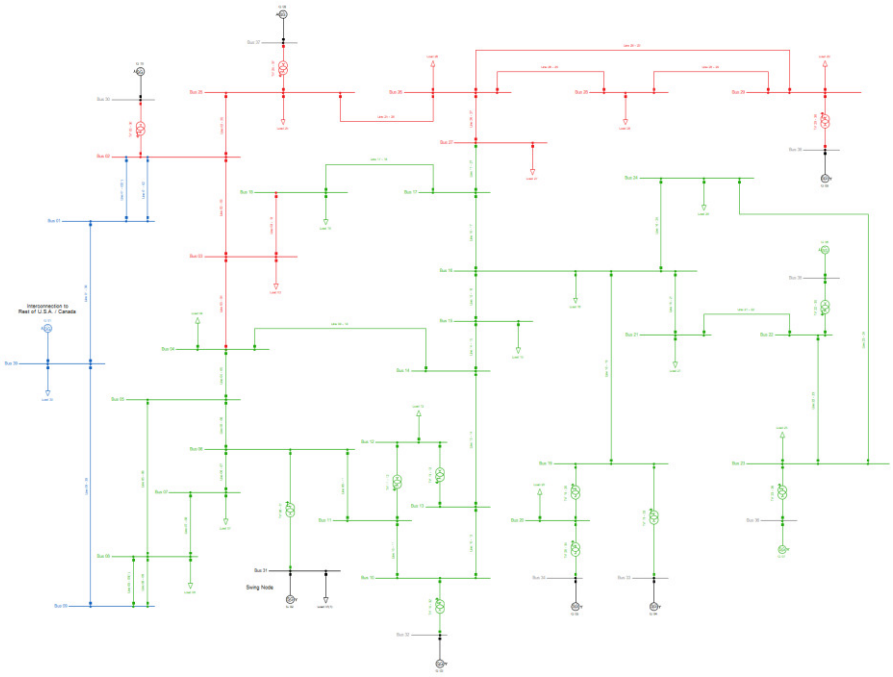

Fig. 3. Zonal one-line diagram of the IEEE 39-bus system, Zone 1: red, Zone 2: green, Zone 3: blue.

C) Load Profiles

The test system is composed of 19 loads with a peak power equal to 6097.1 MW. The test system modified version takes advantage of the load modelling aspects included in

DIgSILENT PowerFactory. These profile characteristics are obtained by a combination of Workday, Saturday, and Sunday behaviors during Winter, Crossing and Summer seasons. The load profiles are defined by peak load, which have three distinct trends based on the following characteristics: (i) L0: General commercial load, (ii) L1: Commercial weekdays load from 8:00 am to 6:00 pm and (iii) L2: Commercial evening load. The load profiles are created using fifteen minutes time resolution; Table 1 shows the leading statistic indicators: minimum, maximum, and average daily value, with the respective occurring time, for each characteristic of the three loads.

Considering the geo-references of Fig. 2, the previous load profiles are used to define three different behaviors in the system's demand required, according to the following criterion. (i) L0 is a load profile to be used at loads installed in the substation close to the city centers. (ii) L1 is the load profile found in suburban areas; therefore, this profile can be allocated to the loads outside the cities. (iii) L2 is supposed to be a load profile used at loads installed in the substations next to the ocean or the ones surrounded by the other load. Table 2 shows the active power peak load, the nominal power factor, the associated characteristic and the falling zone for each load, and Fig. 1 shows the yearly loads utilizing a boxplot. The peak and minimum loads are roughly 5587 MW and 758 MW, respectively, and the required annual load is 21.59 TWh.

For the sake of completeness, Fig. 2 shows the trend of a peak load day (a) and a baseload day (b). The peak load is equal to 5587 MW; it occurs 97 times during the year, i.e., during each Winter working day, whereas the minimum load is equal to 758 MW, and it appears 18 times, i.e., on the Crossing Sundays with total energy required equal to 21.59 TWh. Furthermore, Fig. 3 depicts the yearly zonal load duration curve. Z1 and Z3 have similar behaviors, with a zonal peak load of 1323 and 1094 MW and a minimum load of 197 and 193 MW. On the other hand, Z2 is the most energy-consuming zone during the entire year, with a peak of 3182 MW and a minimum load of 389 MW.

D) Generation Mix

The IEEE 39-bus system is composed of ten generators; the generator at Bus 39 represents the exchange connection with the rest of the transmission network; the remaining are nuclear, hydro or coal power plants. The latter are substituted by several generators of different technology, including RES, to increase the generation flexibility and competition in

the electricity markets. For the sake of simplicity, the term “original” is referred to the IEEE 39-bus system, and “new” is referred to the modified version. For each thermal generator technology, the marginal costs are provided as well. Table 3 reports the rated power of the original and modified version of the IEEE 39-bus system, including the zone, of each generator.

Table 1. Main statistic indicators of the load profiles.

Load Profile		**Main profile values**				
		Min	***Time***	***Max***	***Time***	***Avg***
L0	Summer Saturday	0.278	03:30	0.771	11:45	0.433
	Summer Sunday	0.191	06:00	0.350	21:00	0.268
	Summer Workday	0.221	03:15	0.872	11:45	0.511
	Crossing Saturday	0.279	03:15	0.812	11:45	0.452
	Crossing Summer	0.181	04:30	0.369	20:30	0.273
	Crossing Workday	0.225	03:15	0.924	11:45	0.530
	Winter Sunday	0.264	03:15	0.867	11:15	0.463
	Winter Saturday	0.174	04:30	0.394	19:45	0.270
	Winter Workday	0.198	03:00	1.000	11:45	0.556
L1	Summer Saturday	0.042	01:15	0.100	11:00	0.056
	Summer Sunday	0.038	08:30	0.050	13:00	0.045
	Summer Workday	0.042	03:30	0.697	09:30	0.266
	Crossing Saturday	0.038	02:30	0.128	09:45	0.065
	Crossing Summer	0.038	17:30	0.047	19:15	0.042
	Crossing Workday	0.037	04:30	0.811	11:00	0.309
	Winter Sunday	0.050	04:30	0.120	10:45	0.070
	Winter Saturday	0.050	04:30	0.074	19:00	0.060
	Winter Workday	0.048	04:30	1.000	09:30	0.371
L2	Summer Saturday	0.093	04:30	0.654	18:15	0.382
	Summer Sunday	0.089	04:30	0.581	19:45	0.329
	Summer Workday	0.104	02:30	0.725	20:15	0.413
	Crossing Saturday	0.093	05:30	0.779	18:30	0.444
	Crossing Summer	0.092	05:30	0.667	20:15	0.369
	Crossing Workday	0.104	05:30	0.850	20:30	0.467
	Winter Sunday	0.105	05:30	0.934	18:30	0.517
	Winter Saturday	0.114	05:30	0.802	20:00	0.439
	Winter Workday	0.105	05:30	1.000	18:30	0.532

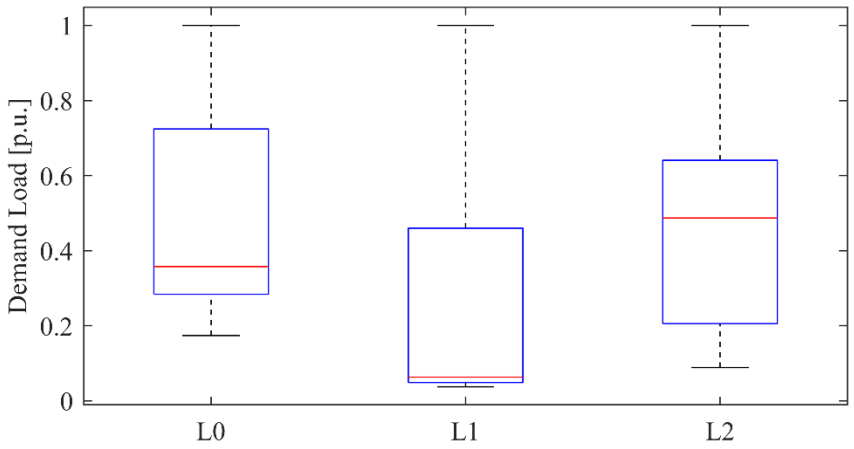

Fig. 1. Yearly load characteristics boxplot of the three profiles.

Table 2. Proposed load profiles and indicators for IEEE 39-bus test system.

Load name	Busbar	Active power [MW]	Power factor	Load characteristic	Zone
Load 03	Bus 03	322.0	0.99997	L2	Zone 1
Load 04	Bus 04	500.0	0.93847	L1	Zone 2
Load 07	Bus 07	233.8	0.94110	L0	Zone 2
Load 08	Bus 08	522.0	0.94759	L1	Zone 2
Load 12	Bus 12	7.5	0.08492	L2	Zone 2
Load 15	Bus 15	320.0	0.90218	L0	Zone 2
Load 16	Bus 16	329.0	0.99521	L0	Zone 2
Load 18	Bus 18	158.0	0.98245	L1	Zone 2
Load 20	Bus 20	628.0	0.98681	L2	Zone 2
Load 21	Bus 21	274.0	0.92208	L1	Zone 2
Load 23	Bus 23	247.5	0.94625	L0	Zone 2
Load 24	Bus 24	308.6	0.95815	L2	Zone 2
Load 25	Bus 25	224.0	0.97851	L0	Zone 1
Load 26	Bus 26	139.0	0.99260	L2	Zone 1
Load 27	Bus 27	281.0	0.96575	L1	Zone 1
Load 28	Bus 28	206.0	0.99114	L2	Zone 1
Load 29	Bus 29	283.5	0.99553	L0	Zone 1
Load 31	Bus 31	9.2	0.89443	L2	Zone 2
Load 39	Bus 39	1104.0	0.97531	L0	Zone 3

The subdivision criterion is to keep the original generator rated power:

$$S_j^G = \sum_{i=1}^{N_j^G} S_{i,j}^G \quad \forall\, j \in N_j^G \tag{34}$$

where S_j^G is the rated power of the j-th generator of the original network, $S_{i,j}^G$ is the rated power of the i-th new generator to substitute the j-th generator, and N_j^G is the number of new generators of the j-th generator. Fig. 4 shows the example of the original generator G 02 split into six photovoltaic (PV) generators, each one with the respective transformer of the same size of the generator in order to allow the voltage regulation.

Table 3. Original and replacing generation rated power and zone belonging.

Original Generators		Replacing Generators		Zone
Gen name	Rated power [MVA]	Gen name	Rated power [MVA]	
G 01	10000	Gen Exchange 01	10000	Z3
G 02 (Nuclear)	700	Gen Solar 01	150	Z2
		Gen Solar 02	90	
		Gen Solar 03	60	
		Gen Solar 04	100	
		Gen Solar 05	180	
		Gen Solar 06	120	
G 03 (Nuclear)	800	Gen Wind 01	150	Z2
		Gen Wind 02	200	
		Gen Wind 03	90	
		Gen Wind 04	200	
		Gen Wind 05	160	
G 04 (Coal)	800	Gen Solar 07	150	Z2
		Gen Solar 08	60	
		Gen Solar 09	100	
		Gen Solar 10	180	
		Gen Solar 11	120	
		Gen Solar 12	190	
G 05 (Coal)	600	Gen Solar 13	220	Z2
		Gen Solar 14	380	
G 06 (Nuclear)	800	Gen CC NG 01	450	Z2
		Gen CT Oil 01	350	
G 07 (Coal)	700	Gen Wind 06	120	Z2
		Gen Wind 07	180	
		Gen Wind 08	200	
		Gen Wind 09	120	
		Gen Wind 10	80	
G 08 (Nuclear)	700	Gen CC NG 02	400	Z1
		Gen ST NG 01	300	
G 09 (Nuclear)	1000	Gen CT NG 01	300	Z1
		Gen ST NG 02	300	
		Gen CC NG 03	400	
G 10 (Hydro)	1000	Gen CT Oil 02	300	Z1
		Gen ST Coal 01	300	
		Gen CC NG 04	400	

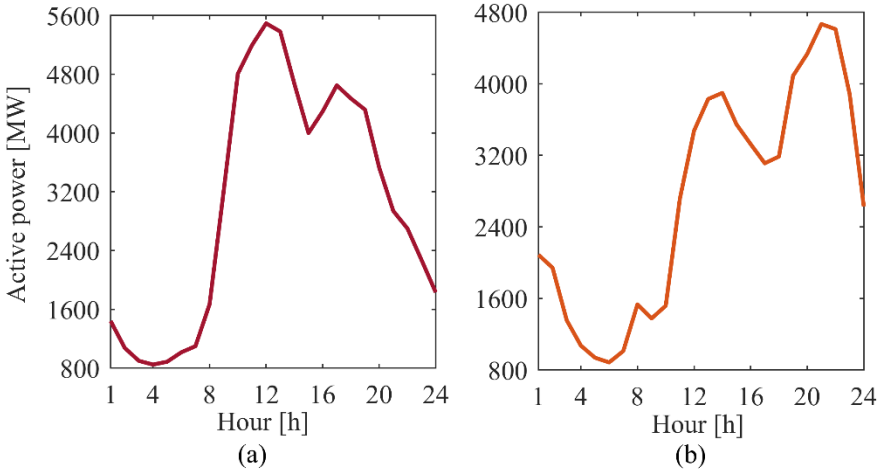

Fig. 2. The system's total power demand considers a peak load day (a) and baseload day (b).

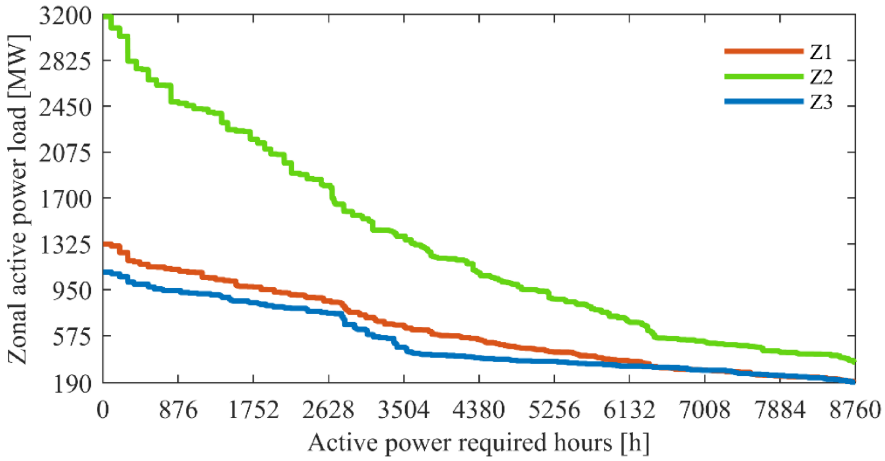

Fig. 3. Zonal active power load duration curve.

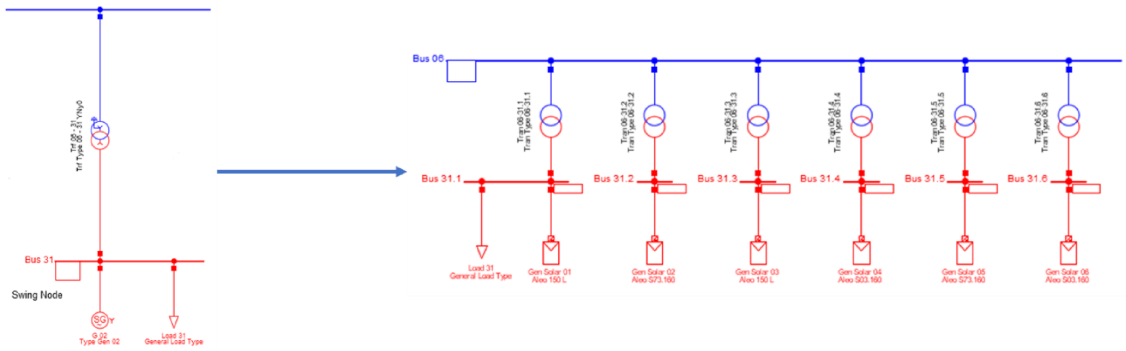

Fig. 4. G 02 splitting in six PV power plants.

Neglecting the external grid generator (G 01), the new test system presents 1500 MVA of wind turbines (WT), 2100 MVA of PV, and 3300 MVA of several thermal power plants as generation capacity with a nominal power factor of 0.85. Fig. 5 shows the percentage installed capacity per each specific technology. It comprises roughly 52% of renewable energy sources (RES), and they are totally installed in Zone 2. The PV power plants' production is estimated according to the forecast weather by DIgSILENT PowerFactory. For the WTs it has been exploited the dataset of [211], [212] to define the yearly profiles. Z1's installed capacity is 2700 MVA, of which 44.5% is a combined cycle (CC), 33.3% is a steam turbine (ST), and 22.2% is a combustion turbine (CT). At the same time, Z2 has 4400 MVA of installed generation with 50% solar, 31.8% wind, 10.2% CC, and 8% CT. Finally, Z3 presents only the exchange generator with a rated power of 10000 MVA. Fig. 6 shows the annual duration curve obtained from the RES production.

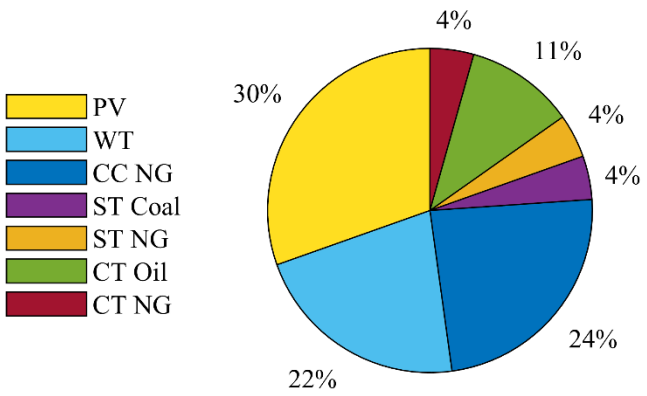

Fig. 5. Generation mix proposed for the modified version of the test system.

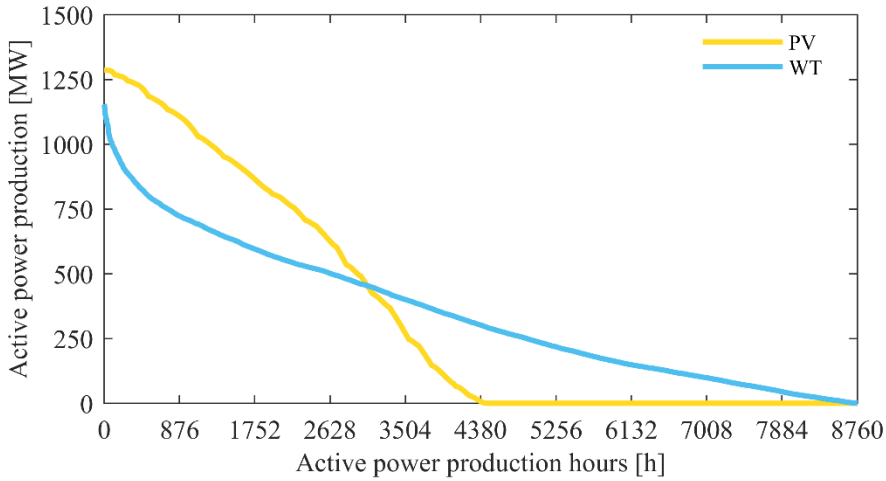

Fig. 6. Duration curve of the RES production of the modified test system.

RES has a marginal price equal to 0.00 $/MWh to develop the energy markets. In contrast, the thermal generators have a marginal price varying according to the technology and the fuel. They are set according to the piecewise costs of [211], [212] and reported in Table 4 with the respective breakpoints (BP). The BP represents the generator marginal cost changing power point. Gen Exchange 01 represents the equivalent exchange with the rest of the US/Canada transmission system. Therefore, its marginal price has been obtained as the average of all the marginal costs of all the generators of [211], [212], to consider RES contributions in the equivalent costs provided in the generation mix. It is important to note that the dataset of [211], [212] is appropriate for these purposes for two main reasons. On the one hand, both are transmission systems from the United States, making them the most reliable WT productions and marginal costs available online. Thermal power plant technologies

presented in this work, on the other hand, are included in the NREL 118, and marginal prices are considered based on the respective rated power and technology.

Table 4. Proposed Generation marginal costs.

Generator	C_g^1 [$/MWh]	BP_1 [MW]	C_g^2 [$/MWh]	BP_2 [MW]	C_g^3 [$/MWh]	BP_3 [MW]
Gen Exchange 01	24.80	2833.00	56.22	5667.00	61.61	8500.00
Gen CC NG 01	35.04	204.00	36.84	293.25	39.56	382.50
Gen CT Oil 01	209.45	159.00	233.88	228.00	264.32	397.50
Gen CC NG 02	27.80	181.00	29.00	261.00	30.80	340.00
Gen ST NG 01	48.67	102.00	49.85	178.20	51.22	255.00
Gen CT NG 01	48.48	161.50	51.20	208.25	55.67	255.00
Gen ST NG 02	48.67	102.00	49.85	178.20	51.22	255.00
Gen CC NG 03	27.80	181.00	29.00	261.00	30.80	340.00
Gen CT Oil 02	218.65	136.00	234.19	195.50	257.97	255.00
Gen ST Coal 01	18.31	161.50	19.67	208.25	21.09	255.00
Gen CC NG 04	27.80	181.00	29.00	261.00	30.80	340.00

2.3. Results and Discussion

2.3.1. Network model validation

The ZDAM has been modelled and solved using the well-known python-based optimization library Pyomo [71]. The ATC values have been set to 1600 MW for Boundary 1 and 1000 MW for Boundary 2 and 3. The load is sampled each hour by the software. The zonal exchange constraints are bound for 1930 hours from Zone 3 to Zone 2, as seen from the duration curve of the interzonal bound percentage values (Fig. 7). Table IV shows the minimum, average and maximum zonal price during the year. Zone 3 is characterized by a lower zonal price due to the congestion among the other zones; therefore, each time it occurs, the market splitting implies clearing more expensive units installed in Zone 2 and Zone 1. Moreover, for 101 hours, the market-clearing price is equal to 0.00 $/MWh; it occurs during early morning hours, with a low required load, in which only wind power plants are dispatched. Furthermore, the wind production forecast is higher than the required load during those hours, causing a total energy production curtailment of 11.28 GWh. The active power dispatched per technology is reported as a duration curve in Fig. 8. Gen Exchange 01, with a dispatched energy of 11.52 TWh, provided the main annual energy amount. RES supply amounts to 3.08 TWh by solar and 2.84 TWh by the wind. Downstream there is the ST and CC production with 2.35 TWh and 1.70 TWh, respectively. Finally, CT has high bid costs, and it provides for 0.10 TWh during the peak.

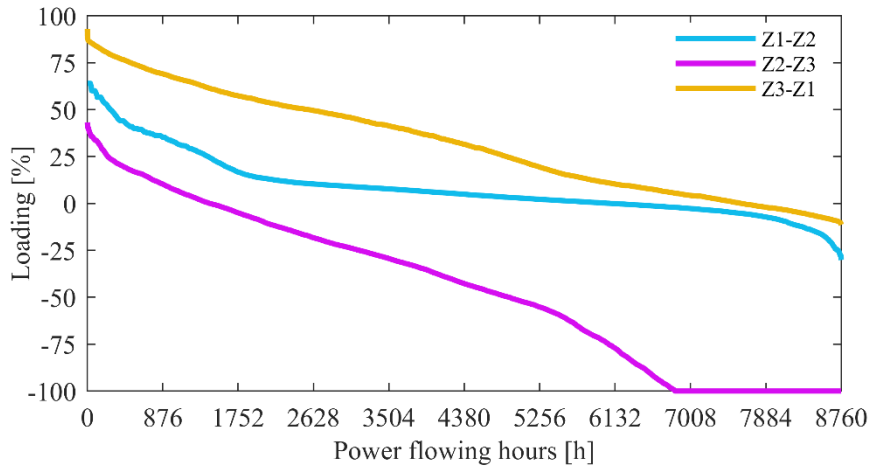

Fig. 7. Interzonal power flow duration curve.

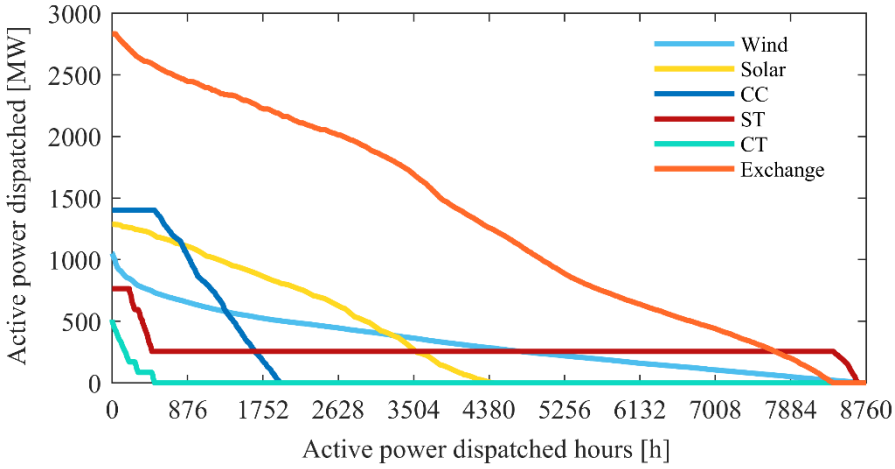

Fig. 8. Technologies' active power dispatched duration curve.

Table 5. Main indicators of the obtained zonal prices.

Zonal prices	Minimum [$/MWh]	Average [$/MWh]	Maximum [$/MWh]
Zone 1	0.00	29.12	233.88
Zone 2	0.00	29.12	233.88
Zone 3	0.00	24.30	29.00

The AC load flows analysis of the proposed test system is performed using the software DIgSILENT PowerFactory, setting the desired voltage of the busbar generators as in [206]. The reference machine is the *Gen Exchange 01*, and *Gen CC NG 03* and *04* are set as must run machines to provide reactive power to control the voltage in Z1. The total active power losses are 467.89 GWh, i.e., the 2.17% of the total yearly load.

Table 6. Test system load flow voltage results.

Busbar	Minimum voltage [p.u.]	Maximum voltage [p.u.]	Average voltage [p.u.]
Bus 01	0.984	1.049	1.035
Bus 02	1.027	1.049	1.042
Bus 03	0.991	1.042	1.027
Bus 04	0.963	1.016	1.000
Bus 05	0.962	1.000	0.988
Bus 06	0.968	0.996	0.986
Bus 07	0.945	1.001	0.984
Bus 08	0.939	1.004	0.985
Bus 09	0.954	1.031	1.011
Bus 10	0.978	0.992	0.987
Bus 11	0.974	0.993	0.986
Bus 12	0.963	1.000	0.985
Bus 13	0.975	0.998	0.990
Bus 14	0.972	1.014	1.000
Bus 15	0.982	1.037	1.017
Bus 16	1.002	1.047	1.032
Bus 17	0.996	1.050	1.033
Bus 18	0.992	1.048	1.031
Bus 19	1.002	1.037	1.024
Bus 20	0.977	0.998	0.990
Bus 21	1.015	1.052	1.040
Bus 22	1.042	1.054	1.050
Bus 23	1.049	1.060	1.056
Bus 24	1.012	1.050	1.038
Bus 25	1.001	1.041	1.027
Bus 26	1.011	1.059	1.042
Bus 27	0.994	1.057	1.038
Bus 28	1.019	1.047	1.037
Bus 29	1.021	1.035	1.031

Voltage results are reported in Table 6, showing minimum, maximum and average values of the load busbars. The minimum value is reached at Bus 08 with 0.974 pu, whereas the maximum occurs at Bus 26 with 1.071 pu, keeping the variation between ±7.1% of rated voltage. Regarding the line loading, Table 7 shows the minimum, maximum and average percentage values obtained during the yearly simulation. The fulfilment of both nodal voltage and line loading demonstrates the total feasibility of the proposed system model and dataset.

Table 7. Test system load flow line loading results.

Line	Minimum loading [%]	Maximum loading [%]	Average loading [%]
Line 01-02	4.5	54.5	21.7
Line 01-39	10.5	54.5	24.4
Line 02-03	5.0	55.3	20.6
Line 02-25	4.9	72.9	31.8
Line 03-04	11.2	49.6	19.5
Line 03-18	1.5	67.4	28.9
Line 04-05	6.0	59.5	27.7

Line 04-14	0.8	28.0	9.1
Line 05-06	0.3	40.8	19.3
Line 05-08	1.4	44.2	17.6
Line 06-07	0.8	32.9	13.4
Line 06-11	0.7	38.5	12.7
Line 07-08	4.7	46.9	20.3
Line 08-09	7.3	50.9	24.1
Line 09-39	8.7	50.9	24.6
Line 10-11	0.4	35.2	11.7
Line 10-13	4.7	59.0	26.0
Line 13-14	4.8	61.8	27.7
Line 14-15	9.8	75.3	31.9
Line 15-16	10.3	58.1	22.7
Line 16-17	1.2	92.5	26.3
Line 16-19	1.6	62.9	28.3
Line 16-21	6.8	30.8	13.4
Line 16-24	7.3	38.8	18.4
Line 17-18	0.8	64.9	25.0
Line 17-27	2.2	48.7	12.0
Line 21-22	4.5	37.8	12.5
Line 22-23	1.8	31.9	10.4
Line 23-24	4.3	21.6	10.3
Line 25-26	5.2	55.3	27.4
Line 26-27	1.4	70.0	12.1
Line 26-28	4.2	25.8	11.8
Line 26-29	5.3	26.1	11.3
Line 28-29	1.4	36.2	7.5

The *N*-1 conditions are evaluated by building five scenarios considering the outage of one of the interzonal lines per time: 01-02 (S1), 03-04 (S2), 03-18 (S3), 08-09 (S4), 17-27 (S5). Fig. 9 shows the duration curve of the most loaded or overload line for each condition. In S2 and S3, overloads occur, respectively, at lines 16-17 and line 14-15. The first reach a maximum overload of 112.6 % with 25 hours of overloading; the second overload is up to 114.2 % with 164 overloading hours. The most loaded line is below the rated power in the remaining scenarios. Line overloads during contingency can be allowed up to a certain threshold, e.g., the author of [213] supposed a margin of 25% higher than the nominal limits. As a result, the system line loading during contingency operation of the above-mentioned lines is met by the boundary limits set in the ZDAM, according to the *N*-1 security criterion.

Finally, the minimum and maximum nodal voltage values are reported in Table 8 for each N-1 scenario. The results show an increase in voltage range variation in each scenario. On Bus 28 occurs the maximum voltage that varies from 1.097 pu in S4 to 1.139 pu in S5. In S3, S4, and S5 bus 25 is subject to the lowest voltage value. Both the buses belong to Z1, and their excursion is related to the low number of active generators to control the voltage in

that market zone, as shown in Fig. 8. In S1 and S2 the lowest voltage value occurs on Bus 08, as in the base case scenario without boundary line outage.

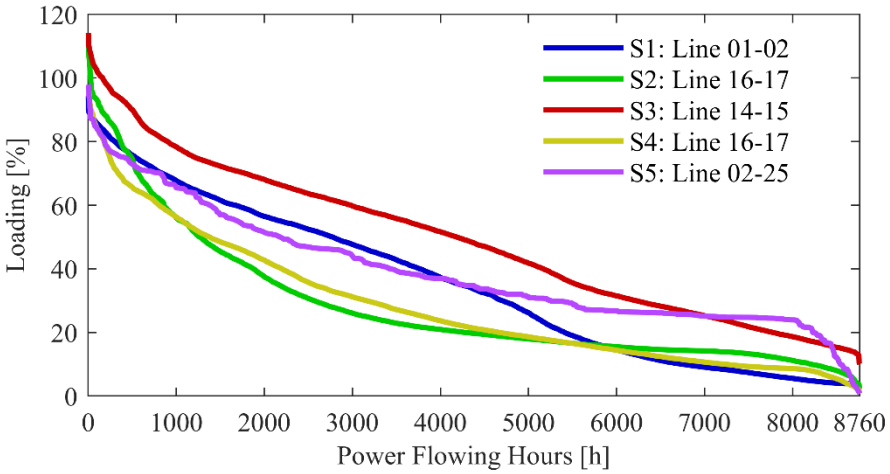

Fig. 9. N-1 scenarios' most loaded lines duration curve.

Table 8. Maximum and minimum voltage values in N-1 contingency scenarios.

Scenario	Minimum voltage		Maximum voltage	
	Bus	***Value [p.u.]***	***Bus***	***Value [p.u.]***
S1	Bus 08	0.926	Bus 28	1.098
S2	Bus 08	0.943	Bus 28	1.112
S3	Bus 25	0.931	Bus 28	1.103
S4	Bus 25	0.925	Bus 28	1.097
S5	Bus 25	0.937	Bus 28	1.139

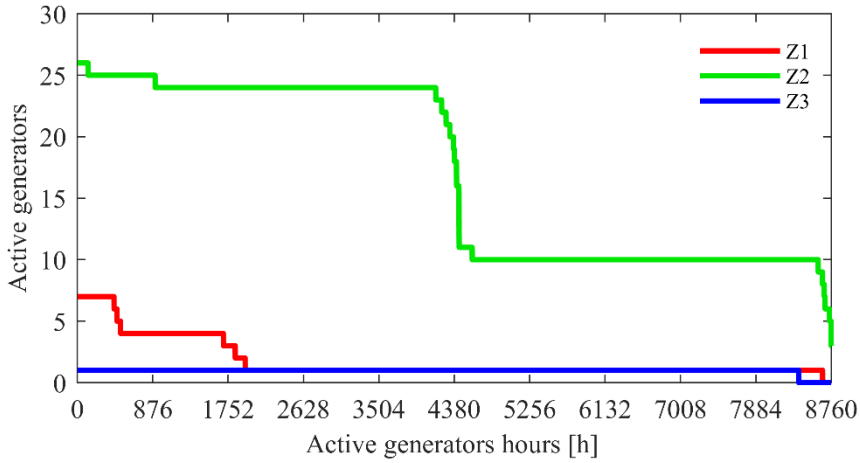

Fig. 10. Zonal active generators duration curve.

2.3.2. SCUCED Results Analysis

The ZDAM has been solved with Pyomo library as well and applied to the winter peak day of the modified IEEE 39-bus system described previously. Neglecting the Exchange

generator, the system has an installed capacity of 52% of RES, and several thermal generation units (TGU), both installed among three market zones called Z1, Z2 and Z3. The TGUs have a piecewise marginal price varying according to the technology and the fuel as defined in Table 4. On the contrary, Table 9 shows the active power limits (P_{MIN} and P_{MAX}), the start-up costs (C_{SU}), and the MUT and MDT of the TGUs. All the parameters, except the maximum power, have been obtained considering the available data of [211], [212]. In particular, they are evaluated concerning each power plant's technology, fuel, and rated power. Therefore, the Exchange is the only generator devoid of proper technical parameters and start-up costs as it represents an equivalent interconnection exchange.

Table 9. GENERATORS PARAMETERS AND START-UP COSTS.

Generator	C_{SU} **[$]**	P_{MIN} **[MW]**	P_{MAX} **[MW]**	***MUT* [h]**	***MDT* [h]**
CC NG 01	31703.82	114.75	382.50	2	2
CC NG 02	28181.70	102.00	340.00	2	2
CC NG 03	28181.70	102.00	340.00	2	2
CC NG 04	28181.70	102.00	340.00	2	2
CT NG 01	27843.52	114.75	255.00	1	1
CT Oil 01	9461.38	89.25	297.50	2	2
CT Oil 02	8109.75	76.50	255.00	2	2
Exchange	0.00	0.00	8500.00	0	0
ST Coal 01	39737.8	114.75	255.00	24	48
ST NG 01	20274.21	25.50	255.00	8	12
ST NG 02	20274.21	25.50	255.00	8	12

The ZDAM simulations are carried out during the yearly peak load day, and its hourly profile is shown in Fig. 11, in which the daily required energy is 72.85 GWh. The resulting dispatched generation is shown in Fig. 12, gathered by fuel and technology. At 4:00 it occurs the minimum load, the wind production is sufficient to balance the load, with a curtailment of 16 MW, and the energy produced during the day is 13.38 GWh. The solar output subsists between 10:00 and 17:00, with a maximum output of approximately 833 MW at 14:00 and a daily production of roughly 5 GWh. Additionally, the figure shows that the ST Coal is the cheapest unit, followed by the Exchange, CC NG, CT NG, ST NG, and CT Oil units, as reported in Table 4. In particular, the last is never cleared because the dispatching of RES and more affordable TGUs can supply the hourly load during the time horizon. Finally, a detail of hour 22 shows that CC NG generation is the marginal one with roughly 14 MW.

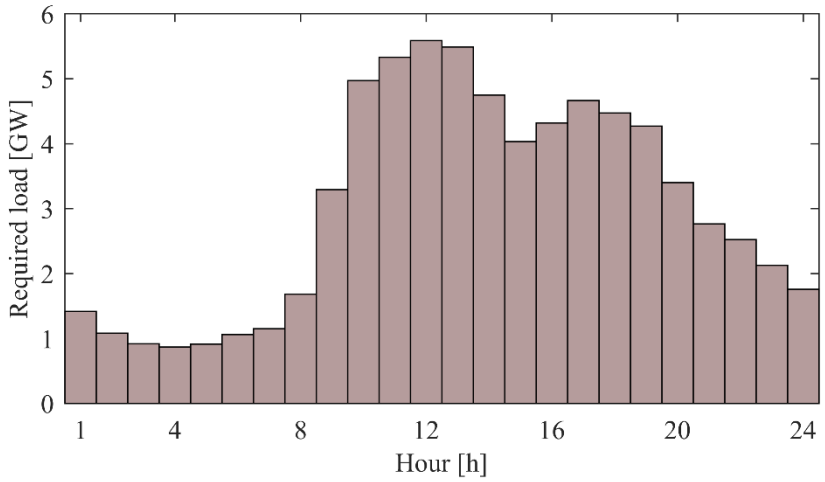

Fig. 11. Hourly load profile of the yearly peak load.

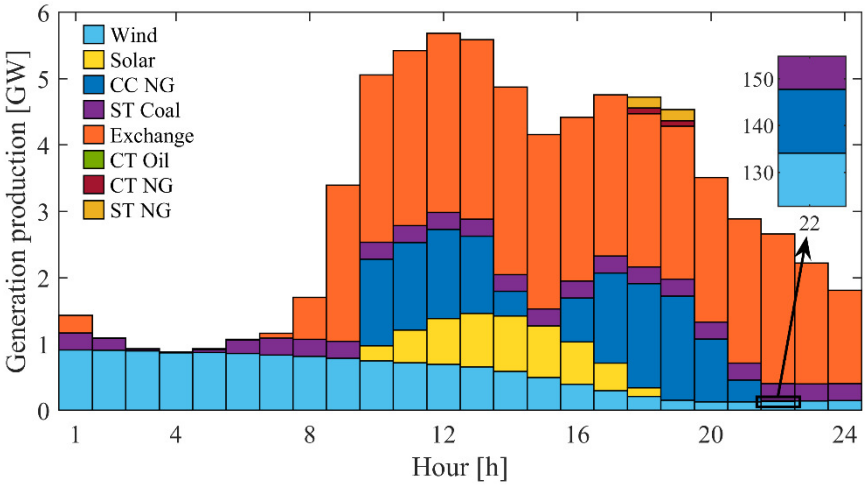

Fig. 12. Dispatched generators after the ZDAM solution gathered by technology and fuel.

Fig. 13 shows the RES penetration percentage of the required load. The RES covers a daily mean of 37% of the total load, above the 32% of the European 2030 target [214]. Fig. 14 depicts the interzonal flow in which the bounds are respectively ±1600, ±1000 and ±1000 [MW] for Z1-Z2, Z2-Z3 and Z3-Z1. From 10:00 to 14:00 and from 16:00 to 22:00 Z2-Z3 reaches the lower bound causing a market splitting of Z3. For this reason, the hourly energy price (Fig. 15) of Z3 is lower of the other zones during the market splitting hours.

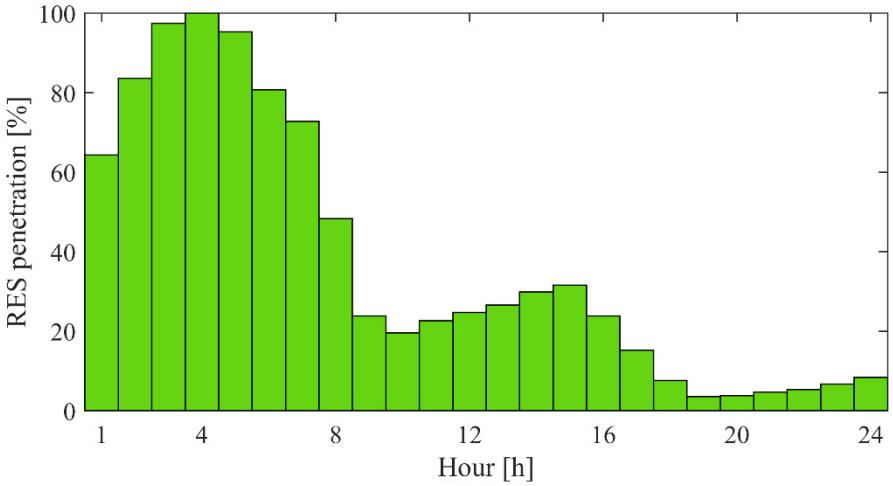

Fig. 13. Hourly RES percentage penetration.

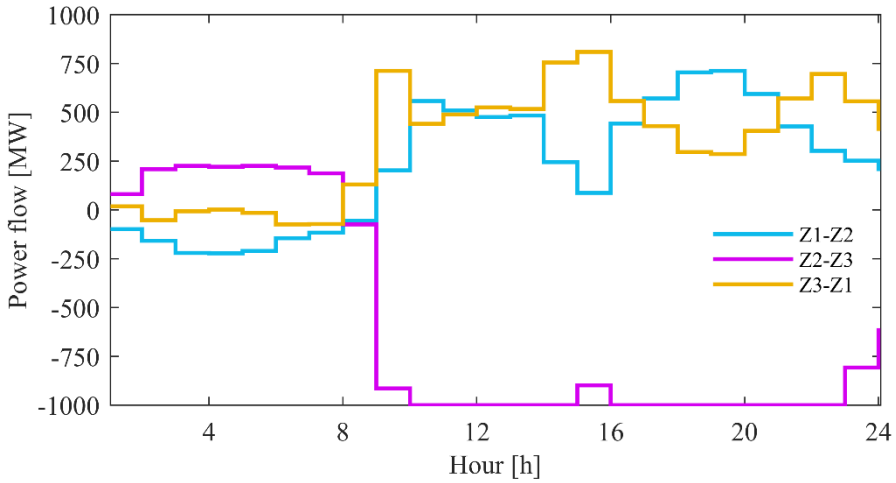

Fig. 14. Interzonal flows after the ZDAM solution.

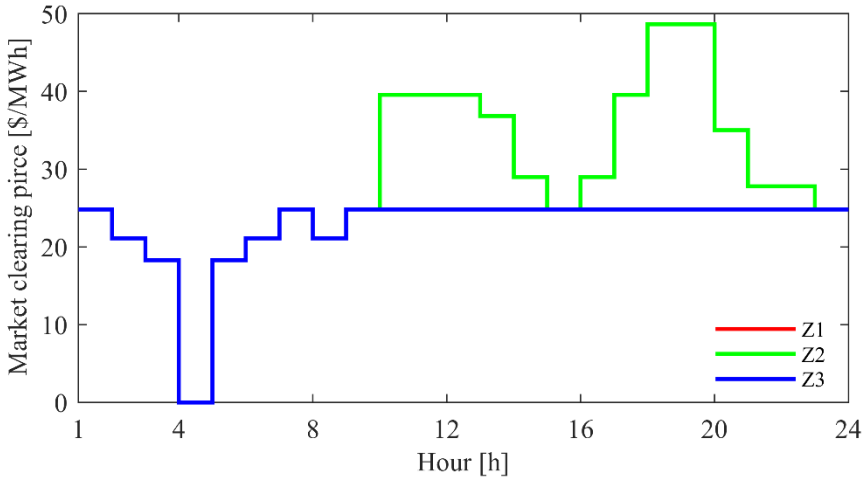

Fig. 15. Zonal market clearing price.

The SCUCED optimization problem is solved in DIgSILENT PowerFactory environment, by means of the module Unit Commitment and Dispatch Optimization. The AC load flow simulations are performed by setting the voltage of the busbar generators as in the original version of the IEEE 39-bus test system [206]. The reference machine is the Exchange. Considering that the desired voltage of the generator connected to bus 36 is 1.0635 pu, in the optimization, the voltage bounds are set ±7% of the rated voltage for all the busses. The maximum acceptable branch loading set in the problem, in percentage, is 100 %. The line rating are provided in the description of the test system in the sub-section 2.2 whereas the start-up costs, as well as the generation parameters, are the ones reported in Table 9. The RES penalty costs for curtailment are set 150 $/MWh. Considering the MUT and MDT of the generator ST Coal 01 and the time window of simulation, the optimization is carried out without a rolling horizon subdivision, whereas the sensitivity factors are updated at each time step.

Fig. 16 shows the net redispatched power after the SCUCED solving. Compared with the results of Fig. 12, it can be seen during 3:00–5:00 that the Coal generator is kept active at minimum power for the MUT constraint. In those hours, being a production lacking, only the reference machine redispatching (Exchange) and wind curtailment can allow the power balance keeping. It is important to pinpoint that the reference machine has the burden of loss compensation, even if it has not been dispatched after the ZDAM. In the market splitting hours, the Exchange is the most exploited generator for upward movement redispatching. It is the second cheaper unit, and due to the *N*-1 security criterium of the ZDAM boundaries, its dispatching was limited in the previous stage. Therefore, the total branch limits included in the SCUCED allow the increase in Exchange production, reducing the NG dispatched power, which is more expensive during those hours. At 18:00 and 19:00 the CT and ST NG units are dispatched in the ZDAM, but downstream the SCUCED solution both are shut down. The ST NG units have a MUT of 8:00, but both the technologies have a marginal price higher than the Exchange.

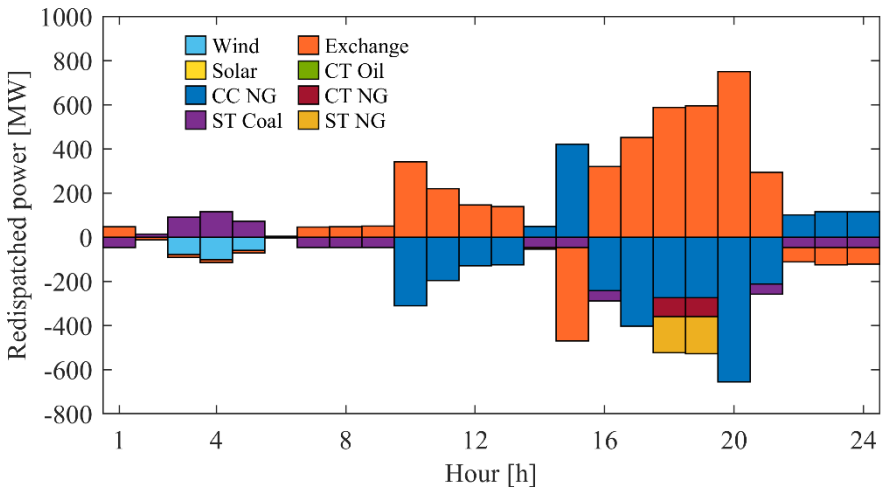

Fig. 16. Hourly net redispatched power per fuel and technology after the SCUCED.

As it can be seen from Fig. 12, at 10:00, all the NG generators are start-up, and even if they are scheduled in the ZDAM, the software includes the start-up costs in the total dispatching. For this reason, at 14:00 and 15:00, the NG is subject to an upper re-dispatch to avoid the start-up costs at 16:00. Moreover, this is a further cause of the CT and ST NG units being shut down. At hour 22, as already said, one CC NG generator is the marginal one, and the software prefers to keep that generator active rather than turn it off in the remaining hours, and even it is more expensive. This occurs because the optimization minimizes the operating costs, and the CC NG generator is slightly lower, with 4.02 k$/h, than the ST Coal one, that is 4.10 k$/h from 22:00 to 24:00 as it can be seen in the detail of Fig. 17. The total net redispatched energy, considering both upward and downward movement, is approximately 10.65 GWh. Regarding the total redispatched costs reported in Fig. 18, the TSO pays the penalty costs in the hours in which the wind production is curtailed, and the total cost is equal of 36.08 k$. During the same hours, the ST Coal generator is kept active; for this reason, the start-up costs are not considered. On the contrary, at 10:00 four CC NG generators are started-up, therefore in addition to the redispatching costs, 116.2 k$ of start-up costs has to be taken into account in the overall costs (Fig. 19). Moreover, in Fig. 16 the CC NG production is reduced because their marginal costs are greater than the Exchange ones. For this reason, from 10:00 to 13:00, and from 17:00 to 19:00 the total revenues from redispatching costs are higher than the expenses for the TSO, with a total profit of 14.94 k$. In the remaining hours, the expenses exceed the revenues with a loss of 48.22 k$. It is worth noting that the CC NG redispatching between 14:00 and 15:00 represents a significant cost savings for the TSO.

Even if the redispatch costs 1.468 k$, the actions taken during those hours saved a further 116.2 k$ from being paid at hour 16:00 to start-up again the CC NG generators.

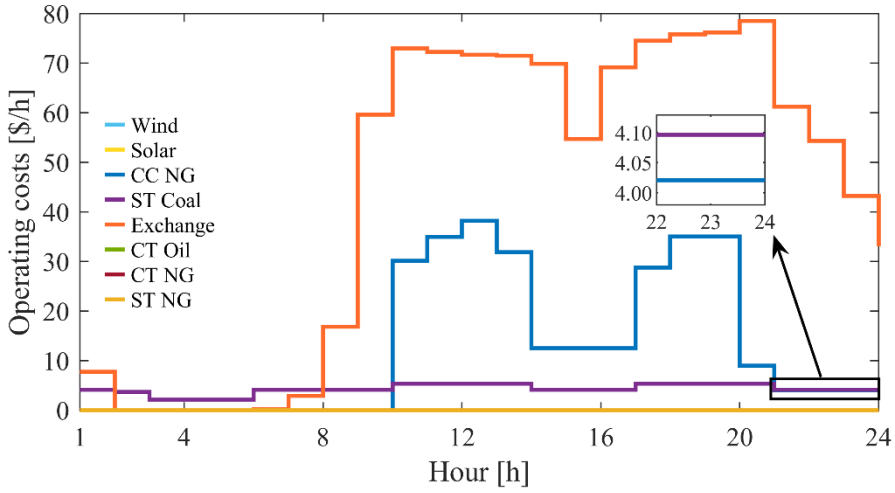

Fig. 17. Operating costs per fuel and technology after the SCUCED.

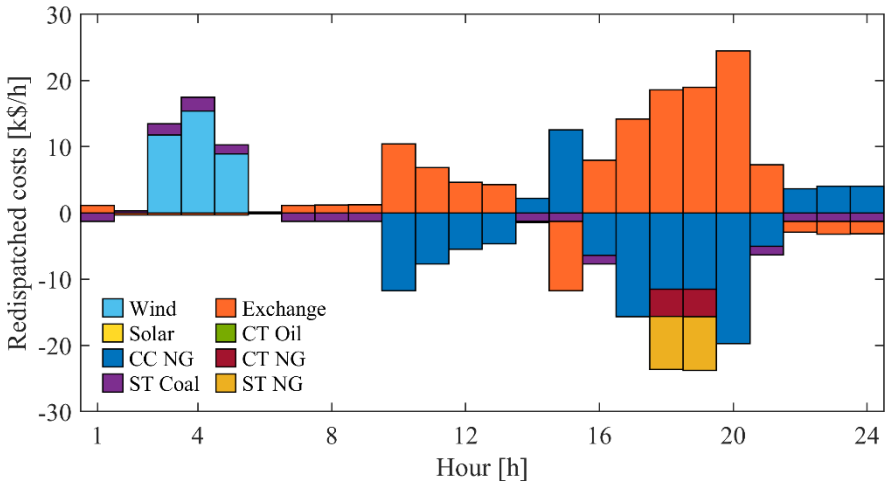

Fig. 18. Hourly total redispatching costs per fuel and technology after the SCUCED.

Finally, Fig. 19 shows the sum of operating, redispatching and start-up costs. It can be seen that the Exchange represent the most expensive unit, due to the greater power supplied and redispatched, with a total daily cost equal to 1,171 k$. Then, there is the CC NG generation with a total daily cost of 339.5 k$. It can be seen that at hour 20 and 21 the downward redispatch costs are higher than the operating costs, and the sum is equal -11.84 k$. The shutdown of the CT NG and ST NG generators during hours 18:00 and 19:00 represents a cost saving of roughly -24.39 k$/MWh. Lastly the daily cost of the Coal generator is 93.55 k$.

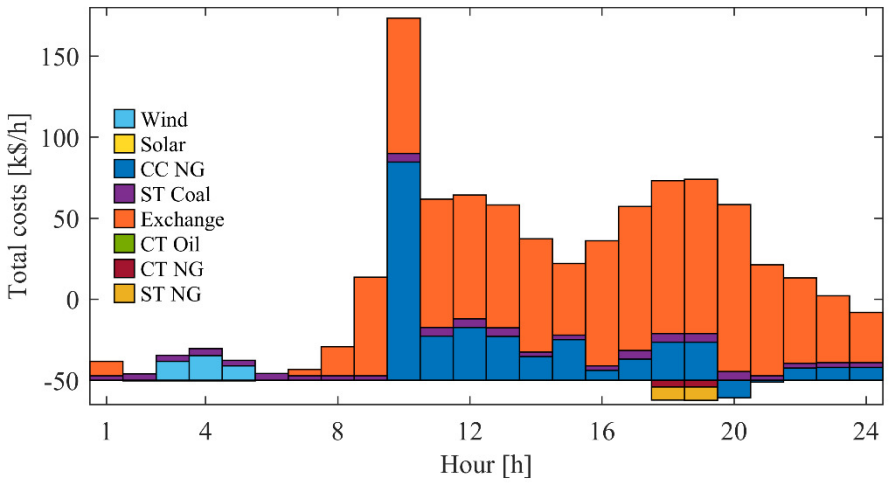

Fig. 19. Total hourly costs per fuel and technology after the SCUCED.

Fig. 20 and Fig. 21 show, respectively, the maximum, mean and minimum values of the nodal voltages and branch loadings after the SCUCED solution. For the nodal voltage, only the PQ busses are shown in Fig. 20 (i.e., from Bus 1 to Bus 29). Both the results respect the constraint limits set in the optimization. To compare the results with those provided before the optimization, in Fig. 22 and Fig. 23 there are the respective differences in the mean values. As shown in the paragraph 2.3, the line loading and nodal voltages do not exceed their limits before the optimization as well. After the re-dispatching, the mean hourly branch loading difference varies from -7.0 % to +9.6 %. Considering the results of the re-dispatched power (Fig. 16), the greater loading difference follows the respective increase and the decrease of the Exchange power production. This occurs because the re-dispatched power of more TGUs spread in the system is balanced by one source located at one busbar. Similar to the voltages, the mean difference is neglectable in the first hours; on the contrary, in the remaining hours, the mean voltage varies from -1.43×10^{-2} pu to $+0.81\times10^{-2}$ pu.

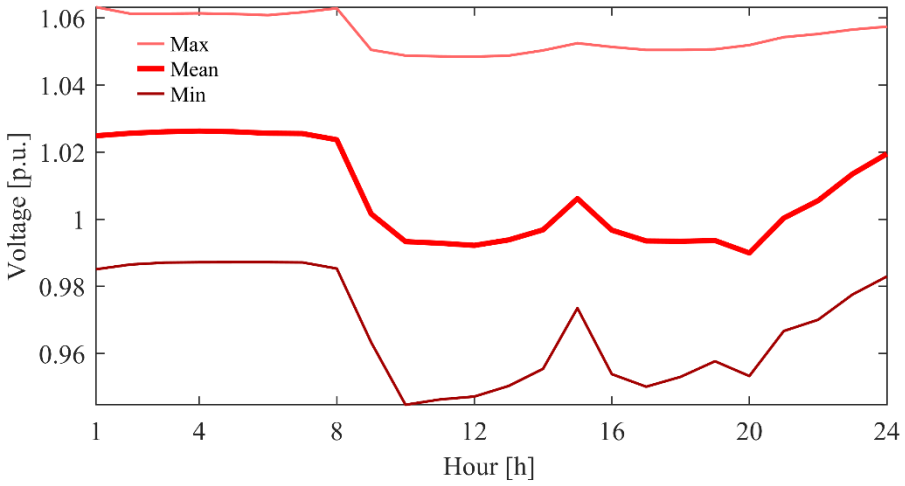

Fig. 20. Hourly maximum, mean and minimum nodal voltages.

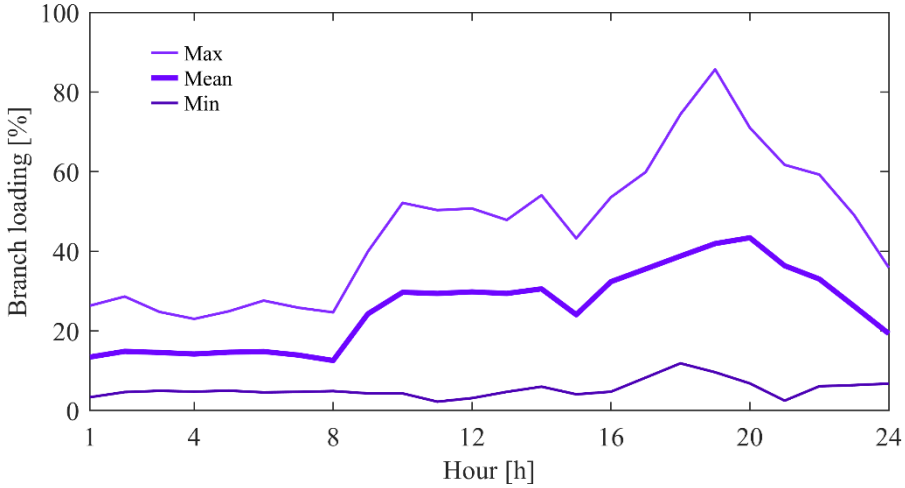

Fig. 21. Hourly maximum, mean and minimum line loadings.

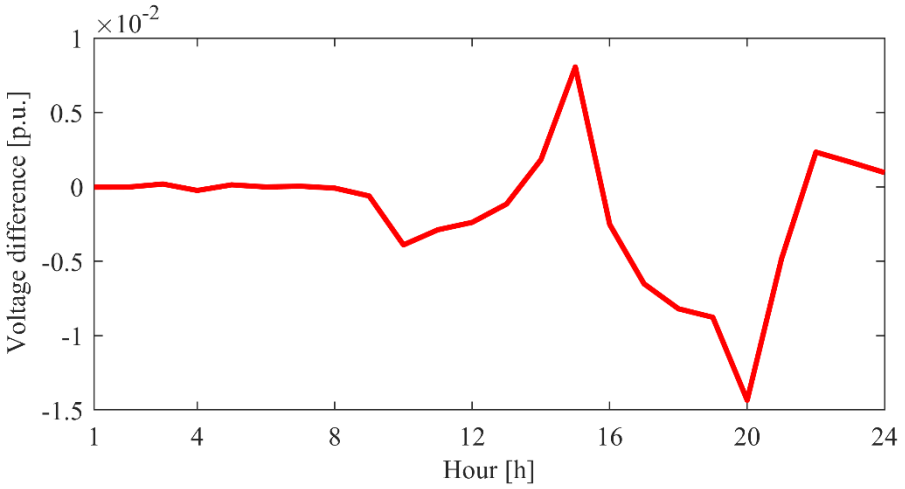

Fig. 22. Mean nodal voltage difference after and before the SCUCED.

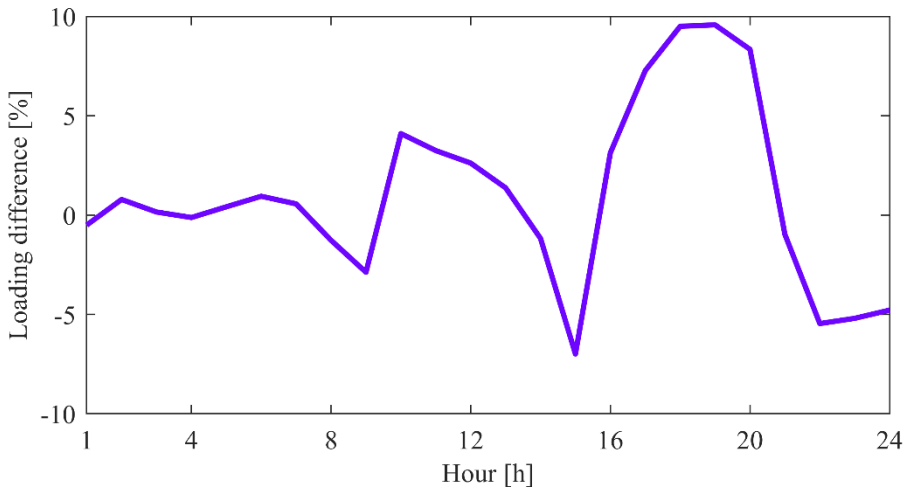

Fig. 23. Mean branch loading difference after and before the SCUCED.

Finally, a comparison of the system losses is presented in Fig. 24. Before the optimization, the minimum and maximum losses were 12.2 MW and 139.8 MW, respectively, whereas after the optimization, they were 11.9 MW and 176.3 MW. The variation of the active power losses is in line with the mean branch loading variation, causing a loss increase of 177.3 MWh during the day, due to the power supplied by the Exchange generator located at bus 39. It is worth to underling that the loss minimization is beyond the purpose of this work.

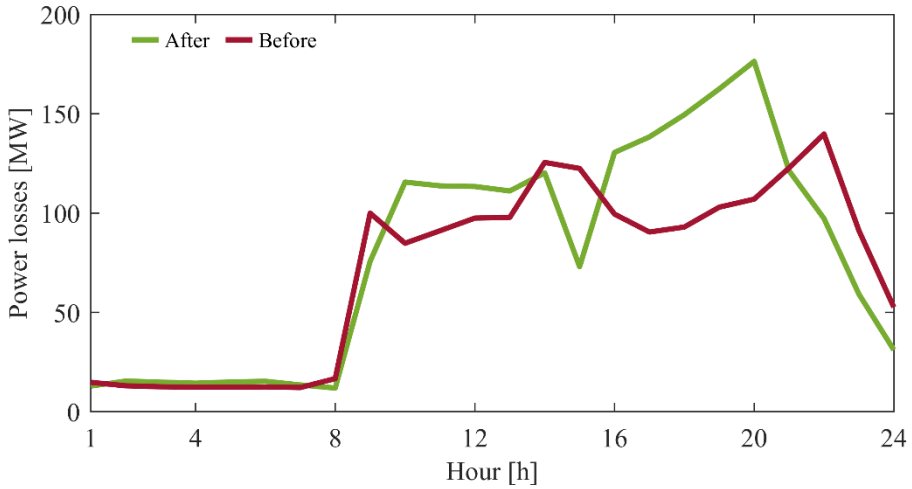

Fig. 24. System losses after and before the SCUCED optimization.

2.4. Conclusions and Future Works

In this chapter it has been proposed a modified version of the IEEE 39-bus system specifically created to allow market and steady-state simulations. The test system consists of 35 generators installed among three market zones. The ZDAM is solved by considering a

merit-order criterion, in which fossil fuel generators present proper marginal costs and ATC is based on *N*-1 security contingency. The transmission system topology has kept the original IEEE 39-bus topology as much as possible. It presents high penetration of RES and several thermal generation unit technologies installed among the three market zones. The new test system has been developed using DIgSILENT PowerFactory. Simulation results have shown that the geographical location plays an essential role as the power production of the PV power plants depends on the solar irradiation, the load profile is based on busbar surrounding (i.e., city centers, suburban areas or close to the ocean). The steady-state performance of the proposed test system is based on the dispatched power of the ZDAM solution in both base case and *N*-1 interzonal conditions. Moreover, two generators of Z1 are set must run in order to control the zonal voltage. The results show that the base case scenario, with the hypothesis mentioned above, is feasible in terms of operational conditions. Furthermore, five N-1 scenarios have been built to test the system in more stressful conditions. The obtained results showed a suitable operation in the whole year for each scenario, especially in terms of line loading. In contrast, the voltage excursions in S2, S3 and S5 are higher by 10% of the nominal voltage due to a lack of active generators to control the voltage in Z1. This means that during the contingency operating conditions, it could be necessary to activate other generators in Z1 to control the voltage. Furthermore, a bi-stage optimization method has been proposed, in which the first stage consists in the ZDAM problem, whereas the second is the SCUCED. The main advantage of this approach is the simulation of SCUCED problems considering linearized sensitivity matrices deriving from AC load flow equations in the optimization problem. Therefore, power flow and voltage, as well as the UC, constraints are embedded in the proposed method. The method has been applied to a modified version of the IEEE 39-bus test system with 37% of RES penetration during the yearly peak hour day. The results show a suitable generation redispatching in order to fulfil both generation and network constraints set in the optimization problem. The RES has been curtailed only in the hours with a low load required, in which only wind power plants are dispatched, to satisfy the MUT constraint of the ST Coal TUG. Moreover, the tool minimizes the costs in each hour, and in six hours, the redispatching revenues are more significant than the expenses. The main drawback of this tool is the addition of start-up costs for the dispatched power scheduled in the previous market; in this work, the ZDAM schedule. This behavior affects the start-up or shut-down of

the involved generators to avoid paying further costs. From the network perspective, the optimal solution does not exceed the system constraints even in the hours when the most energy is re-dispatched. Further works will be developed, including additional UC constraints, extending the time window to one year of simulations, and considering RES and load uncertainties.

Chapter 3. Techno-Economic TEP Methodologies Evaluation

In this chapter, benefits of development projects in power transmission network are assessed, taking into account technical and economic issues by means of two different approaches. On one hand, a flow-based methodology is adopted, including electricity market solution and network analysis with security issues, and exploiting linear sensitivity factors. The sensitivity factors are exploited to develop a security-aimed redispatching action to overcome possible branch overflow of the market-based network solution. The procedure is aimed to analyze an evolution scenario of the network in defined target year, divided in hourly time-step. A comparative analysis is carried out, through proper economic indicators defined according to the redispatching actions, to evaluate the performance of the selected development project. On the other hand, a methodology for performance analysis of a portfolio of network development projects is proposed. In particular, the methodology aims at assessing zonal market framework and AC LF analysis as well, in the base case network to individuate possible candidate projects. The same tools are exploited in the presence of network development candidate project, in order to calculate merit indicators on active power losses, admissible load increase and admissible renewable generation increase , from a technical perspective. Further, investment cost as economic merit indicator is determined from an economic perspective. These indicators are compared among candidate projects by means of Analytic Hierarchy Process (AHP) method, in order to determine the most promising solution under different weights of criteria, representing an evaluation of various evolution scenarios. Both the procedures have been applied to NREL-118 test system, a modified version of the IEEE 118-bus test system with high penetration of RES with a yearly dataset.

3.1 Flow-Based Evaluation

In order to evaluate the impact on power system behavior of a network development project, a procedure to derive performance indicators is adopted, involving electricity market solution and steady-state network study under security conditions. For each operating condition represented by a time interval t_k, the method includes three consecutive sections, as depicted in Fig. 25. First, an electricity market model is solved, to obtain generation dispatch and evaluate market-related benefits. Therefore, steady-state network study is carried out to

evaluate losses. Finally, in the presence of overloads on network connections, a redispatching section is developed, aimed at determining the need of ancillary service and curtailment actions.

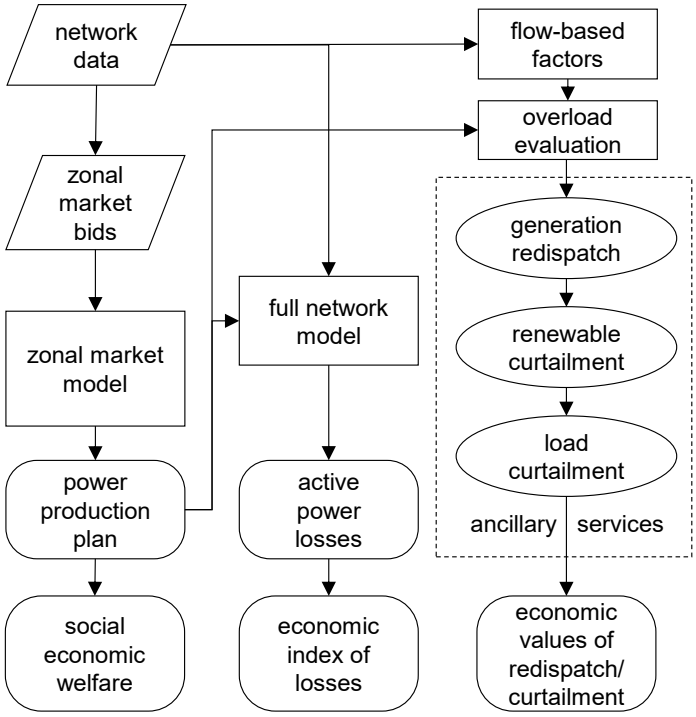

Fig. 25. Overall flowchart of the flow-based methodology.

3.1.1. Energy Market Model

Let us consider an electric power system with N^B buses, N^L branches and N^G generators, including N^Z market zones, with N^I interzonal connections, where generators provide N^S step bids. System behavior is evaluated over a yearly horizon divided into N^T intervals with τ duration. The adopted model of electricity market, to be solved for each time interval t_k, is based on the assumption of inelastic demand. In this case, the market equilibrium is determined by solving the following mixed-integer optimization problem. The objective function is given by stepwise generator bids at constant price levels $c_{i,s}$:

$$\min_{\boldsymbol{P^G}} \sum_{i=1}^{N^G} \sum_{s=1}^{N^S} P_{i,s}^G(t_k)\, c_{i,s} \tag{35}$$

Constraints related to the condition in the analyzed time interval t_k are represented as follows:

$$\sum_{b=1}^{N^B}\sum_{i=1}^{N^G}\sum_{s=1}^{N^S}\beta_{i,b}\,\beta_{b,z}\,P_{i,s}^{G}(t_k)+\sum_{l=1}^{N^I}\beta_{l,z}\,P_{l}^{tie}(t_k)=\sum_{b=1}^{N_B}\beta_{b,z}\,P_{b}^{D}(t_k)\quad\forall\, z\in N^Z \tag{36}$$

$$0\le P_{i,s}^{G}(t_k)\le \bar{u}_{i,s}(t_k)\cdot P_{i,s}^{G,max}(t_k)\quad\forall\, i\in N^G,\forall\, s\in N^S \tag{37}$$

$$u_i(t_k)\cdot P_i^{G,min}\le\sum_{s=1}^{N^S}P_{i,s}^{G}(t_k)\quad\forall\, i\in N^G \tag{38}$$

$$u_i(t_k)\ge\bar{u}_{i,1}(t_k)\ge\bar{u}_{i,2}(t_k)\ge\cdots\ge\bar{u}_{i,N^S}(t_k) \tag{39}$$

$$P_l^{lb}\le P_l^{tie}(t_k)\le P_l^{ub}\quad\forall\, l\in N^I \tag{40}$$

where the state variable vector includes:

- Power generation level of the i-th generator in the s-th bid step $P_{i,s}^{G}$;
- Power exchange at the z-th zonal interface P_l^{tie};
- Binary variable of selection for the s-th bid step of the i-th generator $\bar{u}_{i,1}$;
- Binary variable for on-off status of the i-th generator u_i.

The zonal power balance is expressed in (36), where $P_b^D(t)$ is the inelastic load demand at the b-th bus. Binary parameter $\beta_{i,b}$ is equal to 1 if the i-th generator is connected to the b-th bus and 0 otherwise; moreover, $\beta_{b,z}$ is 1 if the b-th bus is within the z-th zone and 0 otherwise. Finally, $\beta_{l,z}$ is 1 if the l-th exchange is directed towards the z-th zone, -1 if the direction is exiting the z-th zone, and 0 otherwise.

For each bid step, maximum step power $P_{i,s}^{G,max}$ is considered in (37). Non-dispatchable sources have a single bid step equal to maximum power point given by weather conditions and generator features, and negligible price bid. On the contrary, the minimum production constraint is imposed by (38), where $P_i^{G,min}$ is the technical minimum of the i-th generating unit, equal to 0 for non-dispatchable generators. The acceptance relation among bid steps in increasing order is given by (39). Finally, by means of (40), zonal exchanges are limited by available transfer capacities upper (P_l^{ub}) and lower bound (P_l^{lb}), possibly nonsymmetrical.

Ramping constraints and minimum up time relate consecutive time intervals:

$$RD_i \leq \sum_{s=1}^{N^S} P_{i,s}^G(t_k) - \sum_{s=1}^{N^S} P_{i,s}^G(t_{k-1}) \leq RU_i \quad \forall\, i \in N^G \tag{41}$$

$$u_i(t_k) + \sum_{T_k=t_k-MUT_i}^{t_k-1} u_i(T_k) \geq MUT_i \quad \forall\, i \in N^G \tag{42}$$

where RU_i and RD_i represent ramp-up and ramp-down limits of the i-th generator, and MUT_i is minimum up time of the i-th generator as well.

By solving the problem (35)–(42), the dual variable $\lambda_z(t_k)$ related to the balance constraint (36) represents the equilibrium price of the z-th zone in the analyzed time interval. Furthermore, analogously to Italian market structure, the unified price $\lambda(t_k)$ is evaluated as weighed average of zonal prices according to zonal load demand:

$$\lambda(t_k) = \frac{\sum_{z=1}^{N^Z}\left(\lambda_z(t_k)\sum_{b=1}^{N^B}\left(P_b^D(t_k)\cdot\beta_{b,z}\right)\right)}{\sum_{b=1}^{N^B} P_b^D(t_k)} \tag{43}$$

Social welfare (SW) is evaluated as global economic indicator of market solution. It is composed of three contributions: Generator Surplus (GS), User Surplus (US) and Congestion Rent (CR), shown in Fig. 26 and evaluated as follows:

$$GS(t_k) = \sum_{z=1}^{N^Z}\sum_{b=1}^{N^B}\sum_{i=1}^{N^G}\sum_{s=1}^{N^S}\left(\lambda_z(t_k) - c_{i,s}\right)\cdot\beta_{i,b}\beta_{b,z}P_{i,s}^G(t_k) \tag{44}$$

$$US(t_k) = \left(\Lambda - \lambda(t_k)\right)\cdot\sum_{b=1}^{N^B} P_b^D(t_k) \tag{45}$$

$$CR(t_k) = \sum_{l=1}^{N^I}\left|P_l^{tie}(t_k)\right|\cdot\sum_{z=1}^{N^Z}\left|\lambda_z(t_k)\cdot\beta_{l,z}\right| \tag{46}$$

$$SW(t_k) = GS(t_k) + US(t_k) + CR(t_k) \tag{47}$$

where Λ is a conveniently high price value in order to represent virtual consumer bids by inelastic demand, higher than maximum generator offer.

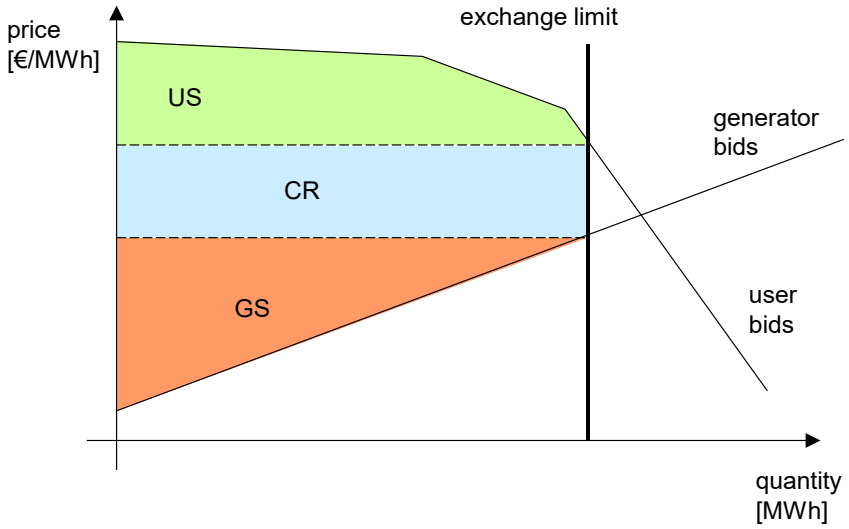

Fig. 26. Definition of socio-economic welfare components.

3.1.2. Steady-state network study

From market analysis, power production level for the i-th generator, P_i^G, at the generic t_k-th time step, is determined as the sum of dispatched power levels over the bid steps:

$$P_i^G(t_k) = \sum_{s=1}^{N^S} P_{i,s}^G(t_k) \quad \forall\, i \in N^G \tag{48}$$

Moreover, total scheduled power production at the b-th bus $P_b^G(t)$ is calculated as follows:

$$P_b^G(t_k) = \sum_{i=1}^{N^G} P_i^G(t_k) \cdot \beta_{i,b} \quad \forall\, b \in N^B \tag{49}$$

Analogously, the power flows on network branches at t_k-th time interval are determined by solving the AC power flow problem:

$$\begin{aligned} \boldsymbol{P}(t_k) - \boldsymbol{P^L}\big(\boldsymbol{\theta}(t_k), \boldsymbol{V}(t_k)\big) &= \boldsymbol{0} \\ \boldsymbol{Q}(t_k) - \boldsymbol{Q^L}\big(\boldsymbol{\theta}(t_k), \boldsymbol{V}(t_k)\big) &= \boldsymbol{0} \end{aligned} \tag{50}$$

where the elements of vectors $\boldsymbol{P}$ and $\boldsymbol{Q}$ are nodal injection of active and reactive power for each bus, as defined in (33). Load reactive power demand is determined according to proper power factor, and reactive power generation descends from bus classification as fixed

voltage, fixed reactive or slack. The losses vectors $\boldsymbol{P^L(\theta, V)}$ and $\boldsymbol{Q^L(\theta, V)}$ derive from network connections and branch model with a π-circuit.

The solution of AC power flow problem yields nodal voltage levels, in terms of magnitude V_b and phase angle θ_b, as well as the active power flow P_j^F through each j-th branch.

Active power losses on j-th branch P_j^L, connecting nodes b and c, at time step t_k can be calculated as follows, where r_j and x_j represent series resistance and reactance, respectively, of the j-th branch:

$$P_j^L(t_k) = \frac{|V_b(t_k) - V_c(t_k)|^2 \cdot r_j}{r_j^2 + x_j^2} \quad \forall\, j\ in\ N^L \tag{51}$$

Economic value of losses (EL) is obtained by means of unified price λ coming from market model, defined in (43):

$$EL(t_k) = \sum_{j=1}^{N^L} P_j^L(t_k) \cdot \lambda(t_k) \tag{52}$$

3.1.3. Security-aimed redispatching

The market-based network solution at time interval t_k could be not feasible if the active power flow through the j-th branch P_j^F exceeds nominal rating $P_{R_j}^F$ According to Italian planning standard [215], overloads OL_j are detected for branches with $P_j^F \geq 1.2\, P_{R_j}^F$ (positive overload) or with $P_j^F \leq -1.2\, P_{R_j}^F$ (negative overload). If overloads are observed, in order to obtain secure operating conditions, the third section of the procedure involves active power redispatching. This should involve a modification of market plans, accounting for the presence of ancillary markets or curtailment actions in actual electricity industry.

At first, for each time interval t_k, the most critical overloaded branch j^* is individuated as follows:

$$j^*(t_k) \quad \ni\ ' \left|OL_{j^*}(t_k)\right| = \max_j \left(\frac{\left|P_j^F(t_k)\right| - 1.2 \cdot P_{R_j}^F}{P_{R_j}^F}, 0 \right) \tag{53}$$

Therefore, the maximum positive/negative overloads for the branch j^*, named $OL_{j^*}^{+}$,$OL_{j^*}^{-}$ respectively, are determined, along with the time interval when they occur $t_{j^*}^{+}, t_{j^*}^{-}$. Their equivalent durations are obtained by averaging all observed critical overloads, as follows:

$$\tau_{j^*}^{+} = \left[\tau \cdot \sum_{t=1}^{N^T} max\left(0, OL_{j^*}(t_k)\right)\right] \cdot \frac{1}{OL_{j^*}^{+}} \tag{54}$$

$$\tau_{j*}^{-} = \left[\tau \cdot \sum_{t=1}^{N^T} min\left(0, OL_{j^*}(t_k)\right)\right] \cdot \frac{1}{OL_{j^*}^{-}} \tag{55}$$

Each maximum overload is therefore solved in the specific time interval $t_{k,j^*}^{+}, t_{k,j^*}^{-}$ exploiting power transfer distribution factors (PTDFs). In particular, the PTDF of the b-th node on the j-th branch $h_{b,j}$ represents the amount of the power injection at the b-th node flowing through the j-th branch to reach the slack bus. PTDFs are determined by means of DC load flow method and matrix approach [216] and can be either positive or negative. In this way, the power flow through the j-th branch P_j^F, at the t_k time step, can be determined as follows:

$$P_j^F(t_k) = \sum_{b=1}^{N^B} P_b(t_k) \cdot h_{b,j} \tag{56}$$

Hence, to avoid a positive overload on the j^*-th branch, power injection at nodes with $h_{b,j^*} > 0$ (concordant PTDF) should be reduced, and power injection at nodes with $h_{b,j^*} < 0$ (discordant PTDF) should be increased by the same amount, keeping global power balance.

The available resources are exploited in a sequential manner. The first resource is the modification of power production levels from dispatchable generators, reducing relevant power production if connected at nodes with concordant PTDF down to the minimum, starting from the higher PTDF value, until the overload is eliminated, i.e., $\left|OL_{j^*}(t_k)\right| = 0$. The power production of dispatchable units at nodes with discordant PTDF is increased, starting from the bottom of the list and up to the maximum level, to balance total power reduction. It can be observed that this preserves the on/off status of generators.

If this first action does not allow to totally solve the overload, the second action is the curtailment of non-dispatchable renewable generators with concordant PTDF. The action

reflects the same property of the previous one, except for the fact that the minimum production level of non-dispatchable generators is zero, and the dispatchable units with discordant PTDF would be called to increase the production to ensure the balance.

As a last resource, load curtailment is exploited. The load reduction is performed first at the node with the highest discordant PTDF. The power balance is attained by reducing the power production at nodes with concordant PTDF as well, having a further positive impact on overload elimination.

At the end of the redispatching action, considering e.g., maximum positive overload, new power production level of i-th generator $P_i^{G,red}(t_{j^*}^+)$ and new load level at b-th bus $P_b^{D,red}(t_{j^*}^+)$ are obtained.

The merit indices of security-aimed redispatching action are related to the three kinds of resources. For each dispatchable generator, within the set Ω_{dis}, the total increasing and decreasing power amount is determined:

$$\Delta P_{dis,i}^{+}(t_{j^*}^{+}) = max\left(P_i^{G,red}(t_{k^*}^{+}) - P_i^{G}(t_{j*}^{+}), 0\right) \quad \forall\, i \in\ \Omega_{dis} \tag{57}$$

$$\Delta P_{dis,i}^{-}(t_{j*}^{-}) = max\left(P_i^{G}(t_{j*}^{+}) - P_i^{G,red}(t_{j*}^{+}), 0\right) \quad \forall\, i \in\ \Omega_{dis} \tag{58}$$

For each non-dispatchable renewable generator, within the set Ω_{ndr}, the total power curtailed is assessed as follows:

$$\Delta P_{ndr,i}^{-}(t_{j^*}^{+}) = P_i^{G}(t_{j^*}^{+}) - P_i^{G,red}(t_{j^*}^{+}) \quad \forall\, i \in\ \Omega_{ndr} \tag{59}$$

whereas load curtailment at b-th node is obtained as:

$$\Delta P_{loa,b}^{-}(t_{j^*}^{+}) = P_b^{D}(t_{j^*}^{+}) - P_b^{D,red}(t_{j^*}^{+}) \quad \forall\, b \in\ N^B \tag{60}$$

The economic evaluation of the redispatching action involves three indicators, namely total cost of generation redispatching $E_{dis}^{R}(t_{j^*}^{+})$, of non-dispatchable generation curtailment $E_{ndg}^{R}(t_{j^*}^{+})$ and of load curtailment $E_{loa}^{R}(t_{j^*}^{+})$. It is assumed that, for dispatchable generators, the production increase and decrease due to redispatch are paid at a higher value with respect to marginal cost, c_i^+ and c_i^- respectively, since the action implies a sub-optimal operation from economic viewpoint. Renewable curtailment is paid at zonal equilibrium price and load

curtailment is linked to value of loss load, indicated as $voll$. Hence, economic values are obtained as:

$$E_{dis}^{R}(t_{j^*}^{+}) = \sum_{i \in \Omega_{dis}} \left(c_i^{+} \ \Delta P_{dis,i}^{+}(t_{j^*}^{+}) + c_i^{-} \ \Delta P_{dis,i}^{-}(t_{j^*}^{+}) \right) \tag{61}$$

$$E_{ndg}^{R}(t_{j^*}^{+}) = \sum_{z=1}^{N^Z} \lambda_z(t_{j^*}^{+}) \cdot \sum_{b=1}^{N^B} \sum_{i \in \Omega_{ndr}} \beta_{i,b} \beta_{b,z} \Delta P_{ndr,i}^{-}(t_{j^*}^{+}) \tag{62}$$

$$E_{loa}^{R}(t_{j^*}^{+}) = voll \cdot \sum_{b=1}^{N^B} \Delta P_{loa,b}^{-}(t_{j^*}^{+}) \tag{63}$$

3.1.4. Total benefit evaluation

Yearly amount of social welfare YSW, of losses economic value YEL, and of the three redispatching components YER_{dis}, YER_{ndr} and YER_{loa} are determined as follows:

$$YSW = \sum_{t_k=1}^{N^T} \tau \cdot SW(t_k) \tag{64}$$

$$YEL = \sum_{t_k=1}^{N^T} \tau \cdot EL(t_k) \tag{65}$$

$$YER_{dis} = \sum_{j^*} \left[\tau_{j^*}^{+} \cdot E_{dis}^{R}(t_{j^*}^{+}) + \tau_{j^*}^{-} \cdot E_{dis}^{R}(t_{j^*}^{-}) \right] \tag{66}$$

$$YER_{ndr} = \sum_{j^*} \left[\tau_{j^*}^{+} \cdot E_{ndg}^{R}(t_{j^*}^{+}) + \tau_{j^*}^{-} \cdot E_{ndg}^{R}(t_{j^*}^{-}) \right] \tag{67}$$

$$YER_{loa} = \sum_{j^*} \left[\tau_{j^*}^{+} \cdot E_{loa}^{R}(t_{j^*}^{+}) + \tau_{j^*}^{-} \cdot E_{loa}^{R}(t_{j^*}^{-}) \right] \tag{68}$$

By cumulating the obtained values, the total yearly evaluation of techno-economic indicators YTE of the network under analysis is obtained.

$$YTE = YSW + YEL + YER_{dis} + YER_{ndr} + YER_{loa} \tag{69}$$

The evaluation of benefits coming from a network development project is carried out through the variation of performance indicators between a Reference Scenario (RS) and the

Evolution Scenario (ES), without and with the project, respectively. The yearly economic evaluation of project benefit YPB is therefore assessed by the difference between the two total values.

$$YPB = YTE_{ES} - YTE_{RS} \tag{70}$$

By accounting for investment cost of the analyzed project IC, the relevant profitability can be evaluated as well by means of net present value NPV, as follows:

$$NPV = IC - \sum_{y=1}^{N^Y} \frac{YPB_y - FC_y}{(1+\alpha)^y} \tag{71}$$

being y the index of years, α the discount rate, FC the fixed maintenance costs and N^Y the lifetime years.

3.2 Techno-Economic Indices Evaluation

The determination of the network development initiative follows a multi-step iterative methodology, synthesized in the following points:

- Study of base case operation according to techno-economic programming over a defined time horizon.
- Individuation of candidate network development projects, able to produce effects on system behavior.
- Carrying out of scenario analysis for each candidate project and determination of the merit indicators.
- Selection of the most promising projects.

3.2.1. Power System Techno-Economic Operation

In order to evaluate the operating conditions of the considered power system, technical and economic considerations should be accounted. The combination of these aspects can be assessed in optimal power flow analysis [217], however in the outline of an unbundled energy sector, the presence of energy markets should be considered. Therefore, the adopted method to determine power system operation is structured as follows. On the contrary of the previous work, here it is proposed a QP optimization problem.

For each operating condition to be analyzed, represented by the t_k-th time step in the considered time window of N^T time steps, the procedure involves the solution of a ZDAM with quadratic generation bids and inelastic load demand, whose formulation can be synthesized as follows:

$$\min_{\boldsymbol{P^G}} \sum_{z=1}^{N^Z} \sum_{i=1}^{N^G} \beta_{i,b}\, \beta_{b,z} \left(\alpha_i\, P_i^G(t_k) + \frac{1}{2} \gamma_i\, {P_i^G}^2(t_k) \right) \tag{72}$$

s.t.

$$\sum_{b=1}^{N^B} \sum_{i=1}^{N^G} \beta_{i,b}\, \beta_{i,z}\, P_i^G(t_k) - \sum_{b=1}^{N^B} \beta_{b,z}\, P_b^D(t_k) - \sum_{l=1}^{N^I} \beta_{l,z}\, P_l^{tie}(t_k) = 0 \quad \forall\, z \in N^Z \tag{73}$$

$$0 \leq P_i^G(t_k) \leq a_i(t_k) P_i^{G,max} \quad \forall\, i \in N^G \tag{74}$$

$$P_l^{lb} \leq P_l^{tie}(t_k) \leq P_l^{ub} \quad \forall\, l \in N^I \tag{75}$$

where, over the variables and parameters described in the previous subchapter, α_i and γ_i are the linear and quadratic bid coefficient costs of the i-th generator, a_i is the availability of the i-th generator. In particular, (73) represents the power balance constraint, (74) explicates the generator technical limits, whereas (75) introduces the zonal interface limit constraints.

The absence of generators technical minimum avoids the presence of block order bids that involve entirely accepted or rejected bids conditions according to the market clearing price, for each hour. These bids entail a Mixed Integer Linear Programming with binary variables that state all-or-nothing constraints, which in turn leads to a counterintuitive market solution called Paradoxically Accepted/Rejected Blocks, described in [218], [219].

It should be remarked that the maximum interzonal power exchange across the l-th border P_l^{ub} is strictly related to the active power flow rating $P_{R_j}^F$ of all the j-th branches constituting the l-th border. For instance, it could represent the Available Transfer Capacity (ATC) value in N or N-1 conditions or come from other security considerations.

The output of the energy market is represented by the power generation plan of the dispatchable generation present in the power system able to minimize the objective (e.g., reduce the generation cost) in the presence of zonal constraints. However, the impact on the behavior of network elements should be assessed as well. Therefore, a steady-state network

analysis is performed, considering the distributed load flow framework with full AC formulation for each time step $t_k \in N^T$ and bus $b \in N^B$ developed as in (32) and reported in the following, in the explicit form:

$$\begin{aligned}
&\sum_{i=1}^{N^G} \beta_{i,b} \bar{P}_i^G(t_k) - P_b^D(t_k) - \sum_{c=1}^{N^B} Y_{bc} v_b(t_k) v_c(t_k) \cos(\theta_b(t_k) - \theta_c(t_k) + \phi_{bc}) = 0 \\
&\sum_{i=1}^{N^G} \beta_{i,b} Q_i^G(t_k) - Q_b^D(t_k) - \sum_{c=1}^{N^B} Y_{bc} v_b(t_k) v_c(t_k) \, sin(\theta_b(t_k) - \theta_c(t_k) + \phi_{bc}) = 0
\end{aligned} \tag{76}$$

s.t.

$$\bar{P}_i^G(t_k) = P_i^G(t_k) + \omega_i \, P^L(t_k) \quad \forall \, i \in N^G \tag{77}$$

$$P^L(t_k) = \sum_{l=1}^{N^L} P_j^L(t_k) = \sum_{j=1}^{N^L} Re\left\{ \frac{\left| \beta_{j,b} \, v_b(t_k) - \beta_{j,c} \, v_c(t_k) \right|^2}{r_j - \mathrm{j} \, x_j} \right\} \tag{78}$$

$$0 \leq \omega_i \leq 1 \quad \forall \, i = 1, \dots, N^G \tag{79}$$

$$\sum_{i=1}^{N^G} \omega_i = 1 \tag{80}$$

where:

- $\bar{P}_i^G$ is the total generated active power by the g-th generator;
- Y_{bc} and ϕ_{bc} are amplitude and phase of the nodal admittance between b and c buses (coming from the construction of the $N_B \cdot N_B$ nodal admittance matrix $\boldsymbol{Y}$;
- v_b and v_c are the complex values of nodal voltage at b-th and c-th bus;
- ω_g is the loss participation factor of i-th generator;
- P^L is the system total active power losses;
- P_j^L is the amount of active power losses across j-th branch;
- $\beta_{j,b}$ and $\beta_{j,c}$ are binary parameters and they indicate if the b-th (c-th) bus is connected (1) or not (0) to the j-th branch;
- r_l and x_l are the resistance and reactance values of the j-th branch;
- j is the imaginary unit.

The distributed load flow is considered in order to share the burden of active power losses balance—not considered in zonal energy market solution—with a limited though diffused stress on the selected generators.

As outcome of the analysis, further than the determination of nodal voltage, the amount of active, reactive and apparent power flowing across the j-th branch, named P_j^F, Q_j^F and S_j^F, is determined from the following complex equation:

$$S_j^F(t_k) = \beta_{j,b} v_b(t_k) \left[\frac{\beta_{j,b} v_b(t_k) - \beta_{j,c} v_c(t_k)}{r_j - j x_j} + y_j \beta_{j,b} v_b(t_k) \right]^* \tag{81}$$

where the superscript * stands for complex conjugate value, and:

$$S_j^F(t_k) = P_j^F(t_k) + \mathrm{j}\, Q_j^F(t_k) \tag{82}$$

$$y_j = r_j + \mathrm{j}\, x_j \tag{83}$$

3.2.2. Selection of the Candidate Projects

From the power system techno-economic operation analysis, and particularly from the determination of power flowing through branches, the loading analysis of network connection can be carried out.

In particular, for each time step $t_k \in N^T$ and branch $j \in N^L$, the loading factor F_j^L is determined as the ratio of absolute value of power flow $\left|S_j^F\right|$ on active power flow rating $P_{R_j}^F$, as follows:

$$F_j^L(t_k) = \frac{\left|S_j^F(t_k)\right|}{P_{R_j}^F} \tag{84}$$

For the base case, the mean value of the loading factor $F_{m_j}^L$ throughout the considered time horizon and a duration curve of loading factor (sorting the values from the highest to the lowest, irrespective of the time step position in the horizon) can provide synthetic evaluation of the operation stress of the j-th branch, thus individuating the paths that would benefit more from a reinforcement project. The formulation of $F_{m_j}^L$ can be generalized as follows:

$$F_{m_j}^{L} = \frac{1}{N^T} \cdot \sum_{t=1}^{N^T} \Delta T(t_k) \cdot F_j^L(t_k) \tag{85}$$

According to the adopted operation planning standard, the overloaded branches can be individuated if the power flow exceeds the rating value by a suitable margin ε; therefore, no overload is observed if the following condition is satisfied

$$F_j^L(t_k) > 1 + \varepsilon \quad \forall\, t = 1, \dots, N^T \; \forall\, j = 1, \dots, N^L \tag{86}$$

From the theoretical framework of the zonal market, it could be expected that more stressed connections are placed across the zones and not within each zone. Therefore, a first selection is made considering the doubling of existing connections across each couple of zones.

However, further connection lines could be individuated as well, in order to improve the network meshing, providing different paths for power routing that could increase the efficiency, although they could represent a more costly solution. A second selection of candidate projects involves new connections between couple of nodes pertaining to different zones, not interested by existing line or market zone connections.

3.2.3. Scenario Analysis of Development Projects

The impact of the candidate project is assessed by means of a PINT approach, therefore each project is analyzed separately, as described in the following.

Differently from the determination of techno-economic benefits at target years according to defined evolution of system generation and demand, the proposed approach aims at determining the effect of the presence of development projects in the considered system through technical and economic merit indicators.

A first indicator is represented by the variation of total active power losses induced by the presence of the *x*-th candidate project. In order to perform this estimation, the energy market in (72)–(75) is solved accounting for the presence of the x-th development project, affecting the inputs of the boundaries of active power exchange P_l^{tie}, and the load flow analysis in (76)–(80) is carried out considering the influence of the *x*-th candidate project on the nodal admittance matrix $\boldsymbol{Y_x}$. Therefore, the global power system operation is varied in each t_k-th time step. The indicator I_x^L quantifies the energy losses reduction benefits, for the x-th

development project over N^T observation periods with duration τ, with respect to the base case network, and it can be expressed as follows:

$$I_x^L = \sum_{t_k=1}^{N^T} \sum_{j=1}^{N^L} \tau \, P_j^L(t_k) - \sum_{t_k=1}^{N^T} \sum_{j=1}^{N^L} \tau \, P_{j,x}^L \quad \forall \, x \in N^X \tag{87}$$

where, N^X is the total number of candidate development projects and x is the candidate project index, $P_{j,x}^L$ represents the j-th branch active losses in the presence of x-th candidate project.

Furthermore, in order to investigate the effect of the project on possible evolution of the generation and demand, and particularly on the attainment of targets for increased energy service for users and reduced environmental impact of power system, the considered power system is subject to increase of load demand and of renewable generation scenarios.

In the load increasing scenario, the load demand is increased by 1% for each iteration for each load bus in each time step. In order to ensure proper balance and avoid power shortage, the generation capacity is incremented uniformly, of the same amount. Therefore, for each load iteration λ the energy market in (72)–(75) and the load flow problem in (76)–(80) are solved with new input parameter of load demand $P_{b,\lambda}^D$ and maximum generation level $P_{i,\lambda}^{G,max}$ in the whole time horizon N^T, defined as follows:

$$P_{b,\lambda}^D(t_k) = (1 + 0.01 \cdot \lambda) \cdot P_b^D(t_k) \;\; \forall \, b = 1, \dots, N^B \tag{88}$$

$$P_{i,\lambda}^{G,max}(t_k) = (1 + 0.01 \cdot \lambda) \cdot P_i^{G,max}(t_k) \;\; \forall \, i = 1, \dots, N^G \tag{89}$$

where $P_i^{G,max}$ varies during the time for non-dispatchable RES (i.e., wind and solar).

At each λ-th load iteration, the branch loading $F_{j,\lambda}^L$ of each j-th branch in each t_k-th time step is determined. Moreover, If no overload is detected according to the adopted planning standard, i.e., (86) is satisfied, the procedure goes on to the next iteration, otherwise the procedure stops at a given iteration number λ_x, and the admissible demand increase (P_x^{DI}) in the network under the x-th candidate study is given by:

$$P_x^{DI} = \sum_{t_k=1}^{N^T} \sum_{b=1}^{N^B} \left[P_{b,\lambda_x}^D(t_k) - P_b^D(t_k) \right] = 0.01 \cdot \lambda_x \cdot \sum_{t_k=1}^{N^T} \sum_{b=1}^{N^B} P_b^D(t_k) \tag{90}$$

The load increase indicator of the x-th candidate project is therefore determined by difference between the result of the developed network (considering the input variation on $P_{l,x}^{ub}$, $P_{l,x}^{lb}$ and $\boldsymbol{Y_x}$ further than the scenario influence) and of the base case (subscript BC), as follows:

$$I_x^D = P_x^{DI} - P_{BC}^{DI} \tag{91}$$

In the renewable increasing scenario, the power generation amount by renewable-based generation technologies is increased by 1% for each ρ-th iteration in each time step. In this case, no intervention on power balance is operated, i.e., load demand and conventional power generation are not varied, since the aim is to investigate the effect of a growing renewable share in the power generation mix. Therefore, for each renewable iteration ρ the energy market in (72)–(75) is solved with new input parameter of maximum generation level $P_{i,\rho}^{G,max}$ applied to the i-th renewable generator (in the subset Ω_{ndg} of non-dispatchable RES generators, in number $N^{NDG} < N^G$) defined as follows:

$$P_{i,\rho}^{G,max}(t_k) = (1 + 0.01 \cdot \rho) \cdot P_i^{G,max}(t_k) \;\; \forall\, i \in \Omega_{ndg} \tag{92}$$

According to energy market results, giving different production levels for all generators $P_{i,\rho}^G$ due to a new equilibrium point, the load flow analysis (76)–(80) is carried out.

At each ρ-th renewable iteration, the branch loading $F_{j,\rho}^L$ of each j-th branch in each t_k-th time step is determined. If no overload is detected according to the adopted planning standard, i.e., condition (86) is satisfied, the procedure goes on to the next iteration, otherwise the procedure stops at a given iteration number ρ_x, and the admissible renewable generation increase (P_x^{RI}) in the network under study is given by:

$$P_x^{RI} = \sum_{t_k=1}^{N^T} \sum_{i \in \Omega_R} \left[P_{i,\rho_x}^G(t_k) - P_i^G(t_k) \right] \tag{93}$$

The renewable generation increase indicator of the x-th candidate project is therefore determined by difference between the result of the developed network (considering the input

variation on $P_{l,x}^{ub}$, $P_{l,x}^{lb}$ and $\boldsymbol{Y_x}$ further than the scenario influence) and of the base case, as follows:

$$I_x^R = P_x^{RI} - P_{BC}^{RI} \tag{94}$$

A representation of the technical merit indicator determination process is depicted in the flowchart reported in Fig. 27. It can be noted that the method involves the storage of network operation analysis under different conditions and in the presence/absence of development project, therefore a specific calculation framework is necessary in order to collect the necessary information.

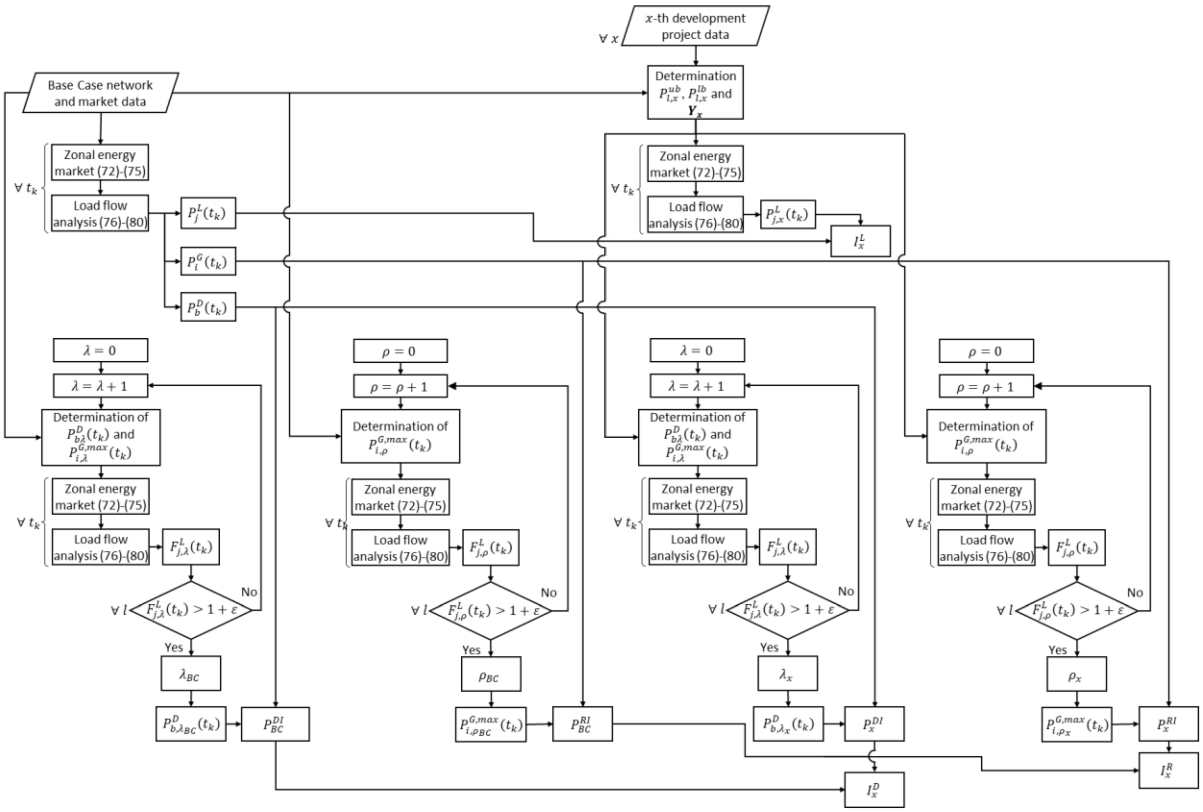

Fig. 27. Flowchart representation of the determination of technical merit indicators of the x-th development project (right), as compared to the base case (left).

Finally, in order to account for economic implications, an estimation of the investment cost IC_x of the x-th candidate project is carried out, according to standard building and installation cost for the single components.

3.2.4. Project Comparison and Selection

As highlighted in the methodology, the three technical merit indicators, plus the economic one, although referring to comparable units, measured as energy amounts over a given

time horizon, are determined according to different operating conditions and evolution frameworks of the system under study. Therefore, in order to carry out a proper comparison among the outcomes of the analysis of candidate projects, Analytic Hierarchy Process (AHP) is adopted [220], [221].

The AHP is based on the determination, for each h-th criterion evaluated for n options, of the $n \times n$ pairwise comparison matrix $\boldsymbol{C}_h$, whose element $c_{h_{i,j}}$ represents the prevalence of the i-th option compared to the j-th one. If the i-th option is preferred to the j-th one, then $c_{h_{i,j}} > 1$, in a scale of values up to 9 according to importance comparison; for equal importance it is $c_{h_{i,j}} = 1$; moreover, the following reciprocal constraint applies:

$$c_{h_{i,j}} \cdot c_{h_{j,i}} = 1 \quad \forall\, c_{h_{i,j}} \in \boldsymbol{C}_h \tag{95}$$

Once the matrix $\boldsymbol{C}_h$ is built, its normalized version $\boldsymbol{C}_h^N$ by column is obtained, and its elements are determined as follows:

$$c_{h_{i,j}}^N = \frac{c_{h_{i,j}}}{\sum_{i=1}^{n} c_{h_{i,j}}} \quad \forall\, c_{h_{i,j}} \in \boldsymbol{C}_h \tag{96}$$

By averaging the entries of each row of $\boldsymbol{C}_h^N$, the $n \times 1$ score vector $\boldsymbol{s}_h$ for the h-th criterion is determined:

$$s_{h_i} = \frac{\sum_{j=1}^{n} c_{h_{i,j}}^N}{n} \quad \forall\, i = 1, \dots, n \tag{97}$$

By padding the vectors $\boldsymbol{s}_h$ by columns, the $n \times m$ score matrix $\boldsymbol{S}$ is obtained:

$$\boldsymbol{S} = [\boldsymbol{s}_1 \dots \quad \boldsymbol{s}_h \dots \quad \boldsymbol{s}_m] \tag{98}$$

Proceeding in the same way, the $m \times m$ pairwise comparison matrix $\boldsymbol{A}$ of the m criteria is determined, in which the element $a_{h,f}$ represents the prevalence of the h-th criterion compared to the f-th one. Applying the same normalization and averaging process described in Equations (95) and (96), the $m \times 1$ criteria weight vector $\boldsymbol{w}$ is determined.

The $n \times 1$ vector of global scores $\boldsymbol{gs}$ is therefore determined by the following matrix operation, where the element gs_i represents the global score assigned by the AHP to the i-th option.

$$\boldsymbol{gs} = \boldsymbol{S} \cdot \boldsymbol{w} \tag{99}$$

For the application to the proposed framework, the candidate projects represent the generic n options, whereas the three indicators I_x^L, I_x^D and I_x^R represent the m criteria.

In addition, the consistency check is performed on pairwise comparison matrices. Taking $\boldsymbol{A}$ as a reference, the consistency index is determined as follows:

$$C^I = \frac{aa - m}{m - 1} \tag{100}$$

where the first term aa is a scalar determined as the average of the elements of the vector obtained by multiplying the rows of $\boldsymbol{A}$ by $\boldsymbol{w}$ and dividing by the corresponding element of $\boldsymbol{w}$:

$$aa = \frac{1}{m} \cdot \sum_{h=1}^{m} \frac{\boldsymbol{a}_h \cdot \boldsymbol{w}}{w_h} \tag{101}$$

The consistency ratio C^R is therefore determined as C^I/R^I where the random index R^I is determined as the average C^I when elements of $\boldsymbol{A}$ are random. It is considered that the consistency is acceptable if $C^R < 0.1$.

3.3 Modified version of IEEE 118-Bus Test System

The proposed methodologies are applied to a modified version of the IEEE 118-bus system, called NREL 118-bus test system, shown in Fig. 28. Yearly generator and load data of the system are reported in [211], [212], divided by hours, therefore τ = 1 h and N_T = 8760. The test system presents a total installed production capacity of 40.5 GW distributed among 327 generators, subdivided among the three zones as reported in Table 10. The installed generation capacity in the Zones 1, 2 and 3 (Z1, Z2 and Z3, respectively) are equal to 26.0%, 48.6% and 25.5% respectively. More than 68% of installed generation capacity is based on natural gas, with combined cycles (CC), combustion turbines (CT) and steam turbines (ST) while non-dispatchable renewables (PV and wind) represent 18.4% of installed capacity. Thermoelectric plants are remarkably present in Z1, whereas Z2 includes hydroelectric power plants up to 85%, and the highest renewable penetration is in Z3 with 30%. Moreover, 21.3% is covered by programmable renewables—mainly hydroelectric in Z2—and 36.2% is represented by photovoltaic, wind—with higher share in Z3—and hydro generators.

Table 10. Zonal installed capacity by technology [MW].

Technology	Number of Generators				Installed capacity [MW]			
	Z1	***Z2***	***Z3***	***Tot***	***Z1***	***Z2***	***Zone 3***	***Tot***
CC gas	19	7	12	38	5,812.1	1,743.9	3,436.1	10,992.1
CT gas	24	7	35	66	1,356.3	374.5	1,549.3	3,280.1
CT oil	3	2		5	223.5	142.4	0.0	365.9
ICE gas		6	1	7	0.0	50.4	3.3	53.7
ST coal	1			1	20.0	0.0	0.0	20.0
ST gas	5		5	10	1,482.2	0.0	978.4	2,460.6
ST other	2			2	35.0	0.0	0.0	35.0
Biomass	32	4	23	59	58.2	16.5	40.2	114.9
Geothermal		1		1	0.0	22.0	0.0	22.0
Hydro prog.		18	1	15	0.0	8,383.6	110.0	8,493.6
Hydro non-disp.	1	18	5	28	0.8	8,506.4	1,649.5	10,156.7
Wind	33	5	37	75	329.0	0.0	749.0	1,078.0
Photovoltaic	132	78	117	327	1,206.0	444.4	1,795.4	3,445.8
Total	zone 1	zone 2	zone 3	Total	10,523.1	19,684.1	10,311.2	40,518.4

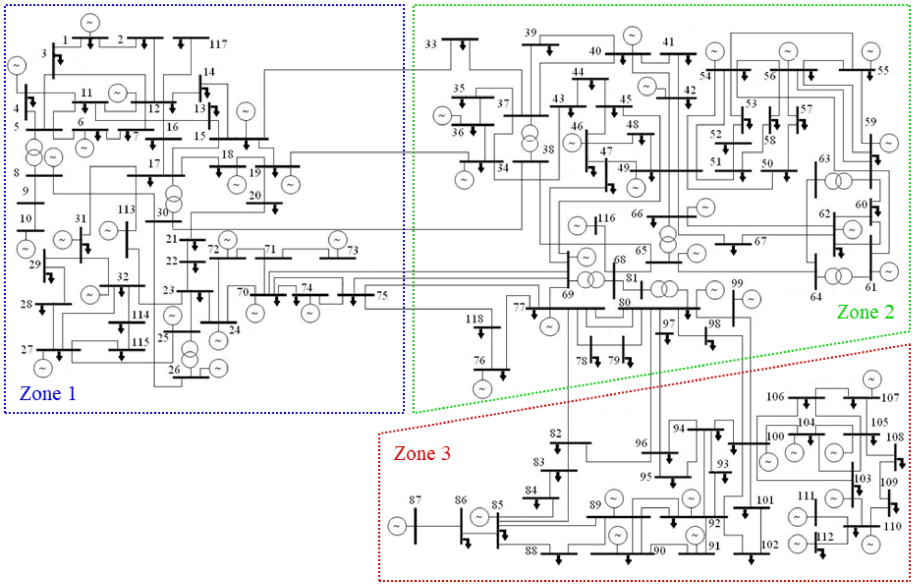

Fig. 28. NREL 118-bus test system with the zonal subdivision.

Minimum and maximum bid prices for fuel-based plants (thermoelectric and biomass) are reported in Table 11, gathered by technology. It can be seen that most of gas-based production has a production cost lower than 30 $/MWh, comparable with biomass, whereas oil-based technology is the less competitive. The parameters Λ and $voll$, present in (45) and (63) respectively, are set to 3,000 €/MWh, well higher than maximum generation bid, and corresponding to average sensibility to interruptions in European framework [222]. Further, the redispatching costs c_i^+ and c_i^- of (61) are estimated at 3 and 2 times maximum power bid of

the i-th generator ($c_{i,N}s$), respectively, according to observed values for reserve bids in Italian ancillary service market [223].

Total yearly demand sums up to 95.95 TWh, whereas the load value ranges from minimum 7.23 GW to maximum 17.29 GW. Load distribution among zones shows that Zone 1 (Z1) has the highest share, between 43.3% and 63.5%, with higher values in winter and lower in summer, whereas Zone 2 (Z2) and Zone 3 have 13.4÷30.6% and 19.4÷33.9% of load respectively. In Fig. 29 a representation of load trend for the days with lowest and highest total load level is reported with the respective zonal distribution. Finally, transfer capacities are equal to 6400 MW between Z1 and Z2 and 3100 MW between Z2 and Z3.

The subdivision of load demand among buses is determined according to fixed ratio provided in [212] not reported for purpose of brevity. For the same reason, the network data for load flow analysis can be found in the database [212].

Table 11. Generation bid price range [$/MWh].

Technology	Minimum	Maximum
CC gas	12.94 ÷ 28.11	27.80 ÷ 66.34
CT gas	15.02 ÷ 28.31	30.22 ÷ 71.49
CT oil	104.72 ÷ 109.32	257.97 ÷ 264.32
ICE gas	21.26 ÷ 21.39	42.52 ÷ 42.78
ST coal	9.15	20.72
ST gas	11.56 ÷ 26.48	23.12 ÷ 64.98
ST other	15.11 ÷ 124.10	30.22 ÷ 290.11
Biomass	12.47 ÷ 16.62	28.45 ÷ 33.24

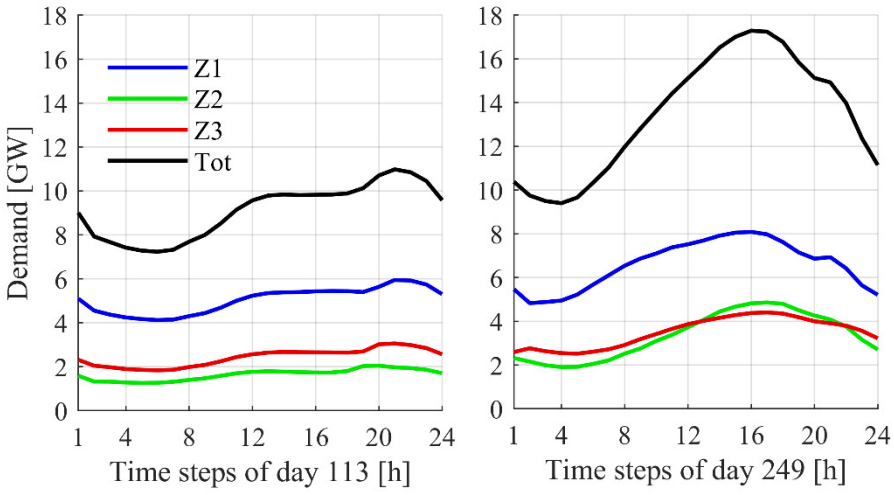

Fig. 29. Trends of zonal demand in lowest load day 113 and highest load day 249.

As regards non-dispatchable renewable generation, the contribution reported in [212] amounts to 2,700 TWh, 7,698 TWh and 2,564 TWh for wind, solar and non-dispatchable hydro, respectively. Correspondently, equivalent yearly duration of 2,505 h, 2,234 h and 253 h for wind, solar and non-dispatchable hydro, respectively is considered. The yearly duration curves are reported in Fig. 30, where it can be seen that wind and hydro show a smooth variation over time, and they do not reach null contribution in any condition, whereas solar power is working for half of total hours, as expectable.

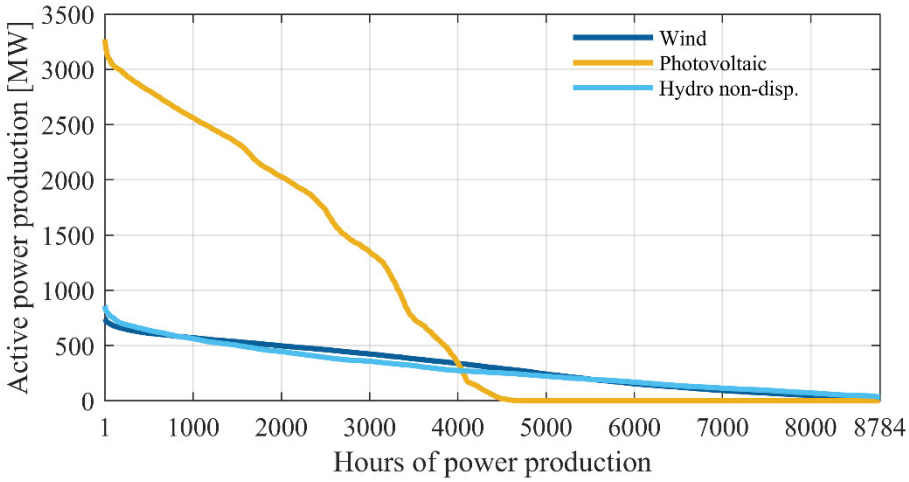

Fig. 30. Duration curves of non-dispatchable renewable production.

3.4 Result Analyses

3.4.1. Flow-Based results

The MATLAB environment is exploited to perform numeric simulations. In particular, zonal market relations are solved by building a proper optimization procedure exploiting *intlinprog* function in the optimization toolbox, whereas the load flow analysis is performed by means of the MATPOWER package [224]. From market analysis in Reference Scenario, it is obtained that zonal exchange limit is attained only from Z3 to Z2 in 41 hours. Therefore, the network development project from Evolution Scenario is selected as the doubling of branch 159, between buses 99 and 100, connecting Z2 with Z3. This allows an increase of transfer capacity between the two zones by 600 MW. Results of market analysis in Reference and Evolution Scenarios are reported in Fig. 31. A slight reduction of average unified price is observed from 24.31 $/MWh to 24.25 $/MWh, although extreme values keep similar. From Table 12, it can be noted that in the Evolution Scenario the occurrences of bounded exchange limits on the border between Zone 2 and Zone 3 is reduced. Yields of social welfare

components, given in Table 13, show that Evolution Scenario implies a strong increase of user surplus and an expected decrease of congestion rent.

Dealing with steady-state network study, the yearly amount of losses is 4816.68 GWh in the Reference Scenario, representing roughly 5% of total yearly load. A 0.06% reduction of losses is obtained in Evolution Scenario, attaining 4815.44 GWh. Moreover, 1918 hourly conditions with at least one overload are observed in Reference Scenario, reducing to 1916 in Evolution Scenario.

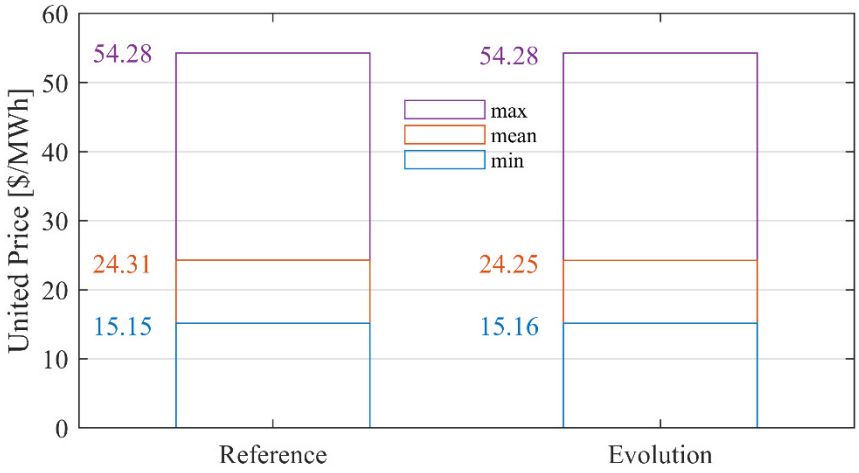

Fig. 31. Unified price: results obtained on yearly horizon.

Table 12. Occurrences of bounded zonal exchange.

Border	**Reference**		**Evolution**	
	Direct	***Reverse***	***Direct***	***Reverse***
Z1–Z2	0	0	0	0
Z2–Z3	0	41	0	3

Table 13. Yearly social welfare components [M$].

Components	***Reference***	***Evolution***
Producer Surplus	392.840	392.858
User Surplus	77679.055	77684.072
Congestion Rent	0.137	0.015
YSW	78072.032	78076.934

Security-aimed redispatching is described in Table 14 and Table 15 in Reference and Evolution Scenarios, respectively. Globally, two lines with total three maximum overloads are detected in Reference Scenario, one in Z1 and the other across Z1 and Z2. Four lines with five maximum overloads are detected in Evolution Scenario, affecting the connection

between Z2 and Z3 as well. Renewables are not affected by any curtailment, whereas dispatchable generators are highly exploited. Moreover, generation and load variations show a reduction by roughly 20% in the Evolution Scenario. Yearly amounts of redispatched energy are reported in Table VII. It can be noted that the total redispatched quantities in Reference Scenario sum up to 0.36% of yearly demand, reducing to 0.29% in Evolution Scenario.

Table 14. Redispatching results of Reference Scenario.

Branch j^*	37	54	54
From-to	8-30	30-38	30-38
$OL_{j^*}^+$, $OL_{j^*}^-$ [p.u.]	-0.2057	1.2290	-0.2920
$t_{j^*}^+$, $t_{j^*}^-$	3876	5994	3396
$\tau_{j^*}^+$, $\tau_{j^*}^-$ [h]	13.93	335.14	6.86
total ΔP_{dis}^+ [MW]	0	1015.6	0
total ΔP_{dis}^- [MW]	152.8	1015.6	1747.7
total ΔP_{ndg}^- [MW]	0	0	0
total ΔP_{loa}^- [MW]	152.8	0	1747.7

Table 15. Redispatching results of Evolution Scenario.

Branch j^*	37	41	54	54	128
From-to	8-30	23-32	30-38	30-38	77-82
$OL_{j^*}^+$, $OL_{j^*}^-$ [p.u.]	-0.2065	0.0106	1.2290	-0.2921	-0.0547
$t_{j^*}^+$, $t_{j^*}^-$	2364	8454	5994	3396	3954
$\tau_{j^*}^+$, $\tau_{j^*}^-$ [h]	11.165	1	267.49	5.524	1
total ΔP_{dis}^+ [MW]	0	62.6	1015.6	0	0
total ΔP_{dis}^- [MW]	153.44	62.6	1015.6	1748.3	128.4
total ΔP_{ndg}^- [MW]	0	0	0	0	0
total ΔP_{loa}^- [MW]	153.44	0	0	1748.3	128.4

Table 16. Yearly results of security-aimed redispatching [GWh].

Resource	**Reference**	**Evolution**
Dispatchable generator increase	340.37	271.72
Dispatchable generator decrease	354.49	283.22
Renewable curtailment	0.00	0.00
Load curtailment	14.12	11.50

The variation of yearly economic indicators between Reference and Evolution Scenarios, giving out total benefit of the analyzed project, are represented in Fig. 32. It can be noted that the total yearly economic benefit YPB is equal to 18.21 M$, and almost 43% is given by the reduction of load curtailment, whereas roughly 28% is due to generation redispatching, 27% is obtained by social welfare, and less than 2% is related to losses.

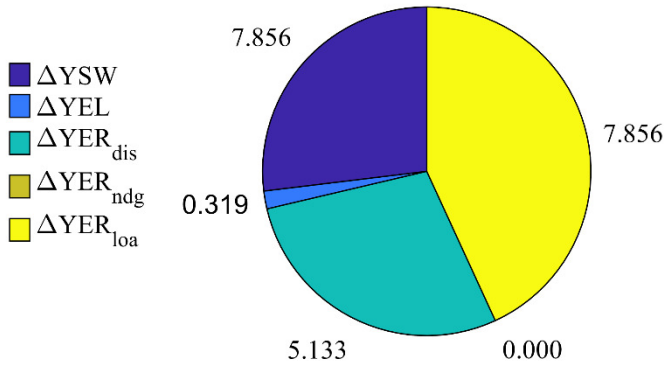

Fig. 32. Variations of economic indicators for the analyzed project [M$].

For investment analysis, it is assumed that the analyzed year is representative of all years in the horizon, hence YPB keeps the same throughout the time horizon. The network development investment cost is determined from line length, individuated at 50 km according to resistance and reactance values per km [225], and taking average installation costs for 138 kV lines with comparable rating at 450 k$/km from[226]. Therefore, for a four-circuit line, a total investment IC =90.2 M$ is determined. By fixing $\alpha = 0.05$ and $FC = 0.01 \cdot IC$, i.e. 900 k€/year, the trend of NPV over years is reported in Fig. 33. It can be noted that investment payback occurs at 6.2 years, and at the end of 20-years horizon NPV = 125.5 M€.

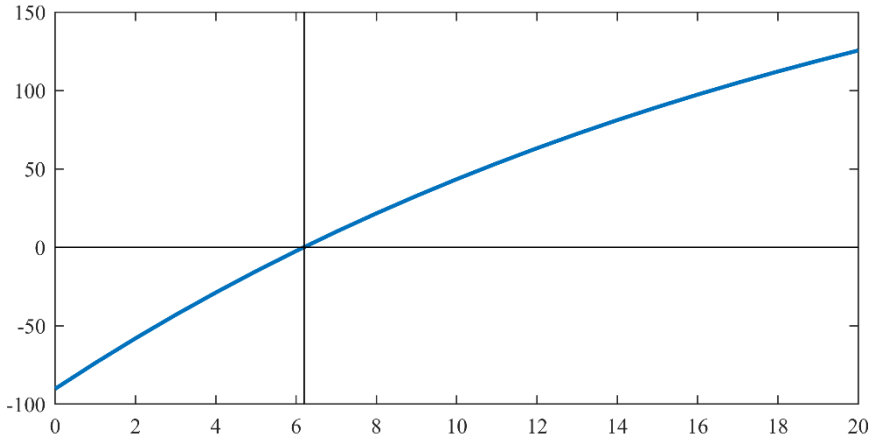

Fig. 33. Net present value trend for the analyzed project.

3.4.2. AHP results

For the scope of zonal market analysis, transfer capacities are assumed equal to the capacity of the set of connection lines; therefore, $P_l^{ub} = P_l^{lb}$ is equal to 6,400 MW between Z1 and Z2, whereas for the boundary Z2-Z3 it has been supposed a lower ATC of 400 MW, therefore P_l^{ub} is 2,700 MW, being the most critical one. Fig. 34 shows the NREL 118-bus

system where the candidate projects are represented by colored lines in the scheme and they are described in the next subsection.

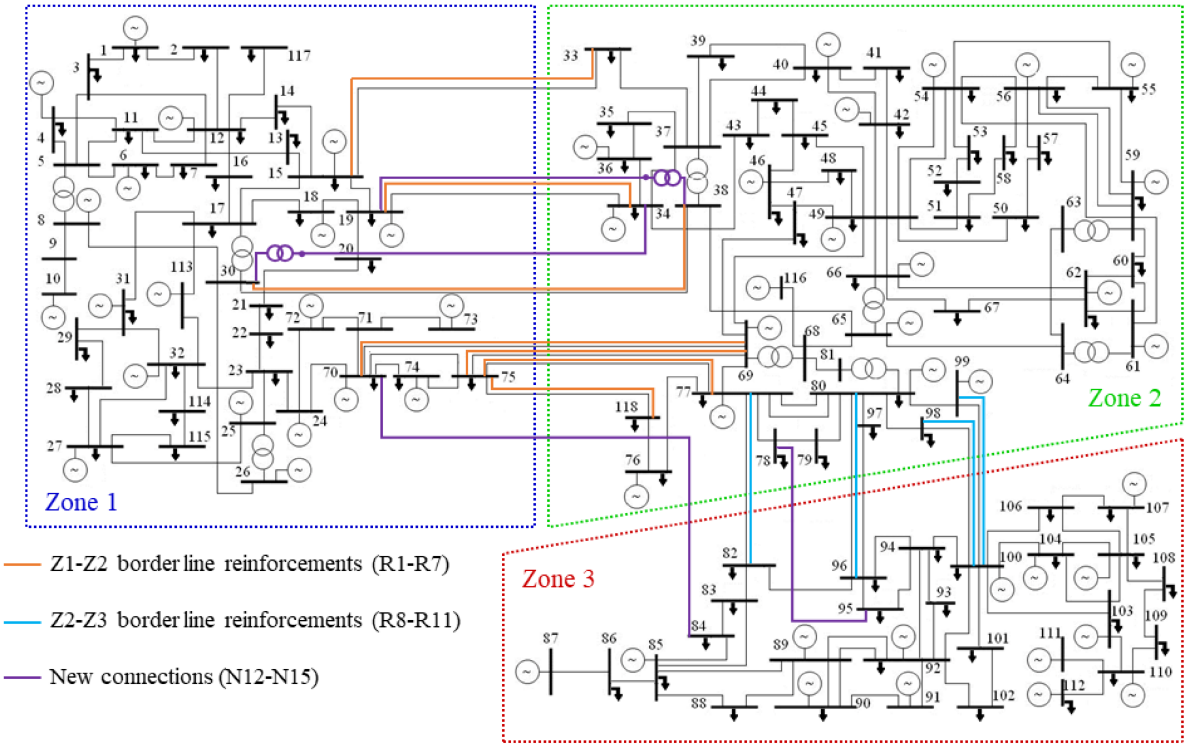

*Fig. 34. **T**he NREL-118 network single-line diagram, reporting with colors the candidate projects for network reinforcements analyzed in the following.*

In order to carry out load flow analysis, the distributed slack is fixed at buses 25, 70, 72 and 107, hosting only conventional power plants with remarkable installed size, according to availability of the plant and to generation level margin. Moreover, it is assumed that all other 55 buses with at least one generator behave as voltage-controlled (PV) buses, considering that even photovoltaic and wind generators are more and more called to take part to voltage/reactive regulation by system operator connection standards [227], [228], and in these buses, voltage levels are fixed at 1.00 p.u. Moreover, according to planning standard of Italian Transmission System Operator, the margin ε to evaluate a line overload considering planning viewpoint is fixed at 0.2, i.e., no overload would be detected until the power flow level is below 120% of line rating [229], [230].

Numerical simulations are also performed using the MATLAB software. The *quadprog* optimization toolbox function has been utilized to solve the electricity market, and MATPOWER has been employed for load flow analysis as well. The determination of merit indicators exploits an iterative framework developed in MATLAB including the previously

mentioned tools. It should be noted that the zonal market and load flow analysis over the yearly time horizon for a single network configuration takes roughly 3 minutes to be solved on an ASUS VivoBook Pro: Processor Intel i7-8750 H, CPU 2.20 GHz 6 Core(s), RAM 16 GB.

A) Base case Network Operation

The application of energy market model to the test system in the base conditions leads to the results synthesized in Fig. 35 in terms of duration curve of zonal active power balance, where the represented values represent the power exchange of each zone. It can be seen that Z3 is always exporting power, having a higher generation excess in winter, and reaching in 6 hours the power exchange limit with Z2. On the contrary, Z1 results an energy importer for most of the analyzed period, with minimum exchange of −2,361.4 MW, well within Z1–Z2 boundaries, albeit it behaves as exporter for 270 hours, especially during summer, reaching maximum exchange of 1,381.0 MW. Finally, Z2 net exchange ranges between 547.3 MW and −2,075.1 MW, and net import is observed for 780 conditions.

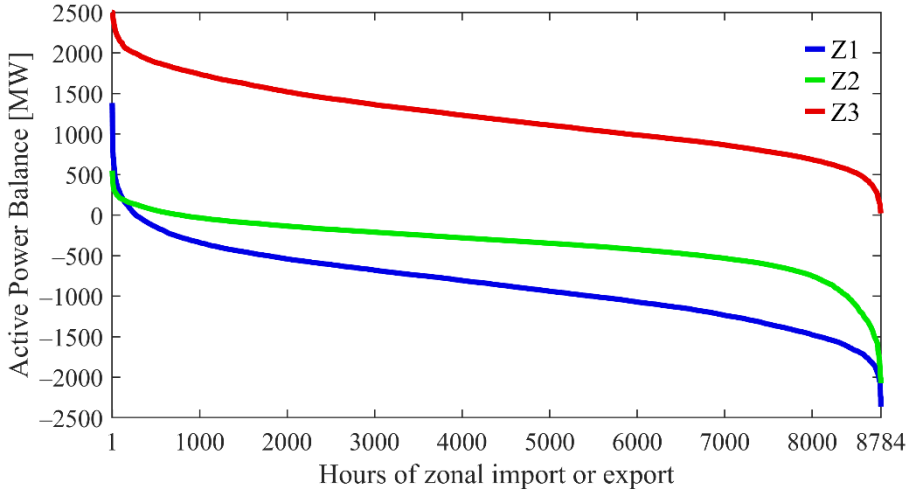

Fig. 35. Duration curve of net power exchange of each zone in energy market analysis for base case network.

As regards steady-state network behaviors and subsequent line loading evaluation by (84)–(86), the analysis of lines at zone boundaries is synthesized in Fig. 36 and Fig. 37 in terms of average loading and duration curve, respectively. It can be observed that boundary lines are, on average, interested by more stressful flow levels as compared to internal lines within each zone, and lines across Z2–Z3 boundary are highly exploited, with line 99–100 reaching the maximum F_j^L of 107%, well within the overload limit of 120%. This branch is

the one on which the flow-based cost-benefit analysis methodology carried out in the previous methodology was focused.

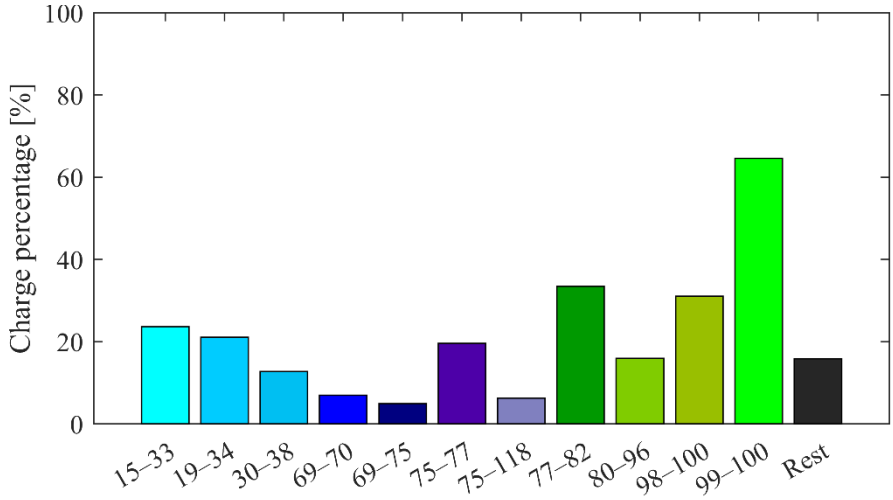

Fig. 36. Yearly mean charge percentage of the candidate branches and of the hourly charge percentage mean of the other network branches (Rest).

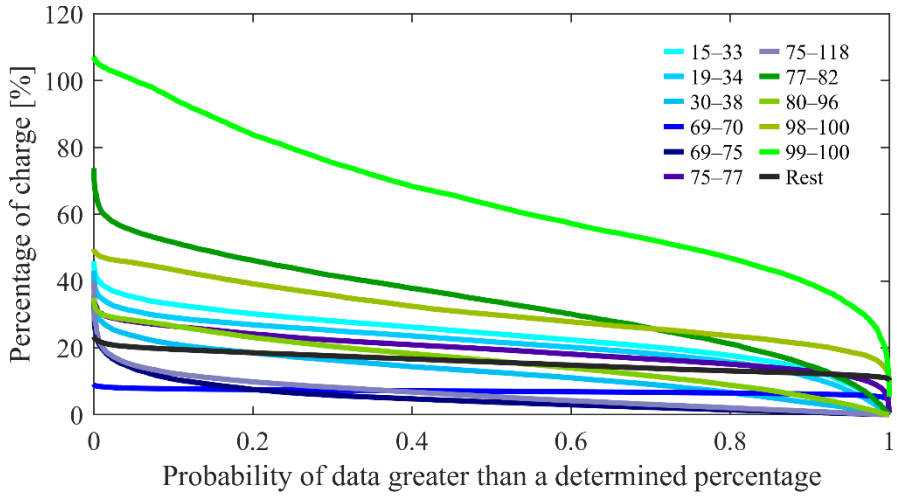

Fig. 37. Probability duration curves of candidate branches and of the hourly charge percentage mean of the other network branches (Rest).

Finally, the total losses are determined, corresponding to 3,431.8 GWh, i.e., roughly 3.57% of total load demand, and in Table 17 minimum and maximum observed values of voltage magnitude (V_M) are reported, in terms of average value over the whole time horizon for each bus and of extreme values attained in a single occurrence. It can be observed that feasible operation values are obtained, keeping in a range of ±11% of nominal voltage.

Table 17. Extreme values of average and absolute observed voltage magnitudes.

Value	Extreme	V_M [p.u.]	Bus
average	minimum	0.967	81

	maximum	1.071	72
absolute	minimum	0.944	95
	maximum	1.109	107

B) Scenario Analysis and Evaluation of Indicators

As explicated in the previous section, the first choice of candidate projects is devoted to the reinforcement of the existing lines across zone borders. In particular, a doubling of existing 11 border lines is considered, numbered from R1 to R11, and relevant characteristics are reported in Table 18. It can be observed that the projects have different impact on electric parameters as well as on energy market exchange level between interested zones.

Table 18. Characteristics of candidate projects of existing line reinforcements.

Candidate Project ID	Nodes	r [p.u.]	x [p.u.]	b [p.u.]	$P^{F}_{R_{j,x}}$ [MW]	Zones	$P^{ub}_{l,x}$ [MW]
R1	15–33	0.00543	0.01777	0.22358	+600	Z1–Z2	7,000
R2	19–34	0.01074	0.03529	0.4424	+600	Z1–Z2	7,000
R3	30–38	0.00066	0.00771	2.954	+600	Z1–Z2	7,000
R4	69–70	0.00032	0.05879	0.71386	+1700	Z1–Z2	8,100
R5	69–75	0.00611	0.02014	0.252	+1700	Z1–Z2	8,100
R6	75–77	0.00441	0.01443	0.7266	+600	Z1–Z2	7,000
R7	75–118	0.00426	0.01219	0.57218	+600	Z1–Z2	7,000
R8	77–82	0.00509	0.026	0.3458	+700	Z2–Z3	3,400
R9	80–96	0.00567	0.02557	0.3332	+600	Z2–Z3	3,300
R10	98–100	0.00257	0.01161	0.1512	+600	Z2–Z3	3,300
R11	99–100	0.00207	0.00687	0.08386	+800	Z2–Z3	3,500

In addition, the presence of further 4 lines creating new connection between nodes of different zones are individuated. In order to define their electric parameters, a reference path of existing lines is followed, and the relevant total impedance is reduced by a defined value in order to account for possible path savings. The features of these new connections, numbered from N12 to N15, are synthesized in Table 19. It can be noted that the projects N12 and N13 involve a transformer doubling and a new line—where path saving assumptions are applied—in order to increase the meshing of the higher voltage section across zones Z1 and Z2, that in the base case involves lines 8–30, 26–30, 30–38, 38–65, 65–68, 68–81. Moreover, the project N15 creates a new zonal connection between Z1 and Z3, not present in all other configurations, therefore a remarkable variation of market equilibrium is expected.

Moreover, due to the bottleneck created by a single connection across zones, its contribution to market exchange level is considered equal to its rated power flow.

Table 19. Characteristics of candidate project for new line connections.

Candidate Project ID	Nodes	Reference Path	Length Reduction	r [p.u.]	x [p.u.]	b [p.u.]	$P^F_{R_{j,x}}$ [MW]	Zones	$P^{ub}_{l,x}$ [MW]
N12	19–38	19–34; 34–37; 37–38	30%	0.01918	0.06258	0.09450	+600	Z1–Z2	7,000
N13	30–34	30–17; 17–18; 18–19; 19–34	30%	0.00811	0.03182	0.09450	+600	Z1–Z2	7,000
N14	78–95	78–77; 77–82; 82–96; 96–95	30%	0.01361	0.04882	0.07560	+600	Z2–Z3	3,300
N15	70–84	70–75; 75–77; 77–82; 82–83; 83–84	30%	0.01749	0.04769	0.32469	+1200	Z1–Z3	1,200

As prospected in the paragraph 3.2.3, the performance analysis of candidate project starts from the determination of total active power losses over the considered year of operation. The evaluation of the indicator I_x^L is reported in the second column of Table 20, and it can be noted that the most favorable effect is attained in the presence of R11 project, giving a 2.0% reduction of total losses, whereas R9 project implies negligible advantage with respect to the base case.

Table 20. Results of merit indicators evaluation for the candidate projects.

Candidate Project ID	I_x^L [MWh]	I_x^D [MWh]	λ_x	Limiting Overload in Load Increase	I_x^R [MWh]	ρ_x	Limiting Overload in Renew. Increase	IC_x [M€]
R1	16,305	1,921	6	30–38	13,868	415	77–82	232.8
R2	30,936	3,840	8	30–38	13,868	415	77–82	462.3
R3	39,077	52,814	59	99–100	13,868	415	77–82	170.6
R4	39,539	4,801	9	30–38	13,868	415	77–82	650.4
R5	43,054	3,840	8	30–38	13,868	415	77–82	222.8
R6	52,637	3,840	8	30–38	13,014	395	77–82	189.0
R7	31,207	3,840	8	30–38	13,014	395	77–82	159.7
R8	9,673	0	4	30–38	15,788	460	75–77	340.6
R9	98	0	4	30–38	0	90	75–77	335.0
R10	25,449	0	4	30–38	3,414	170	75–77	152.1
R11	69,378	960	5	30–38	14,079	420	75–77	90.0
N12	33,644	1,921	6	30–38	13,868	415	77–82	607.7
N13	8,008	44,171	50	99–100	13,868	415	77–82	348.8
N14	25,024	0	4	30–38	4,694	200	75–77	639.6
N15	44,773	0	4	30–38	8,961	300	75–77	624.8

The determination of admissible load increase in the base case results in the procedure stop at iteration λ_{BC} = 4, therefore only 4% of load increase (3,841 GWh roughly) results admissible in the base case network configuration, being the line between nodes 30–38 the first to experience an overload. The evaluation of the indicator I_x^D is reported in the third column of Table 20, and in the fourth one the corresponding λ_x is reported, whereas in the fifth the limiting overloaded line is pointed out. It can be noted that a set of projects (R8, R9, R10, N14 and N15) do not provide remarkable advancement with respect to the Base Case, and many other cases imply a further admissible increase by less than 6% of load demand, being the line 30–38 the limiting overload as well. In R3 and N13, intervening on line 30–38 or in its surroundings, the load increase is higher than 45% and the limiting overload moves to line 99–100.

The determination of admissible renewable generation increase in the base case results in the procedure stop at iteration $\rho_{BC} = 90$, therefore 90% of renewable generation increase (3,840 GWh roughly, closely related to load increase) results admissible in the base case network configuration. In the base case, the limiting overload is observed on the line between nodes 77–82 due to the different distribution of renewable generators with respect to load. The evaluation of the indicator I_x^R, of the corresponding ρ_x and of the limiting overloaded line is illustrated in seventh, eighth and ninth columns of Table 20. It can be seen that all the projects affecting the Z1–Z2 border overcomes 300% of further increase, with the maximum of R8 project equal to global 460% of increase, with limiting overload between nodes 77–82 (Z2–Z3). On the contrary, for projects on Z2–Z3 border or on new Z1–Z3 connection, the limiting overload is for the line between nodes 75–77 (Z1–Z2) but the impact is variable, from no advantage in R9 to levels in R11, N12 and N13 comparable with those of Z1–Z2 lines.

The estimation of investment cost IC_x is reported in the last column of Table 4. Analogously to the results of the other proposed method, the estimation is based on average installation costs for overhead lines [226], considering the different voltage values and flow ratings and determining line length according to typical resistance and reactance values per unit length, whereas for high voltage self-transformers of suitable power ratings the cost estimation is taken from [231]. It can be noted that project R11 is the one with the lowest economic effort, that is considerably higher for R4, interesting a high-rating long line, for

N12 due to mixed voltage level with considerable length, and for N14 and N15 due to the presence of long paths.

C) Selection of Projects

The AHP process explicated in paragraph 3.2.4 is therefore applied to the obtained merit indicators. Since the indicators are all represented by numeric factors (all measured in GWh) in order to determine the pairwise comparison matrix $\boldsymbol{C}_h$ of options, for each pair of candidate projects the difference between the indicators is performed, assigning preference levels from 1 to 9 according to the inclusion in intervals defined in Table 21. This method is applied only if the index of x-th candidate project is not lower than the index of the compared χ-th project, since the reciprocal case has to comply with the constraint in (95). It should be noted that for the investment cost index, the difference is inverted, since in this case the lower the better, differently from technical merit indicators.

Table 21. Thresholds for preference levels in AHP according to values of difference of index between x-th and χ-th candidate project.

AHP level	$I_x^L - I_\chi^L$	$I_x^D - I_\chi^D$	$I_x^R - I_\chi^R$	$C_\chi^I - C_x^I$
1	[0 ; 1,000)	[0 ; 750)	[0 ; 200)	[0 ; 5)
2	[1,000 ; 3,000)	[750 ; 1,500)	[200 ; 1,000)	[5 ; 40)
3	[3,000 ; 9,000)	[1,500 ; 3,000)	[1,000 ; 2,500)	[40 ; 80)
4	[9,000 ; 18,000)	[3,000 ; 5,000)	[2,500 ; 5,000)	[80 ; 180)
5	[18,000 ; 30,000)	[5,000 ; 10,000)	[5,000 ; 8,000)	[180 ; 300)
6	[30,000 ; 40,000)	[10,000 ; 40,000)	[8,000 ; 11,000)	[300 ; 400)
7	[40,000 ; 50,000)	[40,000 ; 49,000)	[11,000 ; 13,500)	[400 ; 450)
8	[50,000 ; 60,000)	[49,000 ; 51,000)	[13,500 ; 14,000)	[450 ; 530)
9	≥60,000	≥51,000	≥14,000	≥530

The outcomes of the consistency test on each matrix is therefore reported in Table 22, where the R^I value of 1.58 for a 15×15 pairwise comparison matrix is exploited, as can be found in [232], [233], It can be seen that consistency level is acceptable for all the three indices, being C^R<0.1 in all cases. The corresponding values of the score matrix $\boldsymbol{S}$ are graphically represented in Fig. 38. It can be observed that, as expectable, candidate projects R11, R6 and N15 show good performances for losses, projects R3, N13 and R4 for demand increase, projects R8 and R11 for renewable increase, and projects R11, R10 and R7 for economic effort. Moreover, by posing a selection threshold of 1/15 = 0.06667, that would be the value of scoring if all projects had the same importance, it can be seen that a number of 6, 3,

9 and 7 projects would pass the threshold for the four criteria, respectively. It can be further observed that R3 passes the threshold in all four indicators, whereas R5 and R11 in three out of four, and R9 and N14 do not show positive performance in all four analyzed aspects.

Table 22. Consistency analysis of the AHP matrices for each index of the candidate projects.

Parameter	$I_x^L - I_\chi^L$	$I_x^D - I_\chi^D$	$I_x^R - I_\chi^R$	$C_\chi^I - C_x^I$
n	15	15	15	15
aa	17.124	16.063	15.892	16.918
C^I	0.1517	0.0759	0.0637	0.137
R^I	1.58	1.58	1.58	1.58
C^R	0.096	0.0481	0.0403	0.0867

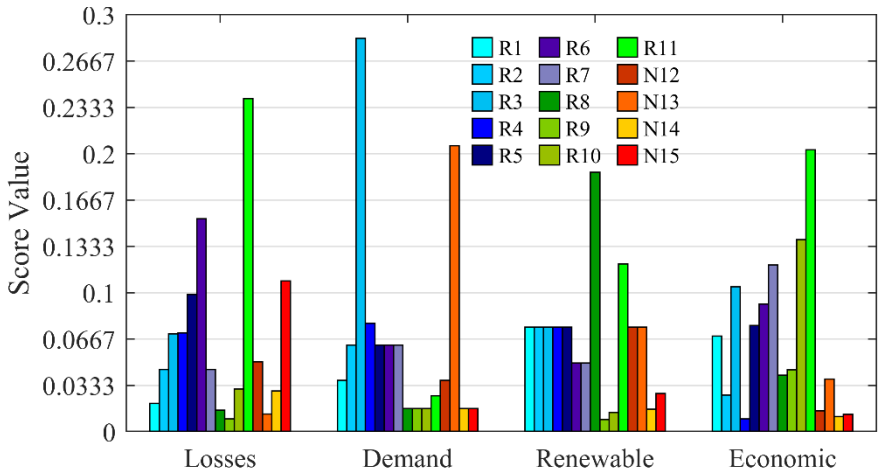

Fig. 38. Graphical representation of score values by column (criteria).

In order to determine the criteria weight vector $\boldsymbol{w}$, a set of different hypotheses has been applied, thus obtaining different estimations. A first assumption is that of equal importance for the three technical indices (Case EIT), giving a vector of equal weight values of 1/3. Therefore, a "slightly more importance" level is assigned to one index per time, thus considering $a_{h,f}$ = 3 for the selected index h, with the aim to investigate the validity of the prevalence of one criterion to the others (Cases LD—losses dominance, DD—demand dominance, RD—renewable dominance). Moreover, assuming the viewpoint of a power system planner aiming at facing the challenges of energetic evolution given by the integration of increasing greener generation with an additional insight to power demand, a dominance level 3 is assigned to renewable increase with respect to losses, and a dominance level 2 is assigned to renewable with respect to demand and to demand with respect to losses (Case PVP, planning viewpoint). These considerations lead to five cases of criteria weight vector $\boldsymbol{w}$, with values reported in Table 23. It is easy to verify that each of the considered cases has a perfect

consistency of pairwise comparison, since $C^I = 0$. The vectors of global scores obtained in the five prospected cases are depicted in Fig. 39. It can be noted that in each case 7 projects pass the selection threshold, with the exception of DD with 6 cases, however the results are different. In EI and DD Cases, R3 is the preferable solution, whereas in LD and DD cases the best compromise is represented by R11, that is the project examined in the previous methodology, in the cost-benefit analysis framework. In PVP Case, representing the reference for the power system planning, the rank of suitable candidate project over the threshold is R3, R11, R8, N13, R4, R5, R6. It can be argued that, under the considered assumptions, there is more value in reinforcement projects than in paving new connections, and the different weighting assumptions, representing contrasting evolution viewpoints, can affect the ranking given the numerical outcomes of the techno-economic analysis and index determination.

Table 23. Criteria weight vectors in the five considered cases.

Criterion \ Case	EIT	LD	DD	RD	PVP
Losses	0.33333	0.6	0.2	0.2	0.16378
Demand	0.33333	0.2	0.6	0.2	0.29726
Renewable	0.33333	0.2	0.2	0.6	0.53896

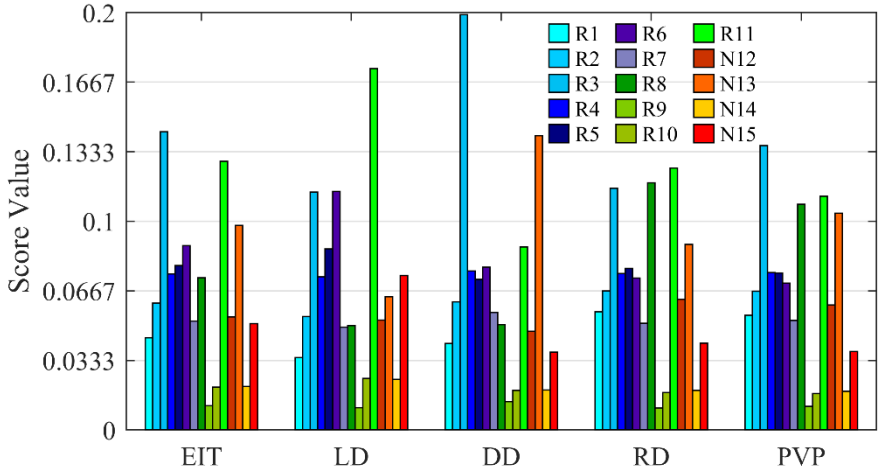

*Fig. 39. Values of global scores **gs** in the five considered cases.*

In order to assess the influence of investment cost in project selection, a further analysis is carried out including the economic effort scores in the AHP. Three further scenarios are therefore analyzed. In the levelized weighting case (Case LW), the four merit indicators assume the same importance, therefore all the elements of the vector of weight values is 1/4. The economic effort dominance (EED) is assessed by imposing a dominance level 5 to economic effort criterion on the three technical indicators, therefore expressing a strong

preference to investment reduction. Finally, the viewpoint of a power system planner is represented by Techno-Economic Planner Perspective (TEPP), where a dominance level 4 is assigned to renewable and economic effort with respect to (w.r.t.) losses, a dominance level 3 is assigned to demand w.r.t. to losses and to economic effort w.r.t. to demand, and a dominance level 2 is assigned to renewable w.r.t. to demand and to economic effort w.r.t. renewable. These considerations lead to three further formulations of criteria weight vector $\boldsymbol{w}$, with values reported in Table 24. It is easy to verify that each of the considered cases has a perfect consistency of pairwise comparison, since $C^I = 0$, except for the TEPP where $C^I = 0.051$.

Table 24. Criteria weight vectors in the three techno-economic cases.

Case / Criterion	LW	EED	TEPP
Losses	0.25	0.125	0.08066
Demand	0.25	0.125	0.17531
Renewable	0.25	0.125	0.28895
Economic effort	0.25	0.625	0.45509

The vectors of global scores obtained in the three techno-economic prospected cases are represented in Fig. 40. It can be seen that in LW and EED cases, as compared to the EIT Case in the previous analysis, the presence of investment cost makes the interest to R7 and R10 increase, due to their cheaper economic effort, to the detriment of R4 and N13. In the TEPP case, 8 projects pass the threshold, i.e., R11, R3, R7, R6, R8, N13, R5 and R10, and the comparison with PVP shows that the economic effort does not remarkably affect the leading projects of the obtained ranking, although further limiting the appeal of more challenging projects (e.g., long new connections or high-rating projects or multi-voltage levels).

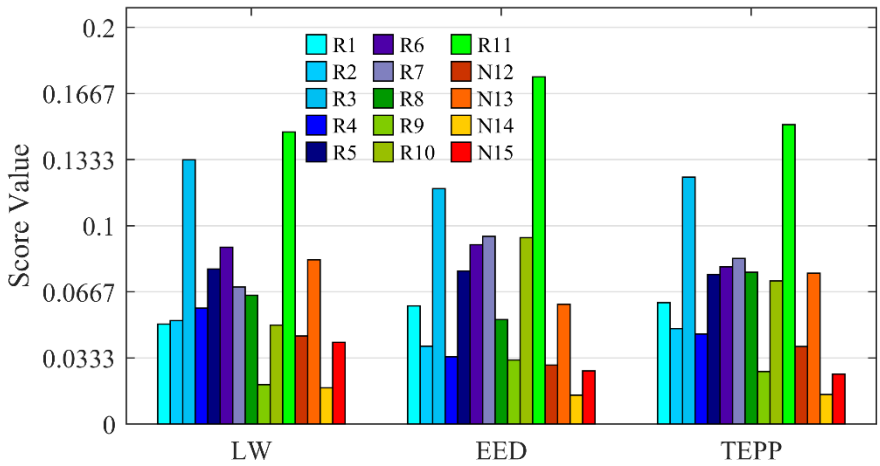

Fig. 40. Values of global scores $\boldsymbol{gs}$ in the three techno-economic considered cases.

3.5 Conclusions

In this chapter, a flow-based as well as AHP procedures to assess the technical and economic benefit of network development project have been carried out. The first methodology involves a threefold analysis: a MILP zonal market solution model to determine social welfare, a load flow analysis to obtain losses and overloads, and a sequential approach based on PTDFs to determine the more effective redispatching actions aiming to reduce overloads. Proper merit indicators have been defined in order to include all aspects in economic benefit evaluation, as a difference of indicators between Reference and Evolution Scenario outputs, in order to evaluate investment profitability. The second one is based on QP energy market and load flow routines as well, however the most profitable development project is evaluated by means of performance indicators, among a set of candidate projects. The development projects' benefits have been compared using the same tools, in order to calculate technical merit indicators on active power losses, admissible load increase and admissible renewable generation increase. In order to perform a comparison of heterogeneous aspects, the outcomes of candidate project study have been analyzed through an Analytic Hierarchy Process method, considering different weighting methods for technical criteria. In addition, the influence of economic effort for project is assessed by including investment cost estimation as a further criterion in AHP method and comparing the classification list of projects under different assumptions. The application of the proposed procedures to the NREL 118 test system over yearly time window has proved the validity of the approaches. In particular, the two procedures are flexible enough to envisage its application to real-scale transmission networks. Furthermore, the indicator comparison through AHP revealed a synthetic though powerful tool to put heterogeneous aspects in a common framework, where evolution scenarios can be efficiently represented by weighting criteria of indicators, prioritizing the attention of the system operator to a subset of projects where a specific cost-benefit analysis could be applied. In ordinary power system operation, N-1 security condition represent a fundamental criterion to assess the generation and load dispatch, and this could affect the evaluation of future network installation, reducing the estimated benefits. For this reason, in a future work, additional CBA and N-1 security criteria could be assessed for the most profitable projects to reduce computational costs concerning network extension.

Chapter 4. Market-driven Sizing and Siting of Generation Investment

A methodology for generation investment analysis is proposed in this chapter, in order to determine the most suitable size and location of generation initiatives in an existing zonal market. In particular, the method aims at determining the new power generation system able to provide competitive bids in energy market through a differential approach, verifying the alleviation of congestions in zonal market environment. Moreover, the potential reduction of network overloads is assessed performing DC load flow analysis in stressful conditions in order to individuate the most suitable location. The method provides static evaluation over a full operation year along with investment profitability analysis. The proposed methodology is applied to the installation of fuel-based generation plants in Sicily, considering Italian energy market results, and including a sensibility analysis on candidate generator sizes and marginal cost levels.

4.1. Investment analysis methodology

The presented generation investment analysis is based on a three-fold methodology involving market, network and economic perspectives. The market studies concern the variation of the DAM results for the candidate zone in terms of zonal price and interzonal power exchanges thanks to the installation of the new generation unit. DC load flow simulations are performed for individuating the site that provides the most benefits to the transmission line power flows. Finally, the economic side entails determining the size of the unit that is economically viable during its whole lifetime. A detailed explanation of the methodology is provided in the following sub-paragraph.

4.1.1. Energy market evaluation

Let us consider the new generation unit of rated power S_r^G with a constant marginal production cost C_n^G, operating in a zonal energy market framework and to be placed in the z-th market zone. The impact in the involved zone of the DAM can be assessed considering the historical MCP results in relation to S_r^G and C_n^G of the new generator as shown in Fig. 41.

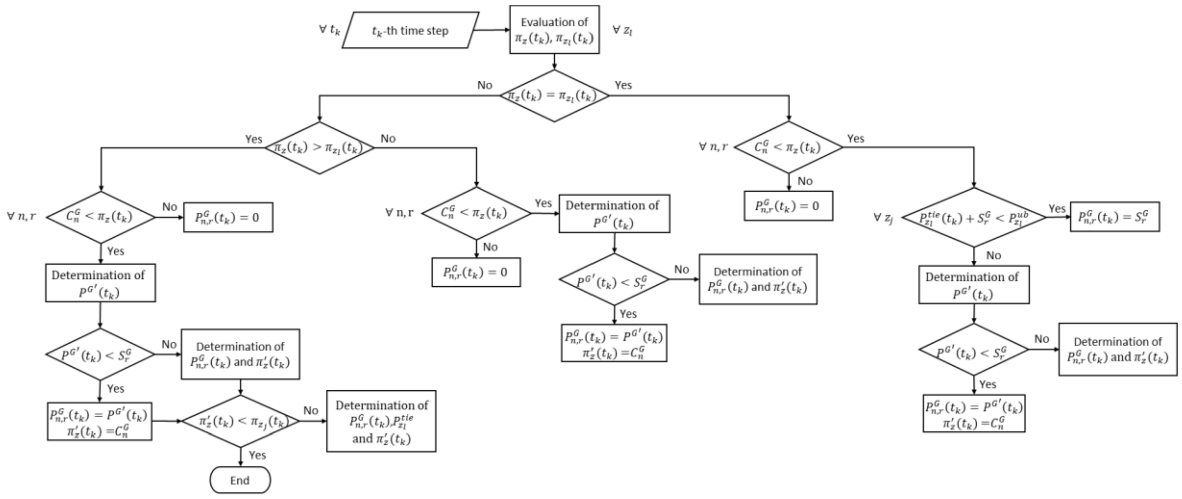

Fig. 41. Flow chart for influence of generation investment in zonal energy market.

For each time step $t_k \in N^T$, when the zonal price of the zone z (π_z) equals the zonal price of each interconnected zone (π_{z_l}), i.e., no power exchange bound is activated, the generator should produce power in the market only if $C_n^G < \pi_z$, otherwise it is not competitive. The cleared power depends on the power exchange with the interconnected zones ($P_{z_l}^{tie}$). If $P_{z_l}^{tie}(t_k) + S_r^G < P_{z_l}^{ub}$, in which $P_{z_l}^{ub}$ is the power exchange upper bound of the z_l-th interconnected zone, the generator will produce S_r^G, and the new zonal price is $\pi_z' = \pi_z$; otherwise $P_{r,n}^G$ and π_z' depend on the rated power and the cleared power by units with a price greater than C_n^G ($P^{G'}$) as well. It is worth to underline that in this condition there is a market splitting with the z_l interconnected zone and $\pi_z' < \pi_{z_l}$. Indicating with $N^{G'}$ the number of generators with a price greater than C_n^G, $P^{G'}$ is equal to:

$$P^{G'}(t_k) = \sum_{i \in N^{G'}} P_i^{G'}(t_k) \tag{102}$$

If at the generic time step t_k $P^{G'}(t_k) > S_r^G$ the generator will produce its rated power, replacing part of the $N^{G'}$ generators, and $\pi_z'(t_k)$ is determined by the new marginal unit; otherwise, the new generator is the marginal one with $P_{r,n}^G(t_k) = P^{G'}(t_k)$ and $\pi_z'(t_k) = C_n^G$.

If $\pi_z(t_k) > \pi_{z_l}(t_k)$ the power exchange with external zones z_l reaches its import limit, and if $C_n^G < \pi_{z_l}(t_k)$ the unit will produce S_G^r while the exchange decreases as follows:

$$P_{z_l}^{tie}(t_k) = P_{z_l}^{lb} + S_r^G - P^{G'}(t_k) \tag{103}$$

only if $P^{G'}(t_k) < S_r^G$, and $\pi_z'(t_k) = \pi_{z_l}(t_k)$, where $P_{z_l}^{lb}$ is the power exchange lower bound (that is negative) of the z_l-th interconnected zone.

If $\pi_{z_l}(t_k) < C_n^G < \pi_z(t_k)$ the power production of the unit depends on $P^{G'}$ as well; if $P^{G'}(t_k) < S_r^G$ the power supplied is $P^{G'}(t_k)$ and $\pi_z'(t_k) = C_n^G$, otherwise the generator is cleared to the rated power, and π_z' depends on the replaced units, hence the new marginal generator energy price, as for previous considerations. In the last case, in which $\pi_z < \pi_{z_i}$, the z_i interconnection power flow reaches its export limit and if $C_n^G < \pi_z$ the new generator will replace the cleared power by the most expensive units up to S_r^G, and π_z' varies according to the new marginal unit, as in previous cases.

4.1.2. Transmission system analysis

Let us suppose a transmission system composed of N^B busbars and N^{ND} non-dispatchable resources (NDR) connected between sub-transmission and distribution system. The zonal market results are used in this stage to run DC load flow simulations to assess the impact of the new generation plant on the transmission system. The zonal dataset of the NDR and loads coming from market are converted to nodal ones thanks to the generation (GPFs) and load participation factors (LPFs), respectively. The power supplied by the most relevant units, on the other hand, are directly associated with the nodes to which they are connected. The GPF and LPF are supposed constant during the year and the first are distinguished by technology:

$$P_{b,n}^G(t_k) = GPF_{b,n} \cdot P_{z,n}^G(t_k) \quad \forall\, n \in N^{ND}, \forall\, b \in N^B \tag{104}$$

$$P_b^D(t_k) = LPF_b \cdot P_z^D(t_k) \quad \forall\, b \in N^B \tag{105}$$

where for the generic time step t_k, $P_{b,n}^G$ is the power supplied by the n-th tecnology at the b-th bus, $P_{z,n}^G$ is zonal power produced by the the n-th tecnology and $GPF_{b,n}$ is the GPF of the the n-th tecnology at the b-th bus; it is zero if at the b-th bus there is not the n-th tecnology installed. Analogusly, P_b^D and LPF_b are respectively the required load and the LPF at the b-th bus, and P_z^D is the zonal demand required. The DC load flow routines are used to determine the most suitable busbar to install the new generator on, taking into account the branches power flow benefits. The DC load flow equations [234] can be written in the matrix form as follows:

$$\boldsymbol{B}^{dc}\theta - P^{dc} = 0 \tag{106}$$

where $\boldsymbol{B}^{dc}$ is the (N^B– 1) x (N^B– 1) symmetric matrix of the conductances obtained neglecting, repsectively, the row and column of the slack bus and reference angle, θ is the vector of dimiention (N^B– 1) of the voltage angles, whereas P^{dc} is the vector of the DC nodal power balance of dimiention (N^B– 1).

4.1.3. Economic investment estimation

The investment analysis is based on the determination of net present value (NPV). Considering a static approach, where the market results over a representative year of operation divided in N^T the time steps are considered valid over the lifetime duration N^Y the NPV is defined as below:

$$NPV = \left(R_y - P_y^C - M_{y,r}\right) \cdot \frac{(1+\alpha)^{N^Y} - 1}{\alpha(1+\alpha)^{N^Y}} - I_r^C \tag{107}$$

where R_y is the yearly revenue from the energy sell:

$$R_y = \sum_{t_k=1}^{N^T} P_{n.r}^G(t_k) \cdot \pi_z'(t_k) \tag{108}$$

moreover P_y^C is the yearly production operating costs:

$$P_y^C = \sum_{t_k=1}^{N^T} P_{n.r}^G(t_k) \cdot C_n^G(t_k) \tag{109}$$

finally, $M_{y,r}$ stands for the yearly maintenance costs and I_r^C is the investment costs, both depending on the size of the new power plant, and α is the discount rate.

4.2. Sicily case study

The method described in the previous section is applied to the Sicily transmission system test case provided by TYNDP of ENTSO-E [235], shown in Fig. 42. It is composed of 127 nodes, distributed among 26 main substations, with several rated voltage as reported in Table 25.

Fig. 42. ENTSO-E Sicily 400 and 230 kV transmission system representation.

Table 25. Number of busbars for each rated voltage

V_r [kV]	Bus number
500	5
400	25
230	34
150	33
<150	30

The nodes at 500 kV are the extremes of new HVDC links to be completed in the next years [236], therefore these parts of the network are not considered active in the study case. The 150 kV nodes are the linking points with the sub-transmission system on which loads and NDR are installed. The buses with the larger size generators have rated voltage lower than 150 kV. The branches are composed of 78 lines, that include interzonal connection with Calabria where a further node is modeled, and 96 transformers, of which 71 are power system transformers, whereas 25 are generator transformers.

The total generation capacity is 9.1 GW: the 39% is installed on the transmission system, and it is composed of wind turbines (108 MW), hydro pumped storage (500 MW) and thermoelectric (2970 MW), with individuated connection nodes. The generators connected to lower voltage levels includes photovoltaic (PV) technology with an installed capacity of 1901 MW, and other 3.6 GW of NDR including other wind power plants, hydropower and biomass, modeled as equivalent generators (EQ) [237]. For PV and EQ, the GPFs reported in (104) are calculated, according to the installed capacity at each node ($P_{b,n}^{\mathrm{G,R}}$) divided by the total installed capacity($P_{z,n}^{\mathrm{G,R}}$):

$$GPF_{b,r} = \frac{P_{b,n}^{\mathrm{G,R}}}{P_{z,n}^{\mathrm{G,R}}} \quad \forall\, n \in \{PV, EQ\}, \forall\, b \in N^B \tag{110}$$

The dataset of ENTSO-E presents one operating condition, with a total required load equal to 2637 MW, distributed among 37 nodes. Analogously to the GPF, the LPF expressed in (105) are defined as the ratio between the nodal load (P_b^D and the total load (P_z^D) in the dataset:

$$LPF_b = \frac{P_b^D}{P_z^D} \quad \forall\, b \in N^B \tag{111}$$

The 2019 Italian DAM findings, which can be found in [238], are used to obtain the generation and load dataset of one year time window, with one hour resolution (i.e., N_T = 8760 hours), for the Sicily market zone, along with power exchanges with neighboring zones and zonal prices. For the generation, the "bell curve" daily PV production profile is considered, for the market ID for PV output establishment; the market ID of the generators connected to the transmission system is linked to the appropriate node; the remaining cleared power is supposed equivalent and distributed to each node according to the GPF.

Fig. 43 shows the duration curve of the power balance of Sicily, it includes the power exchange with Malta and Calabria. The load varies from 3000 to 1200 MW, whereas the total generation from 2550 to 400 MW. Further, an export to Malta for most of the time horizon is detected with a maximum of 199 MW. The import occurs for 320 hours with a maximum of 115 MW. At the contrary, the interchange with Calabria shows an energy import for 8387 hours, reaching the boundary limit of 1100 MW for 2673 hours, and for further 705 hours

with lower exchange limits. Although the maximum export to Calabria is 640 MW, there are 14 hours in which the power flow limit is reached as well. This is because the interchange Sicily-Calabria has asymmetric and time-dependent boundaries.

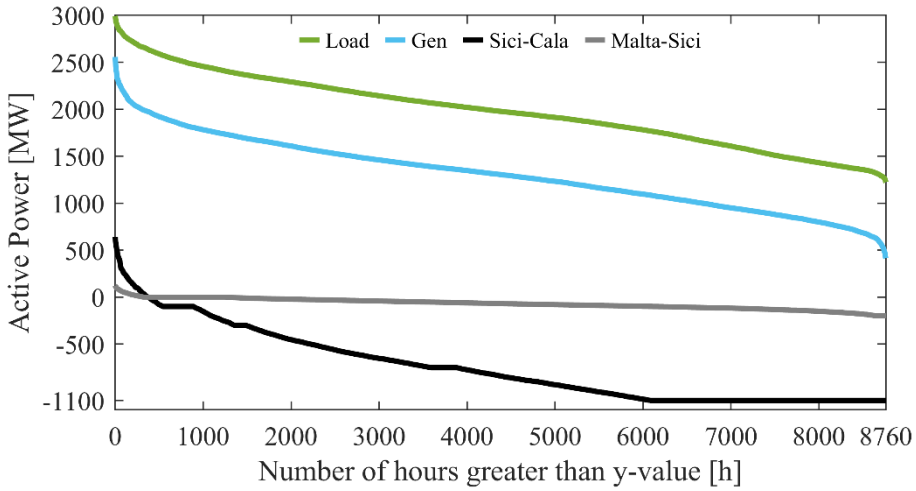

Fig. 43. Sicily yearly active power balance.

Fig. 44 presents the dispatched power after the DAM of the 14 power plants connected to the Sicily's transmission system, by means generation transformers. There are three base-load generator, one generator is cleared roughly half year, and the remaining are peak-load generators. Fig. 45 depicts the duration curve of the zonal price results for the Sicily market zone. The maximum price is 155 €/MWh and only in 65 hours the price is zero. The latter occurs during low load hours or when the renewable production of both South Italy and Sicily is higher than the required load. At contrary, the highest price takes place during high load periods, causing an interzonal congestion with the peninsula.

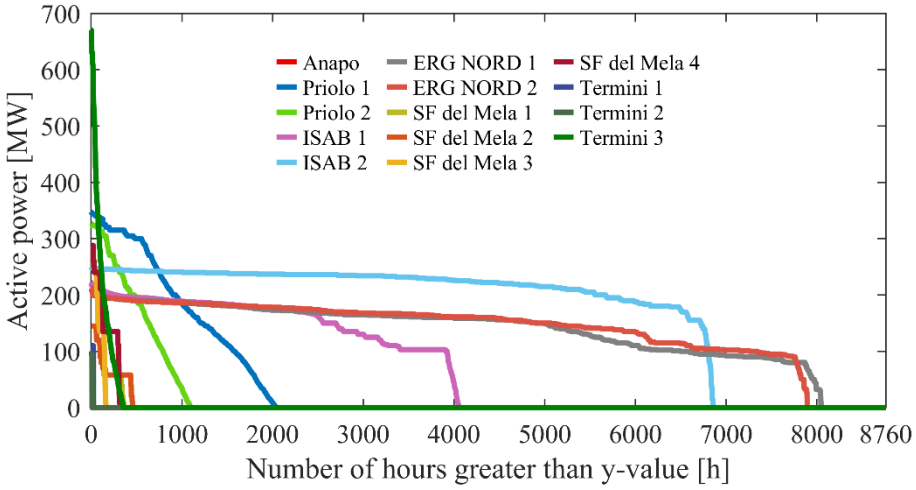

Fig. 44. Yearly dispatched power of the main Sicily's generators.

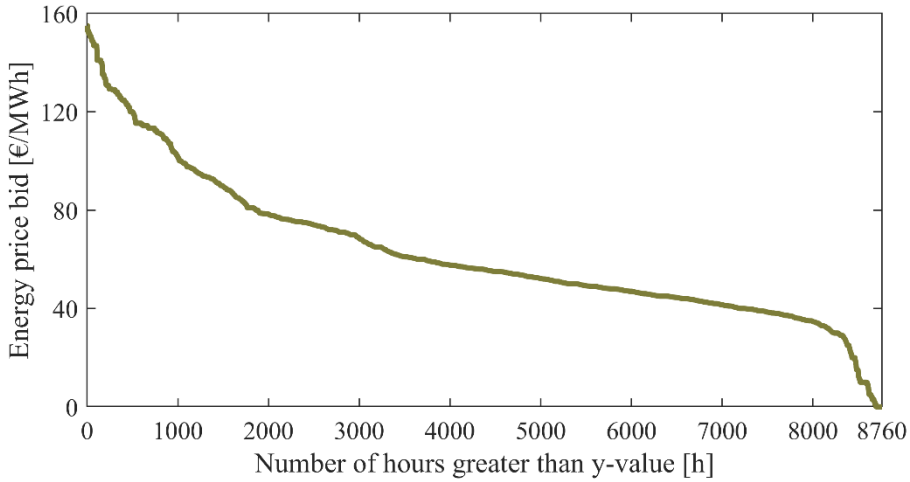

Fig. 45. Hourly MCP of 2019 for the Sicily market zone.

Fig. 46 depicts the system's maximum, mean, and minimum LFP and GPF for distributing load across 20 substations and sub-transmission generation across 17, respectively, and carrying out the nodal DC load flow routines. Melilli substation has the highest GPF (0.277) and LPF (0.133). As a result, the yearly maximum nodal generation and load values are respectively 340.9 MW (hour 8556), and 399.1 MW (hour 4553). Furthermore, Villafranca substation has the lowest GPF (0.028) with the lowest nodal generation of 0.011 MW (hour 7297), and Ferdofin substation has the lowest LPF (0.001), in which the lowest nodal load is 1.47 MW (hour 3656).

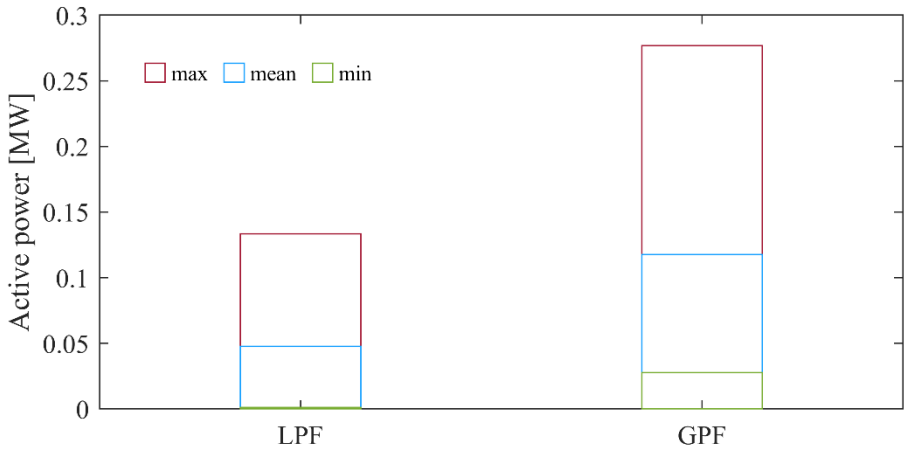

Fig. 46. Minimum, mean and maximum LPF and GPF.

Finally, Table 26 reports the branch overloading for the base case scenario, assuming a rated active power equal to 85% of the rated apparent power. The Caracoli-Termini 220-kV line is overloaded for 10 Winter hours, occurring in three different days, and 4 Autumn

hours, occurring one per day, with a maximum of 107.2% at hour 306. Another overloaded line is the 220-kV Corriolo-Sorgente for 4 hours, all consecutives and during Winter, and its maximum is 111.6% at hour 1196.

Table 26. Base case scenario overloaded lines.

Line	Overloading hours	Max overload
Caracoli-Termini	14	107.2 %
Corriolo-Sorgente	4	111.6%

4.3. Generation Investment results

The method is tested supposing three different sizes and three constant marginal costs, as reported in Table 27. For each of the 9 combinations of (S_r^G, C_n^G) energy production in the DAM is determined and the results are shown in Fig. 47. It can be seen that the lower the price and the rated power, the higher are the hours cleared at rated power, moving from 31 hours for the combination (S_3^G-C_3^G) to 4133 for (S_1^G-C_1^G).

Table 27. New generators parameters.

S_R^G [MW]		C_R^G [€/MWh]	
S_1^G	250	C_1^G	50
S_2^G	500	C_2^G	80
S_3^G	800	C_3^G	100

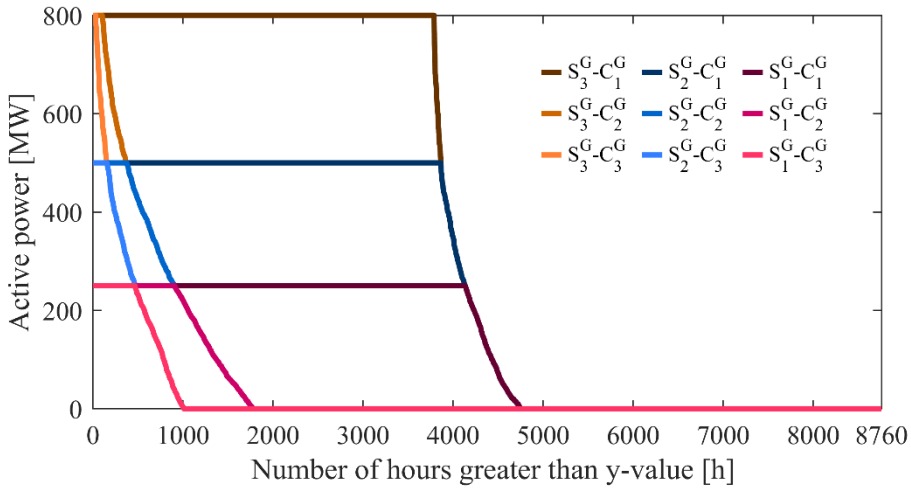

Fig. 47. New generator DAM production for different sizes and costs.

For the sake of clarity, Table 28 shows the yearly equivalent duration hours for each combination ($H_{r,n}$) expressed as ratio between the total energy supplied in one year and the rated power of the unit:

$$H_{r,n} = \frac{1}{S_r^G} \sum_{t_k=1}^{N^T} P_{n,r}^G(t) \qquad \forall\, S_r^G \in S_R^G, \forall\, C_n^G \in C_N^G \tag{112}$$

In case of a marginal cost of 50 €/MWh (C_1^G) the generator will produce for roughly half a year at rated power, with a variation of 211 hours between 250 and 500 MW, and of 349 between 250 and 800 MW. The variation in cost, on the other hand, has a greater impact on the cleared power (e.g., a reduction of three, four, and six times from 50 to 80 €/MWh for a size of 250, 500, and 800 MW, respectively).

Table 28. Equivalent duration hours of the new generator.

$H_{r,n}$	C_1^G	C_2^G	C_3^G
S_1^G	4397	1309	729
S_2^G	4186	962	509
S_3^G	4048	679	348

The yearly peak load in Sicily occurs at hour 4553, Fig. 48 and Fig. 49 show the Calabria-Sicily power exchange and Sicily zonal price variations, respectively caused by the introduction of the new generator during the peak load day, where in the base case the maximum import is reached for each hour, as shown in Fig. 48. The bidding cost 50 €/MWh is lower than Calabria's price in several hours during the peak load day (Fig. 49), when it occurs the power flow is reduced. In fact, for the rated power S_1^G there is a reduction only for one hour (4539) of roughly 63.3 MW. The rated powers S_2^G and S_3^G impact for 12 and 13 hours, respectively, the power flow and at hour 4539 there is the maximum reduction of 313.3 and 613.3 MW. On the contrary, C_n^G has a greater influence on MCP variation, indeed (S_r^G-C_1^G) is the combination with lower zonal MCP, whereas the greater S_G^r the more are the hours in which the generator is marginal, keeping the same C_G^n. This can be observed comparing the MCP of (S_G^3-C_G^3) and (S_G^2-C_G^3) at the peak price, of approximately 113 €/MWh, from hour 4556 to hour 4559. The first has enough margin to replace the most expensive units, becoming the marginal generator, while the second is not able to cover all the high-priced bids (Fig. 50). This is better shown in Fig. 51 where it is represented the yearly Sicily MCP maximum mean and minimum variation for each size and bid offered.

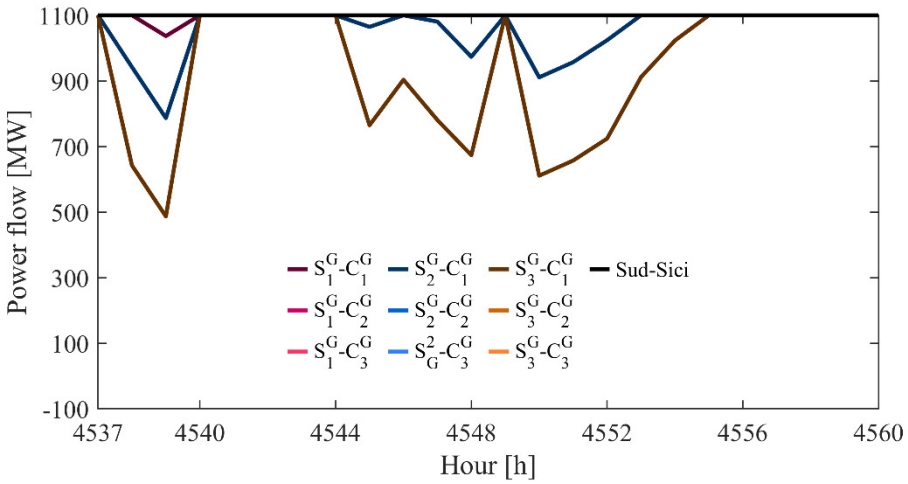

Fig. 48. Calabria-Sicily power flow during the peak load day.

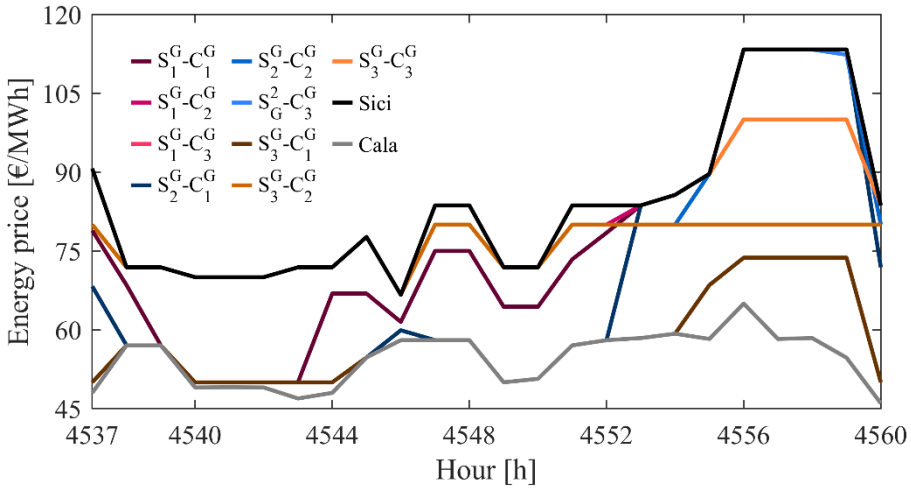

Fig. 49. MCPs for each combination during the peak load day.

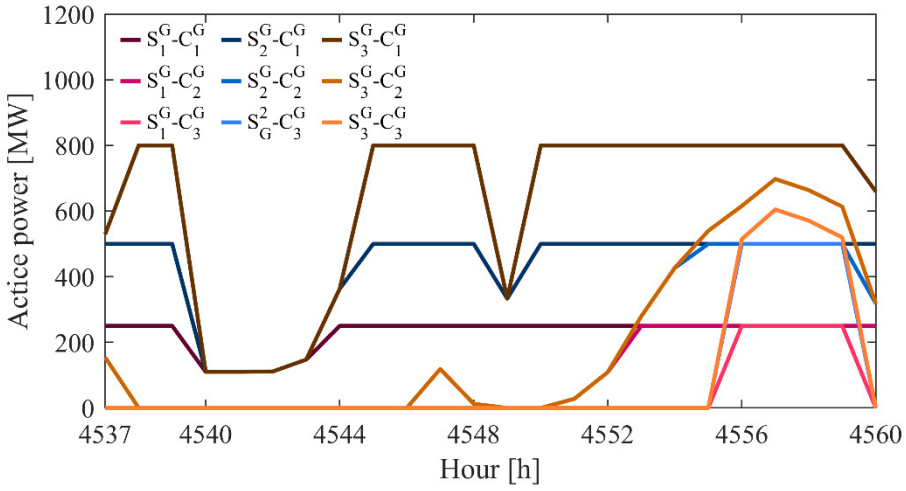

Fig. 50. New generation production during the peak day.

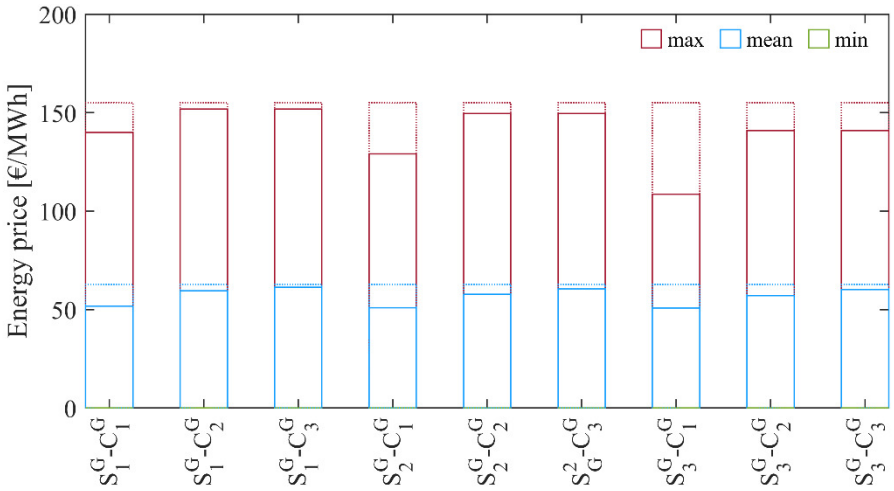

Fig. 51. Maximum, mean and minimum Sicily MCP variation for each combination.

Fig. 52 reports the maximum, mean and minimum interzonal power flow variation for each combination of (S_r^G-C_n^G) over the year. With marginal price C_3^G the power exchange between the market zones keeps at maximum level. This is due to the lower price of Calabria in the whole year than the offered one.

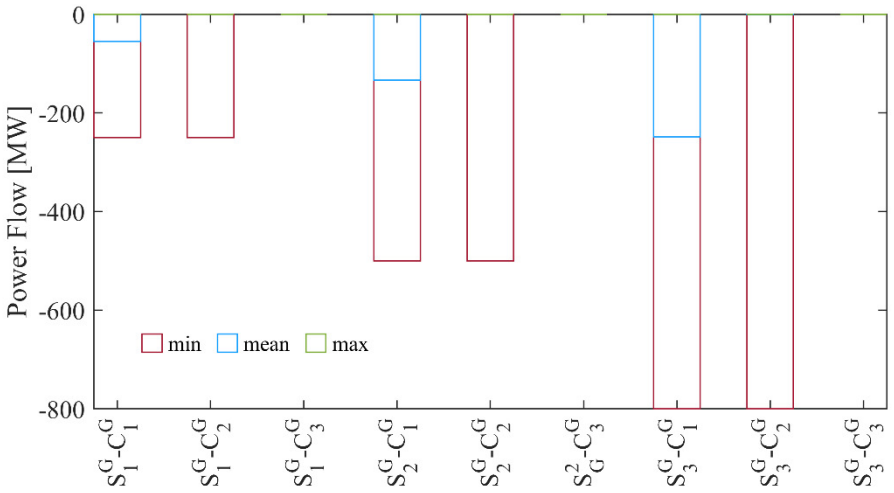

Fig. 52. Calabria-Sicily power flow variation for each combination.

The network impact of the new generation is studied under the worst-case scenario, in which the generator supplies the rated power over the year, in order to assess the more stressful scenario for transmission system operation. The candidate buses where to install the new generator are selected excluding sub-transmission levels due to the chosen sizes, the buses with an existing relevant generator, interzonal and foreign exchange nodes. The results of the DC load flow simulation are shown in Table 29, which includes the base-case hours of overloaded lines as well as possible new ones, for the 5 candidate buses, all at 220 kV level, and

for each possible size of the new generator. S_1^G and S_2^G have the same effect for each candidate bus: the overloads on the Corriolo-Sorgente line are extinguished. On the contrary, the size S_3^G arises further overloads in relation to the selected bus. The worst solution is to locate the new generator at the Ciminna substation, which overloads two other lines for a total of 50 hours. Partanna substation, on the other hand, is the most suitable solution because it reduces the overloads Corriolo-Sorgente as well, without producing further overloads, as the other size.

Table 29. DC load flow results with the new generator.

S_r^G	Lines	Candidate substation overload hours				
		Bellolampo	***Ciminna***	***Favara***	***Partanna***	***Partin***
S_1^G	Caracoli-Termini	14	14	14	14	14
	Corriolo-Sorgente	0	0	0	0	0
S_2^G	Caracoli-Termini	14	14	14	14	14
	Corriolo-Sorgente	0	0	0	0	0
S_3^G	Caracoli-Termini	14	14	14	14	14
	Corriolo-Sorgente	2	5	0	0	0
	Caracoli-Corriolo	15	24	0	0	6
	Caracoli-Sorgente	15	26	0	0	6
	Chiaramonte-Favara	0	0	3	0	0

The investment profitability analysis is carried out considering a specific cost of 617.64 k€/MW for a combined cycle gas plant [239], and the yearly maintenance costs 1% of the investment costs. They are reported in Table 30.

Table 31 shows yearly revenue and production cost per each combination of size and bidding price, as well as the net present value has been calculated supposing α = 5% and N_Y = 30 years. It can be seen that only the generator with sizes 250 MW and 500 MW and marginal cost 50 €/MWh allow an economic investment profit. In particular, the first is the most profitable solution thanks to the higher equivalent duration hour, and the lower reduction of MCP, compared to the other with the same costs.

Table 30. Investment and maintenance costs for each size.

S_r^G	I_r^C [M€]	$M_{y,r}$ [M€/y]
S_1^G	154.41	1.54
S_2^G	308.83	3.09
S_3^G	494.15	4.94

Table 31. New generator investment analysis.

S_r^G	C_n^G	R_y [M€/y]	P_y^C [M€/y]	VAN [M€]
S_1^G	C_1^G	68.48	54.96	29.7
S_1^G	C_1^G	31.83	26.19	–91.46
S_1^G	C_1^G	20.52	18.23	–143.05
S_2^G	C_2^G	127.97	104.65	2.27
S_2^G	C_2^G	42.27	38.49	–298.2
S_2^G	C_2^G	26.88	25.45	–334.23
S_3^G	C_3^G	197.51	161.9	–22.73
S_3^G	C_3^G	44.56	43.49	–553.52
S_3^G	C_3^G	28.18	27.86	–565.14

4.4. Final remarks

The proposed work for a generation investment analysis, based on yearly zonal market dispatch with DC load flow evaluations, has shown that a smaller and cheaper generator is more competitive and leads to lower impacts on zonal prices, seldom becoming marginal, and higher investment benefits. Similarly, as the unit size increases, reduced occurrence of bounded power exchange between zones has been attained along with zonal price reduction, although DC network analysis has limited the candidate buses for generator placement in the network, since investigating maximum production level in the absence of transmission reinforcements additional overloads have been detected in the surroundings of the installation. With this hypothesis the rated power has a relevant impact on branch overflow occurrences over the year: the greater the size the higher the possibility of further overloads. However, in real applications the generation investment optimal solution could be in contrast with non-electric conditions e.g. due to terrains and environmental permissions. Therefore, in the economic evaluation additional costs could be necessary to fit these constraints, such as the installation of own busbar and cable to cover the distance from the closest available place to the selected bus.

The adopted method has proved the determination of the generation impact initiative in a zonal market framework and could be generalized-in further contexts of energy markets. The generation investment viewpoint does not envisage the N-1 security criterion analysis, even if in the market context the zonal boundaries take into account an available transfer capacity lower than the rated power of the involved lines. However, in the network assessment the N-1 security analysis could be taken into account to evaluate if further overflows

arise for the analyzed candidate buses in the most stressful condition. Future works could deal with the impact of strategic bids from the new generator, as well as the influence of expansion for transmission network and generators, e.g., renewables, along with AC load flow models and the possible participation of the new generation plant in other remuneration mechanisms such as ancillary service markets.

Chapter 5. Scenario Clustering and Statistical Estimation of Operating Reserve Requirements

In this chapter, a procedure for the determination of different reserve requirements (RRs) is proposed, taking into account system operating conditions and load, wind and solar uncertainties, as well as load ramp variation uncertainty. the first three uncertainties are assessed using real reference datasets, exploited to determine hourly forecast errors, for each season. The load ramp variation uncertainty is assessed determining the advance/delay of the electrical demand forecast during ramp/deramp conditions, and a proper Ready RRs (ReRRs) is defined in order to cope with this uncertainty. The remaining reserves are the SpRRs and Replacement RRs (RRRs). The three TRRs are determined considering the seasonal influence of the aforementioned uncertainties and the classification of the system operating conditions according to RES penetration and demand request. Moreover, a statistical study is developed to assess the effective RR estimation according to reference system dataset. The proposed methodology is applied to the NREL 118-bus test system with a yearly dataset, where a proper set of eligible generating units to provide the required services is defined. The compatibility of the RRs with generation margins and possible contingency events is eventually assessed. In order to assess the influence of combined energy and service planning in ancillary market framework, the outcome of the reserve requirement estimation—and in particular of secondary reserve—is therefore included in the security constrained economic redispatch procedure.

Main contributions of this chapter can be individuated in:

- a classification method, allowing to draw out the influence on RRs estimation of system operation factors, such as RES production and load demand;
- a real reference system exploitation for supporting RR estimation suitability;
- the RR effective adequacy and feasibility assessment throughout the yearly by means of operating conditions grouping in appropriate specific classes;
- the proposal of a procedure for security constrained redispatch, after day-ahead market, accounting for reserve requirements.

5.1. Reserve Requirement Evaluation

In this section, the methodology to determine the RRs is detailed. The approach is based on Terna (Italian TSO) framework to define them for the Italian transmission system [7]. In particular, the definition of RRs include the Secondary Reserve Requirements (SRR), two TRR types to be delivered within fifteen minutes, and one TRR to be provided up to 2 hours after the TSO request; each TRR is sized according to a combination of specific uncertainties. They are defined for the whole system and for each market zone and the latter are obtained downstream the former according to appropriate proportions.

According to ENTSO-E formulation [240], the SRR is based on the amount of load demand forecast. On the other hand, the first TRR is the upward ReRR, and it is defined to face:

- SRR restoration.
- Advance/delay of the required demand, in relation to the forecast level, in the ramp/deramp load hours.

The second is the upward (downward) SpRR, it is sized to cope:

- SRR and ReRR restoration.
- Unexpected outage of the thermal unit (pumped storage hydro unit) with the maximum cleared power.
- HVDC outage.

The last is the RRR and it is determined to tackle:

- Unexpected outage of the thermal unit (pumped storage hydro unit) with the maximum cleared power.
- Forecast error of required energy demand and of non-dispatchable RES.
- Testing phase thermal unit production lacking with the maximum cleared power (only for upward reserve).
- HVDC outage.

However, the HVDC outage is beyond the scope of the proposed paper, and it represents a further work that can be developed on a proper test case. Moreover, the unit outage in SpRR is redundant, therefore it will be not considered in the following.

5.1.1. Reserve Requirements

According to [241], SRR is evaluated by ENTSO-E formulation [240], and considering a transmission system composed of N^C control areas, for the generic time step $t_k = 1, \dots, N^T$ it is formulated as follows

$$SRR(t_k) = \sum_{c=1}^{N^C} \left(\sqrt{a \cdot P_c^{D,DA}(t_k) + b^2} - b \right) \tag{113}$$

where $P_c^{D,DA}$ is the forecast load of the c-th control area, a=10 MW and b=150 MW.

ReRR is determined supposing a statistical combination of SRR restoration and load ramp/deramp variation (ΔP^R):

$$ReRR(t_k) = \alpha(t_k) SRR(t_k) + \beta(t_k) \Delta P^R(t_k) \tag{114}$$

ΔP^R is defined taking into account two variations: one between two consecutive time steps and the second from DA to RT values. These variations are related to proper thresholds formulated as follows:

$$T_d = \frac{k}{24} \sum_{t_k=1+24(d-1)}^{24d} P^{D,DA}(t_k) \quad \forall\, d = 1, \dots, 365 \tag{115}$$

$$T_y = \sum_{t_k \in \Omega^{T^+}} \frac{\Delta P^D(t_k)}{N^{T^+}} \tag{116}$$

where T_d is the daily mean load threshold and k is a proper weighting coefficient to relate the threshold with mean load of the d-th day. The threshold T_y takes into account that the ReRR is only an upward reserve, therefore it is the yearly mean of positive values of ΔP^D that is the load difference between RT and DA values at t_k-th time step, belonging to Ω^{T^+} set of the N^{T^+} time steps with positive load difference. Hence, the load ramp/deramp variation occurs if the following two conditions are satisfied:

$$|P^{D,DA}(t_k) - P^{D,DA}(t_{k+1})| \geq T_d \quad \forall \begin{cases} t_k \in [1 + 24 \cdot (d-1) \div 24 \cdot d] \\ d = 1, \dots, 365 \end{cases} \tag{117}$$

$$\Delta P^D(t_k) = P^{D,RT}(t_k) - P^{D,DA}(t_k) \geq T_y \;\; \forall\, t_k \in \Omega^{T^+} \tag{118}$$

in which the condition (117) is to evaluate if the t_k-th time step is included in the set Ω^R of ramping time steps, where DA load variation between two consecutive time steps is greater than T_d and condition (118) compares ΔP^D at t_k-th time with T_y. Therefore, ΔP^R is equal to:

$$\Delta P^R(t_k) = \begin{cases} \Delta P^D(t_k) - T_y & \forall\, t \in \left(\Omega^R \cap \Omega^{T^+}\right) \\ 0 & otherwise \end{cases} \tag{119}$$

The SPRR is defined as the statistical combination of SRR and RERR restorations:

$$SpRR(t_k) = \delta(t_k) SRR(t_k) + \gamma(t_k) ReRR(t_k) \tag{120}$$

The RRR is sized to overcome system uncertainties and unexpected generator outage, considering a suitable statistical combination:

$$\begin{aligned} RRR(t_k) = {} & 3\sigma_W(t_k)\tau(t_k) + 3\sigma_{PV}(t_k)\rho(t_k) + 3\sigma_L(t_k)\mu(t_k) \\ & + \max_i P_i^G(t_k)\, \varphi(t_k) \end{aligned} \tag{121}$$

where, for each time step t_k, σ_W, σ_{PV} and σ_L represent the forecast error standard deviation of wind power production, solar power production and load demand, respectively, whereas the last term is the maximum dispatched power in day-ahead market (DAM).

In order to determine reserve amounts, the starting point is constituted by DAM solution, providing economic competitive power generation dispatch. For this aim, a DAM model is developed supposing perfect competition among generators with stepwise bids and an inelastic demand in a zonal framework, in which the objective function aims at minimizing the operating costs for each time step t_k:

$$\min_{\boldsymbol{P^G}} \sum_{i=1}^{N^G} \sum_{s=1}^{N^S} P_{i,s}^G(t_k)\, c_{i,s} \tag{122}$$

where N^G and N^S are the number of generators and bid steps, respectively, $c_{i,s}$ is the marginal cost and $P_{i,s}$ is the variable on the cleared power of the i-th generator of the s-th step. The DAM clearing is subject to four constraints:

$$\sum_{i=1}^{N^G} \sum_{s=1}^{N^S} \beta_{i,z} P_{i,s}^G(t_k) \sum_{l=1}^{N^I} \beta_{l,z} P_l^{tie}(t_k) = P_z^D(t_k) \quad z = 1, \dots, N^Z \tag{123}$$

$$0 \leq \sum_{s=1}^{N^S} P_{i,s}^{G}(t_k) \leq a_i(t_k) P_i^{G,max}(t_k) \quad i = 1, \dots, N^G \tag{124}$$

$$0 \leq P_{i,s}^{G}(t_k) \leq P_{i,s}^{G,max}(t_k) \quad i = 1, \dots, N^G, s = 1, \dots, N^S \tag{125}$$

$$P_l^{lb} \leq P_l^{tie}(t_k) \leq P_l^{ub} \quad l = 1, \dots, N^I \tag{126}$$

in which (123) is zonal power balance, (124) represents generator maximum limits, (125) bounds bid step maximum power, whereas (126) defines interzonal flow bounds. P_l^{tie} represents the power flow of the l-th interzonal transmission line, P_z^D is the total active power demand at the z-th zone, $\beta_{i,z}$ is a binary parameter equal to 1 if the i-th generator belongs to the z-th zone and 0 otherwise. The binary parameter $\beta_{l,z}$, on the other hand, provides information about the direction of the interzonal power flows, and it equals to 1 if the l-th interzonal connection is entering the z-th zone, -1 if it is exiting from the z-th zone, and 0 otherwise. Another binary parameter a_i is aimed to indicate the availability of the i-th generator at each time step to participate to DAM and ancillary service market (ASM) (β_g = 1) or only to ASM (β_g = 0). Moreover, $P_i^{G,max}$ is the rated power of the i-th generator and it varies over the time, as well as $P_{i,s}^{G,max}$ that is the s-th step maximum power of the i-th generator. Finally, P_l^{lb} and P_l^{ub} are the lower and upper bounds of the l-th interzonal transmission line, respectively.

5.1.2. Seasonal classification

The system uncertainties affecting the estimation of reserve requirements vary according to the period of the year and to weather estimation. Therefore, in order to draw uncertainties from historical dataset, a seasonal subdivision method is adopted to cluster the main affecting parameters, and within each season operating conditions are grouped in classes according to RES and load values. Additionally, to correlate the dataset of a real transmission system, called reference, and the one of a test system, the RES and load timeseries can be normalized according to the respective annual peak load to obtain comparable per unit values. This elaboration is intended to provide to interested users (such as generation companies aiming at energy-reserve arbitrage) a straightforward though affordable estimation method

for reserve requirements, by classifying the operating condition in one of the individuated classes.

The classification framework is defined considering the difference between the seasonal minimum and maximum RES production ($P_a^{R,min}$, $P_a^{R,max}$) and load demand ($P_a^{D,min}$, $P_a^{D,max}$) divided in classes defined by discrete intervals as follows:

$$\Delta P_a^{R,tot} = P_a^{R,max} - P_a^{R,min} \tag{127}$$

$$\Delta P_a^{D,tot} = P_a^{D,max} - P_a^{D,min} \tag{128}$$

$$\Delta P_a^{R} = \frac{\Delta P_a^{R,tot}}{N_R} \tag{129}$$

$$\Delta P_a^{D} = \frac{\Delta P_a^{D,tot}}{N_L} \tag{130}$$

where N_R and N_L is the number of the desired RES and load class intervals and a is the generic season. The network behavior can be classified on the bases of RES and load inputs, for each time step:

$$R_{i,a} = \left[P_a^{R,min} + (i-1)\Delta P_a^R \div P_a^{R,min} + i\Delta P_a^R\right] \quad \forall\, i = 1, \dots, N_R \tag{131}$$

$$L_{j,a} = \left[P_a^{D,min} + (j-1)\Delta P_a^D \div P_a^{D,min} + j\Delta P_a^D\right] \quad \forall\, j = 1, \dots, N_L \tag{132}$$

$$\boldsymbol{c}_{i,j,a} = \left\{t_k \ni' \left(P_a^R(t_k) \in R_{i,a} \wedge P_a^D(t_k) \in L_{j,a}\right)\right\} \quad \forall\, t_k \in \Omega^{T_a} \tag{133}$$

where:

- Ω^{T_a} is the set of time steps of the a-th season;
- $R_{i,a}$ is the RES power interval of the i-th RES class in the a-th season;
- $L_{j,a}$ is the load power interval of the j-th load class in the a-th season;
- $\boldsymbol{c}_{i,j,a}$ is the set of time steps of the a-th season included both in the i-th RES class and in the j-th load class.

The RRs are clustered according to the aforementioned classification and for each class their mean values are assessed:

$$SRR_{i,j,\mathrm{a}} = \underset{\boldsymbol{c}_{i,j,a}}{\mathrm{mean}}\big(SRR(t_k)\big) \quad \forall\, i, j, a \tag{134}$$

$$ReRR_{i,j,a} = \underset{\boldsymbol{c}_{i,j,a}}{\text{mean}}\big(ReRR(t_k)\big) \quad \forall\, i,j,a \tag{135}$$

$$SpRR_{i,j,a} = \underset{\boldsymbol{c}_{i,j,a}}{\text{mean}}\big(SpRR(t_k)\big) \quad \forall\, i,j,a \tag{136}$$

$$RRR_{i,j,a} = \underset{\boldsymbol{c}_{i,j,a}}{\text{mean}}\big(RRR(t_k)\big) \quad \forall\, i,j,a \tag{137}$$

5.1.3. Statistical combination

The statistical coefficients reported in (114), (120) and (121) represent the historical occurrence combinations of the considered uncertainties. However, the knowledge of these coefficients requires much experience in on-line operation management. Therefore, the observed RR values of the reference system are exploited to evaluate a total statistical coefficient to be applied to the preliminary of RR estimations in the test system ($ReRR_{i,j,a}^{pre}$, $SpRR_{i,j,a}^{pre}$ and $RRR_{i,j,a}^{pre}$) given by the simple sum of the contributions in (114), (120) and (121). After the application of seasonal classification (127)–(133) to the reference system as well as to the preliminary RR estimations of the test case, the total statistical coefficients are obtained by means of their ratios, evaluated considering the normalized values, obtained on the basis of the respective peak load (P_P^D, $P_P^{D,r}$). The classification of the two systems should is assessed with the same assumptions for the definition of N_R and N_L in (129)–(130); this may provide different occurrences for each RES-load class, although the resulting values keep valid for the ratio evaluation. Therefore, for each seasonal class:

$$\epsilon_{i,j,a} = \frac{\dfrac{ReRR_{i,j,s}^{r}}{P_P^{D,r}}}{\dfrac{ReRR_{i,j,a}^{max}}{P_P^{D}}} \quad \forall\, i,j,a \tag{138}$$

$$\vartheta_{i,j,a} = \frac{\dfrac{SpRR_{i,j,a}^{r}}{P_P^{D,r}}}{\dfrac{SpRR_{i,j,a}^{max}}{P_P^{D}}} \quad \forall\, i,j,a \tag{139}$$

$$\omega_{i,j,a} = \frac{\frac{RRR_{i,j,s}^{r}}{P_P^{D,r}}}{\frac{RRR_{i,j,a}^{max}}{P_P^{D}}} \quad \forall\, i,j,a \tag{140}$$

and these ratios between the normalized reserves represent the overall statistical coefficients to obtain the TRR estimations as follows:

$$\overline{ReRR}(t_k) = \varepsilon_{i,j,a} ReRR_{i,j,a} \quad \forall\, t_k \in \boldsymbol{c}_{i,j,a}, \forall\, i,j,a \tag{141}$$

$$\overline{SpRR}(t_k) = \vartheta_{i,j,a} SpRR_{i,j,a} \quad \forall\, t_k \in \boldsymbol{c}_{i,j,a}, \forall\, i,j,a \tag{142}$$

$$\overline{RRR}(t_k) = \omega_{i,j,a} RRR_{i,j,a} \quad \forall\, t_k \in \boldsymbol{c}_{i,j,a}, \forall\, i,j,a \tag{143}$$

Moreover, an analogous coefficient is applied to the SRR, with the goal to evaluate the reliability of ENTSO-E equation to a real transmission system, therefore:

$$\psi_{i,j,a} = \frac{\frac{SRR_{i,j,a}^{r}}{P_P^{D,r}}}{\frac{SRR_{i,j,\mathrm{a}}}{P_P^{D}}} \quad \forall\, i,j,a \tag{144}$$

$$\overline{SRR}(t_k) = \psi_{i,j,a} SRR_{i,j,a} \quad \forall\, t_k \in \boldsymbol{c}_{i,j,a}, \forall\, i,j,a \tag{145}$$

Finally, the total upward (URR) and downward (DRR) reserve requirements, at t_k-th time step, are defined as follows:

$$URR(t_k) = \overline{SRR}(t_k) + \overline{ReRR}(t_k) + \overline{SpRR}(t_k) + \overline{RRR}(t_k) \tag{146}$$

$$DRR(t_k) = \overline{SRR}(t_k) + \overline{SpRR}(t_k) + \overline{RRR}(t_k) \tag{147}$$

5.2. Security Constrained Unit Commitment and Economic Redispatch Method

The proposed methodology is organized in a multi-stage framework, which is synthesized as follows:

- DAM model: an economic-based merit-order zonal market optimization problem is carried out to define a preliminary dispatched profile;

- ASM generator bids adjustment: a bid adjustment process mechanism is carried out to participate to the ASM, based on DAM results, unit technologies and technical limits;
- DC load flow and sensitivity factors: a network feasibility evaluation of the DAM cleared power is fulfilled, and the PTDFs for the redispatch actions are determined;
- SCUCER optimization problem: a redispatch market to satisfy UC and network constraints as well as to procure secondary reserve requirements (SRRs) is proposed, while minimizing market participant bid costs;

In the following subsections the formulation and a more detailed description of the four stages are provided.

Nomenclature

The notation used throughout this methodology is stated below.

Sets and Indexes:

Ω^B (Index b): Set of N^B transmission branches

Ω^G (Index i): Set of N^G generators

Ω^L (Index l): Set of N^L interconnections between zones

Ω^N (Index n): Set of N^N nodes

Ω_i^S (Index s): Set of N_i^S generators' stepwise bids

Ω^T (Index t): Set of N^T time step

Ω^Z(Index z): Set of N^Z zones

Subsets and Indexes:

$\Omega^H \subset \Omega^G$ (Index i): Set of N^H dispatchable hydroelectric units

$\Omega^{ND} \subset \Omega^{TH}$ (Index i): Set of N^{ND} non-dispatchable thermal units

$\Omega^R \subset \Omega^G$ (Index i): Set of N^R non-dispatchable RES units

$\Omega^{TD} \subset \Omega^{TH}$ (Index i): Set of N^{TD} dispatchable thermal units

$\Omega^{TH} \subset \Omega^G$ (Index i): Set of N^{TH} thermal units

Parameters:

$\Delta D_{n,t}$: Change in active power absorbed by load

$\Delta P_{n,t}^{P}$: Change in active power generated by photovoltaic generators

$\Delta P_{n,t}^{W}$: Change in active power generated by wind generators

C_i^{su}: Fixed start-up cost in €

C^{rc}: Penalty cost for RES curtailment in €/MWh

C^{voll}: Value of lost load cost in €/MWh

$D_{n,t}^{rt}$: Real time load demand

$D_{z,t}^{da}$: Day-ahead zonal forecasted load demand

$E_{i,t-1}^{A}$: Available energy of dispatchable hydroelectric generator at previous time step

$F_{b,t}^{0}$: Active power flow downstream load flow routine

F_b^{max}: Maximum active power flow

F_b^{min}: Minimum active power flow

F_l^{lb}: Interzonal power flow lower bound

F_l^{ub}: Interzonal power flow upper bound

$P_{i,t}^{H,max}$: Dispatchable hydroelectric generator's hourly maximum power

$P_{i,t}^{da}$: Hourly forecasted generated power by RES

$P_{i,t}^{rt}$: Real Time active power output of *non-dispatchable* RES generator

$P_{i,t}^{sh}$: Secondary Reserve Half-bandwidth

$P_{i,t}^{sd}$: Shut-down bid

$P_{i,t}^{su}$: Start-up bid

P_i^{max}: Maximum active power

P_i^{min}: Minimum active power

$S_{n,b}$: Power Transfer Distribution Factors

$a_{i,t}$: Generator's availability

$c_{i,s,t}^{\uparrow}$: Upward energy specific cost for each step of each dispatchable thermal generator in €/MWh

$c_{i,s,t}^{\downarrow}$: Downward energy specific cost for each step of each dispatchable thermal generator in €/MWh

$c_{i,s}$: Energy specific cost for each step of each generator in €/MWh

$c_{i,t}^{sd}$: Variable shut-down cost in €/MWh

$c_{i,t}^{sr\uparrow}$: Upward Secondary Reserve specific cost in €/MWh

$c_{i,t}^{sr\downarrow}$: Downward Secondary Reserve specific cost in €/MWh

$c_{i,t}^{su}$: Variable start-up cost in €/MWh

$e_{i,t}$: Monthly generator's escalator

k_L: Reduction factor for Load Shedding action

$\alpha_{i,z}^{G}$: Binary parameters of zone-generator connections

$\alpha_{z,l}^{F}$: Binary parameters of zone-interzonal line interconnections

$\beta_{i,n}$: Generators-nodes incidence matrix

$\Delta P_{i,s,t}^{max\uparrow}$: Maximum upward energy for each step of each dispatchable thermal generator

$\Delta P_{i,s,t}^{max\downarrow}$: Maximum downward energy for each step of each dispatchable thermal generator

$\Delta P_{i,s}^{max}$: Maximum width for each step of each generator

SRR_t: Secondary Reserve Requirement

Variables:

$\Delta P_{i,s,t}^{\uparrow}$: Continuous var representing upward power for each step of each dispatchable thermal generator

$\Delta P_{i,s,t}^{\downarrow}$: Continuous var representing downward power for each step of each dispatchable thermal generator

$\Delta P_{i,t}^{A}$: Continuous var representing total ASM redispatched active power by dispatchable thermal generator

$D_{n,t}^{ls}$: Continuous var representing curtailed power by load shedding action on *n*-th node

$E_{i,t}^{A}$: Continuous var representing available energy of dispatchable hydroelectric generator

$F_{l,t}$: Continuous var representing the active power flow on interzonal connection

$P_{i,s,t}$: Continuous var representing the cleared active power on the DAM for each step of each generator

$P_{i,t}^{D}$: Continuous var representing the cleared active power output on the DAM of each generator

$P_{i,t}^{rc}$: Continuous var representing curtailed power for each non-dispatchable RES generator

$P_{i,t}^{sr}$: Continuous var representing secondary reserve accepted for each dispatchable thermal generator

$u_{i,t}$: Binary var representing the status ON ($\alpha_{i,t} = 1$) or OFF ($\alpha_{i,t} = 0$) of each dispatchable thermal generator

$u_{i,t}^{\uparrow}$: Binary var representing the upward movement of each dispatchable thermal generator

$u_{i,t}^{\downarrow}$: Binary var representing the downward movement of each dispatchable thermal generator

$u_{i,t}^{sd}$: Shut-down binary var of each dispatchable thermal generator

$u_{i,t}^{sr}$: Secondary Reserve binary var of each dispatchable thermal generator

$u_{i,t}^{su}$: Start-up binary var of each dispatchable thermal generator

$\Delta F_{b,t}$: Continuous var representing change in active power flow on the b-th branch

5.2.1. DAM model

Let us consider an electrical power system composed of N^Z market zones with N^G generators installed among them, and N^L interzonal connections where load demand is assumed to be inelastic in relation to price. A linear programming (LP) optimization problem is proposed to simulate a zonal DAM (ZDAM), with the goal of minimising the stepwise generation costs at a single time step $t \in \Omega^T$ over a time window composed of N^T time steps. As a result, the optimisation problem can be expressed as follows:

$$\min_{P_{i,s,t}} \sum_{i \in \Omega^{TH}} \sum_{s \in \Omega^{S_i}} c_{i,s} P_{i,s,t} \tag{148}$$

s.t.

$$P_{i,t}^{D} = \sum_{s \in \Omega^{S_i}} P_{i,s,t} \quad \forall\, i \in \Omega^{TH} \tag{149}$$

$$0 \le P_{i,s,t} \le \Delta P_{i,s,t}^{max} \quad \forall i \in \Omega^{TH}, \forall s \in \Omega_{\mathrm{i}}^{S} \tag{150}$$

$$0 \le P_{i,t}^{D} \le P_{i,t}^{max} a_{i,t} \quad \forall i \in \Omega^{TH} \tag{151}$$

$$0 \le P_{i,t}^{D} \le P_{i,t}^{da} \quad \forall i \in \Omega^{R} \tag{152}$$

$$0 \le P_{i,t}^{D} \le P_{i,t}^{H,max} \quad \forall i \in \Omega^{H} \tag{153}$$

$$\sum_{i \in \Omega^{G}} P_{i,t}^{D} - \sum_{z \in \Omega^{Z}} D_{z,t}^{da} = 0 \tag{154}$$

$$\sum_{i \in \Omega^{G}} \alpha_{i,z}^{G} P_{i,t}^{D} - \sum_{l \in \Omega^{L}} \alpha_{z,l}^{F} F_{l,t} = D_{z,t}^{da} \quad \forall z \in \Omega^{Z} \tag{155}$$

$$F_{l}^{lb} \le F_{l,t} \le F_{l}^{ub} \quad \forall l \in \Omega^{L} \tag{156}$$

The equality constraint (149) defines the dispatched power of each thermal generator equal to the sum of the accepted bid steps. Inequality (150) limits the power of each bid step within its maximum width. Constraints (151) and (152) are required to ensure that the thermal units never exceed the maximum power and RES never exceed their hourly forecasted power, respectively. The dispatchable hydro (DH) units have an hourly dispatch strategy, and (153) specifies the maximum power available for each hour. The total and zonal active power balances of the system are presented in (154) and(155), respectively, whereas (156) expresses the active power flow boundaries on each interzonal connection. In particular, $\Delta P_{i,s,t}^{max}$ and $P_{i,t}^{MAX}$ are the maximum bid step width and the maximum available power of the i-th generator, respectively, obtained as below:

$$P_{i,t}^{max} = P_{i}^{max}\, e_{i,t} \tag{157}$$

$$\Delta P_{i,s,t}^{max} = \Delta P_{i,s}^{max}\, e_{i,t} \tag{158}$$

5.2.2. ASM generator bids adjustment

A set of bids is required to evaluate the various services to be provided in the ASM. In particular, the quantities offered by qualified units are adjusted based on the dispatched power in the DAM and the technical limits of each generator, while the relevance of each service is considered by applying appropriate time-varying factors to the marginal price. The bids presented by qualified units are the start-up (SU), shut-down (SD), upward redispatch (UR),

downward redispatch (DR), and secondary reserve (SR) bids defined, for each time step t, as described in the following.

- *Start-up bid*

$$P_{i,t}^{su} = min\{P_{i,t}^{min},\ P_{i,t}^{min} - P_{i,t}^{D}\}^{+} \quad \forall\, i \in \Omega^{TD} \tag{159}$$

$$C_{i,t}^{su} = C_{i}^{su}\left(1 - u_{i,t-1}\right) + P_{i,t}^{su}\, c_{i,t}^{su} \quad \forall\, i \in \Omega^{TD} \tag{160}$$

in which

$$P_{i,t}^{min} = P_{i}^{min}\, e_{i,t} \tag{161}$$

$$c_{i,t}^{su} = avg\left(c_{i,s}\right) R_{t}^{su} \tag{162}$$

the SU bid in (159), submitted by dispatchable thermal generators, is the positive minimum between the technical minimum, that varies as defined in(161), and the difference between the technical minimum and the dispatched power after the DAM. The SU cost (160) is the sum of a constant term (C_{i}^{su}) and a time-varying term ($c_{i,t}^{su}$) multiplied by $P_{i,t}^{su}$. The first is taken into account if in the previous time step the generator was shut-down, whereas the second is the average energy marginal costs multiplied by a suitable time-varying factor R_{t}^{su} as in(162).

- *Shut-down bid*

$$P_{i,t}^{sd} = min\{P_{i,t}^{min},\ P_{i,t}^{D}\}^{+} \quad \forall\, i \in \Omega^{TD} \tag{163}$$

$$C_{i,t}^{sd} = P_{i,t}^{sd} \cdot avg\left(c_{i,s}\right) R_{t}^{sd} \quad \forall\, i \in \Omega^{TD} \tag{164}$$

the SD bid of a dispatchable thermal generator, in (163), is the minimum positive quantity between the technical minimum and the cleared power in the DAM. The SD cost (164) has only a variable term evaluated considering a proper time-varying factor R_{t}^{sd} multiplied by the average energy marginal costs.

- *Upward redispatch bids*

$$\Delta P_{i,s,t}^{max\uparrow} = min\{\Delta P_{i,t}^{st}, P_{i,t}^{max} - \left(s\, \Delta P_{i,t}^{st} + P_{i,t}^{D}\right)\} \quad \forall\, i \in \Omega^{TD} \cup \Omega^{H}, s = 1, \dots, N_{i}^{s^{\uparrow}} \tag{165}$$

$$c_{i,s,t}^{\uparrow} = R_{s,t}^{\uparrow} c_{i,s^{\uparrow}} \quad \forall i \in \Omega^{TD} \cup \Omega^{H}, s = 1, \dots, N_{i,t}^{s^{\uparrow}}, s^{\uparrow} = N_{i,t}^{S^{\uparrow}}, \dots, N_{i}^{S} \tag{166}$$

in which

$$\Delta P_{i,t}^{st} = \frac{1}{N_i^S}\left(P_{i,t}^{max} - P_{i,t}^{min}\right) \tag{167}$$

$$N_{i,t}^{S^{\uparrow}} = \left\lceil \frac{P_{i,t}^{max} - P_{i,t}^{D}}{\Delta P_{i,t}^{st}} \right\rceil \tag{168}$$

the UR bids (165) have a power width $\Delta P_{i,s,t}^{max\uparrow}$ equal to the minimum between a predefined quantity $\Delta P_{i,t}^{st}$ and the remaining control margin up to the maximum power of the unit. $\Delta P_{i,t}^{st}$ depends on the bid step number N_i^S and the total control margin, as in (167), whereas $N_i^{s^{\uparrow}}$ is the number of steps required to reach the maximum power expressed in (168). The respective bid cost $c_{i,s,t}^{\uparrow}$, defined in (166) is obtained from a proper time-varying factor $R_{s,t}^{\uparrow}$ and the marginal cost $c_{i,s^{\uparrow}}$ derived from the DAM operating condition.

- *Downward redispatch bids*

$$\Delta P_{i,s,t}^{max\downarrow} = min\left\{\Delta P_{i,t}^{st},\ P_{i,t}^{D} - s\,\Delta P_{i,t}^{st} - P_{i,t}^{min}\right\} \quad \forall\, i \in \Omega^{TD} \cup \Omega^{H}, s = 1, \dots, N_{i,t}^{S^{\downarrow}} \tag{169}$$

$$c_{i,s,t}^{\downarrow} = R_{s,t}^{\downarrow} c_{i,s^{\downarrow}} \quad \forall i \in \Omega^{TD} \cup \Omega^{H}, s = 1, \dots, N_{i,t}^{S^{\downarrow}}, s^{\downarrow} = N_{i,t}^{S^{\downarrow}}, \dots, 1 \tag{170}$$

where:

$$N_{i,t}^{S^{\downarrow}} = \left\lceil \frac{P_{i,t}^{D} - P_{i,t}^{min}}{\Delta P_{i,t}^{st}} \right\rceil \tag{171}$$

the DR bids are formulated based on the previous ones. In particular, the power width $\Delta P_{i,s,t}^{max\downarrow}$ of (169) is the minimum between $\Delta P_{i,t}^{st}$ and the remaining control margin up to the minimum power of the uni. The bid cost $c_{i,s,t}^{\downarrow}$ of (170) is the product of the time-varying factor $R_{s,t}^{\downarrow}$ and $c_{i,s^{\downarrow}}$. Finally, $N_{i,t}^{S^{\downarrow}}$ is the number of steps required to reach the minimum power defined in (171).

- *Secondary reserve bid*

$$P_{i,t}^{sh} = k^{sr}\ P_{i,t}^{max}\ \ \forall\, i \in \Omega^{TD} \tag{172}$$

$$c_{i,t}^{sr\uparrow} = R_t^{sr\uparrow} avg\left(c_{i,s}\right)\ \ \forall\, i \in \Omega^{TD} \tag{173}$$

$$c_{i,t}^{sr\downarrow} = R_t^{sr\downarrow} avg\left(c_{i,s}\right)\ \ \forall\, i \in \Omega^{TD} \tag{174}$$

the SR power bid is the generator's secondary reserve half-bandwidth (SRH), obtained as a certain percentage (k^{sr}) of $P_{i,t}^{max}$, as defined in (172). In particular, the SR is an automatic

control, in which all the cleared units are dispatched simultaneously, providing the required percentage of the reserved quantity. Therefore, in the clearing process, $P_{i,t}^{sh}$ must be equal in both upward and downward action. The costs for supplying upward and downward SR, provided in (173) and (174), respectively, considering proper upward ($R_t^{sr\uparrow}$) and downward ($R_t^{sr\downarrow}$) time-varying factors applied to the average marginal costs.

- *Bidding flowchart*

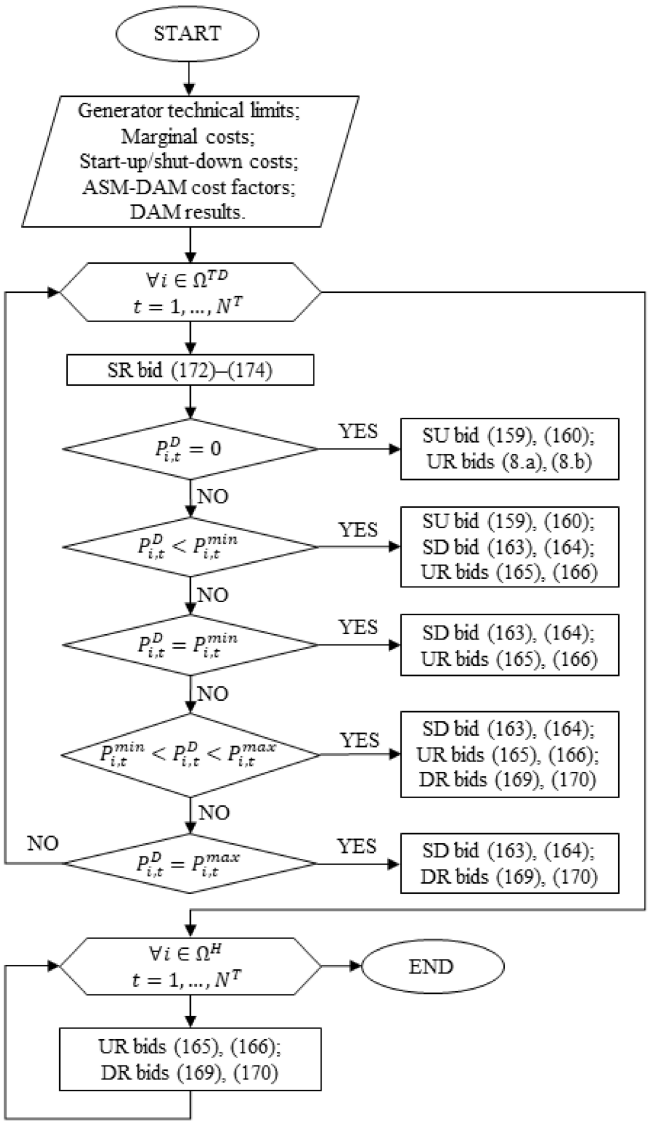

Fig. 53. ASM bids adjustment flowchart.

The ASM bids adjustment mechanism is synthetised in Fig. 53, where the bids presented for the ASM by each eligible unit are shown in relation to the technical limits, the $P_{i,t}^{DAM}$ and the unit technology, i.e. thermal or DH. In particular, DH units have $P_{i,t}^{MIN} = 0$,

therefore the DH bid adjustment process concerns the UR and DR bids, and $\Delta P_{i,t}^{st}$ in (167) is defined from 0 to $P_{i,t}^{MAX}$. On the other hand, after the DAM, thermal units can be dispatched below the technical minimum, so proper SU and SD bid adjustment is defined in (159) and (163), respectively.

5.2.3. DC load flow and sensitivity factors

DC Load Flow (DCLF) calculations are performed, for each time step of the considered time horizon, in order to assess the effective branches' power flow due to the dispatched generation of the ZDAM. Considering a power system composed of N^N nodes and N^B branches, for each time step t, the nodal matrix form of the DCLF equations can be written as follows:

$$\boldsymbol{B}^{dc}\theta_t - P_t^{dc} = 0 \tag{175}$$

where $\boldsymbol{B}^{dc}$ is the (N^N– 1) x (N^N– 1) symmetric matrix of the conductances, obtained neglecting, repsectively, the row and column of the slack bus and reference angle, θ is the vector of dimiention (N^N– 1) of the voltage angles, whereas P^{dc} is the vector of the DC nodal power balance of dimiention (N^B– 1), and:

$$N_{i,t}^{S^{\downarrow}} = \left\lceil \frac{P_{i,t}^{D} - P_{i,t}^{min}}{\Delta P_{i,t}^{st}} \right\rceil \tag{176}$$

is the active power flowing through each branch obtained multiplying the voltage angle difference between the interconnected buses and the and the branch susceptance.

Subsequently, DC sensitivity factors are calculated to quantify how an incremental change in the nodal active power affects the branch power flows. For this purpose, and to avoid lack of generality, DC power transfer distribution factors (PTDF) are calculated by a distributed slack bus DCLF [242]. Because the DCLF is a linearized calculation tool, the resulting PTDF are linear as well, depending only on the network topology.

5.2.4. SCUCER formulation

The proposed DAM aims to minimize the generation costs based on the forecasted load demand and solar and wind production. However, neglecting the generation constraints and considering a zonal market framework, the solution may result in an infeasible global optimum operating condition from the network perspective. As a result, a security constrained

unit commitment and economic redispatch (SCUCER) optimization problem is developed to account for the network and generation constraints, the SRR procurement, and updated load, wind and solar forecasts. For this purpose, the objective function seeks to minimize the UR and DR costs, the SU and the SD costs, the SR provision costs, the load shedding (LS) costs and the RES curtailment (RC) costs as below, for each $t \in \Omega^T$:

$$\min\left[C_t^{\uparrow} - C_t^{\downarrow} + C_t^{SU} - C_t^{SD} + C_t^{SR} + C_t^{LS} + C_t^{RC}\right] \tag{177}$$

where selling bids, i.e. those that increase the dispatched power, represent an expense for the TSO vice versa for the buying bids. In particular, the costs are defined as follows:

$$C_t^{\uparrow} = \sum_{i \in \Omega^{TD} \cup \Omega^H} \sum_{s=1}^{N_{i,t}^{S^{\uparrow}}} c_{i,s,t}^{\uparrow} \, \Delta P_{i,s,t}^{\uparrow} \tag{178}$$

$$C_t^{\downarrow} = \sum_{i \in \Omega^{TD} \cup \Omega^H} \sum_{s=1}^{N_{i,t}^{S^{\downarrow}}} c_{i,s,t}^{\downarrow} \, \Delta P_{i,s,t}^{\downarrow} \tag{179}$$

$$C_t^{SU} = \sum_{i \in \Omega^{TD}} C_{i,t}^{su} \, u_{i,t}^{su} \tag{180}$$

$$C_t^{SD} = \sum_{i \in \Omega^{TD}} C_{i,t}^{sd} \, u_{i,t}^{sd} \tag{181}$$

$$C_{i,t}^{SR} = \sum_{i \in \Omega^{TD}} \left(c_{i,t}^{sr\uparrow} - c_{i,t}^{sr\downarrow}\right) P_{i,t}^{sr} \tag{182}$$

$$C_t^{LS} = \sum_{n \in \Omega^N} C^{voll} \, D_{n,t}^{ls} \tag{183}$$

$$C_t^{RC} = \sum_{i \in \Omega^R} C^{rc} \, P_{i,t}^{rc} \tag{184}$$

The optimisation problem is subject to several constraints that can be gathered in: UR and DR constraints (185)–(187); thermal unit constraints (188)-(202); DH unit constraints (203)-(205); RC and LS constraints (208), (209); and network constraints (210)-(212); defined and described in the following.

$$\Delta P_{i,s,t}^{\downarrow} - \Delta P_{i,s,t}^{max\downarrow} u_{i,t}^{\downarrow} \leq 0 \quad s = 1, \dots, N_{i,t}^{S^{\downarrow}} \tag{185}$$

$$\Delta P_{i,s,t}^{\uparrow} - \Delta P_{i,s,t}^{max\uparrow} u_{i,t}^{\uparrow} \leq 0 \quad s = 1, \dots, N_{i,t}^{S^{\uparrow}} \tag{186}$$

$$u_{i,t}^{\uparrow} + u_{i,t}^{\downarrow} \leq 1 \tag{187}$$

where (185) and (186) limit the UR and DR bids to the maximum step width, whereas (187) avoids the simultaneous UR and DR.

For each $i \in \Omega^{TD}$ the thermal unit constraints are:

$$\Delta P_{i,t}^{A} - \sum_{s=1}^{N_{i,t}^{S^{\uparrow}}} \Delta P_{i,s,t}^{\uparrow} + \sum_{s=1}^{N_{i,t}^{S^{\downarrow}}} \Delta P_{i,s,t}^{\downarrow} - P_{i,t}^{su} u_{i,t}^{su} + P_{i,t}^{sd} u_{i,t}^{sd} = 0 \tag{188}$$

$$P_{i,t}^{min} u_{i,t} - \Delta P_{i,t}^{A} + P_{i,t}^{sh} u_{i,t}^{sr} \leq P_{i,t}^{D} \tag{189}$$

$$P_{i,t}^{max} u_{i,t} - \Delta P_{i,t}^{A} - P_{i,t}^{sh} u_{i,t}^{sr} \geq P_{i,t}^{D} \ , \forall i \in \Omega^{TD} \tag{190}$$

$$u_{i,t} - \frac{P_{i,t}^{D} + \Delta P_{i,t}^{A}}{P_{i,t}^{max}} \geq 0 \tag{191}$$

$$u_{i,t} = 0 \text{ if } a_{i,t} = 0 \tag{192}$$

$$u_{i,t} - u_{i,t}^{\uparrow} \geq 0 \tag{193}$$

$$u_{i,t} - u_{i,t}^{su} \geq 0 \tag{194}$$

$$u_{i,t} + u_{i,t}^{sd} \leq 1 \tag{195}$$

$$u_{i,t}^{su} - u_{i,t}^{\uparrow} \geq 0 \quad \text{if } P_{i,t}^{D} < P_{i,t}^{min} \tag{196}$$

$$u_{i,t}^{su} = 0 \quad \text{if } P_{i,t}^{D} \geq P_{i,t}^{min} \tag{197}$$

$$u_{i,t}^{su} + u_{i,t}^{sd} = 1 \quad \text{if } 0 < P_{i,t}^{D} < P_{i,t}^{min} \tag{198}$$

$$\sum_{s=1}^{N_{i,t}^{S^{\downarrow}}} \Delta P_{i,s,t}^{\downarrow} - \sum_{s=1}^{N_{i,t}^{S^{\downarrow}}} \Delta P_{i,s,t}^{max\downarrow} u_{i,t}^{sd} \geq 0 \quad \text{if } P_{i,t}^{D} > P_{i,t}^{min} \tag{199}$$

$$u_{i,t} - u_{i,t}^{sr} \geq 0 \tag{200}$$

$$P_{i,t}^{sr} - P_{i,t}^{sh}\, u_{i,t}^{sr} \leq 0 \tag{201}$$

$$\sum_{i \in \Omega^{TD}} P_{i,t}^{sr} \geq SRR_t \tag{202}$$

the equality constraint (188) defines the total power redispatch as algebraic sum of the redispatch quantities accepted in the ASM. The technical minimum and maximum constraints are defined in (189) and (190), respectively. The constraint (191) defines the status of the thermal units according to DAM and ASM results. In (192) the generator status is bound to its availability. The constraints, (193), (194) and (195) allow the UR, the SU and the SD, respectively, according to the unit status. The units below the technical minimum after the DAM are constrained, in (196), to be SU before accepting the UR bids, whereas in (197) the units above the technical minimum cannot be SD. The units dispatched between 0 and the technical minimum are forced to be SU or SD in the constraint (198). For the units above the technical minimum, constraint (199) binds the SD bid clearance only if all the DR bids are accepted. In (200) the SR bid is conditioned to the generator status, and (201) limits the SR provision to the SRH of each thermal unit, whereas (202) defines the minimum SR to be procured, where the value of SRR_t is determined as in the previous paragraph.

For each $i \in \Omega^H$ the hydro unit constraints are:

$$\Delta P_{i,t}^{A} - \sum_{s=1}^{N_{i,t}^{S^{\uparrow}}} \Delta P_{i,s,t}^{\uparrow} + \sum_{s=1}^{N_{i,t}^{S^{\downarrow}}} \Delta P_{i,s,t}^{\downarrow} = 0 \tag{203}$$

$$E_{i,t}^{A} - E_{i,t-1}^{A} + \tau \Delta P_{i,t}^{A} = 0 \tag{204}$$

$$-\tau P_{i,t}^{D} \leq \tau \Delta P_{i,t}^{A} \leq min\left\{\tau\left(P_{i}^{max} - P_{i,t}^{D}\right), E_{i,t-1}^{A}\right\} \tag{205}$$

where (203) is the analogous total power redispatch for the DH units, (204) updates the available energy of the units according to the accepted bids in the ASM, whereas (205) limits the DAM and ASM dispatched power to the minimum between the available energy of the previous step and the rated power of the units. In particular, τ is expressed as fraction of hour and represents the duration of each time step.

The daily available energy for the DH units ($E_{i,d}^{M}$) varies from month to month and is divided into two parts: a major portion that is bid to the DAM in accordance with five

different trends based on typical load profiles as described in [243], and a minor portion that is stored for bidding in the ASM. As a result, $E^{A}_{i,t-1}$ is daily updated, adding the new daily available energy to the accepted quantities in the DAM and ASM as follows:

$$E^{A}_{i,t-1} = \sum_{\hat{d}=1}^{d} E^{M}_{i,\hat{d}} - \sum_{\hat{t}=1}^{t} \tau P^{D}_{i,\hat{t}} - \sum_{\hat{t}=1}^{t-1} \tau \Delta P^{A}_{i,\hat{t}} \quad \forall\, t \in \Omega^{T}, d = 1, \dots, N^{D} \tag{206}$$

where N^{D} is the number of days in the considered time window. Furthermore, it is supposed a maximum storable energy for each DH unit as follows:

$$E^{A}_{i,t-1} = \sum_{\hat{d}=1}^{d} E^{M}_{i,\hat{d}} - \sum_{\hat{t}=1}^{t} \tau P^{D}_{i,\hat{t}} - \sum_{\hat{t}=1}^{t-1} \tau \Delta P^{A}_{i,\hat{t}} \quad \forall\, t \in \Omega^{T}, d = 1, \dots, N^{D} \tag{207}$$

in which k^{H} is a positive integer number.

The RC and LS are limited to an upper bound defined as:

$$0 \le P^{rc}_{i,t} \le P^{rt}_{i,t} \quad , \forall\, i \in \Omega^{R} \tag{208}$$

$$0 \le D^{ls}_{n,t} \le k^{L} D^{rt}_{n,t} \quad , \forall\, n \in \Omega^{N} \tag{209}$$

Finally, network constraints are:

$$\sum_{i \in \{\Omega^{TD} \cup \Omega^{H}\}} \left[P^{D}_{i,t} + \Delta P^{A}_{i,t}\right] + \sum_{i \in \Omega^{ND}} P^{D}_{i,t} + \sum_{i \in \Omega^{R}} \left[P^{rt}_{i,t} - P^{rc}_{i,t}\right] - \sum_{n \in \Omega^{N}} \left[D^{rt}_{n,t} - D^{ls}_{n,t}\right] = 0 \tag{210}$$

$$F^{min}_{b} \le F^{0}_{b,t} + \Delta F_{b,t} \le F^{max}_{b} \quad \forall b \in \Omega^{B} \tag{211}$$

$$\Delta F_{b,t} = \sum_{n \in \Omega^{N}} S_{n,b} \left(\sum_{i \in \{\Omega^{TD} \cup \Omega^{H}\}} \beta_{i,n} \Delta P^{A}_{i,t} + \Delta P^{W}_{n,t} + \Delta P^{P}_{n,t} - \Delta D^{L}_{n,t} + D^{ld}_{n,t} - \sum_{i \in \Omega^{R}} \beta_{i,n} P^{rc}_{i,t} \right) \quad \forall b \in \Omega^{B} \tag{212}$$

where (210) represents the power balance, (211) limits the branches power flow to the upper and lower bounds, whereas (212) defines the power flow variation according to the PTDF and the redispatched quantities and the forecast update of load demand wind and solar production.

5.3. NREL 118-Bus Test System

The proposed methodology is applied to the NREL 118-bus test system, characterized by high penetration of RES and several thermal power plants, distributed on three market zones, as shown in Fig. 54 [211], [212]. The forecast uncertainties are obtained from Terna's RRs and load dataset [244], [245], and RES measurement data provided by research projects. In addition to the information provided in the paragraph 3.3, the zonal installed capacity is roughly 10.5 GW in Zone 1, 19.7 GW in Zone 2 and 10.3 GW in Zone 3. Combined cycle (CC) technology is the most spread in Zone 1 with 5.81 GW, followed by steam turbine (ST) and combustion turbine (CT) with respectively 1.48 GW and 1.36 GW; each one supplied by natural gas (NG). Hydro power generation is mostly installed in Zone 2, with 8.38 GW of dispatchable capacity and 8.51 GW of non-dispatchable (ND) capacity. The main technologies of Zone 3 are CC NG, hydro ND, and CT NG with respectively 3.44 GW, 1.65 GW and 1.55 GW of installed capacity. The total solar photovoltaic (PV) installed capacity is 3.45 GW of which 35% is present in Zone 1, 50% in Zone 3, and the remaining 15% in Zone 3. Finally, wind power plants are installed in Zone 1 and Zone 3 with 0.33 and 0.75 GW respectively. The installed capacity is distributed among 327 generators, gathered in 132, 78 and 117 from Zone 1 to Zone 3.

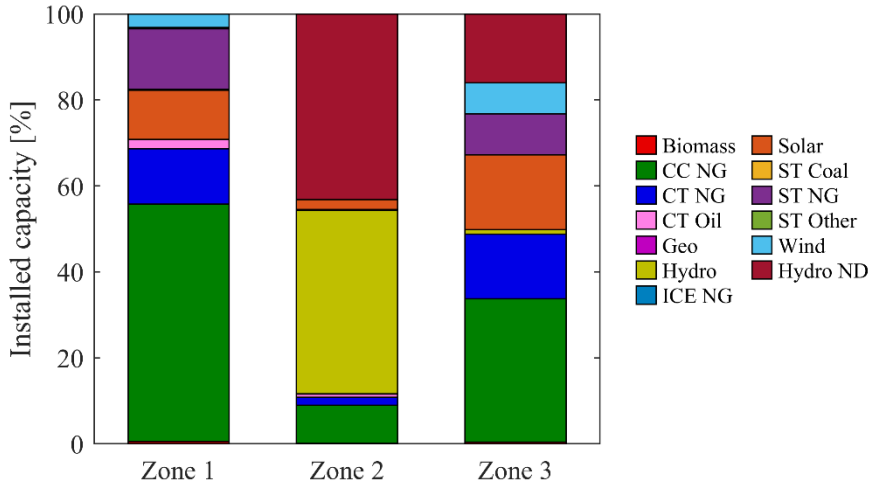

Fig. 54. Zonal generation capacity per technology and fuel.

Table 32. Interzonal lines and rated powers.

Interconnected zones	Interconnected buses	Rated power [MW]
Z1-Z2	15-33	600

Z1-Z2	19-34	600
Z1-Z2	30-38	600
Z1-Z2	70-69	1700
Z1-Z2	75-69	1700
Z1-Z2	75-77	600
Z1-Z2	75-118	600
Z2-Z3	77-82	700
Z2-Z3	80-96	600
Z2-Z3	97-96	600
Z2-Z3	98-100	600
Z2-Z3	99-100	600

The zonal market framework of the network presents two interconnections, one between Zone 1 and Zone 2 (Z1-Z2) and the other between Zone 2 and Zone 3 (Z2-Z3). Table 32 reports the interconnection lines between market zones with their rated power, with total maximum transfer capacity equal to 6400 MW and 3100 MW, for Z1-Z2 and Z2-Z3 zonal connections respectively. Applying the N-1 security criterion to the line with the greatest rated power, for the zonal market, the available transfer capacity (ATC) for Z1-Z2 is 4700 MW, whereas for Z2-Z3 is 2400 MW. Generator marginal costs range per each technology are the same defined in Table 11.

Fig. 55 shows the yearly energy supplied by each technology, as result of the DAM optimization problem (122)–(126) during the year. Half of the required load is covered by CC technology, roughly one quarter by Hydro and the remaining quarter among Solar, Wind and CT. Biomass and Geo have low installed capacity, whereas ST has several expensive units therefore it is cleared only during peak load hours. However, in order to participate in the ASM, power plants must meet certain technical requirements set by the system operator. For this purpose, following the Italian Grid Code [6], the dispatchable candidate units have rated power greater than or equal to 10 MW. As a result, there are 88 units allowed to provide ancillary services, of which 28 are CC, 52 are CT, 8 are ST, with total zonal nominal power of 8181.18 MW, 2282.76 MW, and 5766.17 MW for Zone 1, Zone 2, and Zone 3. The DAM clearing yields the total increasing and decreasing power margins of the 88 units, shown in Fig. 56. The increasing margin ranges from 3.1 GW to 14.8 GW, while the decreasing margin ranges from -0.7 GW to -12.2 GW. According to the dynamic rated power of the generators, the total available margin fluctuates monthly, by maximum ±0.5 GW, with an average value

of roughly 15 GW. Finally, Fig. 57 depicts the duration curve of the total power variation (TPV) from DA forecast to RT operation of net load (difference between demand and Solar and Wind production), showing the maximum positive and negative unbalance of 3.5 GW and –3.3 GW, respectively, and average value of –141.2 MW.

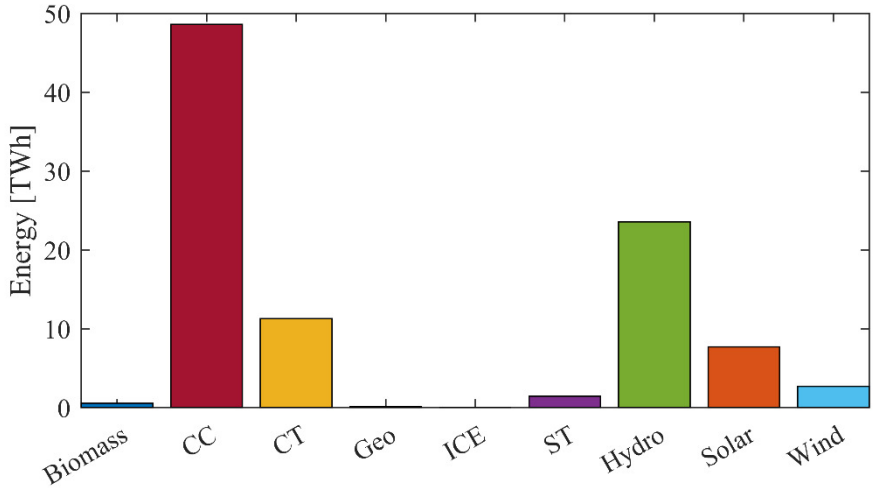

Fig. 55. Yearly energy production per technology.

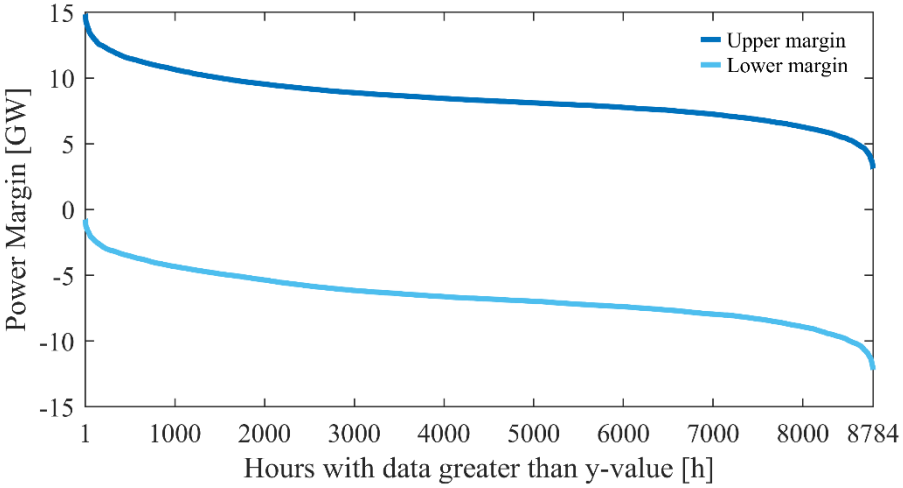

Fig. 56. Upper and lower power margin of the eligible generating units.

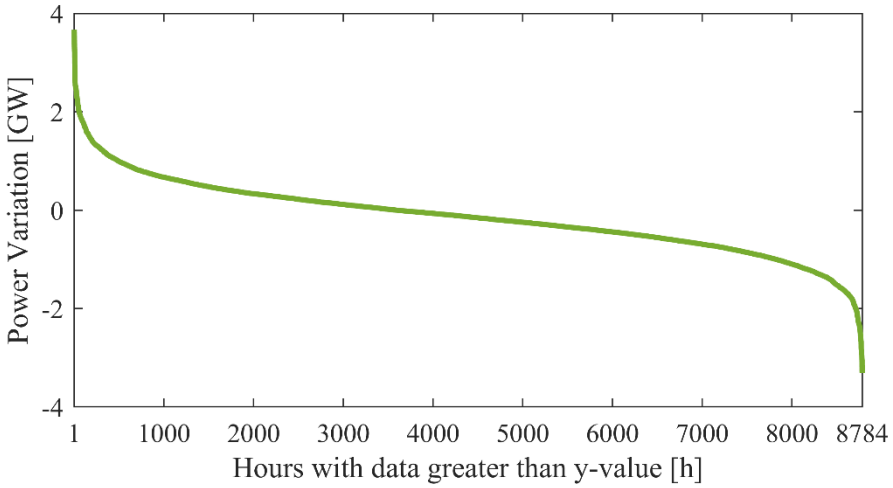

Fig. 57. Total power variation from DA to RT of load, wind and solar.

Fig. 58, Fig. 59 and Fig. 60, show, respectively, load, PV and wind standard deviation of the forecast errors used in (121) and normalized according to the yearly peak load. The standard deviations are evaluated obtaining mean values for each season and hour for load and wind power plants, instead the PV standard deviation mean values has been obtained for each hour and bimonthly with the same daylight duration (i.e., June and July, May, and August, etc.). As results, the bell-shaped trends obtained have different temporal windows and peak according to months.

The highest load forecast error is roughly 0.024 pu in Summer and the lowest is 0.009 pu in Autumn. For the PV, the higher standard deviation trend occurs during the months April-September with a peak value of 0.013 pu, whereas in June-July the trend is peak-shaved in the central hours, due to the more accurate prediction in the presence of clear sky , where the minimum peak value is equal to 0.008 pu. During the season, daily wind production forecast errors are more consistent, and during the year it varies from a minimum of 0.004 pu (Summer) up to 0.010 pu (Spring).

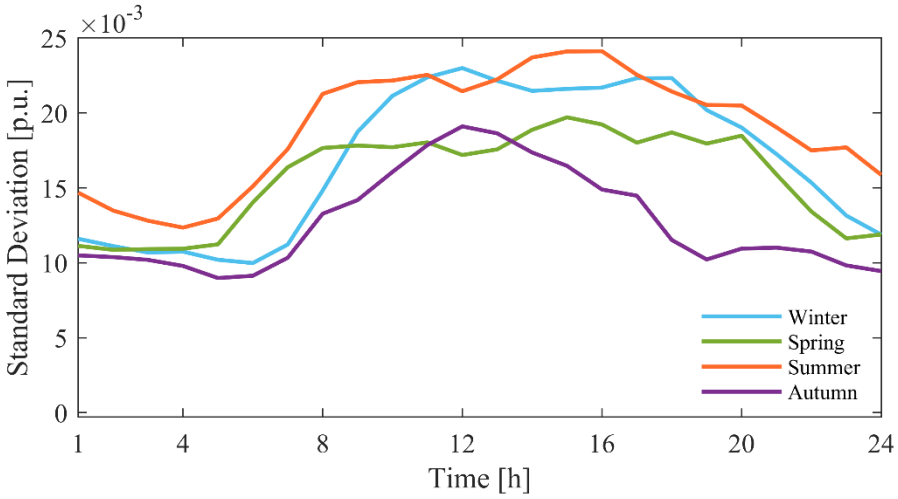

Fig. 58. Seasonal load standard deviation.

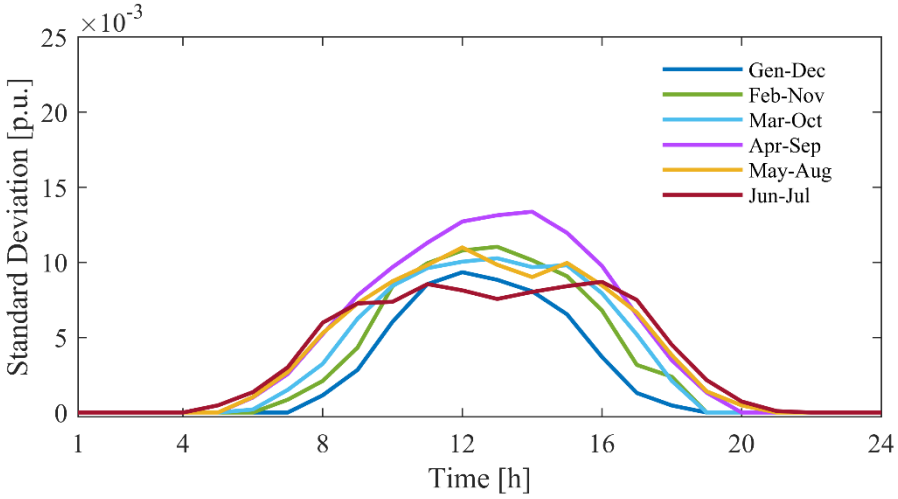

Fig. 59. Bimonthly PV standard deviation.

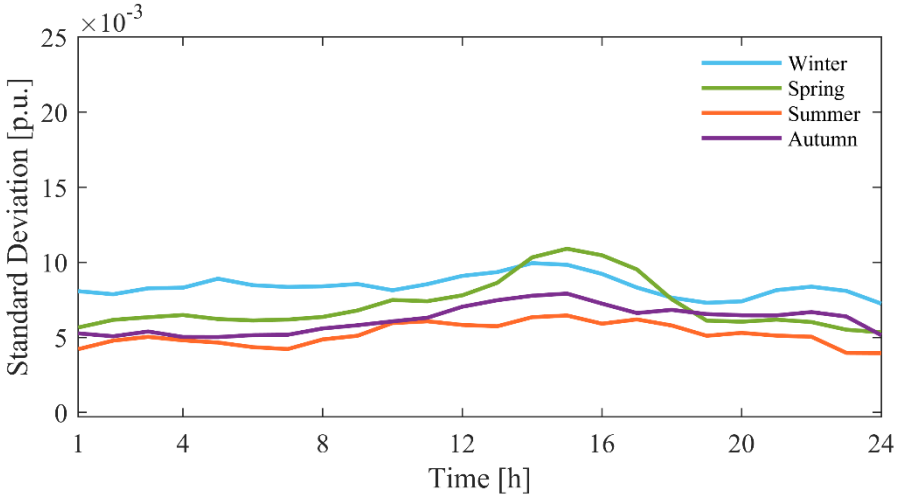

Fig. 60. Seasonal wind standard deviation.

5.4. Reserve Sizing

The procedure is applied to the whole year operation data reported in the dataset [212] For the sake of exemplification, in Fig. 61 the values obtained for the yearly peak load day are shown, in particular SRR is calculated from (113), and the preliminary TRRs are determined as in (114), (120) and (121) as explained in the previous section, in pu value of peak load. A similar trend for SRR and preliminary ReRR, ranging from 0.0107 pu to 0.0174 pu, is observed during the day, indicating that no ramp variation is detected, therefore the maximum SpRR is the double of SRR. The preliminary RRR has values between 0.0940 pu and 0.1708 pu, roughly ten times greater of SRR. The minimum and maximum values of SRR, ReRR, and SpRR occur at the same time steps, i.e. during the minimum load at hour 3 and the maximum load at hour 15. However, the lowest RRR occurs for two consecutive time steps, hours 3 and 4, while the highest RRR occurs at hour 14. This demonstrates that the first three RRs are strictly related to the forecast load, whereas the RRR is affected by uncertainties that vary throughout the day independently from the load.

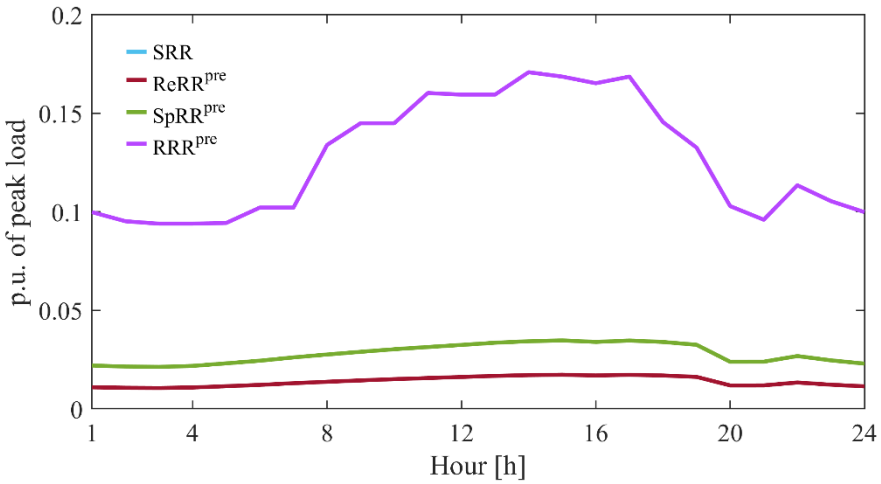

Fig. 61. RRs during the yearly peak day.

5.3.1. Seasonal Classification

The application of the classification reported in (127)–(130) to the yearly dataset of the test system is synthetized in the Table 33. In particular, for each a-th season, $N_R = N_L = 10$ classes are defined for RES generation and load demand, and each class is identified by $R_{i,a}$ and $L_{j,a}$ with $i, j = 1, \ldots, 10$. On the bases on the data reported in Table 33, the class R_1-L_1

in Winter season includes all the time steps with RES generation between 6 MW and 360.8 MW and with load demand between 6,666 MW and 7,415.9 MW.

Exploiting this classification, the number of hours categorized in each class (i.e., the number of elements of $\boldsymbol{c}_{i,j,a}$) is depicted in Fig. 62. The most frequent classes are with low RES penetration (R_1 and R_2) – mainly driven by PV unavailability during evening and night – and several load requirements. Later on, there are the classes with higher RES penetration and middle load demand (L_5, L_6 and L_7). The more extreme the load and RES classes, the lesser the samples. Furthermore, the seasonal peak load occurs for higher RES classes during Summer and Autumn, vice versa for the rest of the seasons. For instance, in the class R_1-L_1 in Winter season 87 time steps are included.

Table 33. NREL 118-bus test system seasonal classification values of load and RES [MW].

Season	$P_a^{R,min}$	$P_a^{R,max}$	ΔP_a^R	$P_a^{D,min}$	$P_a^{D,max}$	ΔP_a^D
Winter	6	3,554	354.8	6,666	14,165	749.9
Spring	21	3,947	392.6	6,286	15,756	974.0
Summer	19	3,601	352.8	6,976	17,288	1,031.2
Autumn	2	3,273	327.1	6,410	15,604	919.4

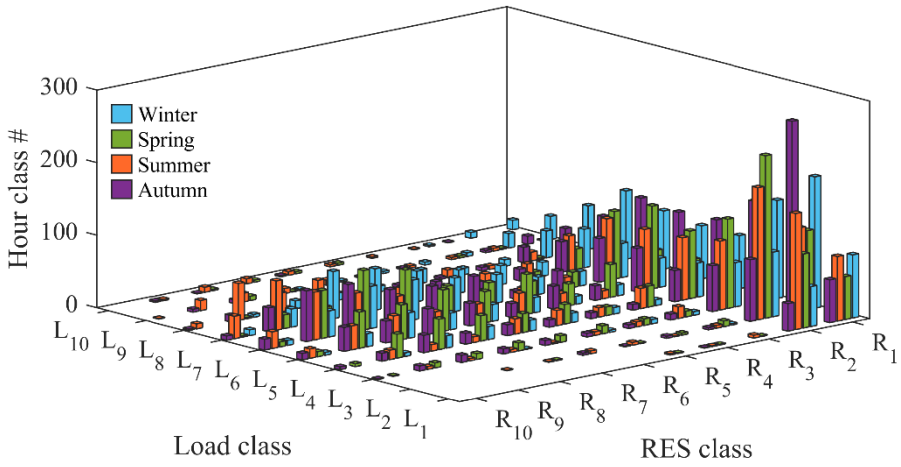

Fig. 62. Seasonal class hour recurrences of the test system.[3]

5.3.2. Reserve Requirement Preliminary Sizes

Supposing $k = 0.04$ in (115) the hourly mean seasonal load ramp variation of the NREL 118-bus test system is shown in Fig. 63. Only in 149 hours occurs a load ramp variation

[3] For the sake of visualization improvement, in this figure RES axis is reported from the highest class (R_{10}) to the lowest one (R_1).

during the time window, in which 45 occur in Winter, 24 in Spring, 52 in Summer, and 25 in Autumn. The mean values have been evaluated also considering the hours in which $\Delta P^R = 0$ in order to evaluate its impact during the season. It can be seen that Spring and Autumn have low mean error with a maximum mean impact of 0.001 pu. In particular, in Spring there are errors from hour 3 to 20 with few gaps, whereas in Autumn the gap is within the morning hours. In Winter, the peak is roughly 0.0025 pu at 5, in the central hours there is not ramp variation, whereas in the evening and the night there are two lower peaks. Finally, in the Summer only from hour 1 to 3 there is not ramp error, and the peak is reached at 5 with an approximate value of 0.004 pu.

The average of SRR and preliminary ReRR, evaluated for each season and class and normalized by the yearly peak load (17.28 GW), are depicted in Fig. 64 and Fig. 65, respectively. Maximum SRR value is 0.0171 pu and occurs in the highest load class in Summer, whereas minimum SRR value is detected in the lowest load class in Spring and it is equal to 0.0089 pu. Among the seasons, the preliminary SRR reaches the lowest value in Winter with 0.0149 pu, whereas the minimum SRR assumes the highest value in Summer with 0.0097 pu. These values are in line with the load required per each season. In particular, the lowest and the highest seasonal values are obtained respectively in class L_1 and L_{10} for ReRR: 0.0149 pu and 0.0093 pu, 0.0161 pu and 0.0089 pu, 0.171 pu and 0.0097 pu and 0.0162 pu and 0.0092 pu from Winter to Summer.

Considering that for k = 0.04 the hourly mean of seasonal ramp/deramp error ΔP^R has a maximum value of 0.004 pu (Fig. 63), that is lower than the half of minimum SRR, this error is determined only in 149 ramp/deramp hours. Therefore, a limited impact on preliminary ReRR is expectable, and this depends on the ramp/deramp occurrences in each class. For a better visualization, Fig. 66 shows the percentage difference between mean values of preliminary ReRR and SRR per each season and class. The classes with the highest percentage difference are in Autumn: in L_8-R_6 it reaches 0.0223 %; in L_2-R_5 it is roughly 0.0183 %. Furthermore, in Fig. 67 the influence of this parameter k in the determination of ΔP^R and in the number of occurrences is shown, and it can be inferred that a decrease of threshold implies increase of maximum ΔP^R and of the occurrences. In particular, the maximum value moves from 0.120 pu for k = 0.055 to 0.133 pu for k = 0.025, whereas ramp/deramp conditions are individuated in 128 hours for k = 0.055 up to 240 hours for k = 0.025. Therefore, the choice

of the daily threshold parameter slightly affects the determination of the mean ReRR in each class, although keeping importance in the analysis of a specific ramp/deramp operation condition. Finally, Fig. 68 shows the preliminary SpRR evaluated for each season and class as well, where the lowest and the highest seasonal values are obtained respectively in class L_1 and L_{10} with 0.0299 and 0.0186, 0.0322 and 0.0178, 0.0342 and 0.0194 and 0.0325 and 0.0184 from Winter to Summer.

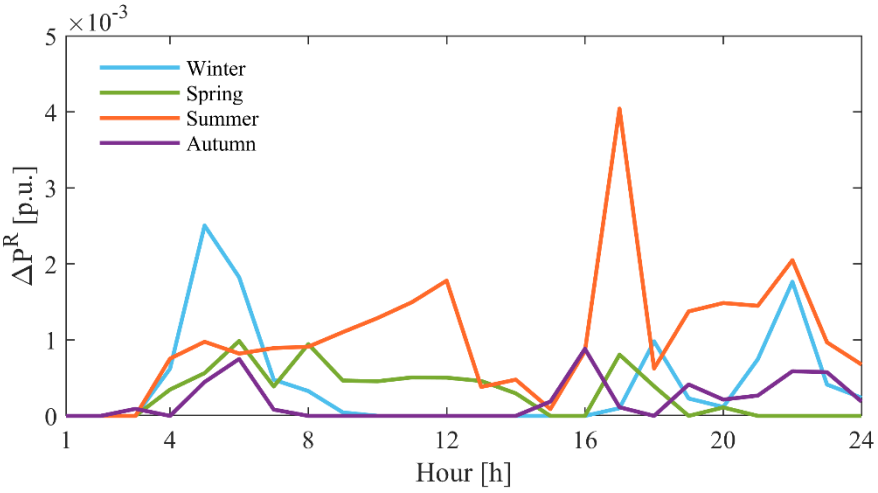

Fig. 63. Seasonal mean load ramp variation.

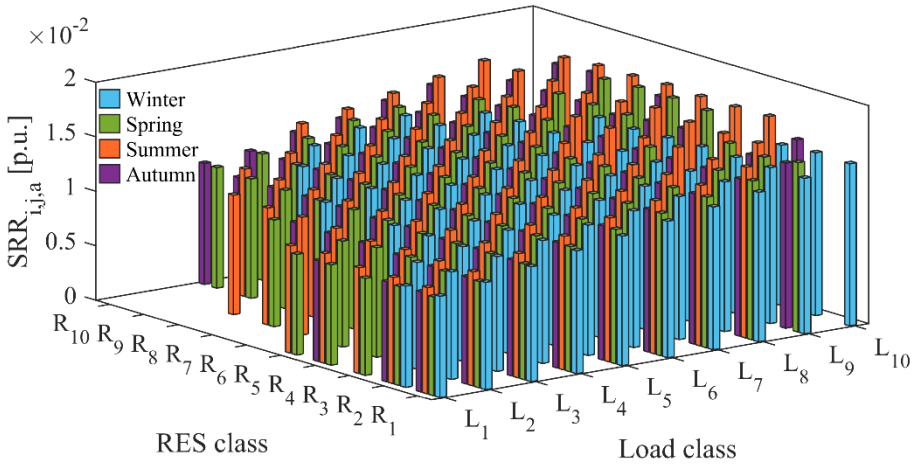

Fig. 64. Seasonal SRR for each class in relative value.

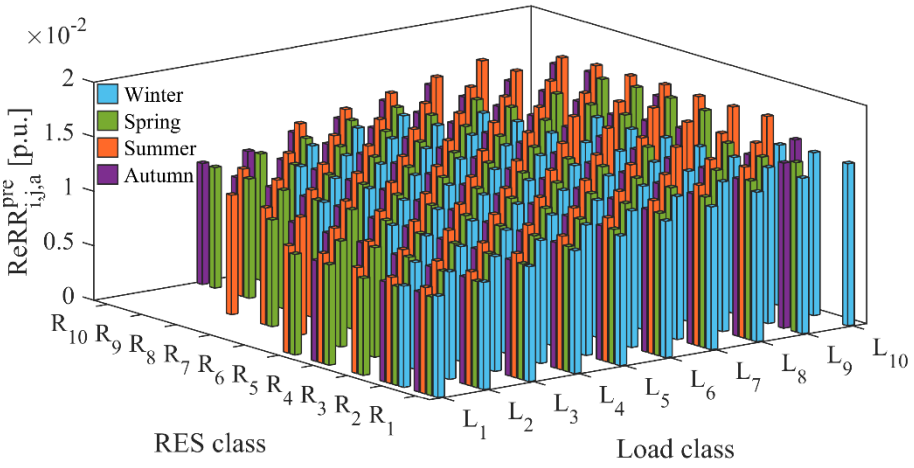

Fig. 65. Seasonal preliminary ReRR for each class in relative value.

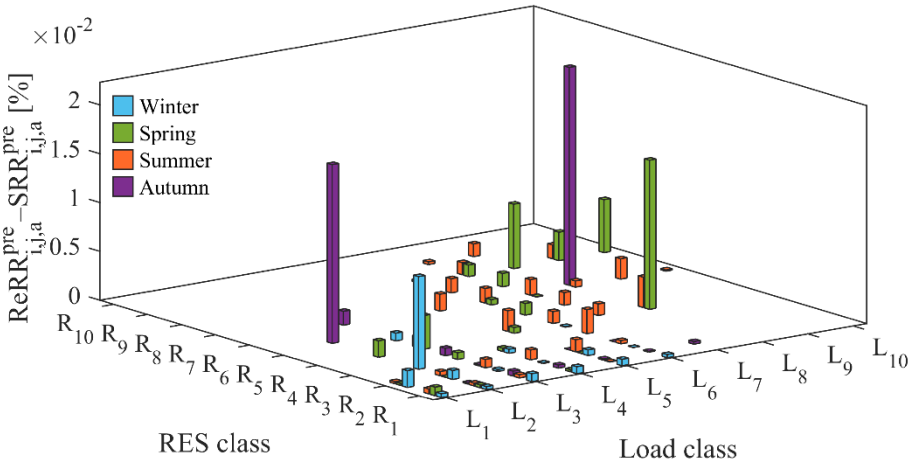

Fig. 66. Percentage difference between ReRR and SRR.

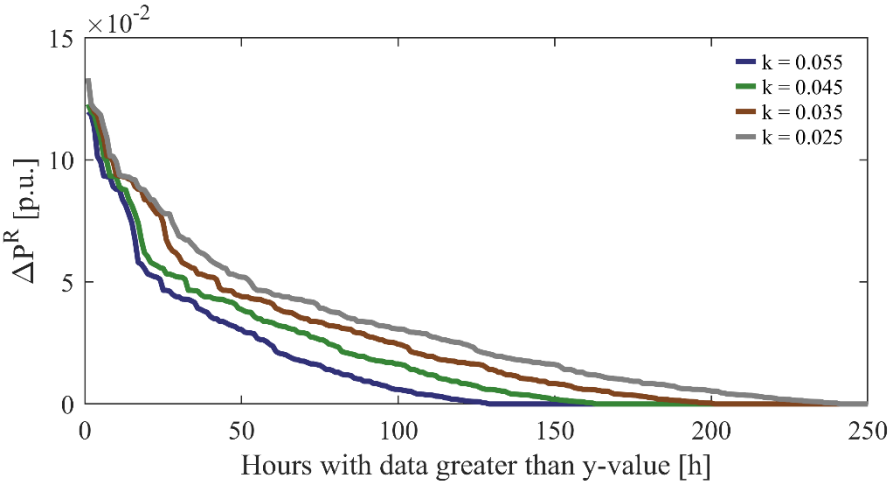

Fig. 67. Evaluation of ΔP^R varying k.

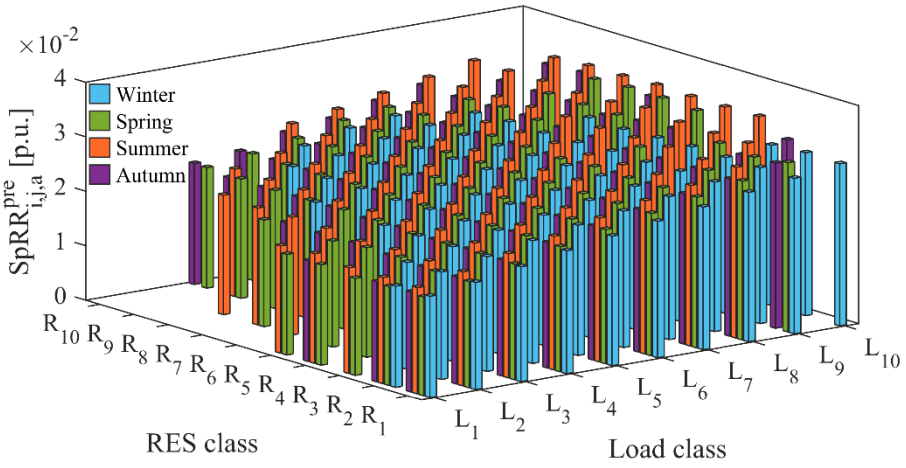

Fig. 68. Seasonal preliminary SpRR for each class in relative value.

From (121) RRR estimation depends on load, solar and wind seasonal forecast errors, as well as the maximum dispatched power in DAM. The first three terms have been deeply analyzed in the test case paragraph, whereas in Fig. 69 the mean value of the maximum dispatched power in DAM is depicted, per each season and class, in per unit values of peak load as well. It can be observed that, for each season, the higher the load class, the greater the maximum dispatched power in DAM. In Winter, an average value of 0.0458 pu is obtained, and slight differences among classes are observed, roughly [–10 % ÷ +2 %]. Summer classes, on the other hand, are characterized by highest variability, with an average of 0.0537 pu and a variation range within [–29 % ÷ +40 %], moreover extreme values reached in summer, equal to 0.0383 pu and 0.0753 pu, respectively, represent the extreme values observed over the entire year. This is primarily due to two correlated factors: the mean RES penetration and the load variation. During the winter, in fact, RES production is mostly ascribable to wind generators, whereas solar provides the most part of RES supply during Summer, with a sharp distinction between the daylight and night time steps. On the contrary, as shown by the statistical data in Table 33, the load trend has different profiles throughout the seasons. In addition, it should be noted that generators are subject to availability in DAM throughout the year that affects the cleared power solution.

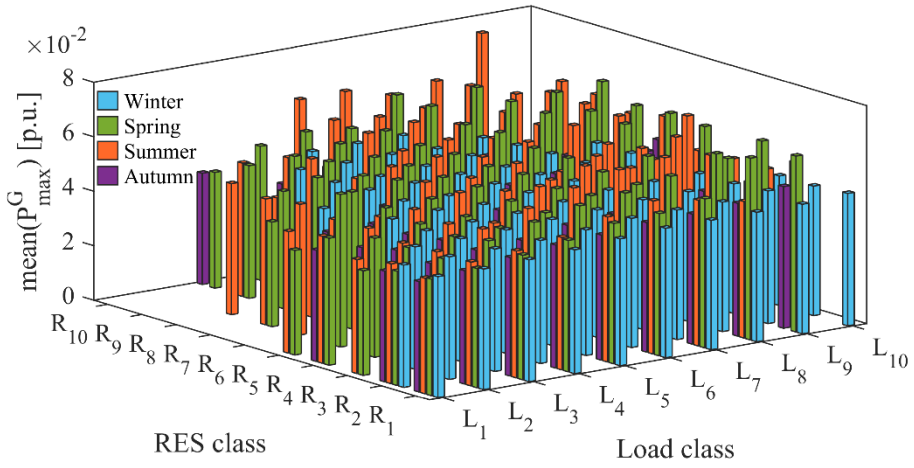

Fig. 69. Seasonal maximum DAM cleared power mean.

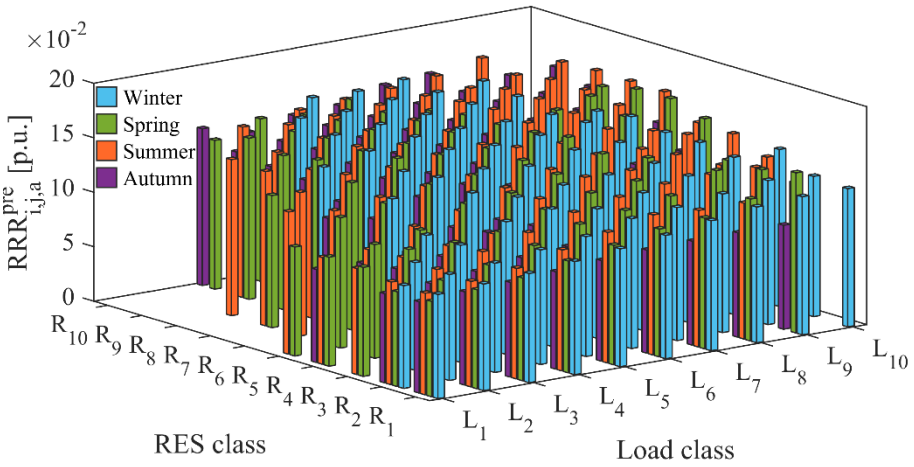

Fig. 70. Seasonal preliminary RRR for each class in relative value.

In order to evaluate the influence of the maximum dispatched power in DAM on RRR calculation, Fig. 70 shows seasonal preliminary RRR per each class, and Table 34 reports relevant minimum, average and maximum values. It can be noted that, differently from the other reserves, RRR is affected by both classification parameters, and its values are roughly ten times higher than ReRR, representing a more challenging target to be reached by gathering reserve provision. The maximum seasonal values occur in class L_8-R_9 during Winter with 0.1653, in class L_{10}-R_6 during Spring with 0.1610, in class L_9-R_{10} during Summer and Autumn respectively with 0.1663 pu and 0.1589 pu. The minimum seasonal values occur in class L_1-R_2 during winter, spring and autumn with 0.0943, 0.0869 and 0.0818, respectively. For summer the minimum RRR occurs in scenario L_1-R_1 and the value is equal to 0.0934. From the comparison with Fig. 69 , it can be seen that the maximum dispatched power in

DAM is approximately one third of the RRR, whereas the remaining two thirds depend on load, wind and solar uncertainties. In fact, the highest seasonal RRR values are obtained in classes with high RES production and required load, especially in Summer where the highest solar production and load demand occur (see $P_a^{R,max}$ and $P_a^{D,max}$ in Table 33) [211], [212].

Table 34. Preliminary RRR minimum, mean and maximum seasonal values [p.u.].

Season	***Minimum***	*Mean*	***Maximum***
Winter	0.0943	0.1354	0.1653
Spring	0.0869	0.1323	0.1610
Summer	0.0934	0.1389	0.1663
Autumn	0.0818	0.1194	0.1589

5.3.3. Evaluation of the Statistical Coefficients

In order to apply the Reference Statistical Combination of effective estimations of RRs, the Italian power system dataset is considered as reference system. Therefore, the seasonal classification (127)–(130) is applied to the Italian TS dataset of RES and load dataset throughout the year 2019 [244] considering ten classes for load and RES as well, as synthetized in Table 35. Comparing with Table 33 it can be observed that the two power systems, although characterized by different scales, present similar load and RES trends over the seasons. In particular, the yearly peak load is observed in Summer, moreover the maximum and minimum RES production is experienced in Spring and Autumn, respectively. The reference system occurrences for each class and season are depicted in Fig. 71. It can be noted that, as for the test system (Fig. 62), the most populated classes are characterized by low seasonal RES generation and low load demand, whereas the middle level of class population is represented by high seasonal load demand.

The determination of the overall statistical coefficients in (138)–(140), (144) is carried out taking into account the reserve requirements of the reference system at 2019 [245]. In those equations, when the reference system does not show any value in a populated class of the test system, the ratio is assumed to be equal to 1.

Table 35. Italian system seasonal seasonal classification values of load and RES [MW].

Season	$P_a^{R,min}$	$P_a^{R,max}$	ΔP_a^R	$P_a^{D,min}$	$P_a^{D,max}$	ΔP_a^D
Winter	266	16,992	1,672.6	17,512	53,434	3,592.2
Spring	125	17,473	1,734.8	19,518	53,581	3,406.3
Summer	105	16,987	1,688.2	22,540	59,526	3,698.6
Autumn	128	15,059	1,493.1	21,061	51,390	3,032.9

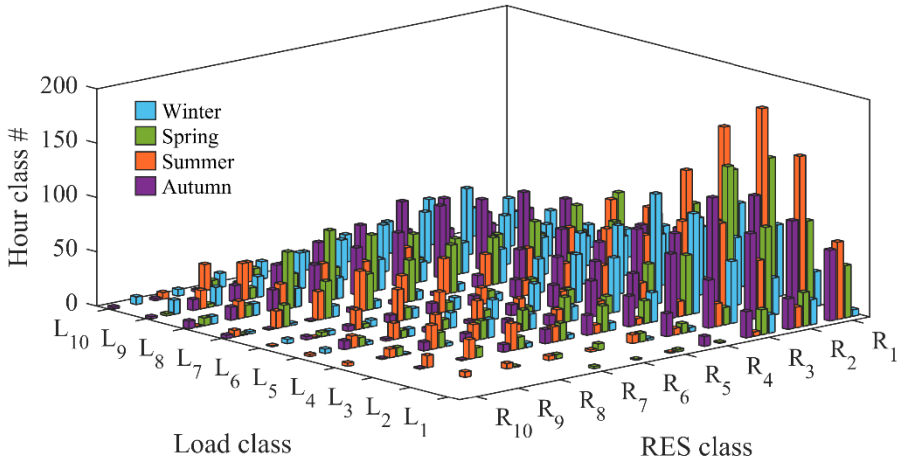

Fig. 71. Seasonal class hour recurrences of the Italian system.[4]

In Fig. 72 , the values of the ratio $\psi_{i,j,a}$, are shown for each class and season, in order to compare the results of the implemented SRR formulation (113) with the SRR values in the reference system. In particular, in Winter only in four classes the ratio is above 1, and minimum and maximum values are 0.5630 and 1.0574 in classes L_5-R_1 and L_4-R_9, respectively, with a mean seasonal value of 0.7615. In Spring all the values are lower than 1, with a minimum of 0.5041 in L_5-R_{10} and maximum of 0.9711 in L_6-R_3 and the seasonal mean is 0.6625. A similar condition is observed in Summer, obtaining ratios between 0.5637 in L_2-R_8 and 0.8591 in L_2-R_2 with an average seasonal value of 0.6529. Finally, Autumn has 32 classes with ratio greater than 1, mostly occurring with low RES production (classes R_1-R_4), minimum and maximum ratios equal to 0.6870 (in L_6-R_9) and 1.2603 (in L_6-R_2), respectively, and the average ratio is 0.9672.

The most interesting aspect is that $\psi_{i,j,a}$ varies from values below and above the unity, even if ENTSO-E defines (113) as the minimum SRR [240].

[4] See footnote 1.

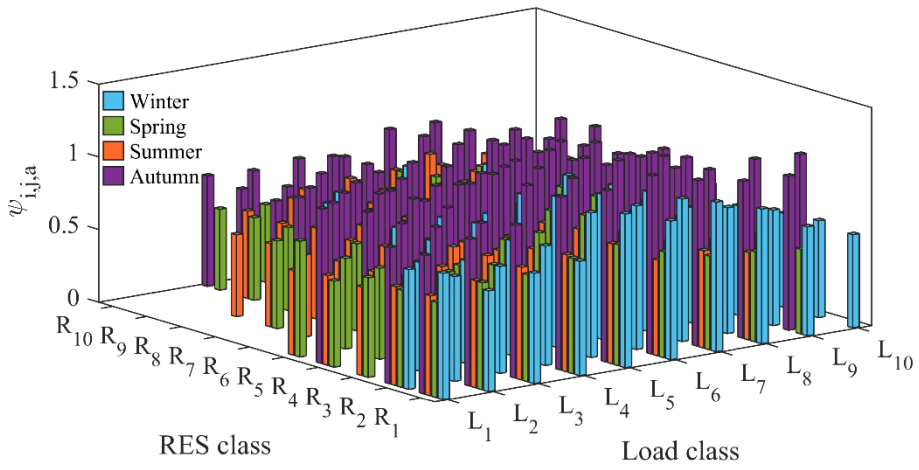

Fig. 72. Seasonal SRR ratio per each class.

In Fig. 73, Fig. 74 and Fig. 75 the ReRR, SpRR and RRR ratios are shown, respectively, according to (138)–(140). As regards ReRR, Fig. 73 shows that minimum seasonal ratios occur in Winter class L_4-R_9 with 0.5834, in Spring class L_3-R_{10} with 0.5508, in Summer class L_5-R_{10} with 0.5818 and in Autumn class L_6-R_{10} with 0.7005. The maximum ratios occur in Winter class L_7-R_1 with 1.1560, in Spring class L_6-R_3 with 1.0170, in Summer class L_5-R_2 with 0.8884 and in Autumn class L_6-R_2 with 1.3126 and the seasonal average ratio are 0.8034, 0.6929, 0.6763 and 0.9924, respectively. In Fig. 74 it can be seen that the SpRR seasonal minimum ratios take place in the class L_{10}-R_7 for both Spring and Summer, with 0.8270 and 0.7840 values, respectively. In winter, the minimum value is equal to 0.8708 in the class L_6-R_{10} and in Autumn it is equal to 0.8317 in the class L_{10}-R_9. At the contrary, the maximum ratios for all the seasons occur in the class L_7-R_2 and assume the following values 1.4249 (Winter), 1.3588 (Spring), 1.2638 (Summer) and 1.3552 (Autumn). The seasonal average ratios are equal to 1.0903, 1.0518, 0.9696 and 1.0404 in Winter, Spring, Summer and Autumn, respectively. Finally, the RRR ratio is reported in Fig. 75, where the seasonal ratios have average values equal to 0.4145 (Winter), 0.4160 (Spring), 0.3975 (Summer) and 0.4800 (Autumn). The minimum ratios are 0.3193 in Winter (class L_4-R_9), 0.3193 in Spring (class L_4-R_8), 0.3186 in Summer (class L_8-R_7), and 0.3539 in Autumn (class L_4-R_9). The maximum are 0.5309 in Winter (class L_3-R_4), 0.7250 in Spring (class L_1-R_4), 0.5215 in Summer (class L_2-R_4), and 0.7258 in Autumn (class L_1-R_4).

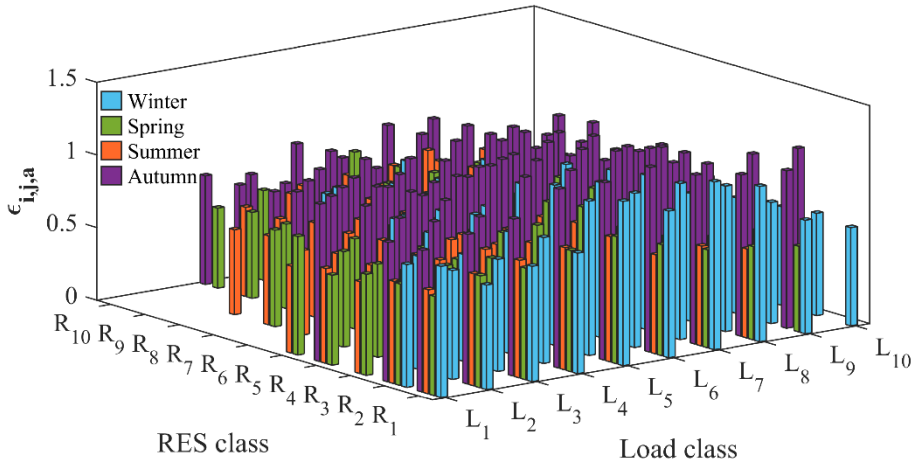

Fig. 73. Seasonal ReRR ratio per each class.

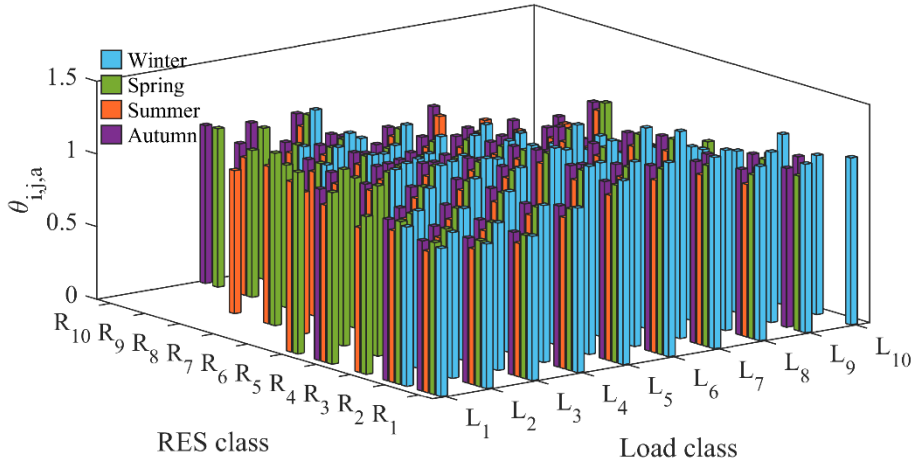

Fig. 74. Seasonal SpRR ratio per each class.

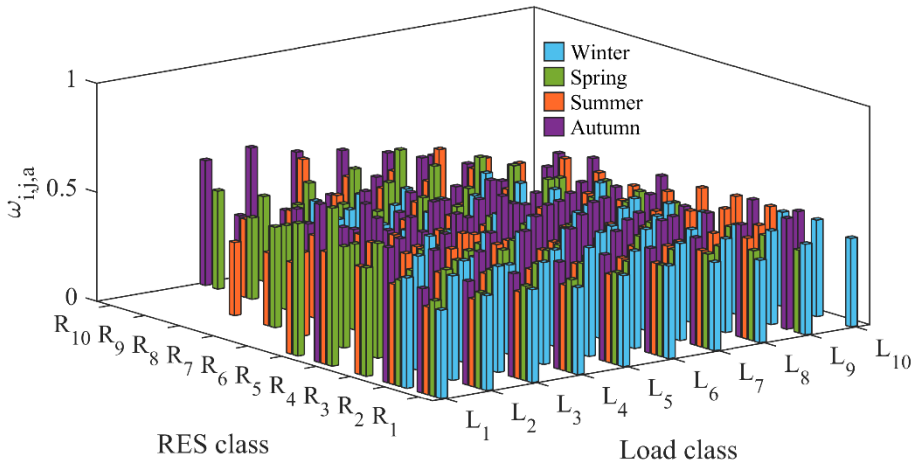

Fig. 75. Seasonal RRR ratio per each class.

Applying the statistical coefficients to the test system, evaluated at each hour according to the pertaining class, the effective estimation of each RR is obtained. In particular, results of effective RR estimations for the peak load day are shown in Fig. 76. Comparing with the preliminary RRs in the same day (Fig. 61) it can be noted that the effective SRR is reduced averagely by 33.2 % with a minimum of 16.8 % at hour 22 and a maximum of 44.1 % at hour 13, and an analogous behavior is observed for the ReRR. The estimation of SpRR is lower than the preliminary estimation in most of the day, reaching a maximum reduction of 22.7 % at hour 12, on the contrary from hour 19 to 23 the application of the statistical coefficients leads to an increase of the SpRR estimation up to 43.5 %. Finally, the application of the statistical coefficients to the preliminary RRR provides a general reduction throughout the day, with a variation range within 46.2 % and 67.4 %.

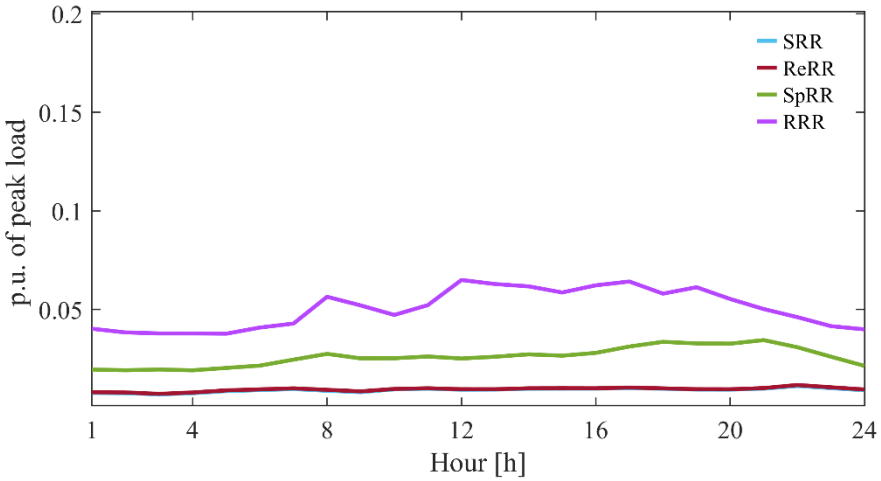

Fig. 76. RRs estimation during the yearly peak day.

5.3.4. Result discussion

From the analysis of the statistical coefficients and the estimation of RRs, it is useful to draw out some considerations.

With the normalization assumptions, $\psi_{i,j,a}$ is expected to be higher than 1, since EN-TSO-E defines the formulation (113) as the minimum SRR [240]. However, as it can be seen from Fig. 72, this condition is often experienced in classes with low-RES generation, showing that the evaluation of SRR in the reference system is based on the field network load, measured at higher voltage level, where the RES production at lower voltage levels is already deducted.

On the contrary, an overestimation of ReRR in the majority of classes, with ratios lower than 1, is obtained from Fig. 73, whereas for the middle load and high RES classes, preliminary ReRR is underestimated in Summer and Autumn. Comparing with SRR ratios of Fig. 72, their trends are similar with a slight increase of the seasonal average ratios $\epsilon_{i,j,a}$, stating that in the reference system the load ramp variation is more frequent and has a higher impact with respect to the RRs obtained in the test system. The effective ReRR is lower than preliminary estimate in all Summer classes, whereas in Autumn, Winter and Spring some classes show the opposite, in particular with low RES generation, and mostly in the middle load demand classes, reflecting the obtained results of the SRR.

The mean seasonal values of $\theta_{i,j,a}$, shown in Fig. 74, indicate a slight overestimation of the effective SpRR, except in Summer, where the mean of $\theta_{i,j,a}$ is lower than 1. Winter is the season with the highest maximum and mean ratio and only in 19 classes the SpRR is underestimated, followed by Spring (25 classes), Autumn (32 classes) and Summer (55 classes). The overestimation is mainly observed in low RES generation classes in all the seasons, and this is expectable from SRR and ReRR ratio results and considering that SpRR, defined in (120), depends on them.

The effective RRR underestimation is more than half of the RRR value in the reference system, as shown in Fig. 75, moreover a higher required load and RES generation entails an increase of $\omega_{i,j,a}$, although this ratio is more affected by RES due to the solar and wind uncertainties modeled in (9). In Autumn the mean $\omega_{i,j,a}$ is higher than those of other seasons because of the lowest load uncertainty forecast error, as well as the lowest RES production in both systems (see Table 35 and Table 33), resulting in a smaller overestimation of the RRR. In Spring and Autumn, the averagely lower load demand and RES production yield lower variation of $\omega_{i,j,a}$ among classes, as compared to Summer and Winter.

In order to prove the feasibility of the obtained effective RR estimations, it is crucial to verify their possible provision with respect to the available power margins of the units eligible to provide the ancillary services downstream of the DAM (see Fig. 56). Hence, per each hour, the net upper margin (difference between upper margin and URR) and net lower margin (difference between lower margin and DRR) are determined, and the relevant duration curves are illustrated in Fig. 77. From this figure, possible critical conditions can be

individuated where net margins are below 0 MW. In particular, it can be noted that the total margin is sufficient to cover the URR for the entire year, whereas the DRR is not satisfied for 18 hours, resulting in a mean unmet DRR of about 260 MW. In these critical conditions the TSO should evaluate the possibility to redispatch the eligible units, or to involve other units (such us RES) in the provision of services.

The verification is extended to the RRs adequacy in the most challenging situations. To this purpose, in a first instance, the TPV from DA to RT (reported in Fig. 57), is compared, for each hour, with the URR estimation when positive and to the DRR estimation when negative. The relevant duration curves are shown in Fig. 78, where it can be observed that the URR and DRR estimation are mostly suitable to cope with the TPV, whereas in 91 hours the URR is not enough and in other 301 hours the DRR is insufficient. The expected energy not served (EENS) for the 91 hours is 41.2 GWh, roughly 0.4% of the yearly load, whereas the possible RES curtailment, during the 301 hours, is approximately 112.3 GWh, approximately 1.1% of yearly RES production. In these conditions, TSOs need to procure further redispatch from the qualified units, even if not cleared to provide real-time services, exploiting the total margin [6]. A further investigation of RRs adequacy is carried out to assess the system ability to respond to a generation outage, comparing, per each hour, the URR estimation with the maximum $P_{g,t}^{DAM}$. The obtained duration curve is depicted in Fig. 78 as well, and it can be seen that, in all conditions, the URR is suitable to cover the generation outage, even leaving a residual amount to accomplish further balancing operations.

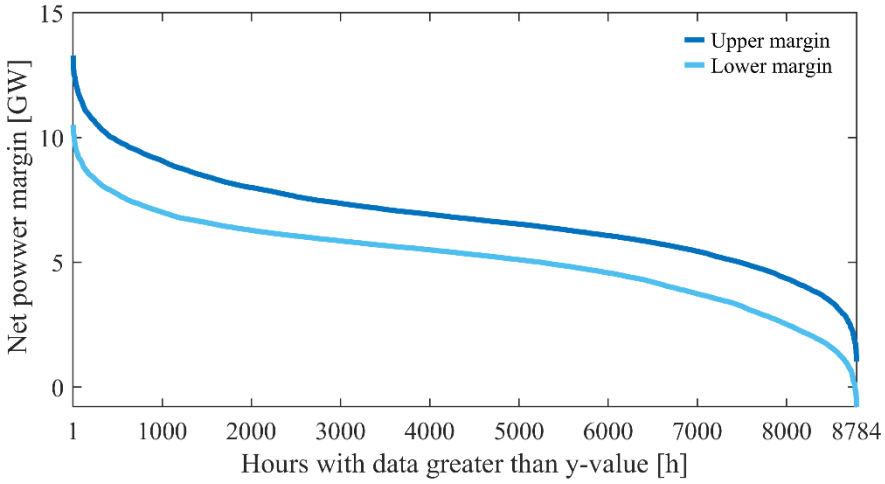

Fig. 77. Hourly residual power margins of RR feasibility.

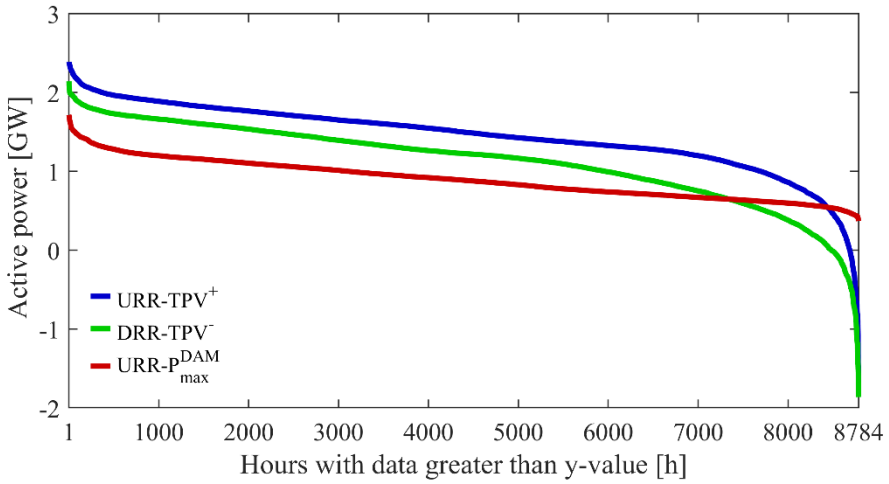

Fig. 78. URR and DRR adequacy evaluation.

5.5. SCUCER preliminary results

The methodology proposed in the paragraph 5.2.4 is preliminarily tested during the RT peak load day of the NREL 118-bus test system occurring at hour 15:00 of the 4th of July. In particular, Fig. 79 and Fig. 80 show RES and load variation from DA forecast to RT operation, respectively. A production underestimation is observed in the whole daylight window for the solar, with total of 1.96 GWh and in the central hours for the wind, with a total of 1.12 GWh, whereas in the remaining hours the overestimated energy is 1.48 GWh. In addition, the load demand is characterized by an underestimation as well for a total of 28.57 GWh, except in first and the last 4 hours of the day where an overestimation of 1.68 GWh Is observed. Therefore the TPV varies from +0.77 GW at hour 22:00 to −3.31 GWh at hour 10:00. Moreover, hour 10:00 represents the maximum negative variation of shown in Fig. 57.

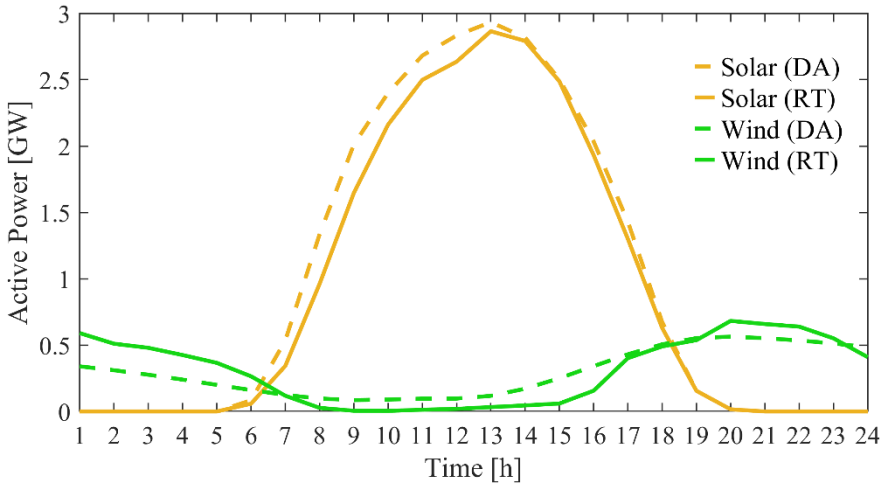

Fig. 79. Solar and Wind production variation from DA to RT during the peak day load.

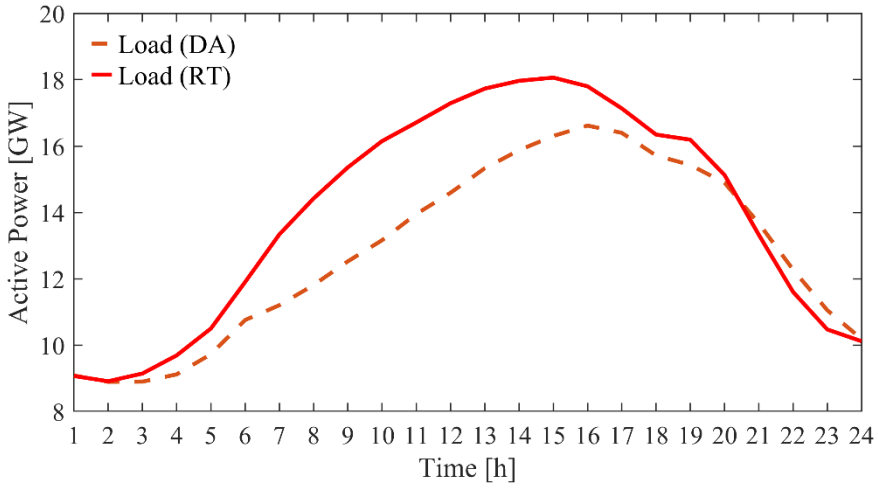

Fig. 80. Load demand variation from DA to RT during the peak day load.

The overall SCUCER results are shown in Fig. 81 during the peak load day and the adjacent days as well, where the peak hour is highlighted in green and it is equal to18.06 GW, with an increase of the 10.8% compared to forecasted one. As it can be seen, to keep the power balance in RT a TPV reduction is overwhelming detected during the three days requiring upward redispatching actions, whereas in few night hours the TPV is greater than the forecasts and therefore downward redispatch is needed.

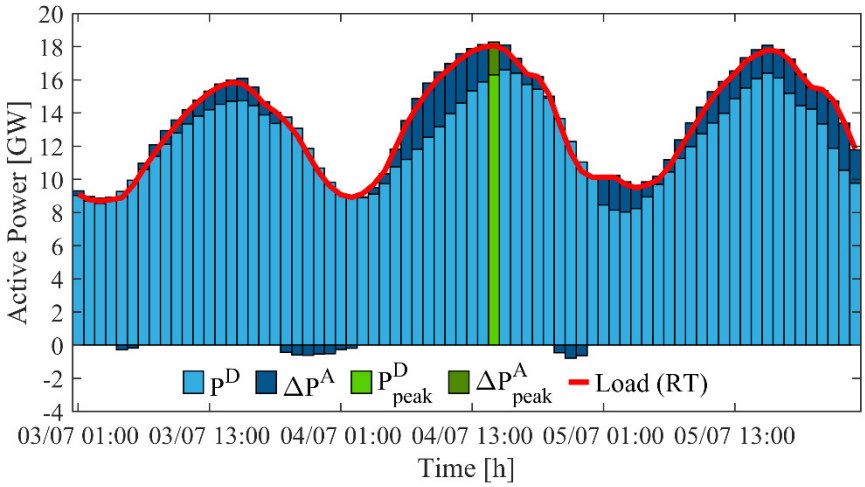

Fig. 81. SCUCER results of peak load day and adjacent ones.

Finally, the SRR procured after the SCUCER solution is shown in Fig. 82 gathered for each technology. The SRR varies form a minimum of 110.5 MW up to a maximum of 215.6 MW. It can be observed that only CC and CT technologies provide the service, where on a total of 11.30 GWh required energy the 53.7% is provided by CC power plants and the remaining 46.3 % is procured by CT ones. The marginal costs reported in Table 11 testify that

ST technologies are the most affordable ones, except for "ST Other", therefore they are cleared ad maximum power after the DAM, whereas CC and CT costs are comparable and greater than ST ones. Moreover, according to network operating conditions and the RT load they are redispatched and/or cleared to provide SR service.

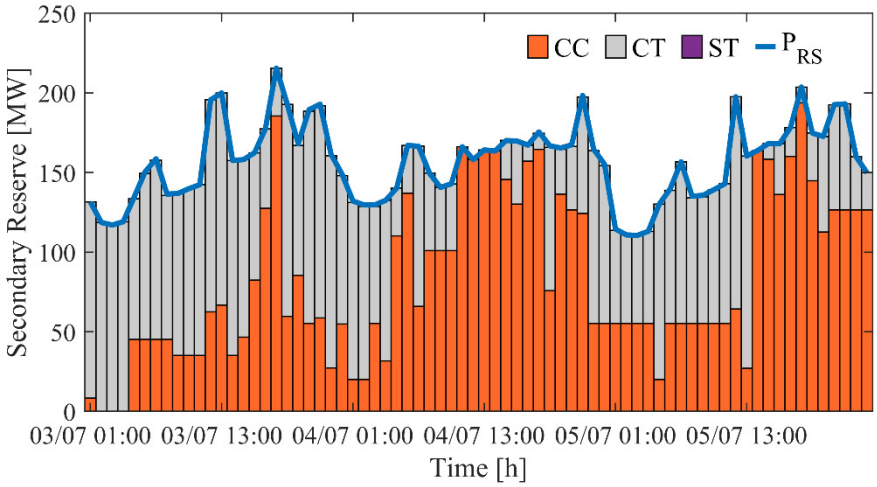

Fig. 82. SRR procured for each technology during the peak load day and adjacent ones.

5.6. Final Conclusions and Remarks

The proposed methodology for the estimation of secondary and tertiary reserve requirements has led to the awareness about the ancillary service procurement mechanisms deriving from power system operation uncertainties. In particular, the RR estimation based on the seasonal classification has pointed out the different impacts of RES and load levels on each reserve amount, and analogous behavior with respect to a real reference system has been observed. By comparing RR estimation with operation conditions, the possible challenging situations can be individuated, revealing the reserve feasibility and adequacy.

These analyses could constitute a useful tool for electric industry operators in order to understand the rationale of TSO ancillary service requirements, and to plan their strategies in energy and service bidding in markets according to the adopted classification.

Finally, the preliminary results obtained from the SCUCER optimization problem have been shown in the paragraph 5.5.The method has been tested in yearly peak day, representing one possible challenging condition, and the results have proved the effectiveness of the procedure application for this kind of investigation. Currently, the method is in the whole-year

simulation stage, where the computational time is of roughly 43.5 seconds for each time step, and the full results are aimed to be elaborated in the next works.

In the proposed optimization problem, the N-1 security constraint can be embedded by implementing the line outage distribution factors, however a preliminary selection of the most critical line outages and further redispatch implications can be related to avoid unfavorable operating conditions and limit the additional computation burden.

Chapter 6. Markets impact on Southern Italy Transmission System

This final chapter proposes a market-based study of the Southern Italy Transmission System (SITS). The work is developed to evaluate TSO strategies from energy market (i.e., DAM plus IM) to the BM, in order to ensure the system's security operation. To achieve this goal, preliminary hypotheses and analyses are conducted to distribute the zonal framework markets outcomes to the generation and absorption buses of the modelled network. Then, ex-ante and ex-post the BM, steady-state simulations are performed by daily AC load flow routines on DIgSILENT PowerFactory software, creating a Python-based automatism to elaborate and import the market results into the software, and export the obtained results. The SITS grid is made up of the 400 kV and 230 kV sections of Apulia, Basilicata, Calabria, and Campania regions, the interconnection lines with the rest of the Italian transmission system and the exchange with Greece, as depicted in Fig. 83. The considered regions belong to three different market zones, Apulia, Basilicata are in the South (SUD) market zone, Calabria represents a market zone itself, whereas Campania is part of the Centre-South (CSUD) [246], however before 2019 Calabria belonged to SUD zone but was classified as "virtual zone" because the generation was subject to further system's security constraints. This zonal market distribution represents a crucial issue for the nodal distribution of the obtained results because it requires proper data managing.

6.1. Market-based Load Flow Analysis

The proposed work aims at providing a methodologic framework to handle the zonal results of the public dataset given by Italian energy (GME) and ancillary service (Terna) market operators. In addition to the work developed in the Chapter 4 for the Sicily transmission system, further consideration are taken into account to run AC load flow simulations. The data management to define the operating point of each load and generator in the system is described in the following paragraphs.

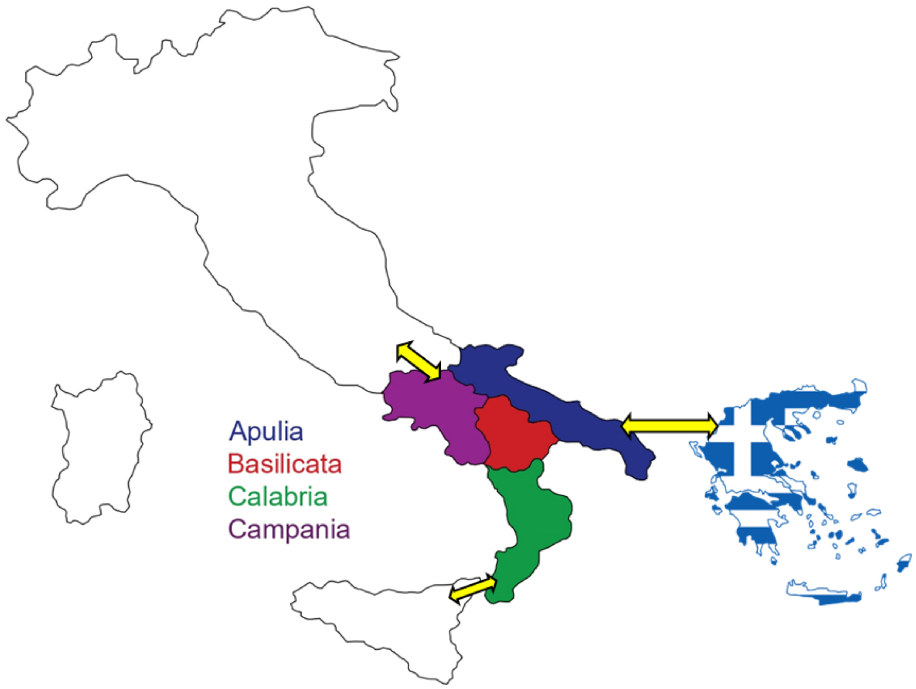

Fig. 83. Geographical location of SITS regions.

6.1.1. Generation Handling

The AC load flow simulations are run with two types of generators: those that can provide voltage control (PV) and those that cannot (PQ). PV generators, in particular, are those connected to the transmission system via proper HV/MV transformers, whereas PQ generators are those connected to the sub-transmission. Furthermore, PV generators are equipped with technology-appropriate capabilities. Defined the generation set up, specific strategies are applied at each PV generator, depending on their technology, to obtain their own operating point.

A) PV generation

The active power dispatched of each PV generator is defined by coupling the market ID to the generator of the respective supplying unit (SU). However, a SU can be made up of several generators (i.e., a combined cycle gas turbine (CCGT) is made up of at least one GT and one steam turbine (ST) generating unit), hence a strategy to split the market results among the SUs' generators is required. This strategy is consequential to the number of active generators for the voltage control, as well as for the capability reactive power limits. Therefore, three different strategies are defined based on the technologies made up of more

generators, that are: 1 GT + 1 ST (1+1) CCGT, 2 GT + 1 ST (2+1) CCGT, and pumped storage hydro (PSH) power plants.

The operating points of the two generators of a 1+1 CCGT are strictly related in this power plant category because the ST is used and sized to recover the waste thermal power produced by the GT in order to increase system efficiency. As a result, a coupled operating mode must be defined between the generators, splitting the cleared power according to the rated power. Therefore, indicating with N^{C1} the number of 1+1 CCGT units, for each time step t_k, the dispatched power between the GT ($P_p^{G,gt}$) and the ST ($P_p^{G,st}$) units is defined as follows:

$$\begin{cases} P_p^{G,gt}(t_k) = \dfrac{P_p^m(t_k)\, S_p^{N,gt}}{S_p^{N,gt} + S_p^{N,st}} \\ P_p^{G,st}(t_k) = \dfrac{P_p^m(t_k)\, S_p^{N,st}}{S_p^{N,gt} + S_p^{N,st}} \end{cases} \quad p = 1, \dots, N^{C1} \tag{213}$$

in which P_p^m is the dispatched power of the p-th generator, downstream the m-th market, $S_p^{N,gt}$ and $S_p^{N,st}$ are the apparent rated power of the GT and ST units of the p-th generator, respectively.

Even in the 2+1 CCGT the GTs and ST are coupled, however the ST is sized according to the waste thermal power produced by both the GTs. Therefore, over the ST, if the cleared power is greater than half of the active maximum power of the entire system ($P_q^{G,max}$), supposing that all generators have a nominal power factor ($\cos(\varphi^N)$) of 0.85, then both the GTs are supplying the same power; otherwise, only one GT is supplying power. Hence, defining with N^{C2} the number of 2+1 CCGT units, for each time step t_k, the dispatched power between the two GTs and the ST generators is formulated as below:

$$\begin{cases} P_q^{G,gt_1}(t_k) = \dfrac{P_q^m(t_k)\, S_q^{N,gt}}{S_q^{N,gt} + \dfrac{S_q^{N,st}}{2}} \\ P_q^{G,gt_2}(t_k) = 0 \\ P_q^{G,st}(t_k) = \dfrac{P_q^m(t_k) \dfrac{S_q^{N,st}}{2}}{S_q^{N,gt} + \dfrac{S_q^{N,st}}{2}} \end{cases} \quad q = 1, \dots, N^{C2} \wedge P_q^m(t_k) \leq P_q^{G,max} \tag{214}$$

$$\begin{cases} P_q^{G,gt_1}(t_k) = \dfrac{P_q^m(t_k)\, S_q^{N,gt}}{2S_q^{N,gt} + S_q^{N,st}} \\ P_q^{G,gt_2}(t_k) = P_q^{G,gt_1}(t_k) \\ P_q^{G,st}(t_k) = \dfrac{P_q^m(t_k)\, S_q^{N,st}}{2S_q^{N,gt} + S_q^{N,st}} \end{cases} \quad q = 1, \dots, N^{C2} \wedge P_q^m(t_k) > P_q^{G,max} \tag{215}$$

where $P_q^{G,max} = \cos(\varphi^N)\left(2\, S_q^{N,gt} + S_q^{N,st}\right)$. It can be noted that in (214) it has been used half of $S_q^{N,st}$, this because in the 1+1 set up the ST can produce no more than half of the maximum power, because the thermal power is recovered only from one GT.

In contrast to previous technologies, PSH power plants with more generators are independent from one another and therefore, they are dispatched one at a time until the maximum power is reached. The dispatched power of each PSH generator can be defined as follows, for the generic time step t_k, where N^H is the number of PSH units and N_h^G is the number of generators of the h-th PSH unit:

$$N_h^{max}(t_k) = \left\lfloor \frac{P_h^m(t_k)}{P_h^{G,max}} \right\rfloor \quad h = 1, \dots, N^H \tag{216}$$

$$P_{h,o}^G(t_k) = P_h^{G,max} \quad o = 1, \dots, N_h^{max}(t_k) \ \wedge \ h = 1, \dots, N^H \tag{217}$$

$$if\ N_h^{max}(t_k) < N_h^G$$
$$P_{h,o}^G(t_k) = P_h^m(t_k) - N_h^{max}(t_k) P_h^{G,max} \quad o = N_h^{max}(t_k) + 1 \ \wedge h = 1, \dots, N^H \tag{218}$$

$$if\ N_h^{max}(t_k) + 1 < N_h^G$$
$$P_{h,o}^G(t_k) = 0 \quad o = N_h^{max}(t_k) + 2, \dots, N_h^G \wedge h = 1, \dots, N^H \tag{219}$$

equation (216) identifies the number of generators suppling the maximum power for each PSH unit (N_h^{max}) at time step t_k, in (217) the $P_h^{G,max}$ value is assigned to the generators from 1 to $N_h^{max}(t_k)$; if not all the generators have been cleared to the maximum power the $N_h^{max}(t_k)+1$ generator of the h-th PSH unit is dispatched at the remaining power amount as defined in (218); finally, if there are further generators, their dispatched power is equal to 0 MW as shown in (219).

The generators are given with the appropriate capabilities in accordance with the own turbine technology for the voltage control. The GT, ST, and PSH turbine (PSHT) are obtained based on [247]–[249] and are reported in Fig. 84, Fig. 85, and Fig. 86 in relative values, respectively. Technical constraints on minimum and maximum power (respectively equal to 0.85 and 0.2 pu) limit the theoretical GT and ST capabilities. On the contrary, the PSHT is seamless from 1 to -1 pu, except at 0 pu to avoid the voltage control when a PSH unit is not cleared. In addition to the theoretical active power limits, the market-accepted bids for the generators specify the effective minimum and maximum active powers.

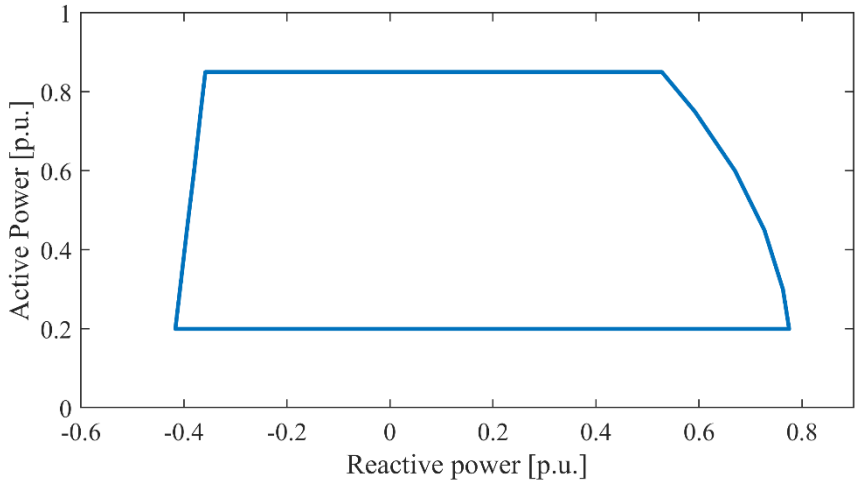

Fig. 84. GT capability in relative values.

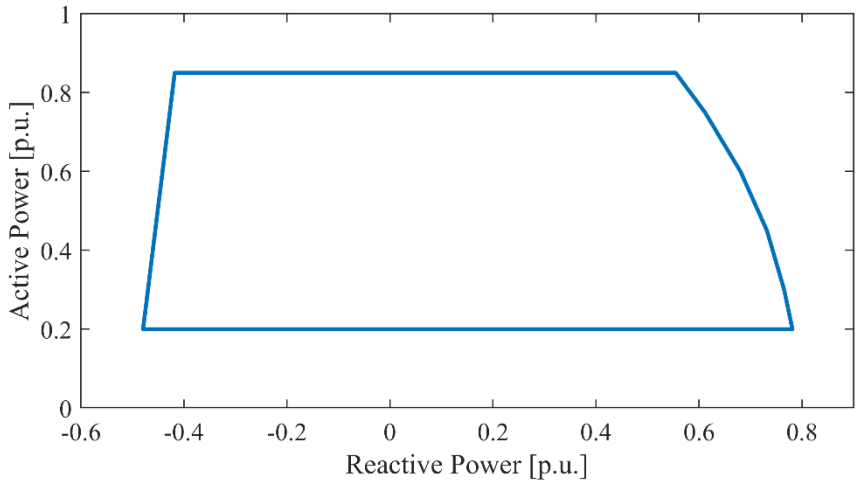

Fig. 85. ST capability in relative values.

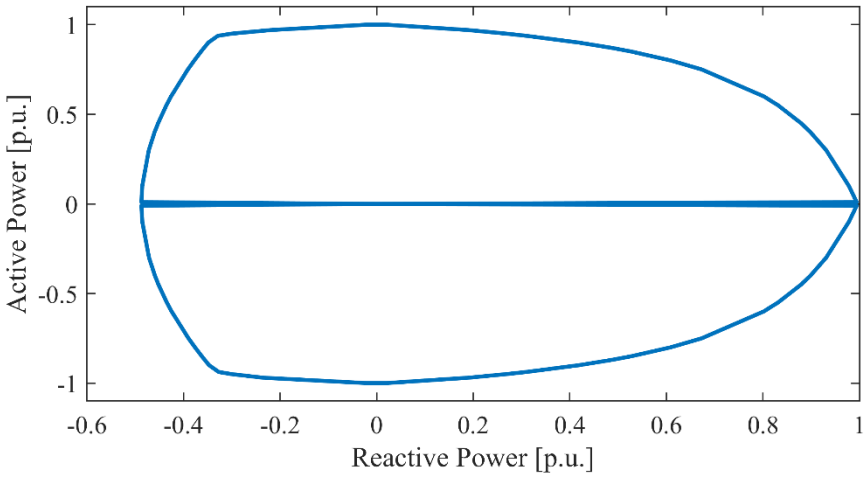

Fig. 86. PSHT capability in relative values.

B) PQ generation

Let us consider the set of the market zones of interest Ω^Z, the PQ generation downstream the m-th market ($P_z^{PQ,m}$) is identified as the difference between the zonal cleared generation ($P_z^{G,m}$) and the one defined as PV generation of the investigated market zone z:

$$P_z^{PQ,m}(t_k) = P_z^{G,m}(t_k) - \sum_{i=1}^{N^{G,PV}} P_{i,z}^{G,m}(t_k) \quad \forall\, z \in \Omega^Z \tag{220}$$

As in Chapter 5, the solar generation (here it is called SO to avoid ambiguity with PV generators) is split from the rest of the equivalent generation (EQ) exploiting the "bell-shaped" daily SO production profile, obtained from the $P_z^{PQ,m}$. Then, the generation of the two technologies are split by region according to the installed capacity provided in [250]:

$$P_{r,n}^{PQ,m}(t_k) = P_{n,z}^{PQ,m}(t_k)\frac{P_{n,r}^{max}}{\sum_{r\in\Omega_z^R} P_{n,r}^{max}} \quad n \in \{SO, EQ\}, \forall\, r \in \Omega_z^R, \forall\, z \in \Omega^Z \tag{221}$$

in which Ω_z^R is the set of the regions included in the z-th market zone, $P_{n,r}^{max}$ is the installed capacity of the n-th technology and r-th region, whereas $P_{r,n}^{PQ,m}$ is the supplied power from the n-th technology in the r-th zone. With regard to the transmission system modelled, this method enables the removal of external regions' generation, and distribute only the internal one. In particular, the nodal distribution of the PQ generation is determined by taking into account the subset of the buses of each region ($\Omega_r^B \subset \Omega^B$) and the generation participation factors ($GPF_{b,n}$):

$$P_{b,n}^{PQ,m}(t_k) = P_{r,n}^{PQ,m}(t_k)\, GPF_{b,n} \quad \forall\, b \in \Omega_r^B, \forall\, r \in \Omega^R, n \in \{SO, EQ\} \tag{222}$$

where Ω^R is the set of the modelled regions. In particular, $GPF_{b,r,n} = 0$ if on the b-th bus the n-th technology is not installed, otherwise $GPF_{b,n} < 1$; and they are characterized by the following property:

$$\sum_{b=1}^{N_r^B} GPF_{b,n} = 1 \;\; \forall\, r \in \Omega^R, n \in \{SO, EQ\} \tag{223}$$

The PQ generation subsists from the sub-transmission to the distribution system, hence the reactive power injections to control the voltage cannot be noticed for the local impact. For this reason, it has been supposed that the PQ generation does not provide any reactive power contribution.

6.1.2. Load Distribution

Similar to how PQ generation is distributed, the load distribution is based on a regional split that is derived from the statistical regional report on annual regional and provincial energy consumption provided in [251]. First, for each time step t_k, the regional load obtained from the m-th market ($P_r^{D,m}$) is established in order to determine the network's required load and to exclude the one of the external regions:

$$P_r^{D,m}(t_k) = P_z^{D,m}(t_k)\frac{E_r^D}{\sum_{r\in\Omega_z^R} E_r^D} \quad \forall\, r \in \Omega_z^R, \forall\, z \in \Omega^Z \tag{224}$$

where E_r^D is the yearly energy consumption of the r-th region and $P_z^{D,m}$ is the zonal required load obtained from the m-th market. Second, the provincial split is calculated exploiting the provincial energy consumption (E_a^D), for the region of interest (Ω^R):

$$P_a^{D,m}(t_k) = P_r^{D,m}(t_k)\frac{E_a^D}{\sum_{a\in\Omega_r^A} E_a^D} \quad \forall\, a \in \Omega_r^A, \forall\, r \in \Omega^R \tag{225}$$

in which Ω_r^A is the set of the provinces, or areas, of the r-th region. Finally, the provincial load participation factors ($LPF_{b,a}$) are employed to the network buses distribution:

$$P_b^{D,m}(t_k) = P_a^{D,m}(t_k)\, LPF_{b,a} \quad \forall\, b \in \Omega_a^B, \forall\, a \in \Omega_r^A, \forall\, r \in \Omega^R \tag{226}$$

where Ω_a^B is the subset of the provincial nodes ($\Omega_a^B \subset \Omega_r^B \subset \Omega^B$).

To carry out the AC load flow simulations, the load reactive power is defined for each bus ($Q_b^{D,m}$) exploiting proper power factors:

$$Q_b^{D,m}(t_k) = P_b^{D,m}(t_k)\, tg(\varphi_b) \quad b = 1, \dots, N^B \tag{227}$$

6.1.3. Power Exchange

The interconnection lines between the SITS model, Greece and the rest of the Italian transmission system are listed in Table 36. While the SITS has five interconnecting lines on the side heading towards northern Italy, both interconnections with Sicily and Greece are made up of a single line. Therefore, a technique to divide the interzonal power flow among more lines is necessary, and this task is made more difficult by the asymmetry between the modelled network and the network's zonal subdivision. The zonal framework is represented in Fig. 87 considering the SITS model boundary, the neighboring regions and the SUD-CSUD boundary provided by the market (a) and the desired one to fit the network boundary (b).

Table 36. Interconnection lines with the neighboring zones

Line	V^N [kV]	Type	Interconnected Regions
Rotello-San Severo	400 kV	HVAC	Molise-Apulia
Valmontone-Presenzano	400 kV	HVAC	Lazio-Campania
Latina-Garigliano	400 kV	HVAC	Lazio-Campania
Ceprano-Garigliano	400 kV	HVAC	Lazio-Campania
Popoli-Capriati	230 kV	HVAC	Abruzzi-Campania
Sorgente-Calabria	400 kV	HVAC	Sicily-Calabria

Arachthos-Galatina	400 kV	HVDC	Greece-Apulia

The regional load and generation distribution developed in the previous paragraphs is useful to adjust the SUD-CSUD boundary power flow as well. Defining with $F^{SC,m}$ the SUD-CSUD power flow boundary yields from the m-th market and with $F^{I,m}$ the SITS Internal boundary power flow towards northern Italy from the m-th market; for each time step t_k, the last quantity can be obtained from the first one through the following equation:

$$F^{I,m}(t_k) = F^{SC,m}(t_k) - P^{m}_{Mol}(t_k) + P^{m}_{Cam}(t_k) \tag{228}$$

in which

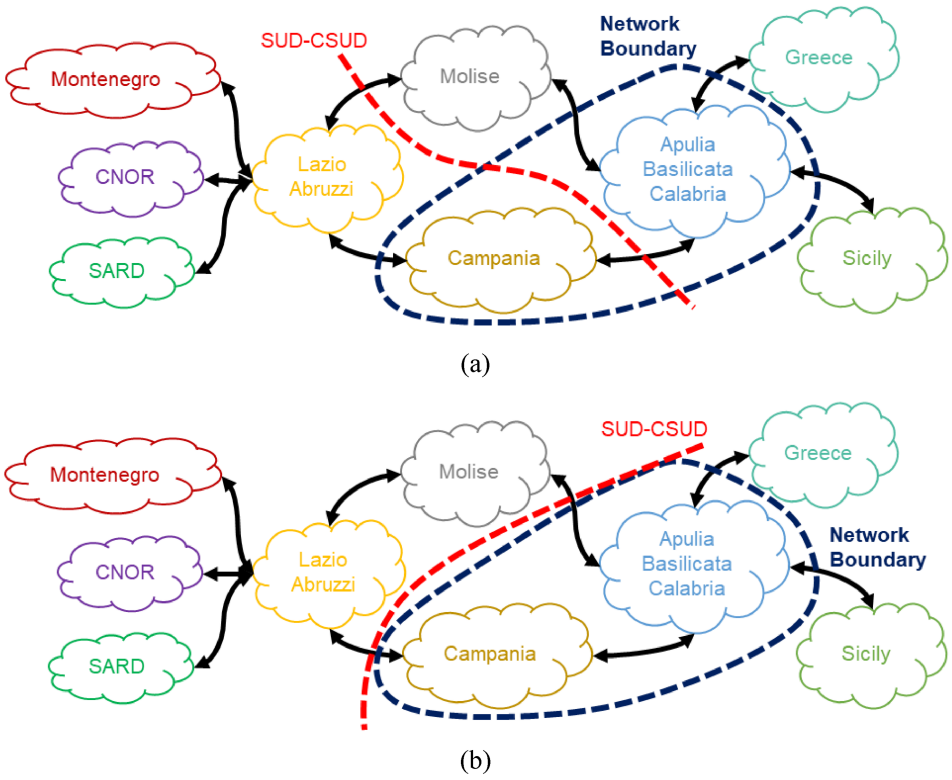

Fig. 87. Zonal power flow SUD-CSUD provided by market results (a) and the desired one for the model of the SITS (b)

$$P^{m}_{Mol}(t_k) = P^{D,m}_{Mol}(t_k) - P^{G,m}_{Mol}(t_k) \tag{229}$$

is the Molise's net power and

$$P^{m}_{Cam}(t_k) = P^{D,m}_{cam}(t_k) - P^{G,m}_{Cam}(t_k) \tag{230}$$

is the Campania's net power.

The resulting boundary power flow is then split by the five lines, and the contributions of each are calculated using two methodologies: one based on Sorgenia's experience, and the other on the rated power of the lines, as shown below:

$$F_x^m(t_k) = F^{N,m}(t_k)\frac{S_{R_x}^F}{\sum_{x\in\Omega^X} S_{R_x}^F} \quad \forall\, x \in \Omega^X \tag{231}$$

where Ω^X is the set of the boundary interconnection lines, F_x^m is the power flow on the x-th interconnection line after the m-th market and finally $S_{R_x}^F$ is the rated apparent power of the x-th interconnection line.

Except for the HVDC interconnection with Greece, which is supposed to be a PQ generator with no reactive power provision because it is a 20-year-old technology, the exchange power flows have been modelled as PV generators. Even if the modeling of power flows as PV generators may not be equivalent to reality, it must be remembered that the real power system has several equipment distributed through the network to support the voltage control (such as shunt, synchronous condenser, etc.).

6.1.4. Load Flow Routines Automatization

To perform quasi-dynamic AC load flow simulations, a Python-based automatization process is developed for data handling according to the equation described in the preceding paragraphs, import the data, run the simulations, and export the obtained results via DIgSILENT PowerFactory software, as shown in Fig. 88 and Fig. 89, respectively. A quasi-dynamic load flow is a time varying load flow calculation tool that can be used for medium to long term simulation studies. In particular, quasi-dynamic load flow completes a series of load flow simulations, in series or in parallel, spaced in time, with a certain flexibility to select the simulation time horizon as well as the time step size.

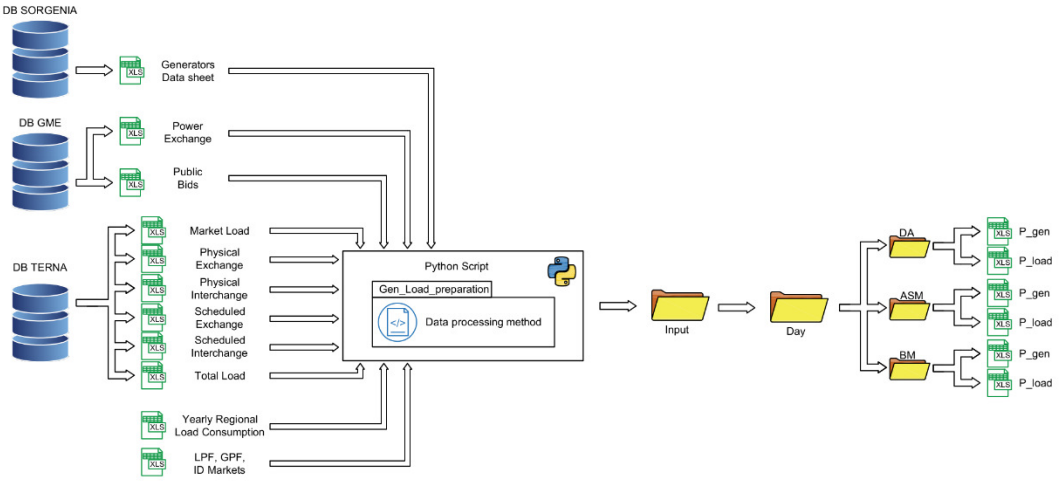

Fig. 88. Market data handling automatization process.

The first script processes the data based on the interested market, which can be day-ahead market plus intraday market (DA), ancillary service market (ASM), or balancing market (BM). In particular, for DA simulations the processed data are the ones provided by GME, whereas for ASM and BM the data provided by Terna are processed as well. GME, on one hand, provides market results for each SU and consuming unit of each market, including ASM and BM. Terna, on the other hand, publishes load, RES and power exchange and interchange updates from energy to real-time markets. Sorgenia has provided an empirical-based generation datasheet to determine the SU rated power and regional location. Finally, two Excel files have been created for the load and generation data processes to be properly elaborated and converted to PowerFactory-readable data format. This script generates an hourly profile for each generator and load of the system, which are saved in two Excel files. According to the analyzed day and market, a specific path is generated to save the files.

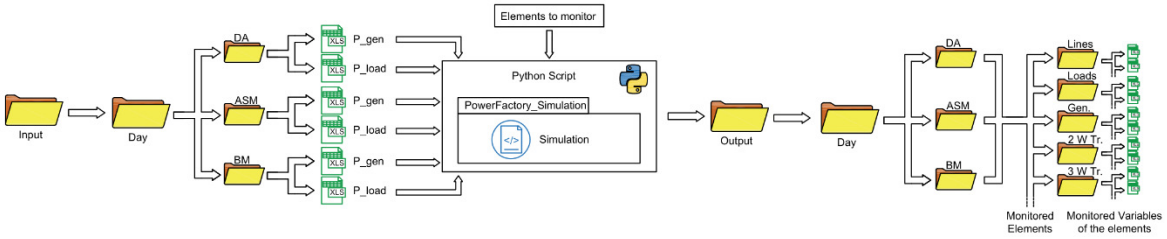

Fig. 89. AC load flow routine automatization process.

The second script makes use of the output data of the first script as well as a Python-based object oriented programming library, in order to set, run, and export the outcomes of quasi-dynamic AC load flow using the program DIgSILENT PowerFactory. The flexibility to adapt this procedure to a different day or scenario is the significant advantage of this

library. The obtained results are saved in several folders, one folder for each network element type, storing the variables of interest (i.e., for the line on variable of interest is the loading percentage) and, as for the input data, a specific path is produced according to the day and market under consideration.

6.2. The Southern Italy Transmission System Test Case

The SITS network has been modeled based on TYNDP of ENTSO-E [235] and exploiting Terna's transmission evolution planning (TEP) reports to identify the developing projects [252]. It is composed of 159 busbars, 142 lines, 72 two-winding transformers, 6 synchronous condenser, and 14 shunts. Fig. 90 shows a simplified geographical location with the Sicily and Internal boundaries. The sub-transmission level, or 150 kV, has been neglected in this model, as shown by Table 37, and the load and equivalent generators are connected directly to the 400 kV or 230 kV busbars. The 230 kV system is mainly located in the Naples' area and is distinguished by an underground cable installation. The system is composed of 24 SUs for a total of 47 PV generators with a capacity of 11.8 GW among HPS (1.1 GW), CCGT (7.9 GW) and ST (3.0 GW) power plants. A proper two-winding transformer is used to connect each of the 47 PV generators on the system's busbar, as shown in Fig. 91 for the Modugno's 2+1 CCGT power plant. A station controller is set up among the generators of the same power plant to coordinate the voltage control, allowing the target voltage to be defined directly on the 400 kV busbar (i.e. the busbar named Modugno in Fig. 91).

Fig. 90. SITS network geographical representation.

Table 37. Number of busbars for each rated voltage

V_r [kV]	Bus number
400	59
230	53
<20	47

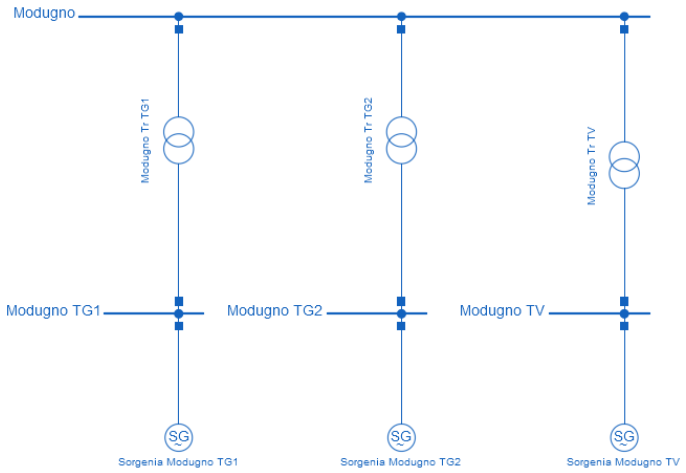

Fig. 91. 2+1 CCGT power plant of Modugno.

The SITS network has 60 loads and 70 PQ equivalent generators installed. Table 38 shows the regional RES installed capacity from sub-transmission to distribution system

updated to the 31/12/2020 [250] to obtain the regional subdivision of (221). With penetration rates of 61.8%, 38.0%, and 40%, respectively, Apulia has the most installed capacity for solar, wind, and biomass; meanwhile, Calabria has the highest hydro penetration with 62.1%. With a 24.5% penetration rate, Campania is the second region for RES installed capacity. On the other hand, Fig. 92 displays the annual energy consumption for each province and region in 2020 [251]. The province of Naples (NA) in Campania consumes the most energy, with 7.2 TWh consumed, followed by Taranto (TA) and Bari (BA) in Apulia, with 4.6 and 4.0 TWh consumed, respectively. From Apulia to Campania, a total of 15.6, 2.6, 4.8, and 15.8 TWh of energy are needed. The GPF and LPF determined in (110) and (111), respectively, remain in effect, but the first was determined for each region and the second for each province.

Table 38. RES installed capacity updated at the end of 2020 [MW].

Region	Solar	Wind	Hydro	Biomass
Apulia	2826.50	2560.30	3.70	359.90
Basilicata	371.00	1300.30	162.20	93.90
Calabria	536.50	1151.10	911.30	218.20
Campania	833.30	1733.00	390.10	257.00

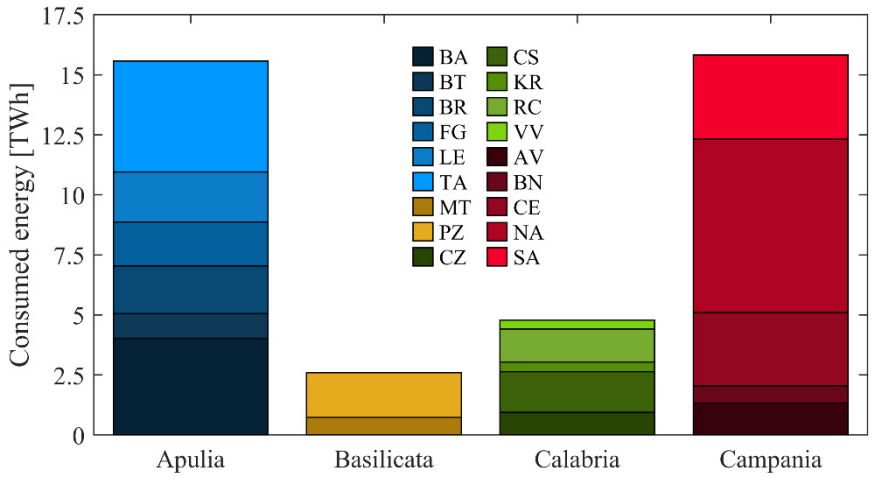

Fig. 92. Yearly province energy consumption.

The daily system power balance following DA and BM are depicted in Fig. 93 and Fig. 94, respectively. After DA, the required load is 107.15 GWh and it varies between 3.25 GW at hour 4:00 and 5.54 GW at 20:00, but after BM, the load reaches 6.40 GW and the minimum is changed to hour 5:00 with a require load of 3.56 GW and the total required energy is increased to 121.83 GWh. PQ generation ranges from 1.65 GW at hour 23:00 to 3.34 GW at

hour 12:00 in the DA, whereas after MB the minimum PQ generation is 2.49 GW at hour 24:00, and the maximum occurs at hour 1:00 suppling 4.50 GW, and until hour 5:00 the PQ generation is greater than the required load. During the day, PQ generation supplied from 59.82 GWh in DA to 90.94 GWh in BM. This increase, over the RES generation forecast error, is due to the exceeding self-consumption of the units that do not participate to the market [244]. While the interzonal flow with Sicily and the Internal Boundaries change trend from DA to BM, the power exchange with Greece is zero for the whole day in both scenarios. In particular, the Internal Boundary exports 1.55 GWh after DA from 19:00 to 23:00, however real-time operations changed the tendency to a full import scenario in BM with an average of 1.5 GW. On the contrary, throughout the day, the import from Sicily has risen from 1.29 GWh to 4.07 GWh.

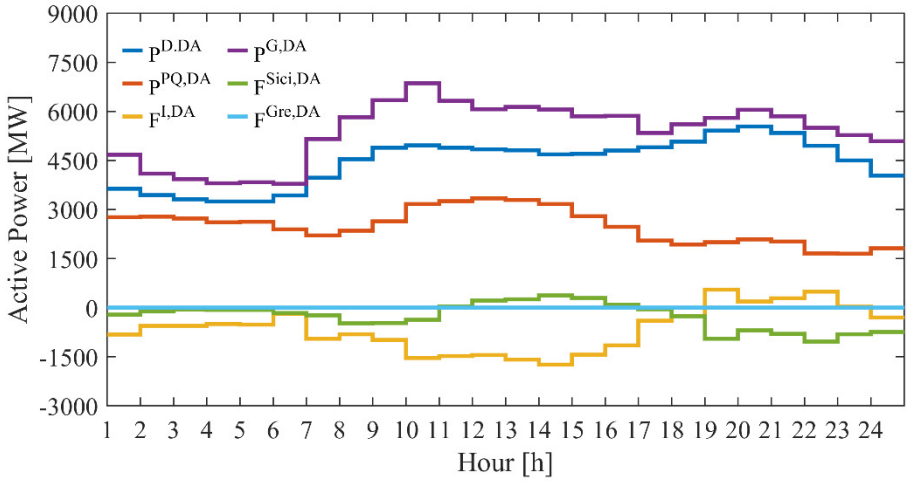

Fig. 93. Hourly power balance after DA.

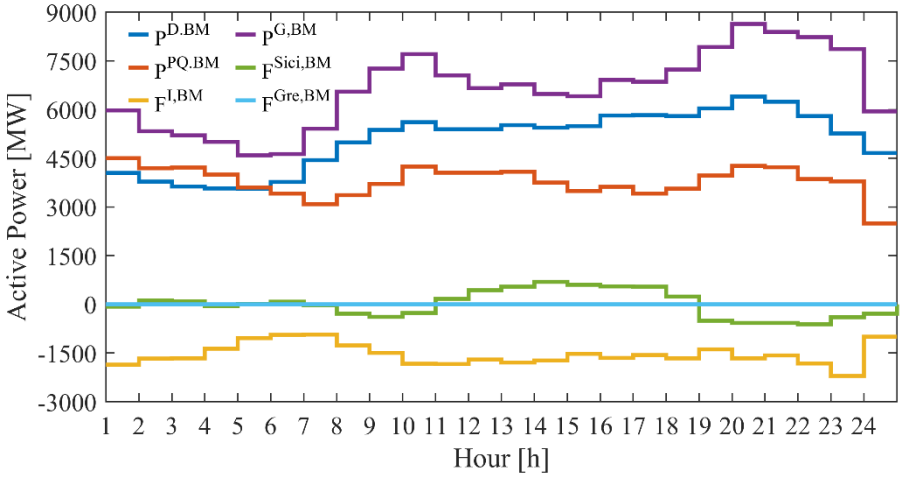

Fig. 94. Hourly power balance after BM.

6.3. Steady-State Results

The target voltage of 1 pu is set to the 400 kV busbars controlled by the PV power plants, in order to carry out the quasi-dynamic AC load flow. Only, the shunt inductors installed on the two terminals of the Scilla-Villafranca branch are turned on throughout the day because the cable connecting with Sicily has a significant capacitive nature. The load power factors of (227) are obtained from the nodal active and reactive power of the TYNDP network, adjusting their distribution in relation to the future installation provided by Terna's TEP reports [253].

The main objective of this work is to examine the start-up of Altomonte, Sparanise 2 and Modugno SUs—situated in Calabria, Campania and Apulia, respectively—from DA to BM results. In particular, Fig. 95 shows the DA results, while Table 39 reports the hours and the corresponding dispatched minimum power of the SUs as result of the BM. After DA Altomonte is cleared from 15:00 to the end of the day, Sparanise 2 is cleared for the entire day save for the time window 2:00-5:00, whereas Modugno is running from 7:00 to 16:00. The TSO ordered Altomonte start-up in the morning and that Sparanise 2 and Modugno continue to run, for the BM.

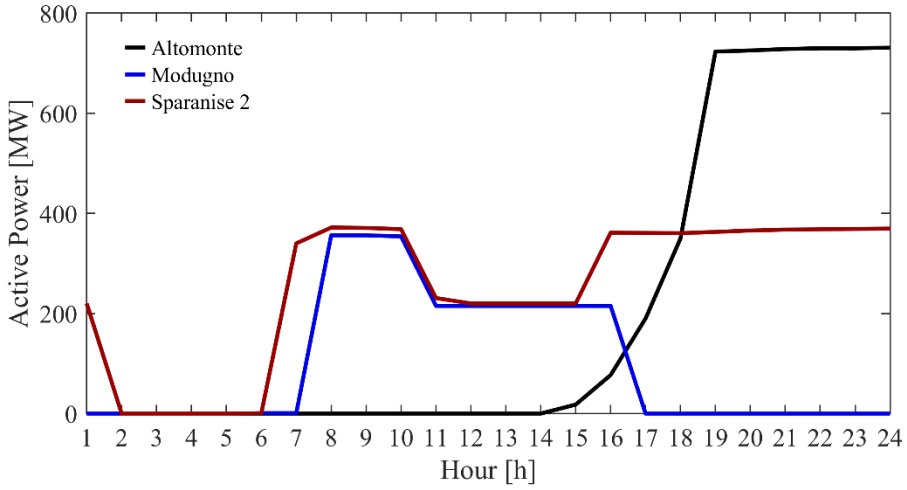

Fig. 95. Dispatched power after DA results of the supplying units of interest.

Table 39. Start-up SUs from DA to BM.

UP \ h	1	2	3	4	5	6	…	17	18	19	20	21	22	23	24
Altomonte	190	190	190	190	190	190									
Sparanise 2		220	220	220	220	220									
Modugno								215	215	215	215	215	215	215	215

For this purpose, three scenarios have been considered and they are described below:

- Base case scenario (BC): according to the experience of Sorgenia, the Internal Italy boundary power flow is divided among the lines; a detailed comparison of the two markets is then presented highlighting the main system critical issues, and the first motives behind the start-up of the generators are identified.
- Modugno not running scenario (MNR): using the same hypotheses as the previous scenario, Modugno's cleared power from 17:00 to 24:00 is supposed to be denied after BM, distributing its dispatched power among the operational PV generators; this scenario aims to uncover additional factors that might influence the TSO's decision to continue operating Modugno.
- Internal flow rated power division scenario (IFD): in this scenario (228) is exploited to define the power flow among the interconnecting lines of the Internal Italy boundary. This additional scenario has been defined to evaluate the impact of the northen power flow distribution on the system.

6.3.1. Base Case Scenario

The boundary power flow division through the interconnection lines of the Internal Italy following AC load flow simulations are shown in Fig. 96 and Fig. 97, after DA and BM, respectively. Four lines belong to the Tyrrhenian side, as indicated in Fig. 90, and only Rotello-San Severo (which is situated between Foggia and Larino) permits the flow exchanged on the Adriatic side. As a result of the border power flow increase, it is clear that the lines from DA to BM are susceptible to a higher power flow. In both situations, Rotello-San Severo is the most heavily loaded one; in Fig. 97 the line reaches its peak active power between 19:00 and 22:00.

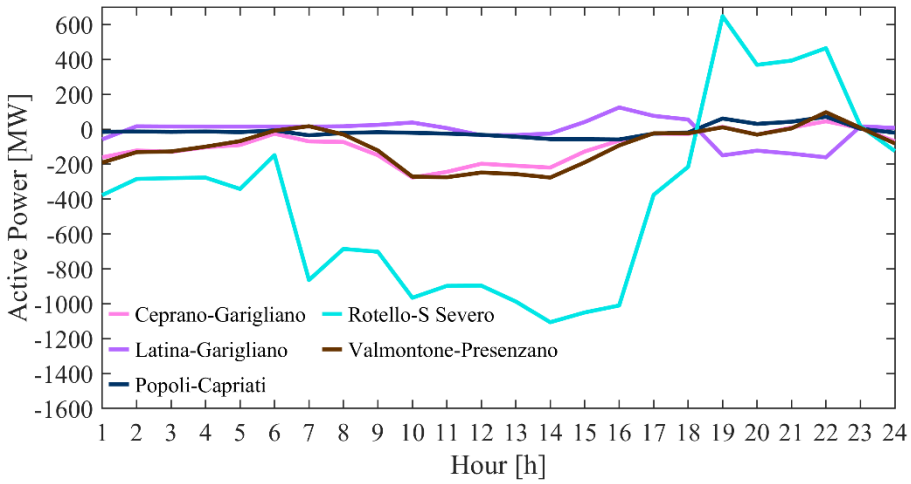

Fig. 96. BC Internal Italy boundary splitting after DA.

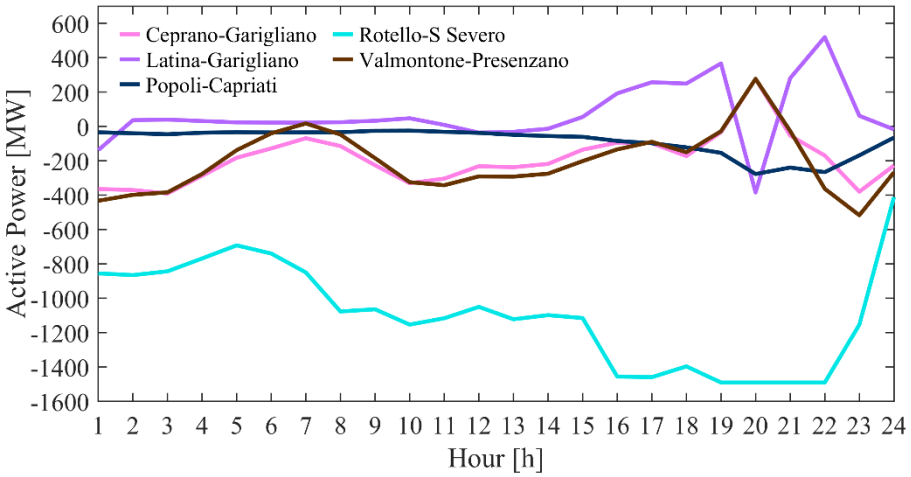

Fig. 97. BC Internal Italy boundary splitting after BM.

The obtained voltage results after the DA market are shown in Fig. 98 in terms of absolute minimum and maximum values, as well as mean one. An overvoltage condition occurs in the early morning, with a maximum and mean voltage of 1.058 pu and 1.025 pu, respectively. During the same hours in Fig. 99 there are buses in undervoltage operation, with the lowest at 8:00 a.m. with 0.938 pu.

Minimum voltage values occur at PV generation buses in both simulations, particularly on Calabria's ones, to balance the capacitive nature of the system. In fact, Fig. 100 depicts the buses on which the maximum voltage occurs, at least for one hour of the day, as output of DA AC load flow simulation, and Laino and Rossano, that are located in Calabria, are the buses where the maximum voltage occurs in the early morning. Plotting the same buses'

results after BM, as depicted in Fig. 101, it is straightforward that Altomonte's start-up provides a voltage benefit in the Calabria region, lowering those voltages to less than 1.02 pu.

As observed by the analogues AC load flow results focused on the BM minimum voltage buses, respectively in Fig. 102 and Fig. 103, this benefit requires a strong reactive power supply from Altomonte. After BM simulation (Fig. 102) the ST bus of Altomonte has the lowest voltage from 1:00 to 6:00, whereas after DA simulation (Fig. 103) the buses have the same overvoltage as the Calabria region. Presenzano is an additional SU that is dispatched in BM, but it is a PSH, and due to the fast response and high cost of this technology, it is usually called for balancing purposes, indeed it lacks of start-up bid [238].

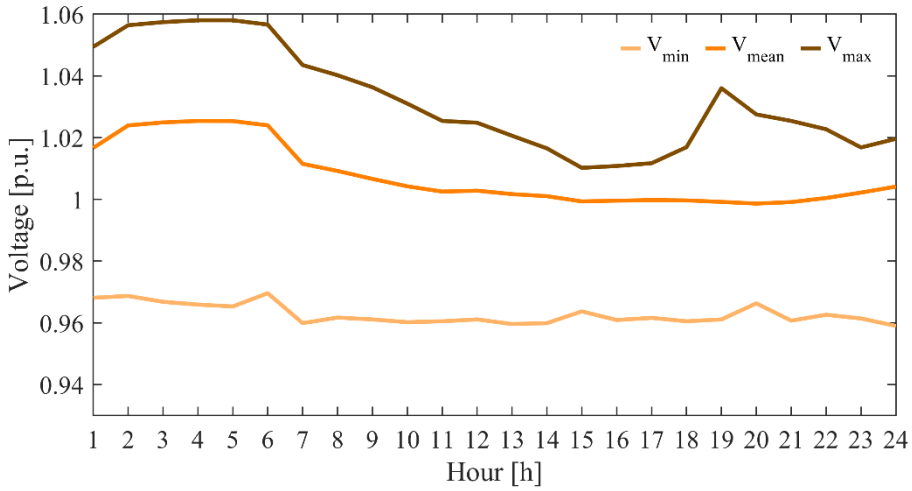

Fig. 98. BC statistical voltage values after DA load flow results.

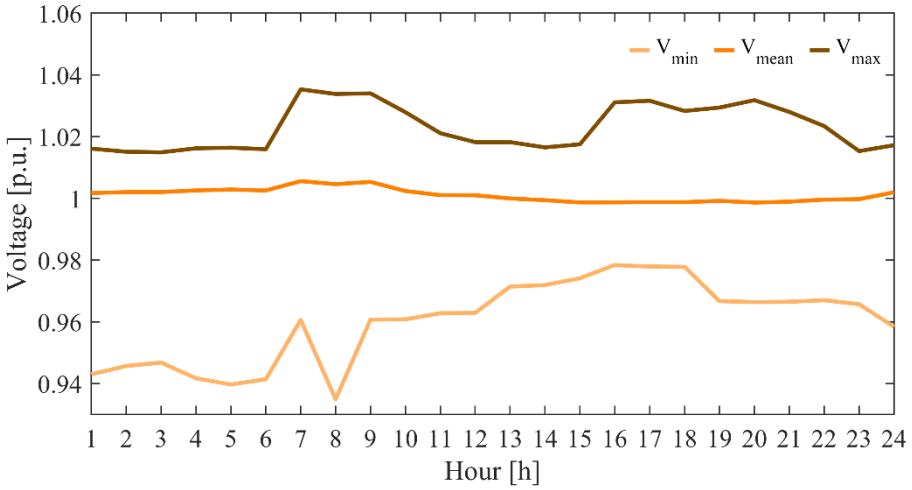

Fig. 99. BC statistical voltage values after BM load flow results.

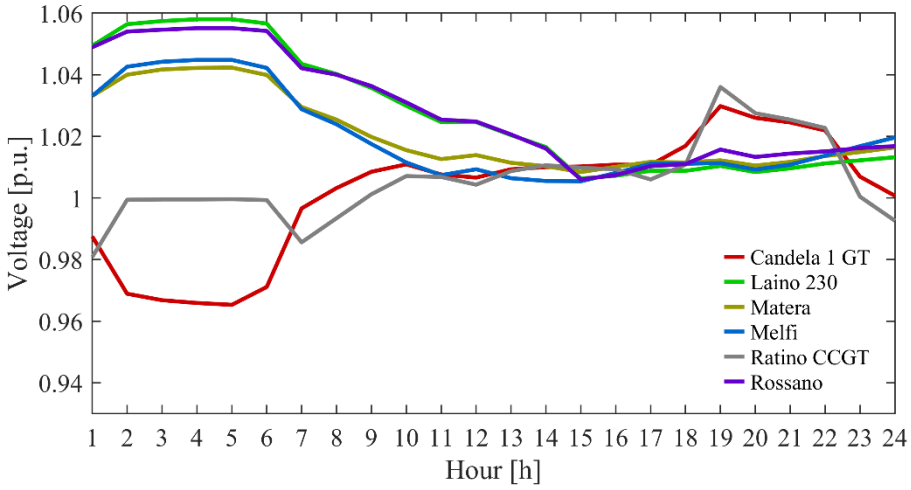

Fig. 100. BC maximum voltage buses of DA after DA load flow simulation.

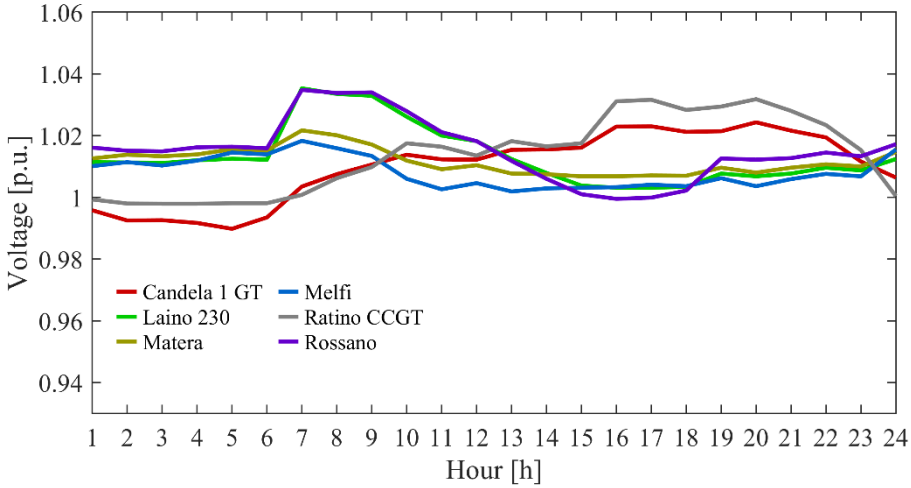

Fig. 101. BC maximum voltage buses of DA after BM load flow simulation.

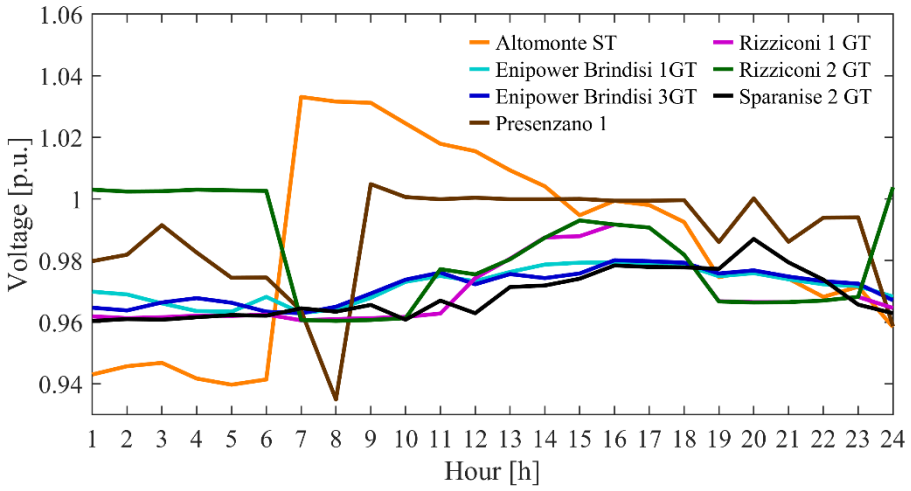

Fig. 102. BC minimum voltage buses of BM after BM load flow simulation.

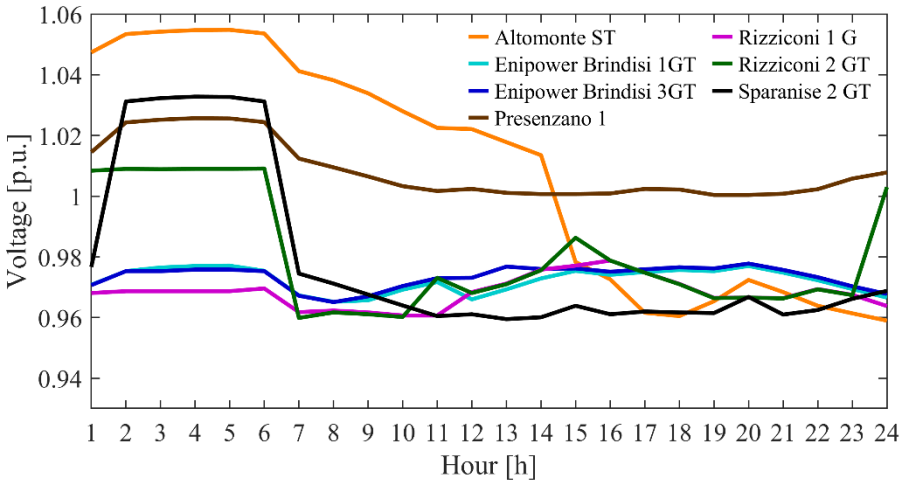

Fig. 103. BC minimum voltage buses of BM after DA load flow simulation.

PV generators' reactive power supply can lead to additional considerations on the obtained results. Therefore, Fig. 104 and Fig. 105 show the reactive power provided by SUs and interconnection generators after DA results, respectively. From 7:00 to the end of the day, the northern Apulian SUs are the only ones operating in over-excitation, while the rest of the SUs are operating in under-excitation, demonstrating the overall capacity reactive power required by the system. A similar behavior is observed for the interconnection generators, with Sorgente and Ceprano generators being the most heavily used in the early morning, providing an average of -380 MVAr and -280 MVAr, respectively.

The BM simulation results are depicted in Fig. 106 and Fig. 107 for the PV and interconnection generators, respectively. The start-up of Sparanise 2 and the clearing of Presenzano reduced the capacity reactive power supply from the Tyrrhenian side exchange generators by approximately 400 MVAr per each hour of the early morning. Similarly for Sicily, Altomonte's start-up reduced reactive power by approximately 200 MVAr from 1:00 to 6:00. On the contrary, even though Modugno is start-up from 17:00 until the end of the day, the required inductive reactive power of North Apulian area is increased. This is due to the increase in power balance from DA to BM, as well as the nodal distribution of load and generation based on yearly consumption (Fig. 92) and the RES installed capacity (Table 38).

Fig. 108 and Fig. 109 depict the maximum and mean branch loading after DA and BM simulation, respectively. The power balance increase leads to a slight increase of the line mean loading from DA to BM, exceeding the 20 % at hour 20:00, while the maximum value

of 90 % is reached in the time window 19:00-22:00 due to the power flowing though the Rotello-San Severo line.

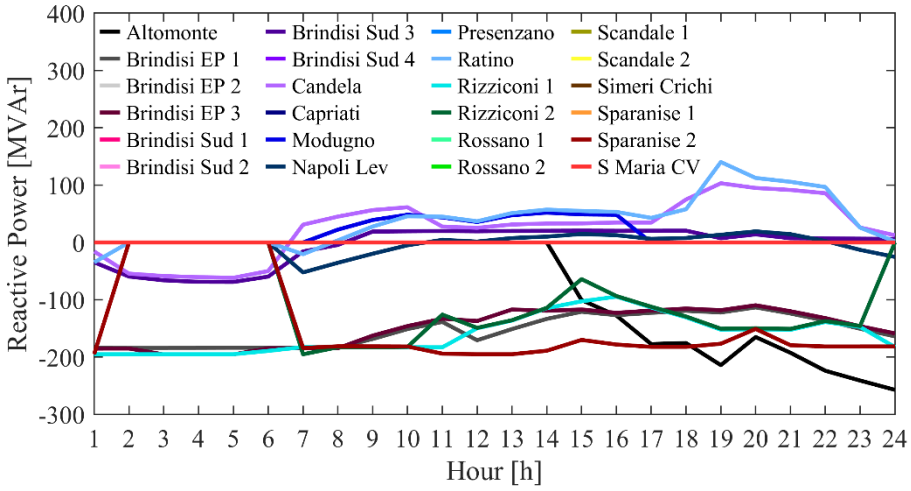

Fig. 104. BC SUs reactive power supply after DA simulation.

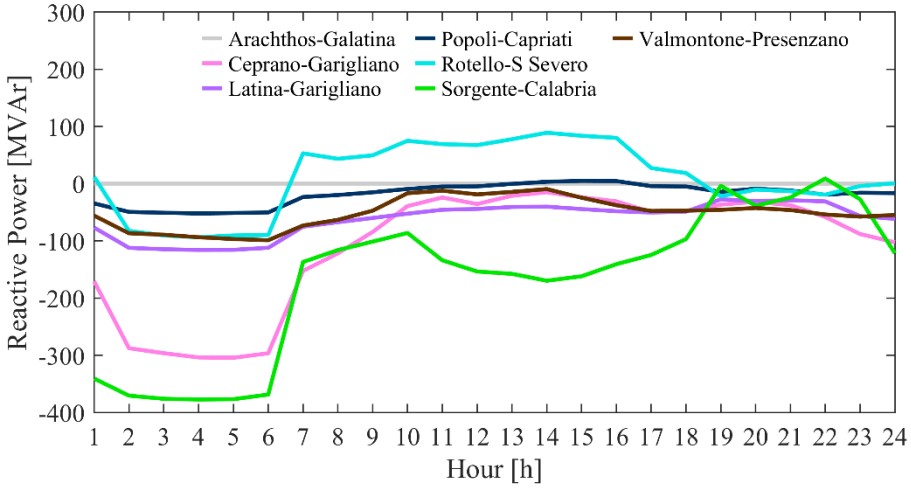

Fig. 105. BC exchange generators reactive power supply after DA simulation.

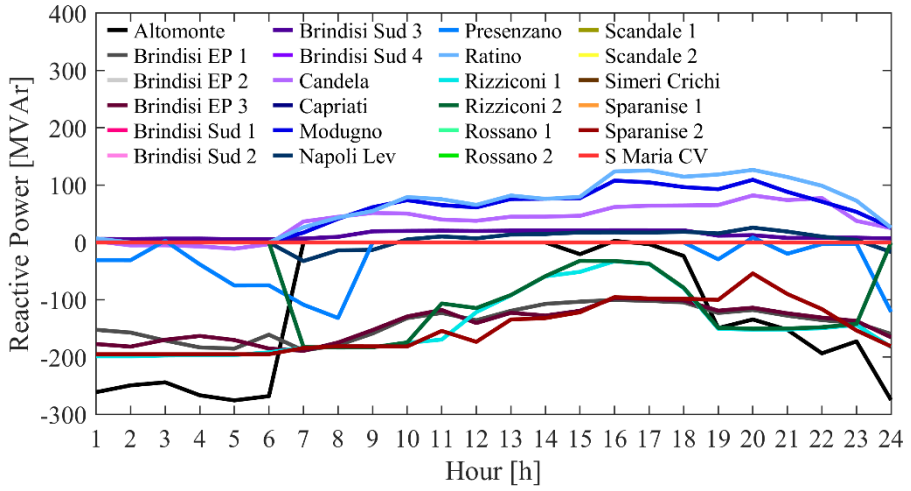

Fig. 106. BC SUs reactive power supply after BM simulation.

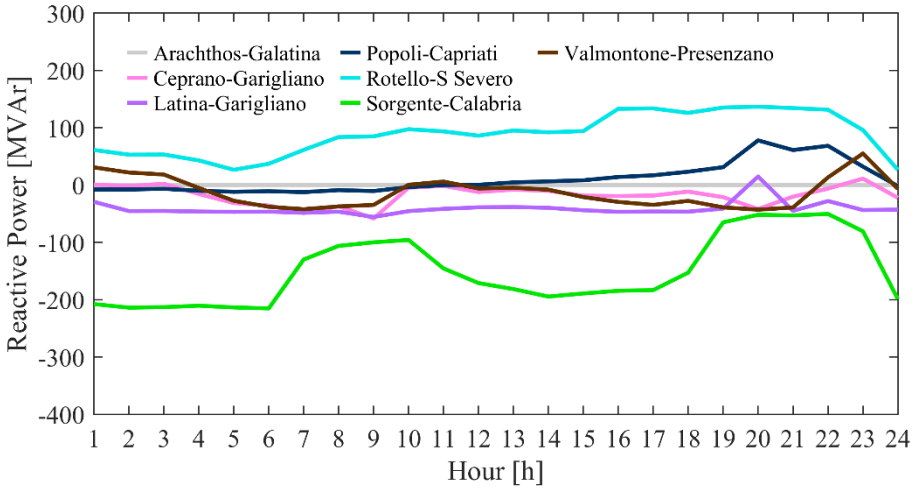

Fig. 107. BC exchange generators reactive power supply after BM simulation.

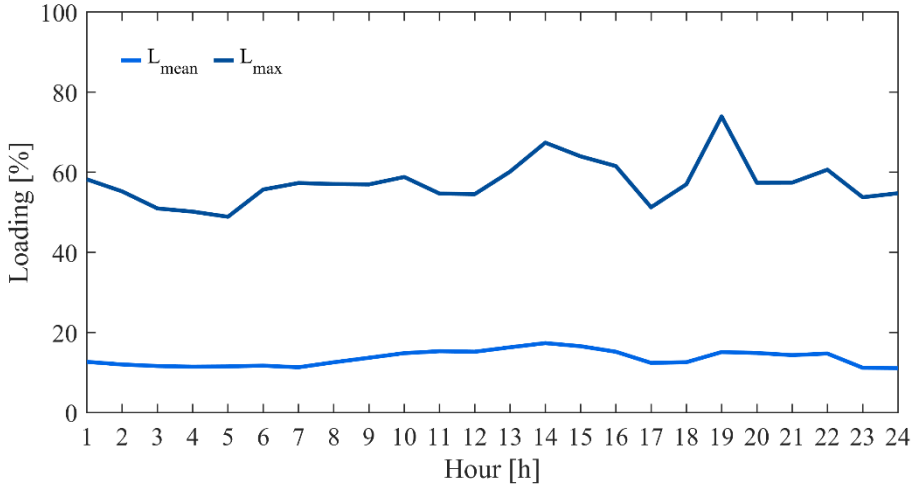

Fig. 108. BC maximum and mean branch loading after the DA simulation.

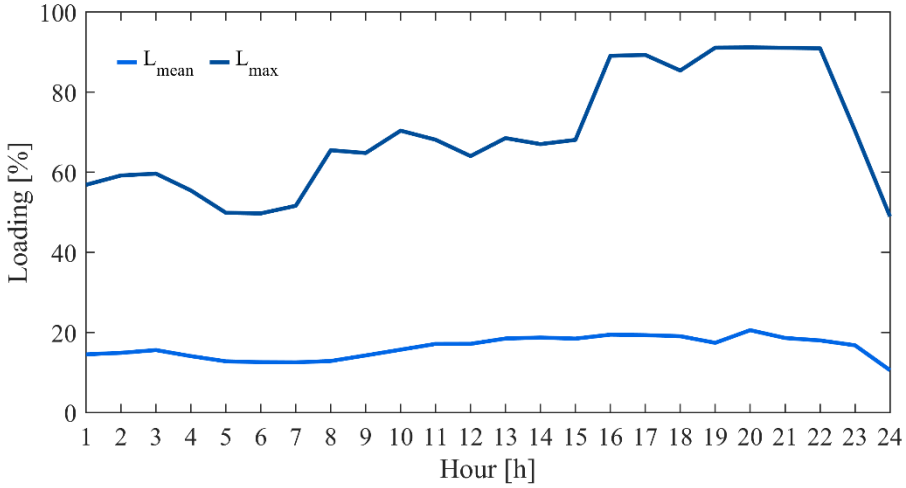

Fig. 109. BC maximum and mean branch loading after the BM simulation.

6.3.2. Modugno not Running Scenario

In addition to the previous hypothesis, for a better understating of the reasons to keep running Modugno power plant, in this scenario it is supposed to be shut-down from 17:00 to 24:00 during BM simulation. Therefore, defining with $\Omega^G(t_k)$ and $P_i^{G,PV}(t_k)$ the set of the cleared SUs and the dispatched power of the i-th PV generator at time t_k = 17, …, 24, respectively, the new dispatched power is:

$$P'^{G,PV}_i(t_k) = P_i^{G,PV}(t_k) + \frac{P^G_{Mod}(t_k)}{N^G(t_k)} \quad \forall\, i \in \Omega^G(t_k) \wedge P_i^{G,PV}(t_k) < P_i^{G,max} \tag{232}$$

where P^G_{Mod} is the cleared power of Modugno reported in Table 39 and N^G is the number of operating SUs below their rated power ($P_i^{G,max}$) at time t_k.

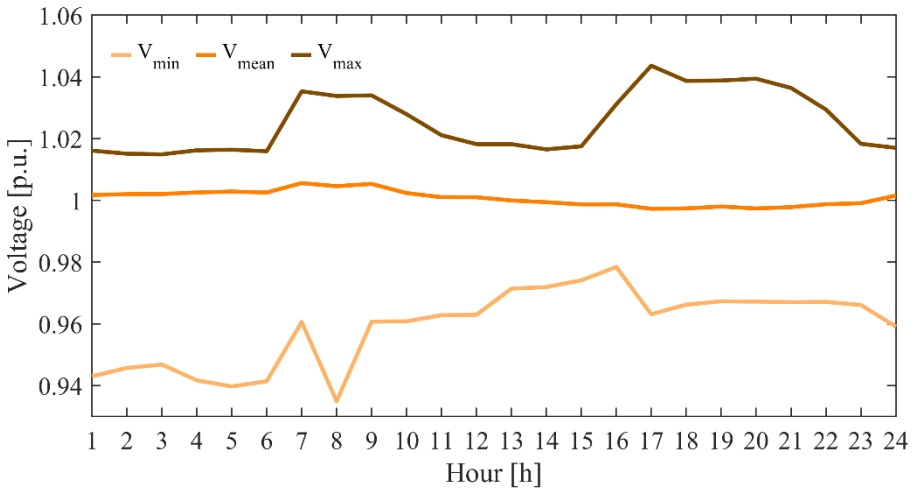

Fig. 110. MNR statistical voltage values after BM load flow results.

The maximum, mean and minimum voltage values are shown in Fig. 110 and the operating condition of the system from 17:00 to 24:00 is still within 1.05 and 0.95 pu. When compared to the results in Fig. 97, the maximum voltage is higher, with a peak of over 1.04 pu at hour 17:00, but the mean voltage follows the same trend. Therefore, the dispatch of Modugno provides a benefit to the Apulia North area voltages, but it is not essential as for Altomonte for the Calabria area voltages.

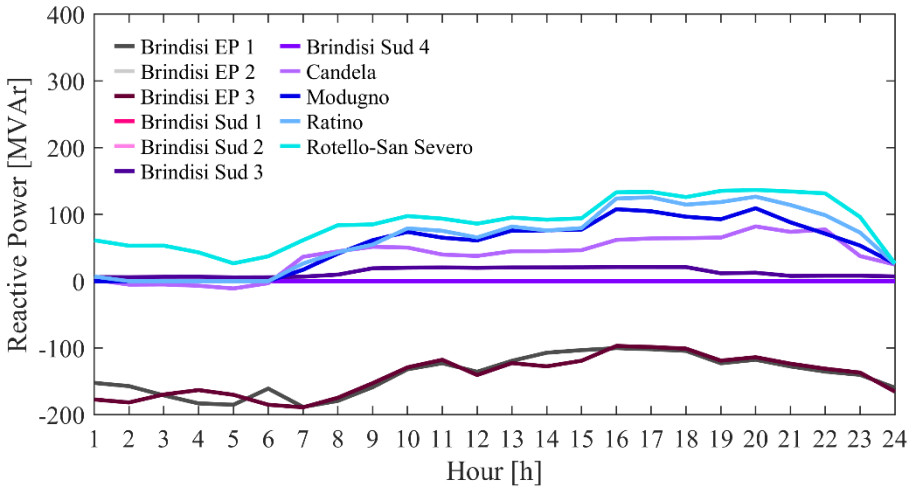

Fig. 111. BC Apulian generators reactive power.

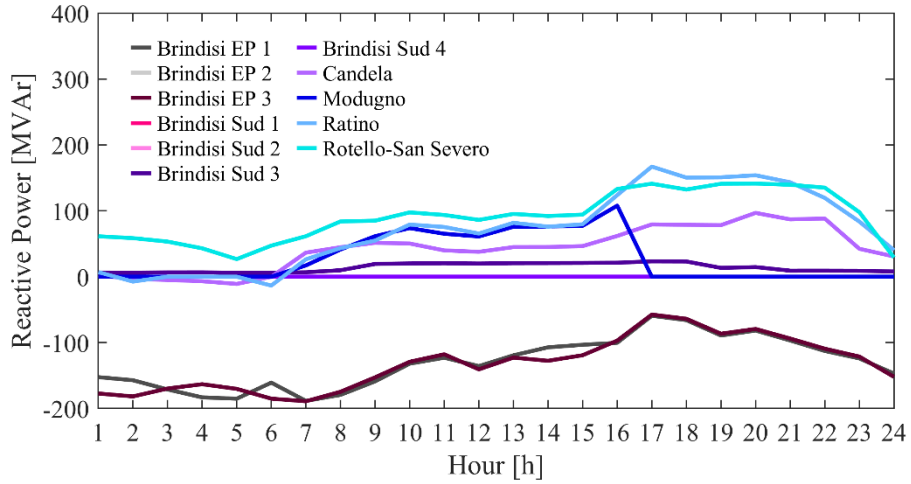

Fig. 112. MNR Apulian generators reactive power.

For the sake of completeness, the reactive power provided by the Apulian SUs are depicted in Fig. 111 for the BC scenario and Fig. 112 for the MNR scenario, respectively. In the base case scenario from 17:00 to 20:00 Modugno provided roughly 100 MVAr, while in the new scenario the reactive power variation is equal to the reactive power amount that Modugno was suppling. In particular, the two SUs in Brindisi reduced their supply of capacitive reactive power, while the rest of the generators increased their supply of inductive reactive power, and Ratino is the SU with the greatest variation of roughly 30 MVAr (it is the bus on which occur the maximum voltage at hour 20:00). In the remaining hours Modugno provided less than 50 MVAr; therefore, the generators' operating condition variation between the scenarios is negligible.

6.3.3. Internal Flow Rated Power Division Scenario

Following BM simulations, the Rotello-San Severo reached its maximum active power in the base case scenario for four hours (19:00-22:00). However, a phase shifter transformer (PST) is strategically placed between Foggia and Benevento to support the system's power flow from the Adriatic to the Tyrrhenian sides. Since the power exchanged is modeled as a PV generation, their values will not change adjusting the PST taps. Therefore, this scenario is realized exploiting the power flow split of (231) to evaluate a different Internal Boundary configuration, and Fig. 113 illustrates the results after DA, while Fig. 114 illustrates the results after BM load flows. As opposed to the BC scenario, the flows are concordant among them and two lines of the Tyrrhenian side are more loaded compared to the Rotello-San Severo one.

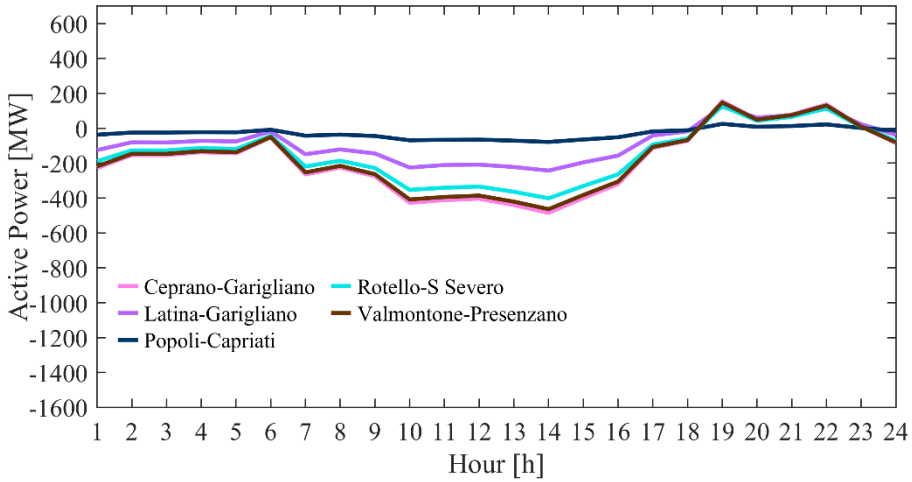

Fig. 113. IFD Internal Italy boundary splitting after DA.

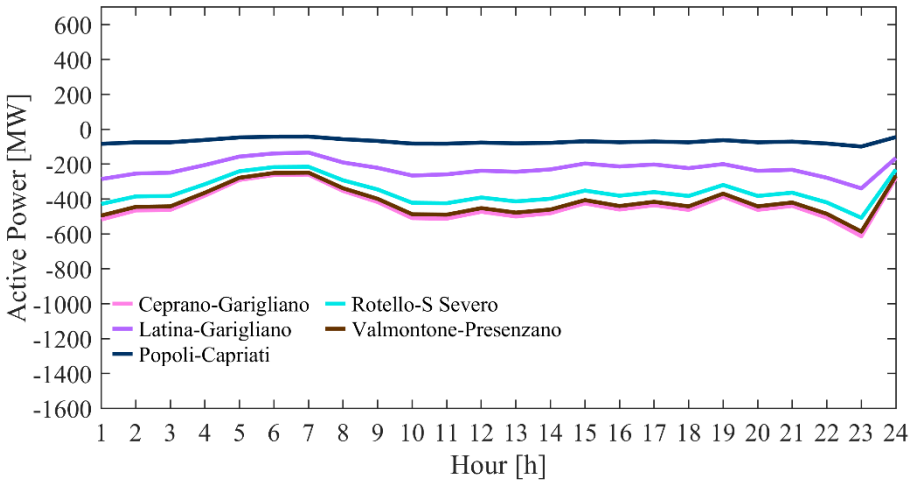

Fig. 114. IFD Internal Italy boundary splitting after BM.

The statistical voltage values are shown in Fig. 115 and Fig. 116 after DA and BM simulations, respectively. The maximum voltages in the early morning after the DA are equal to those in Fig. 98, due to the distance of Calabria area from the Internal boundary, whereas the maximum voltage drops to values around 1.02 pu during the night. This is because, as shown in Fig. 117, lower voltages are needed on the PV generation buses in north Apulian zone in order to achieve 1 pu on the 400 kV buses as a result of the Adriatic side power import reduction (comparing Fig. 113 with Fig. 96). Furthermore, in this scenario the mean voltage is close to 1 pu from 10:00 to 22:00, while in the BC scenario it is close to 1 pu starting from 13:00. The reactive power supplied by PV and interconnection generators after DA simulation are not analyzed because their variation is neglectable.

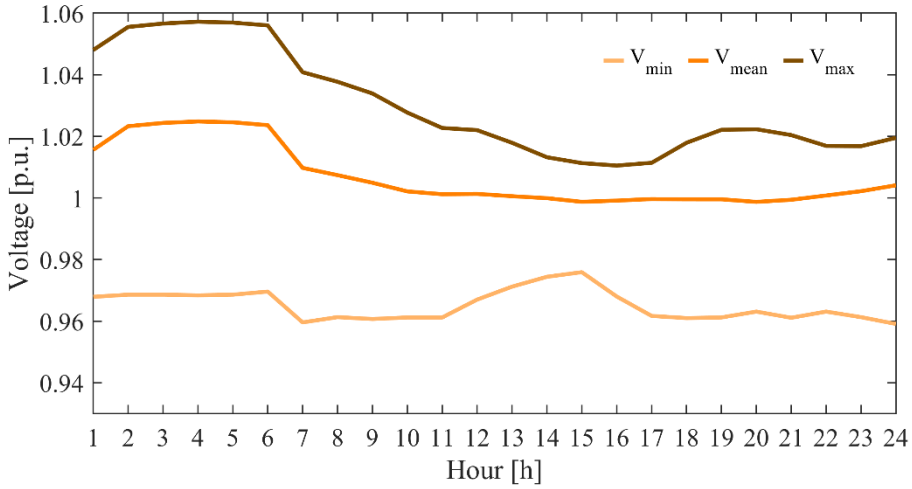

Fig. 115. IFD statistical voltage values after DA load flow results.

When compared to the BM results in Fig. 116 with the ones in Fig. 99, the voltages are subject to a slight benefit in the early morning hours. In particular, the minimum voltage between 1:00 and 6:00 is greater than 1.04 pu and at hour 8:00 the minimum is 0.96 pu. For the rest of the day the maximum voltage varies within 1.02 pu and 1.03 pu. Furthermore, Fig. 118 displays the buses where the hourly minimum voltage occurs, and contrary to the findings of Fig. 102, Presenzano's bus voltage is higher than 1 pu for several hours of the day and at hour 8:00 its nodal voltage is significantly improved moving from 0.983 pu to 0.938 pu of the BC scenario. Finally, Fig. 119 shows the reactive power supplied by the interconnection generators, which are the most varied ones with respect to the BC scenario, while Arachthos-Galatina is omitted because there is any exchange throughout the day. Sorgente provides the same amount of reactive power as the BC scenario (Fig. 107), while the Internal

lines reduced their reactive power injection, particularly Rotello-San Severo which produces 100 MVAr less between 16:00 and 22:00. As a result, the Tyrrhenian side requires more inductive reactive power under this new operating condition, vice versa for the Adriatic one.

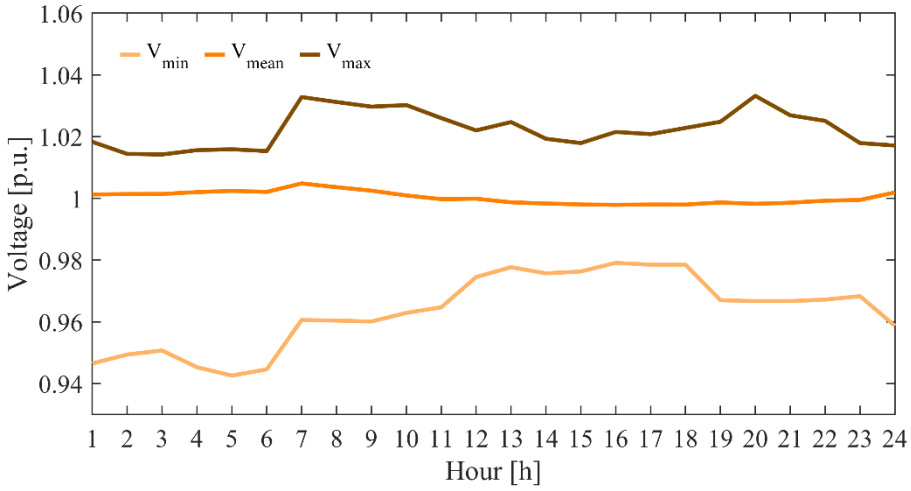

Fig. 116. IFD statistical voltage values after BM load flow results.

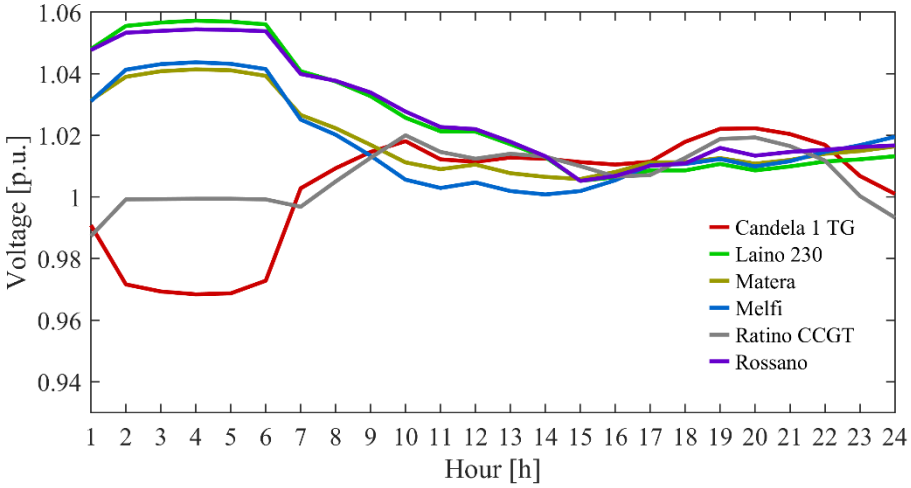

Fig. 117. IFD maximum voltage buses of DA after DA load flow simulation.

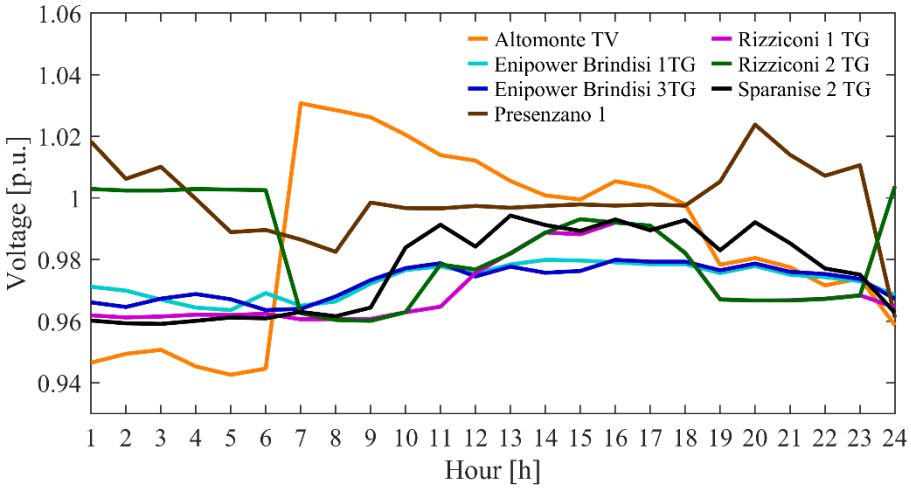

Fig. 118. IFD minimum voltage buses of BM after BM load flow simulation.

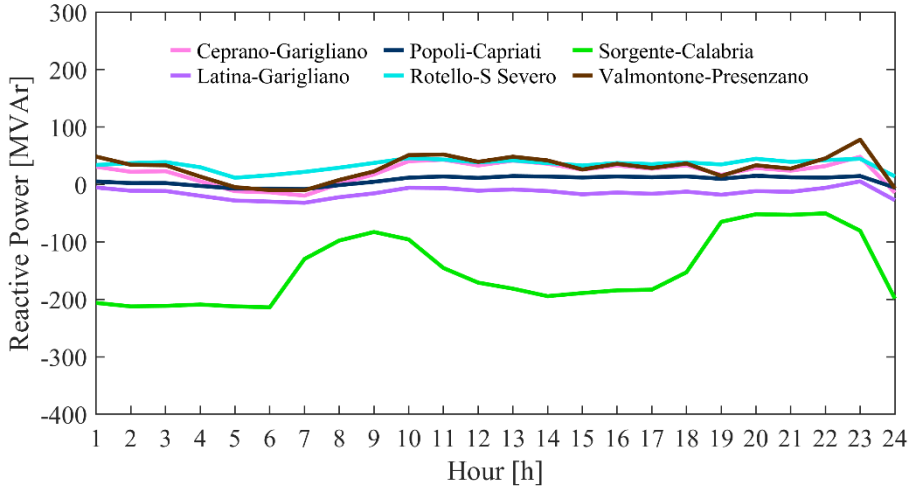

Fig. 119. IFD exchange generators reactive power supply after BM simulation.

6.4. Final Understanding

In this chapter an approach to evaluate the operations of a TSO to ensure the system security by means of BM is proposed. The method aims to handle the market outcomes following DA and BM in order to obtain a suitable nodal distribution and perform a quasi-dynamic AC load flow simulation. The test case, on which the methodology is applied, is the 400 kV and 230 kV SITS of Apulia, Basilicata, Calabria and Campania regions. In particular, three scenarios are developed and analyzed in order to deduce the factors that led to start-up or keep run the SUs of Altomonte, Modugno and Sparanise 2. Altomonte was started up in the early morning hours, and the results have shown that its contribution to voltage control has a significant positive impact on the area of Calabria during those hours by reducing the maximum voltage from 1.058 pu to 1.02 pu. Contrarily, Modugno and Sparanise 2, which

were kept run, did not prove relevant for the voltage control, despite a marginal improvement in the voltage of the corresponding region, i.e. Apulia and Campania, is detected. Therefore, these two SUs are called by the TSO to balance the power during real time operations, whereas Altomonte is crucial for the voltage control of the Calabria's area. Further answers can be obtained from the N-1 security conditions and/or from considerations on dynamic behaviour, in particular, to identify the motivations to justify form a technical perspective the actions on Sparanise 2 to be kept running.

Bibliography

[1] NEMO, “All NEMO Committee.” [Online]. Available: https://www.nemo-committee.eu/index

[2] GME, “Italian Electrical Market Integration With Single Intra-Day Coupling (SIDC).” [Online]. Available: https://www.mercatoelettrico.org/it/MenuBiblioteca/Documenti/20200331_DCO_Xbid.pdf

[3] ACER, “Complementary Regional Intraday Auctions proposal for Italy North Capacity Calculation Region in accordance with Article 63 of the Commission Regulation (EU) 2015/1222 of 24 July 2015 establishing a Guideline on Capacity Allocation and Congestion Manageme.” [Online]. Available: https://acer.europa.eu/en/Electricity/MARKET-CODES/CAPACITY-ALLOCATION-AND-CONGESTION-MANAGEMENT/9 CRIDA/Italian borders Action 9a - CRIDA amended proposal IB.pdf

[4] GME, “Glossary.” [Online]. Available: https://www.mercatoelettrico.org/en/Tools/Glossario.aspx#X

[5] GME, “SIDC: XBID-CRIDA.” [Online]. Available: https://www.mercatoelettrico.org/en/Mercati/MercatoElettrico/XBID.aspx

[6] Terna, “Grid Code: Chapter 4 – Dispatching regulations.” [Online]. Available: https://download.terna.it/terna/220701_Chapter_4_8da5ad23d90ecdc.pdf

[7] Terna, “Annex A.22 – Method for the resources selection in the planning stage of ASM,” 2021. [Online]. Available: https://download.terna.it/terna/20211004 Allegato_A.22_8d987427a7fc012.pdf

[8] ENTSO-E, “TERRE - Trans European Replacement Reserves Exchange.” [Online]. Available: https://www.entsoe.eu/network_codes/eb/terre/

[9] ENTSO-E, “Cross Border Electricity Balancing Pilot Projects.” [Online]. Available: https://docstore.entsoe.eu/major-projects/network-code-implementation/cross-border-electricity-balancing-pilot-projects/Pages/default.aspx

[10] ENTSO-E, “Common opinion from AEEGSI, CNMC, CRE, ElCom, ERSE and OFGEM on TERRE project design.” [Online]. Available: https://docstore.entsoe.eu/Documents/Events/2018/terre/NRAs_2nd_opinion_paper_endorsed_at_working_level.pdf

[11] P. Denholm and M. Hand, “Grid flexibility and storage required to achieve very high penetration of variable renewable electricity,” *Energy Policy*, vol. 39, no. 3, pp. 1817–1830, 2011, doi: 10.1016/j.enpol.2011.01.019.

[12] A. J. Conejo, Y. Cheng, N. Zhang, and C. Kang, “Long-term coordination of transmission and storage to integrate wind power,” *CSEE J. Power Energy Syst.*, vol. 3, no. 1, pp. 36–43, 2017, doi: 10.17775/cseejpes.2017.0006.

[13] A. J. Conejo and L. Baringo, “Unit Commitment and Economic Dispatch,” in *Power System Operation*, Switzerland, 2018, pp. 197–232. doi: 10.1007/978-3-319-69407-8_7.

[14] M. Paturet, U. Markovic, S. Delikaraoglou, E. Vrettos, P. Aristidou, and G. Hug, “Stochastic unit commitment in low-inertia grids,” *IEEE Trans. Power Syst.*, vol. 35, no. 5, pp. 3448–3458, 2020, doi: 10.1109/TPWRS.2020.2987076.

[15] M. Ellahi, G. Abbas, G. B. Satrya, M. R. Usman, and J. Gu, “A Modified Hybrid Particle Swarm Optimization with Bat Algorithm Parameter Inspired Acceleration Coefficients for Solving Eco-Friendly and Economic Dispatch Problems,” *IEEE Access*, pp. 82169–82187, 2021, doi: 10.1109/ACCESS.2021.3085819.

[16] Q. Xia, Y. H. Song, B. Zhang, C. Kang, and N. Xiang, “Effective decomposition and co-ordination algorithms for unit commitment and economic dispatch with security constraints,” *Electr. Power Syst. Res.*, vol. 53, no. 1, pp. 39–45, 2000, doi: 10.1016/S0378-7796(99)00035-8.

[17] E. Du, N. Zhang, C. Kang, and Q. Xia, “A High-Efficiency Network-Constrained Clustered Unit Commitment Model for Power System Planning Studies,” *IEEE Trans. Power Syst.*, vol. 34, no. 4, pp. 2498–2508, 2019, doi: 10.1109/TPWRS.2018.2881512.

[18] X. Zhu, Z. Yu, and X. Liu, “Security Constrained Unit Commitment with Extreme Wind Scenarios,” *J. Mod. Power Syst. Clean Energy*, vol. 8, no. 3, pp. 464–472, 2020, doi: 10.35833/MPCE.2018.000797.

[19] ENTSO-E, “Glossary.” [Online]. Available: https://www.entsoe.eu/outlooks/midterm/glossary/

[20] M. Van Vyve and others, “Linear prices for non-convex electricity markets: models and algorithms,” 2011.

[21] S. Edition, *The Authoritative Dictionary of IEEE Standards Terms*. 2000.

[22] A. Martin, J. C. Müller, and S. Pokutta, “Strict linear prices in non-convex European day-ahead

electricity markets," *Optim. Methods Softw.*, vol. 29, no. 1, pp. 189–221, 2013, doi: 10.1080/10556788.2013.823544.
[23] J. Gan, Deqiang; Feng, Donghan; Xie, "Introduction," in *Electricity Markets and Power System Economics*, 1rst ed., CRC Press, 2014, pp. 1–9.
[24] D. Shah and S. Chatterjee, "A comprehensive review on day-ahead electricity market and important features of world's major electric power exchanges," *Int. Trans. Electr. Energy Syst.*, vol. 30, no. 7, pp. 1–39, 2020, doi: 10.1002/2050-7038.12360.
[25] A. I. Cohen and S. H. Wan, "A Method for Solving the Fuel Constrained Unit Commitment Problem," *IEEE Trans. Power Syst.*, vol. 2, no. 3, pp. 608–614, 1987, doi: 10.1109/TPWRS.1987.4335178.
[26] K. Sepetanc and H. Pandzic, "Convex Polar Second-Order Taylor Approximation of AC Power Flows: A Unit Commitment Study," *IEEE Trans. Power Syst.*, vol. 36, no. 4, pp. 3585–3594, 2021, doi: 10.1109/TPWRS.2020.3046970.
[27] T. S. Dillon, K. W. Edwin, H.-D. Kochs, and R. J. Taud, "Integer Programming Approach to the Problem of Optimal Unit Commitment with Probabilistic Reserve Determination," *IEEE Trans. Power Appar. Syst.*, vol. PAS-97, no. 6, pp. 2154–2166, 1978, doi: 10.1109/TPAS.1978.354719.
[28] J. Ortega and D. Watts, "Operating Reserves And Unit Commitment Considering Variable Renewable Energies : An Academic Review," vol. 15, no. 11, pp. 2108–2119, 2017.
[29] Y. Xu, T. DIng, M. Qu, and P. Du, "Adaptive Dynamic Programming for Gas-Power Network Constrained Unit Commitment to Accommodate Renewable Energy with Combined-Cycle Units," *IEEE Trans. Sustain. Energy*, vol. 11, no. 3, pp. 2028–2039, 2020, doi: 10.1109/TSTE.2019.2951616.
[30] H. Liu *et al.*, "Application of modified progressive hedging for stochastic unit commitment in electricity-gas coupled systems," *CSEE J. Power Energy Syst.*, vol. 7, no. 4, pp. 840–849, 2021, doi: 10.17775/CSEEJPES.2020.04420.
[31] Y. Zhou, M. Shahidehpour, Z. Wei, Z. Li, G. Sun, and S. Chen, "Distributionally Robust Unit Commitment in Coordinated Electricity and District Heating Networks," *IEEE Trans. Power Syst.*, vol. 35, no. 3, pp. 2155–2166, 2020, doi: 10.1109/TPWRS.2019.2950987.
[32] Y. Zhou, M. Shahidehpour, Z. Wei, G. Sun, and S. Chen, "Multistage robust look-ahead unit commitment with probabilistic forecasting in multi-carrier energy systems," *IEEE Trans. Sustain. Energy*, vol. 12, no. 1, pp. 70–82, 2021, doi: 10.1109/TSTE.2020.2979925.
[33] M. A. Mirzaei, M. Nazari-Heris, B. Mohammadi-Ivatloo, K. Zare, M. Marzband, and S. A. Pourmousavi, "Robust Flexible Unit Commitment in Network-Constrained Multicarrier Energy Systems," *IEEE Syst. J.*, vol. 15, no. 4, pp. 5267–5276, 2021, doi: 10.1109/JSYST.2020.3012338.
[34] Q. P. Zheng, J. Wang, S. Member, and A. L. Liu, "Stochastic Optimization for Unit Commitment — A Review," *IEEE Trans. Power Syst.*, pp. 1–12, 2014.
[35] N. Yang *et al.*, "A Comprehensive Review of Security-constrained Unit Commitment," *J. Mod. Power Syst. Clean Energy*, vol. 10, no. 3, pp. 562–576, 2022, doi: 10.35833/MPCE.2021.000255.
[36] N. Muralikrishnan, L. Jebaraj, and C. C. A. Rajan, "A Comprehensive Review on Evolutionary Optimization Techniques Applied for Unit Commitment Problem," *IEEE Access*, vol. 8, pp. 132980–133014, 2020, doi: 10.1109/ACCESS.2020.3010275.
[37] S. Virmani, E. C. Adrian, K. Imhof, and S. Mukherjee, "Implementation of a Lagrangian relaxation based unit commitment problem," *IEEE Trans. Power Syst.*, vol. 4, no. 4, pp. 1373–1380, 1989, doi: 10.1109/59.41687.
[38] A. Bhardwaj, V. K. Kamboj, V. K. Shukla, B. Singh, and P. Khurana, "Unit commitment in electrical power system - A literature review," *2012 IEEE Int. Power Eng. Optim. Conf. PEOCO 2012 - Conf. Proc.*, no. June, pp. 275–280, 2012, doi: 10.1109/PEOCO.2012.6230874.
[39] M. Bavafa, H. Monsef, and N. Navidi, "A new hybrid approach for unit commitment using lagrangian relaxation combined with evolutionary and quadratic programming," *Asia-Pacific Power Energy Eng. Conf. APPEEC*, 2009, doi: 10.1109/APPEEC.2009.4918069.
[40] X. Yu and X. Zhang, "Unit commitment using Lagrangian relaxation and particle swarm optimization," *Int. J. Electr. Power Energy Syst.*, vol. 61, pp. 510–522, 2014, doi: 10.1016/j.ijepes.2014.03.061.
[41] G. C. Contaxis and J. Kabouris, "Short term scheduling in a wind/diesel autonomous energy system," *IEEE Trans. Power Syst.*, vol. 6, no. 3, pp. 1161–1167, 1991, doi: 10.1109/59.119261.
[42] T. Senjyu, T. Miyagi, A. Y. Saber, N. Urasaki, and T. Funabashi, "Emerging solution of large-scale unit commitment problem by Stochastic Priority List," *Electr. Power Syst. Res.*, vol. 76, no. 5, pp. 283–292, 2006, doi: 10.1016/j.epsr.2005.07.002.
[43] CAISO, "Appendix A – Master Definition Supplement." [Online]. Available:

https://www.caiso.com/Documents/AppendixA_Definitions_Aug1_2014.pdf
[44] G. Tricarico, F. Gonzalez-longatt, L. S. Azuara-grande, and J. L. Rueda, "Security Constrained Unit Commitment and Economic Dispatch applied to the Modified IEEE 39-bus system Case," in *2022 IEEE Biennial Congress of Argentina (ARGENCON)*, 2022.
[45] C. K. Simoglou, P. N. Biskas, and A. G. Bakirtzis, "Optimal self-scheduling of a thermal producer in short-term electricity markets by MILP," *IEEE Trans. Power Syst.*, vol. 25, no. 4, pp. 1965–1977, 2010, doi: 10.1109/TPWRS.2010.2050011.
[46] D. Pettersen, E. Melfald, A. Chowdhury, M. N. Acosta, F. Gonzalez-Longatt, and D. Topic, "TSO-DSO Performance Considering Volt-Var Control at Smart-Inverters: Case of Vestfold and Telemark in Norway," in *2020 International Conference on Smart Systems and Technologies (SST)*, 2020, pp. 147–152. doi: 10.1109/SST49455.2020.9264097.
[47] B. Knueven, J. Ostrowski, and J. P. Watson, "On mixed-integer programming formulations for the unit commitment problem," *INFORMS J. Comput.*, vol. 32, no. 4, pp. 857–876, 2020, doi: 10.1287/ijoc.2019.0944.
[48] J. Holzer, Y. Chen, Z. Wu, F. Pan, and A. Veeramany, "Fast Simultaneous Feasibility Test for Security Constrained Unit Commitment," 2022, doi: 10.36227/techrxiv.20280384.v1.
[49] A. F. M. K. Chowdhury, J. Kern, T. D. Dang, and S. Galelli, "PowNet: A network-constrained unit commitment/economic dispatch model for large-scale power systems analysis," *J. Open Res. Softw.*, vol. 8, no. 1, 2020, doi: 10.5334/JORS.302.
[50] G. E. Constante-Flores, A. J. Conejo, and F. Qiu, "AC Network-Constrained Unit Commitment via Relaxation and Decomposition," *IEEE Trans. Power Syst.*, vol. 37, no. 3, pp. 2187–2196, 2022, doi: 10.1109/TPWRS.2021.3120180.
[51] K. Cheung *et al.*, "Toward scalable stochastic unit commitment: Part 2: solver configuration and performance assessment," *Energy Syst.*, vol. 6, no. 3, pp. 417–438, 2015, doi: 10.1007/s12667-015-0148-6.
[52] H. Abdi, "Profit-based unit commitment problem: A review of models, methods, challenges, and future directions," *Renew. Sustain. Energy Rev.*, vol. 138, no. November 2020, p. 110504, 2021, doi: 10.1016/j.rser.2020.110504.
[53] S. M. Moosavian, M. Modiri-Delshad, J. Selvaraj, and N. A. Rahim, "Solution techniques for optimal power dispatch problems-a review," *IET Conf. Publ.*, vol. 2016, no. CP688, pp. 1–7, 2016, doi: 10.1049/cp.2016.1274.
[54] M. B. Maskar, A. R. Thorat, and I. Korachgaon, "A review on optimal power flow problem and solution methodologies," in *2017 International Conference on Data Management, Analytics and Innovation, ICDMAI 2017*, 2017, pp. 64–70. doi: 10.1109/ICDMAI.2017.8073487.
[55] M. Shafiullah, S. D. Ahmed, and F. A. Al-Sulaiman, "Grid Integration Challenges and Solution Strategies for Solar PV Systems: A Review," *IEEE Access*, vol. 10, pp. 52233–52257, 2022, doi: 10.1109/ACCESS.2022.3174555.
[56] R. Sharma and K. K. Sharma, "Review of Economic Load Dispatch Problems by Intelligence based Optimization," *2022 2nd Int. Conf. Adv. Comput. Innov. Technol. Eng. ICACITE 2022*, pp. 1646–1650, 2022, doi: 10.1109/ICACITE53722.2022.9823513.
[57] W. Warsono, C. S. Ozveren University Of Abertay, D. J. King, and DBradley, "A review of the use of genetic algorithms in economic load dispatch," *Proc. Univ. Power Eng. Conf.*, 2008, doi: 10.1109/UPEC.2008.4651530.
[58] Y. Liu, L. Wu, and J. Li, "A Fast lp-based approach for robust dynamic economic dispatch problem: A feasible region projection method," *IEEE Trans. Power Syst.*, vol. 35, no. 5, pp. 4116–4119, 2020, doi: 10.1109/TPWRS.2020.3004058.
[59] M. Ellahi and G. Abbas, "A Hybrid Metaheuristic Approach for the Solution of Renewables-Incorporated Economic Dispatch Problems," *IEEE Access*, vol. 8, pp. 127608–127621, 2020, doi: 10.1109/ACCESS.2020.3008570.
[60] F. Safdarian, A. Kargarian, and A. Kargarian, "Temporal Decomposition-Based Stochastic Economic Dispatch for Smart Grid Energy Management," *IEEE Trans. Smart Grid*, vol. 11, no. 5, pp. 4544–4554, 2020, doi: 10.1109/TSG.2020.2993781.
[61] R. Ponciroli, N. E. Stauff, J. Ramsey, F. Ganda, and R. B. Vilim, "An improved genetic algorithm approach to the unit commitment/economic dispatch problem," *IEEE Trans. Power Syst.*, vol. 35, no. 5, pp. 4005–4013, 2020, doi: 10.1109/TPWRS.2020.2986710.
[62] B. Chen, W. Wu, and H. Sun, "Coordinated Heat and Power Dispatch Considering Mutual Benefit and

Mutual Trust: A Multi-party Perspective," *IEEE Trans. Sustain. Energy*, vol. 13, no. 1, pp. 251–264, 2022, doi: 10.1109/TSTE.2021.3108997.
[63] Y. Yang, W. Wu, B. Wang, and M. Li, "Chance-Constrained Economic Dispatch Considering Curtailment Strategy of Renewable Energy," *IEEE Trans. Power Syst.*, vol. 36, no. 6, pp. 5792–5802, 2021, doi: 10.1109/TPWRS.2021.3081120.
[64] and J. X. D. Gan, D. Feng, "Fundamentals of Power System Operation," in *Electricity markets and power system economics*, CRC Press, 2014, pp. 11–59.
[65] J. Löfberg, "YALMIP: A toolbox for modeling and optimization in MATLAB," *Proc. IEEE Int. Symp. Comput. Control Syst. Des.*, pp. 284–289, 2004, doi: 10.1109/cacsd.2004.1393890.
[66] G. E. P. Vayanos Q. Jin, "{ROCPP} Version v2020.0140," 2022, doi: 10.5281/zenodo.6360996.
[67] K. O'Hara, "OptimLib, a lightweight C++ library of numerical optimization methods for nonlinear functions," 2017. https://www.kthohr.com/optimlib.html
[68] M. Eldred, Michael S.; Giunta, Anthony A.; van Bloemen Waanders, Bart G.; Wojtkiewicz, Steven F.; Hart, William E., Jr. & Alleva, "DAKOTA, A Multilevel Parallel Object-Oriented Framework for Design Optimization, Parameter Estimation, Uncertainty Quantification, and Sensitivity Analysis Version 3.0 Reference Manual," Albuquerque, New Mexico, 2001. [Online]. Available: https://digital.library.unt.edu/ark:/67531/metadc741294/citation/#top
[69] Fortran Wiki, "Libraries." https://fortranwiki.org/fortran/show/Libraries
[70] P. Virtanen *et al.*, "SciPy 1.0: fundamental algorithms for scientific computing in Python," *Nat. Methods*, vol. 17, no. 3, pp. 261–272, 2020, doi: 10.1038/s41592-019-0686-2.
[71] W. E. Hart, C. Laird, J.-P. Watson, and D. L. Woodruff, *Pyomo – Optimization Modeling in Python*, vol. 67. 2012. [Online]. Available: http://link.springer.com/10.1007/978-1-4614-3226-5
[72] S. Koretsky *et al.*, "Adapting Quantum Approximation Optimization Algorithm (QAOA) for Unit Commitment," *Proc. - 2021 IEEE Int. Conf. Quantum Comput. Eng. QCE 2021*, pp. 181–187, 2021, doi: 10.1109/QCE52317.2021.00035.
[73] Q. Zhao and E. Ma, "Analysis of PDG, penalty-BFGS and KKT in economic dispatch problems," *Proc. - 2020 5th Int. Conf. Mech. Control Comput. Eng. ICMCCE 2020*, pp. 2249–2254, 2020, doi: 10.1109/ICMCCE51767.2020.00488.
[74] I. B. M. I. Cplex, "V12. 1: User's Manual for CPLEX," *Int. Bus. Mach. Corp.*, vol. 46, no. 53, p. 157, 2009.
[75] encoord, "Scenario Analysis Interface for Energy Systems (SAInt)." https://encoord.com/SAInt.html#top
[76] O. J. Guerra, B. Sergi, M. Craig, K. A. Pambour, C. Brancucci, and B. M. Hodge, "Coordinated operation of electricity and natural gas systems from day-ahead to real-time markets," *J. Clean. Prod.*, vol. 281, p. 124759, 2021, doi: 10.1016/j.jclepro.2020.124759.
[77] M. Craig, O. J. Guerra, C. Brancucci, K. A. Pambour, and B. M. Hodge, "Valuing intra-day coordination of electric power and natural gas system operations," *Energy Policy*, vol. 141, no. December 2019, p. 111470, 2020, doi: 10.1016/j.enpol.2020.111470.
[78] B. Sergi and K. Pambour, "An Evaluation of Co-Simulation for Modeling Coupled Natural Gas and Electricity Networks," *Energies*, vol. 15, no. 14, 2022, doi: 10.3390/en15145277.
[79] PowerWorld Corporation, "Power Market." https://www.powerworld.com/solutions/power-markets
[80] K. De Vos, J. Morbee, J. Driesen, and R. Belmans, "Impact of wind power on sizing and allocation of reserve requirements," *IET Renew. Power Gener.*, vol. 7, no. 1, pp. 1–9, 2013, doi: 10.1049/iet-rpg.2012.0085.
[81] T. Niknam, R. Azizipanah-Abarghooee, and M. R. Narimani, "Reserve constrained dynamic optimal power flow subject to valve-point effects, prohibited zones and multi-fuel constraints," *Energy*, vol. 47, no. 1, pp. 451–464, 2012, doi: 10.1016/j.energy.2012.07.053.
[82] T. Ding, Z. Wu, J. Lv, Z. Bie, and X. Zhang, "Robust co-optimization to energy and reserve joint dispatch considering wind power generation and zonal reserve constraints in real-time electricity markets," *Appl. Sci.*, vol. 7, no. 4, pp. 1547–1557, 2016, doi: 10.3390/app7070680.
[83] L. Zhang, Y. Yuan, X. Yuan, B. Chen, D. Su, and Q. Li, "Spinning Reserve Requirements Optimization Based on an Improved Multiscenario Risk Analysis Method," *Math. Probl. Eng.*, vol. 2017, no. ii, 2017, doi: 10.1155/2017/6510213.
[84] J. M. Morales, A. J. Conejo, and J. Pérez-Ruiz, "Economic valuation of reserves in power systems with high penetration of wind power," *2009 IEEE Power Energy Soc. Gen. Meet. PES '09*, vol. 24, no. 2, pp. 900–910, 2009, doi: 10.1109/PES.2009.5260229.

[85] ENTSO-E, "Electricity Balancing Guideline." [Online]. Available: https://www.entsoe.eu/network_codes/eb/
[86] B. Mohandes, M. S. El Moursi, N. Hatziargyriou, and S. El Khatib, "A Review of Power System Flexibility with High Penetration of Renewables," *IEEE Trans. Power Syst.*, vol. 34, no. 4, pp. 3140–3155, 2019, doi: 10.1109/TPWRS.2019.2897727.
[87] M. A. Ortega-Vazquez and D. S. Kirschen, "Optimizing the spinning reserve requirements using a cost/benefit analysis," *IEEE Trans. Power Syst.*, vol. 22, no. 1, pp. 24–33, 2007, doi: 10.1109/TPWRS.2006.888951.
[88] M. A. Ortega-Vazquez and D. S. Kirschen, "Estimating the spinning reserve requirements in systems with significant wind power generation penetration," *IEEE Trans. Power Syst.*, vol. 24, no. 1, pp. 114–124, 2009, doi: 10.1109/TPWRS.2008.2004745.
[89] M. Ghiasi, E. Ahmadinia, M. J. Lariche, H. Zarrabi, and R. Simoes, "A New Spinning Reserve Requirement Prediction with Hybrid Model," *Smart Sci.*, vol. 6, no. 3, pp. 212–221, 2018, doi: 10.1080/23080477.2018.1460890.
[90] J. Wu, B. Zhang, W. Deng, and K. Zhang, "Application of Cost-CVaR model in determining optimal spinning reserve for wind power penetrated system," *Int. J. Electr. Power Energy Syst.*, vol. 66, pp. 110–115, 2015, doi: 10.1016/j.ijepes.2014.10.051.
[91] P. Nikolaidis, S. Chatzis, and A. Poullikkas, "Optimal planning of electricity storage to minimize operating reserve requirements in an isolated island grid," *Energy Syst.*, vol. 11, no. 4, pp. 1157–1174, 2020, doi: 10.1007/s12667-019-00355-x.
[92] J. Zhao, C. Wan, Z. Xu, and K. P. Wong, "Spinning Reserve Requirement Optimization Considering Integration of Plug-In Electric Vehicles," *IEEE Trans. Smart Grid*, vol. 8, no. 4, pp. 2009–2021, 2017, doi: 10.1109/TSG.2016.2597098.
[93] F. Liu, Z. Bie, S. Liu, and T. Ding, "Day-ahead optimal dispatch for wind integrated power system considering zonal reserve requirements," *Appl. Energy*, vol. 188, pp. 399–408, 2017, doi: https://doi.org/10.1016/j.apenergy.2016.11.102.
[94] M. Bucksteeg, L. Niesen, and C. Weber, "Impacts of dynamic probabilistic reserve sizing techniques on reserve requirements and system costs," *IEEE Trans. Sustain. Energy*, vol. 7, no. 4, pp. 1408–1420, 2016, doi: 10.1109/TSTE.2016.2555483.
[95] G. M. Mohammad, K. Afshar, and N. Bigdeli, "Optimal Reserve Determination Considering Demand Response in the Presence of High Wind Penetration and Energy Storage Systems," *Iran. J. Sci. Technol. - Trans. Electr. Eng.*, vol. 44, no. 4, pp. 1403–1428, 2020, doi: 10.1007/s40998-020-00328-2.
[96] J. Saez-Gallego, J. M. Morales, H. Madsen, and T. Jónsson, "Determining reserve requirements in DK1 area of Nord Pool using a probabilistic approach," *Energy*, vol. 74, pp. 682–693, 2014, doi: https://doi.org/10.1016/j.energy.2014.07.034.
[97] V. Dvorkin, S. Delikaraoglou, and J. M. Morales, "Setting reserve requirements to approximate the efficiency of the stochastic dispatch," *IEEE Trans. Power Syst.*, vol. 34, no. 2, pp. 1524–1536, 2019, doi: 10.1109/TPWRS.2018.2878723.
[98] S. K. Kim, J. H. Park, and Y. T. Yoon, "Determination of secondary reserve requirement through interaction-dependent clearance between ex-ante and ex-post," *J. Electr. Eng. Technol.*, vol. 9, no. 1, pp. 71–79, 2014, doi: 10.5370/jeet.2014.9.1.071.
[99] K. F. Krommydas, C. N. Dikaiakos, G. P. Papaioannou, and A. C. Stratigakos, "Flexibility study of the Greek power system using a stochastic programming approach for estimating reserve requirements," *Electr. Power Syst. Res.*, vol. 213, no. August, p. 108620, 2022, doi: 10.1016/j.epsr.2022.108620.
[100] S. Riahinia, A. Abbaspour, M. Fotuhi-Firuzabad, and M. Moeini-Aghtaie, "Impact of correlation on reserve requirements of high wind-penetrated power systems," *Int. J. Electr. Power Energy Syst.*, vol. 73, pp. 576–583, 2015, doi: 10.1016/j.ijepes.2015.05.026.
[101] N. Costilla-Enriquez, M. Ortega-Vasquez, A. Tuohy, A. Motley, and R. Webb, "Operating Dynamic Reserve Dimensioning Using Probabilistic Forecasts," *IEEE Trans. Power Syst.*, vol. 8950, no. c, pp. 1–14, 2022, doi: 10.1109/TPWRS.2022.3163106.
[102] B. Park, Z. Zhou, A. Botterud, and P. Thimmapuram, "Probabilistic Zonal Reserve Requirements for Improved Energy Management and Deliverability with Wind Power Uncertainty," *IEEE Trans. Power Syst.*, vol. 35, no. 6, pp. 4324–4334, 2020, doi: 10.1109/TPWRS.2020.2992763.
[103] J. D. Lyon, K. W. Hedman, and M. Zhang, "Reserve requirements to efficiently manage intra-zonal congestion," *IEEE Trans. Power Syst.*, vol. 29, no. 1, pp. 251–258, 2014, doi: 10.1109/TPWRS.2013.2278537.

[104] A. Goudarzi, Z. N. C. Viray, P. Siano, A. G. Swanson, J. V. Coller, and M. Kazemi, "A probabilistic determination of required reserve levels in an energy and reserve co-optimized electricity market with variable generation," *Energy*, vol. 130, pp. 258–275, 2017, doi: 10.1016/j.energy.2017.04.145.
[105] A. Ahmed and M. Khalid, "A review on the selected applications of forecasting models in renewable power systems," *Renew. Sustain. Energy Rev.*, vol. 100, no. October 2018, pp. 9–21, 2019, doi: 10.1016/j.rser.2018.09.046.
[106] K. Parker and P. Barooah, "A Probabilistic Method for Reserve Sizing in Power Grids with High Renewable Penetration," *IEEE Trans. Power Syst.*, vol. 36, no. 3, pp. 2473–2480, 2021, doi: 10.1109/TPWRS.2020.3030041.
[107] J. Yun, H. Ma, Z. Yan, and S. Member, "Distributionally Robust Optimization based Restoration for Integrated Electricity-Gas System Incorporating Wind Power and Flexible Reserve Capacity Allocation," *CSEE J. Power Energy Syst.*, 2021, doi: 10.17775/CSEEJPES.2021.01650.
[108] S. Wang, H. Gangammanavar, S. Ekşioğlu, and S. J. Mason, "Statistical estimation of operating reserve requirements using rolling horizon stochastic optimization," *Ann. Oper. Res.*, vol. 292, no. 1, pp. 371–397, 2020, doi: 10.1007/s10479-019-03482-x.
[109] K. Dietrich, J. Latorre, and L. Olmos, "Stochastic unit commitment considering uncertain wind production in an isolated system," *4th Conf. ...*, pp. 1–6, 2009, [Online]. Available: http://www.iit.upcomillas.es/aramos/papers/20090315_article_mod.pdf
[110] A. Muzhikyan, A. M. Farid, and K. Youcef-Toumi, "An a priori analytical method for the determination of operating reserve requirements," *Int. J. Electr. Power Energy Syst.*, vol. 86, pp. 1–17, 2017, doi: 10.1016/j.ijepes.2016.09.005.
[111] N. Lu, R. Diao, R. P. Hafen, N. Samaan, and Y. V Makarov, "A comparison of forecast error generators for modeling wind and load uncertainty," in *2013 IEEE Power & Energy Society General Meeting*, 2013, pp. 1–5. doi: 10.1109/PESMG.2013.6672978.
[112] D. Niu, Y. Zhang, and J. Liu, "The application of time series seasonal multiplicative model and GARCH error amending model on forecasting the monthly peak load," *IFCSTA 2009 Proc. - 2009 Int. Forum Comput. Sci. Appl.*, vol. 3, pp. 135–138, 2009, doi: 10.1109/IFCSTA.2009.272.
[113] S. Tiwari, R. Sabzchgar, and M. Rasouli, "Short Term Solar Irradiance Forecast Using Numerical Weather Prediction (NWP) with Gradient Boost Regression," *2018 9th IEEE Int. Symp. Power Electron. Distrib. Gener. Syst. PEDG 2018*, 2018, doi: 10.1109/PEDG.2018.8447751.
[114] R. Bessa, C. Moreira, B. Silva, and M. Matos, "Handling renewable energy variability and uncertainty in power systems operation," *Wiley Interdiscip. Rev. Energy Environ.*, vol. 3, no. 2, pp. 156–178, 2014, doi: 10.1002/wene.76.
[115] European Commission, "Renewable Energy Targets." [Online]. Available: https://energy.ec.europa.eu/topics/renewable-energy/renewable-energy-directive-targets-and-rules/renewable-energy-targets_en#:~:text=Building on the 20%25 target,possible upwards revision by 2023
[116] European Environment Agency, "Total Electricity Consumption – Outlook from EEA." [Online]. Available: https://www.eea.europa.eu/data-and-maps/indicators/total-electricity-consumption-outlook-from-eea/total-electricity-consumption-outlook-from-1
[117] International Electrotechnical Commission, "Electropedia: The World's Online Electrotechnical Vocabulary." [Online]. Available: https://www.electropedia.org/
[118] D. S. Kirschen and G. Strbac, "Investing in Transmission," in *Fundamentals of Power System Economics*, John Wiley & Sons, Ltd, 2004, pp. 227–264. doi: https://doi.org/10.1002/0470020598.ch8.
[119] J. Gan, Deqiang; Feng, Donghan; Xie, "Market Design: Common Cost Allocations," in *Electricity Markets and Power System Economics*, 1st ed., CRC Press, 2014, pp. 113–157.
[120] ENTSO-E, "Scenarios." [Online]. Available: https://tyndp.entsoe.eu/scenarios/
[121] ENTSO-E, "TYNDP-2022 Scenario Report." [Online]. Available: https://2022.entsos-tyndp-scenarios.eu/wp-content/uploads/2022/04/TYNDP2022_Joint_Scenario_Full-Report-April-2022.pdf
[122] D. S. Kirschen and G. Strbac, "Basic Concepts from Economics," in *Fundamentals of Power System Economics*, John Wiley & Sons, Ltd, 2004, pp. 11–47. doi: https://doi.org/10.1002/0470020598.ch2.
[123] European Central Bank, "The impact of the war in Ukraine on euro area energy markets." [Online]. Available: https://www.ecb.europa.eu/pub/economic-bulletin/focus/2022/html/ecb.ebbox202204_01~68ef3c3dc6.en.html
[124] Timera Energy, "A tour of European capacity markets." [Online]. Available: https://timera-energy.com/a-tour-of-european-capacity-markets/

[125] B. Burgholzer and H. Auer, “Cost/benefit analysis of transmission grid expansion to enable further integration of renewable electricity generation in Austria,” *Renew. Energy*, vol. 97, no. 1364, pp. 189–196, 2016, doi: 10.1016/j.renene.2016.05.073.
[126] C. Kemfert, F. Kunz, and J. Rosellón, “A welfare analysis of electricity transmission planning in Germany,” *Energy Policy*, vol. 94, pp. 446–452, 2016, doi: 10.1016/j.enpol.2016.04.011.
[127] Q. Ploussard, L. Olmos, and A. Ramos, “An Operational State Aggregation Technique for Transmission Expansion Planning Based on Line Benefits,” *IEEE Trans. Power Syst.*, vol. 32, no. 4, pp. 2744–2755, 2017, doi: 10.1109/TPWRS.2016.2614368.
[128] Z. Wu, X. Du, W. Gu, X. P. Zhang, and J. Li, “Automatic Selection Method for Candidate Lines in Transmission Expansion Planning,” *IEEE Access*, vol. 6, pp. 11605–11613, 2018, doi: 10.1109/ACCESS.2018.2798063.
[129] M. Mehrtash, A. Kargarian, and M. Rahmani, “Security-constrained transmission expansion planning using linear sensitivity factors,” *IET Gener. Transm. Distrib.*, vol. 14, no. 2, pp. 200–210, 2020, doi: 10.1049/iet-gtd.2019.0844.
[130] P. F. S. Freitas, L. H. Macedo, and R. Romero, “A strategy for transmission network expansion planning considering multiple generation scenarios,” *Electr. Power Syst. Res.*, vol. 172, no. February, pp. 22–31, 2019, doi: 10.1016/j.epsr.2019.02.018.
[131] M. Sun, F. Teng, I. Konstantelos, and G. Strbac, “An objective-based scenario selection method for transmission network expansion planning with multivariate stochasticity in load and renewable energy sources,” *Energy*, vol. 145, pp. 871–885, 2018, doi: 10.1016/j.energy.2017.12.154.
[132] Z. Zhuo, E. Du, N. Zhang, C. Kang, Q. Xia, and Z. Wang, “Incorporating Massive Scenarios in Transmission Expansion Planning with High Renewable Energy Penetration,” *IEEE Trans. Power Syst.*, vol. 35, no. 2, pp. 1061–1074, 2020, doi: 10.1109/TPWRS.2019.2938618.
[133] C. A. Sima, G. C. Lazaroiu, and V. Dumbrava, “Transmission expansion planning optimization for improving RES integration on electricity market,” *2017 10th Int. Symp. Adv. Top. Electr. Eng. ATEE 2017*, pp. 855–859, 2017, doi: 10.1109/ATEE.2017.7905085.
[134] M. Franken, H. Barrios, A. B. Schrief, and A. Moser, “Transmission expansion planning via power flow controlling technologies,” *IET Gener. Transm. Distrib.*, vol. 14, no. 17, pp. 3530–3538, 2020, doi: 10.1049/iet-gtd.2019.1897.
[135] M. Franken, A. B. Schrief, H. Barrios, R. Puffer, and A. Moser, “Co-optimization of multi-stage transmission expansion planning and grid operation,” *Electr. Power Syst. Res.*, vol. 189, no. April, p. 106686, 2020, doi: 10.1016/j.epsr.2020.106686.
[136] R. García-Bertrand and R. Mínguez, “Dynamic Robust Transmission Expansion Planning,” *IEEE Trans. Power Syst.*, vol. 32, no. 4, pp. 2618–2628, 2017, doi: 10.1109/TPWRS.2016.2629266.
[137] S. Dehghan, S. Member, N. Amjady, S. Member, A. J. Conejo, and A. Indices, “Adaptive Robust Transmission Expansion Planning Using Linear Decision Rules,” *IEEE Trans. POWER Syst.*, vol. 32, no. 5, pp. 4024–4034, 2017.
[138] X. Zhang and A. J. Conejo, “Candidate line selection for transmission expansion planning considering long- and short-term uncertainty,” *Int. J. Electr. Power Energy Syst.*, vol. 100, no. March, pp. 320–330, 2018, doi: 10.1016/j.ijepes.2018.02.024.
[139] S. Dehghan, N. Amjady, and A. J. Conejo, “A Multistage Robust Transmission Expansion Planning Model Based on Mixed Binary Linear Decision Rules - Part I,” *IEEE Trans. Power Syst.*, vol. 33, no. 5, pp. 5341–5350, 2018, doi: 10.1109/TPWRS.2018.2799946.
[140] D. Huppmann and J. Egerer, “National-strategic investment in European power transmission capacity,” *Eur. J. Oper. Res.*, vol. 247, no. 1, pp. 191–203, 2015, doi: 10.1016/j.ejor.2015.05.056.
[141] S. Lumbreras *et al.*, “Large-scale transmission expansion planning: From zonal results to a nodal expansion plan,” *IET Gener. Transm. Distrib.*, vol. 11, no. 11, pp. 2778–2786, 2017, doi: 10.1049/iet-gtd.2016.1441.
[142] C. Rathore, P. B. Thote, S. Kamble, V. Naik, P. Singh, and M. Jukaria, “Transmission Network Expansion Planning Considering Transmission Switching and Pumped-Storage,” *WIECON-ECE 2017 - IEEE Int. WIE Conf. Electr. Comput. Eng. 2017*, no. December, pp. 161–164, 2018, doi: 10.1109/WIECON-ECE.2017.8468901.
[143] E. Mortaz and J. Valenzuela, “Evaluating the impact of renewable generation on transmission expansion planning,” *Electr. Power Syst. Res.*, vol. 169, no. March 2018, pp. 35–44, 2019, doi: 10.1016/j.epsr.2018.12.007.
[144] H. Du *et al.*, “A Decision Support System for Transmission Expansion Planning Considering

Vulnerability," *IEEE Power Energy Soc. Gen. Meet.*, vol. 2019-Augus, 2019, doi: 10.1109/PESGM40551.2019.8973704.
[145] M. Divya Sri and M. Veera Kumari, "Transmission Expansion Planning Using Differential Evolution Multi-Objective Differential Evolution and Multi-Criteria Decision Making Methods," *2018 Natl. Power Eng. Conf. NPEC 2018*, pp. 1–5, 2018, doi: 10.1109/NPEC.2018.8476707.
[146] M. S. El-bages and W. T. Elsayed, "Social spider algorithm for solving the transmission expansion planning problem," *Electr. Power Syst. Res.*, vol. 143, pp. 235–243, 2017, doi: 10.1016/j.epsr.2016.09.002.
[147] A. M. Leite Da Silva, M. R. Freire, and L. M. Honório, "Transmission expansion planning optimization by adaptive multi-operator evolutionary algorithms," *Electr. Power Syst. Res.*, vol. 133, pp. 173–181, 2016, doi: 10.1016/j.epsr.2015.12.027.
[148] B. Ghaddar and R. A. Jabr, "Power transmission network expansion planning: A semidefinite programming branch-and-bound approach," *Eur. J. Oper. Res.*, vol. 274, no. 3, pp. 837–844, 2019, doi: 10.1016/j.ejor.2018.10.035.
[149] S. Verma and V. Mukherjee, "Investigation of static transmission expansion planning using the symbiotic organisms search algorithm," *Eng. Optim.*, vol. 50, no. 9, pp. 1544–1560, 2018, doi: 10.1080/0305215X.2017.1408085.
[150] E. J. De Oliveira, C. A. Moraes, L. W. Oliveira, L. M. Honório, and R. P. B. Poubel, "Efficient hybrid algorithm for transmission expansion planning," *Electr. Eng.*, vol. 100, no. 4, pp. 2765–2777, 2018, doi: 10.1007/s00202-018-0744-2.
[151] D. Z. Fitiwi, L. Olmos, M. Rivier, F. de Cuadra, and I. J. Pérez-Arriaga, "Finding a representative network losses model for large-scale transmission expansion planning with renewable energy sources," *Energy*, vol. 101, pp. 343–358, 2016, doi: 10.1016/j.energy.2016.02.015.
[152] W. Wu, Z. Hu, Y. Song, G. Sansavini, H. Chen, and X. Chen, "Transmission Network Expansion Planning Based on Chronological Evaluation Considering Wind Power Uncertainties," *IEEE Trans. Power Syst.*, vol. 33, no. 5, pp. 4787–4796, 2018, doi: 10.1109/TPWRS.2018.2809728.
[153] A. Papaemmanouil, L. Bertling Tjernberg, L. A. Tuan, and G. Andersson, "Improved cost-benefit analysis for market-based transmission planning, a European perspective," *Energy Policy*, vol. 63, pp. 215–223, 2013, doi: 10.1016/j.enpol.2013.08.066.
[154] J. Gorenstein Dedecca, R. A. Hakvoort, and P. M. Herder, "Transmission expansion simulation for the European Northern Seas offshore grid," *Energy*, vol. 125, pp. 805–824, 2017, doi: 10.1016/j.energy.2017.02.111.
[155] S. Abbasi, H. Abdi, S. Bruno, and M. La Scala, "Transmission network expansion planning considering load correlation using unscented transformation," *Int. J. Electr. Power Energy Syst.*, vol. 103, no. May, pp. 12–20, 2018, doi: 10.1016/j.ijepes.2018.05.024.
[156] S. Cole, P. Martinot, S. Rapoport, and G. Papaefthymiou, "Cost-benefit analysis of a coordinated grid development in the North Sea," *2015 IEEE Eindhoven PowerTech, PowerTech 2015*, 2015, doi: 10.1109/PTC.2015.7232385.
[157] S. Jaehnert, O. Wolfgang, H. Farahmand, S. Völler, and D. Huertas-Hernando, "Transmission expansion planning in Northern Europe in 2030-Methodology and analyses," *Energy Policy*, vol. 61, pp. 125–139, 2013, doi: 10.1016/j.enpol.2013.06.020.
[158] K. Vandyshev, S. D. A. De Graaff, J. Van Casteren, and D. Klaar, "Using optimized flow based market capacity indices in TSO investment evaluation," *Int. Conf. Eur. Energy Mark. EEM*, vol. 2016-July, 2016, doi: 10.1109/EEM.2016.7521257.
[159] S. Lumbreras and A. Ramos, "The new challenges to transmission expansion planning. Survey of recent practice and literature review," *Electr. Power Syst. Res.*, vol. 134, pp. 19–29, 2016, doi: 10.1016/j.epsr.2015.10.013.
[160] M. Mahdavi, C. Sabillon Antunez, M. Ajalli, and R. Romero, "Transmission Expansion Planning: Literature Review and Classification," *IEEE Syst. J.*, vol. 13, no. 3, pp. 3129–3140, 2019, doi: 10.1109/JSYST.2018.2871793.
[161] A. M. L. Da Silva, L. S. Rezende, L. A. F. Manso, and G. J. Anders, "Transmission expansion planning: A discussion on reliability and 'N-1' security criteria," *2010 IEEE 11th Int. Conf. Probabilistic Methods Appl. to Power Syst. PMAPS 2010*, pp. 244–251, 2010, doi: 10.1109/PMAPS.2010.5528652.
[162] O. B. Tor, A. N. Guven, and M. Shahidehpour, "Promoting the investment on IPPs for optimal grid planning," *IEEE Trans. Power Syst.*, vol. 25, no. 3, pp. 1743–1750, 2010, doi: 10.1109/TPWRS.2009.2039947.

[163] ENTSO-E, “2nd ENTSO-E Guideline for Cost Benefit Analysis of Grid Development Project.” [Online]. Available: https://www.entsoe.eu/news/2018/10/12/commission-approves-2d-entso-e-guideline-for-cost-benefit-analysis-of-grid-development-projects/
[164] Terna, “Metodologia Analisi Costi-Benefici—ACB 2.0.” [Online]. Available: https://download.terna.it/terna/0000/1009/13.pdf
[165] W. Ho and X. Ma, “The state-of-the-art integrations and applications of the analytic hierarchy process,” *Eur. J. Oper. Res.*, vol. 267, no. 2, pp. 399–414, 2018, doi: 10.1016/j.ejor.2017.09.007.
[166] R. W. Saaty, “The analytic hierarchy process-what it is and how it is used,” *Math. Model.*, vol. 9, no. 3–5, pp. 161–176, 1987, doi: 10.1016/0270-0255(87)90473-8.
[167] J. L. Ceciliano Meza, M. B. Yildirim, and A. S. M. Masud, “A multiobjective evolutionary programming algorithm and its applications to power generation expansion planning,” *IEEE Trans. Syst. Man, Cybern. Part ASystems Humans*, vol. 39, no. 5, pp. 1086–1096, 2009, doi: 10.1109/TSMCA.2009.2025868.
[168] S. Malkawi, M. Al-Nimr, and D. Azizi, “A multi-criteria optimization analysis for Jordan’s energy mix,” *Energy*, vol. 127, pp. 680–696, 2017, doi: 10.1016/j.energy.2017.04.015.
[169] R. Jing *et al.*, “A multi-objective optimization and multi-criteria evaluation integrated framework for distributed energy system optimal planning,” *Energy Convers. Manag.*, vol. 166, no. November 2017, pp. 445–462, 2018, doi: 10.1016/j.enconman.2018.04.054.
[170] M. E. Gardeshi and A. Rahimi-Kian, “Invasive weed optimization feature in market-based transmission expansion planning,” *2011 16th Int. Conf. Intell. Syst. Appl. to Power Syst. ISAP 2011*, pp. 1–4, 2011, doi: 10.1109/ISAP.2011.6082175.
[171] S. Majumder, R. M. Shereef, and S. A. Khaparde, “A Two-Stage Algorithm for Efficient Transmission Expansion Planning with Renewable Energy Resources,” *IET Renew. Power Gener.*, vol. 11, no. 3, pp. 320–329, 2016.
[172] L. U. Liang, Z. Hong, C. Shaorong, L. Yiben, J. Li, and W. Yuhong, “Comprehensive Evaluation of Transmission Network Planning Schemes Based on IFAHP,” *2020 4th Int. Conf. HVDC, HVDC 2020*, pp. 375–381, 2020, doi: 10.1109/HVDC50696.2020.9292895.
[173] S. Z. Moghaddam, H. Monsef, and M. Jafari, “A new heuristic method for transmission expansion planning using AHP,” *2011 10th Int. Conf. Environ. Electr. Eng. EEEIC.EU 2011 - Conf. Proc.*, 2011, doi: 10.1109/EEEIC.2011.5874831.
[174] H. Zhao, H. Liu, D. You, and X. Zhao, “Comprehensive Evaluation Index System for Screening and Sequencing Power Transmission Grid Planning Projects,” *DEStech Trans. Environ. Energy Earth Sci.*, no. appeec, pp. 314–322, 2018, doi: 10.12783/dteees/appeec2018/23538.
[175] E. A. C. Aranha Neto *et al.*, “An AHP multiple criteria model applied to transmission expansion of a Brazilian southeastern utility,” *2010 IEEE/PES Transm. Distrib. Conf. Expo. Lat. Am. T D-LA 2010*, pp. 575–580, 2011, doi: 10.1109/TDC-LA.2010.5762940.
[176] A. Gonzalez, J. Rodriguez, F. Fernandez, G. Blanco, and V. Oxilia, “Multi-criteria Analysis of the Expansion Plan of the Transmission System of Paraguay,” *IEEE Chil. Conf. Electr. Electron. Eng. Inf. Commun. Technol. CHILECON 2019*, no. 1, pp. 1–6, 2019, doi: 10.1109/CHILECON47746.2019.8988081.
[177] N. E. Koltsaklis and A. S. Dagoumas, “State-of-the-art generation expansion planning: A review,” *Appl. Energy*, vol. 230, no. September, pp. 563–589, 2018, doi: 10.1016/j.apenergy.2018.08.087.
[178] P. J. Hibbard and T. Schatzki, “The Interdependence of Electricity and Natural Gas: Current Factors and Future Prospects,” *Electr. J.*, vol. 25, no. 4, pp. 6–17, 2012, doi: 10.1016/j.tej.2012.04.012.
[179] V. Oree, S. Z. Sayed Hassen, and P. J. Fleming, “Generation expansion planning optimisation with renewable energy integration: A review,” *Renew. Sustain. Energy Rev.*, vol. 69, no. December 2016, pp. 790–803, 2017, doi: 10.1016/j.rser.2016.11.120.
[180] I. C. Gonzalez-Romero, S. Wogrin, and T. Gómez, “Review on generation and transmission expansion co-planning models under a market environment,” *IET Gener. Transm. Distrib.*, vol. 14, no. 6, pp. 931–944, 2020, doi: 10.1049/iet-gtd.2019.0123.
[181] I. Sharan and R. Balasubramanian, “Integrated generation and transmission expansion planning including power and fuel transportation constraints,” *Energy Policy*, vol. 43, pp. 275–284, 2012, doi: 10.1016/j.enpol.2012.01.004.
[182] F. D. Munoz, B. F. Hobbs, and J. P. Watson, “New bounding and decomposition approaches for MILP investment problems: Multi-area transmission and generation planning under policy constraints,” *Eur. J. Oper. Res.*, vol. 248, no. 3, pp. 888–898, 2016, doi: 10.1016/j.ejor.2015.07.057.

[183] J. Aghaei, N. Amjady, A. Baharvandi, and M. A. Akbari, "Generation and transmission expansion planning: MILP-based probabilistic model," *IEEE Trans. Power Syst.*, vol. 29, no. 4, pp. 1592–1601, 2014, doi: 10.1109/TPWRS.2013.2296352.
[184] N. Gupta, M. Khosravy, N. Patel, and T. Senjyu, "A Bi-Level Evolutionary Optimization for Coordinated Transmission Expansion Planning," *IEEE Access*, vol. 6, pp. 48455–48477, 2018, doi: 10.1109/ACCESS.2018.2867954.
[185] M. S. Sepasian, H. Seifi, A. A. Foroud, and A. R. Hatami, "A multiyear security constrained hybrid generation-transmission expansion planning algorithm including fuel supply costs," *IEEE Trans. Power Syst.*, vol. 24, no. 3, pp. 1609–1618, 2009, doi: 10.1109/TPWRS.2009.2021218.
[186] S. Yin and J. Wang, "Generation and Transmission Expansion Planning Towards a 100% Renewable Future," *IEEE Trans. Power Syst.*, vol. 37, no. 4, pp. 3274–3285, 2022, doi: 10.1109/TPWRS.2020.3033487.
[187] M. T. Askari, M. Z. A. Ab Kadir, H. Hizam, and J. Jasni, "Evaluation of uncertainties on generation expansion planning," *Proc. 2013 IEEE 7th Int. Power Eng. Optim. Conf. PEOCO 2013*, no. June 2013, pp. 273–276, 2013, doi: 10.1109/PEOCO.2013.6564556.
[188] A. Schwele, J. Kazempour, and P. Pinson, "Do unit commitment constraints affect generation expansion planning? A scalable stochastic model," *Energy Syst.*, vol. 11, no. 2, pp. 247–282, 2020, doi: 10.1007/s12667-018-00321-z.
[189] C. Guo, M. Bodur, and D. J. Papageorgiou, "Generation expansion planning with revenue adequacy constraints," *Comput. Oper. Res.*, vol. 142, no. January, 2022, doi: 10.1016/j.cor.2022.105736.
[190] K. Mason, M. Qadrdan, and N. Jenkins, "Investing in generation and storage capacity in a liberalised electricity market: An agent based approach," *Appl. Energy*, vol. 294, no. April, p. 116905, 2021, doi: 10.1016/j.apenergy.2021.116905.
[191] Sarjiya, R. F. S. Budi, and S. P. Hadi, "Game theory for multi-objective and multi-period framework generation expansion planning in deregulated markets," *Energy*, vol. 174, pp. 323–330, 2019, doi: 10.1016/j.energy.2019.02.105.
[192] P. A. J. Fonseka, T. K. Saha, and Z. Y. Dong, "A price-based approach to generation investment planning in electricity markets," *IEEE Trans. Power Syst.*, vol. 23, no. 4, pp. 1859–1870, 2008, doi: 10.1109/TPWRS.2008.2002287.
[193] G. Liu, J. H. Zhao, F. Wen, X. Yin, and Z. Y. Dong, "Option-game-based method for generation investment analysis considering uncertain carbon reduction policy in the electricity market," *IET Gener. Transm. Distrib.*, vol. 4, no. 8, pp. 917–927, 2010, doi: 10.1049/iet-gtd.2009.0439.
[194] A. L. Wilson, C. J. Dent, and M. Goldstein, "Quantifying uncertainty in wholesale electricity price projections using Bayesian emulation of a generation investment model," *Sustain. Energy, Grids Networks*, vol. 13, pp. 42–55, 2018, doi: 10.1016/j.segan.2017.11.003.
[195] S. Taheri, V. Kekatos, and S. Veeramachaneni, "Strategic Generation Investment in Energy Markets: A Multiparametric Programming Approach," *IEEE Trans. Power Syst.*, vol. 37, no. 4, pp. 2590–2600, 2022, doi: 10.1109/TPWRS.2021.3125624.
[196] V. Dvorkin, J. Kazempour, L. Baringo, and P. Pinson, "A Consensus-ADMM Approach for Strategic Generation Investment in Electricity Markets," *Proc. IEEE Conf. Decis. Control*, vol. 2018-Decem, no. Cdc, pp. 780–785, 2018, doi: 10.1109/CDC.2018.8619240.
[197] T. Oderinwale, D. Papadaskalopoulos, Y. Ye, and G. Strbac, "Investigating the impact of flexible demand on market-based generation investment planning," *Int. J. Electr. Power Energy Syst.*, vol. 119, no. January, p. 105881, 2020, doi: 10.1016/j.ijepes.2020.105881.
[198] S. Kaminski, M. Dolanyi, K. Bruninx, and E. Delarue, "Comparative analysis of risk-aversion and strategic investment behavior in generation expansion," *Electr. Power Syst. Res.*, vol. 210, no. February, p. 108082, 2022, doi: 10.1016/j.epsr.2022.108082.
[199] X. Zou, C. Zhu, M. Ling, and X. Chang, "Decision analysis of nuclear power investment development under carbon price," in *2020 8th International Conference on Orange Technology, ICOT 2020*, 2020. doi: 10.1109/ICOT51877.2020.9468800.
[200] J. Valinejad, T. Barforoshi, M. Marzband, E. Pouresmaeil, R. Godina, and J. P. S. Catalão, "Investment incentives in competitive electricity markets," *Appl. Sci.*, vol. 8, no. 10, pp. 1–23, 2018, doi: 10.3390/app8101978.
[201] S. J. Kazempour, S. Member, A. J. Conejo, and C. Ruiz, "Strategic Generation Investment Using a Complementarity Approach," *IEEE Trans. Power Syst.*, vol. 26, no. 2, pp. 940–948, 2011.
[202] C. Li, A. J. Conejo, J. D. Siirola, and I. E. Grossmann, "On representative day selection for capacity

expansion planning of power systems under extreme operating conditions," *Int. J. Electr. Power Energy Syst.*, vol. 137, no. September 2021, p. 107697, 2022, doi: 10.1016/j.ijepes.2021.107697.
[203] M. A. Pourmoosavi and T. Amraee, "Low carbon generation expansion planning with carbon capture technology and coal phase-out under renewable integration," *Int. J. Electr. Power Energy Syst.*, vol. 128, no. January, p. 106715, 2021, doi: 10.1016/j.ijepes.2020.106715.
[204] S. Pineda and J. M. Morales, "Chronological time-period clustering for optimal capacity expansion planning with storage," *IEEE Trans. Power Syst.*, vol. 33, no. 6, pp. 7162–7170, 2018, doi: 10.1109/TPWRS.2018.2842093.
[205] V. Hinojosa, "Static generation capacity expansion planning using linear transmission distribution factors," *2016 IEEE PES Transm. Distrib. Conf. Expo. Am. PES T D-LA 2016*, 2017, doi: 10.1109/TDC-LA.2016.7805678.
[206] A. Pai, *Energy Function Analysis for Power System Stability*. Springer, 1989. doi: 10.1080/07313569008909464.
[207] ENTSO-E, "Single Day-Ahead Coupling (SDAC)."
[208] ENTSO-E, "Single Intraday Coupling (SIDC)." [Online]. Available: https://www.entsoe.eu/network_codes/cacm/implementation/sidc/
[209] L. Ding, F. M. Gonzalez-Longatt, P. Wall, and V. Terzija, "Two-step spectral clustering controlled islanding algorithm," *IEEE Trans. Power Syst.*, vol. 28, no. 1, pp. 75–84, 2013, doi: 10.1109/TPWRS.2012.2197640.
[210] Terna, "Reference requirements and characteristics of electrical lines and substations of National Transmission System." [Online]. Available: https://download.terna.it/terna/0000/0105/20.pdf
[211] I. Pena, C. Brancucci, and B. M. Hodge, "An Extended IEEE 118-bus Test System with High Renewable Penetration," *IEEE Trans. Power Syst.*, vol. 8950, no. c, 2017, doi: 10.1109/TPWRS.2017.2695963.
[212] I. Pena, C. Brancucci, and B. M. Hodge, "An Extended IEEE 118-Bus Test System With High Renewable Penetration." [Online]. Available: https://item.bettergrids.org/handle/1001/120
[213] N. Fan, R. Chen, and J.-P. Watson, "N-1-1 contingency-constrained optimal power flow by interdiction methods," in *2012 IEEE Power and Energy Society General Meeting*, 2012, pp. 1–6. doi: 10.1109/PESGM.2012.6345713.
[214] Renewable Energy, *Moving Towards a Low Carbon Economy*. Eur. Commission, Brussels, Belgium, 2018.
[215] Joint Working Group CIGRE/CIRED C1.29, "Planning criteria for future transmission networks in the presence of a greater variability of power exchange with distribution systems," March 2017.
[216] B. Aluisio *et al.*, "The application of a flow-based methodology for yearly network analysis according to market data," in *2017 14th International Conference on the European Energy Market (EEM)*, 2017, pp. 1–6. doi: 10.1109/EEM.2017.7981918.
[217] S. Frank, I. Steponavice, and S. Rebennack, "Optimal power flow: A bibliographic survey I Formulations and deterministic methods," *Energy Syst.*, vol. 3, no. 3, pp. 221–258, 2012, doi: 10.1007/s12667-012-0056-y.
[218] A. G. Vlachos and P. N. Biskas, "Adjustable profile blocks with spatial relations in the day-ahead electricity market," *IEEE Trans. Power Syst.*, vol. 28, no. 4, pp. 4578–4587, 2013, doi: 10.1109/TPWRS.2013.2273560.
[219] G. A. Dourbois, P. N. Biskas, and A. G. Vlachos, "A new concept for the clearing of European Power Exchange day-ahead markets with complex orders," *Int. Conf. Eur. Energy Mark. EEM*, 2014, doi: 10.1109/EEM.2014.6861236.
[220] T. L. Saaty, *The Analytic Hierarchy Process: Planning, Priority Setting, Resource Allocation*. McGraw-Hill International Book Company, 1980. [Online]. Available: https://books.google.it/books?id=Xxi7AAAAIAAJ
[221] O. S. Vaidya and S. Kumar, "Analytic hierarchy process: An overview of applications," *Eur. J. Oper. Res.*, vol. 169, no. 1, pp. 1–29, 2006, doi: 10.1016/j.ejor.2004.04.028.
[222] ACER - CEPA, "Study on the value of lost load of electricity supply in Europe," 2018. [Online]. Available: acer.europa.eu
[223] GME, "Italian Electricity Market." [Online]. Available: www.mercatoelettrico.org
[224] R. D. Zimmerman, C. E. Murillo-Sánchez, and R. J. Thomas, "MATPOWER: Steady-State Operations, Planning, and Analysis Tools for Power Systems Research and Education," *IEEE Trans. Power Syst.*, vol. 26, no. 1, pp. 12–19, 2011, doi: 10.1109/TPWRS.2010.2051168.

[225] M. Reta-Hernández, “Transmission Line Parameters,” *Electr. Power Gener. Transm. Distrib. Electr. Power Eng. Handb.*, 2018.
[226] Terna, “Conventional Technical Solution for the Connection to Main Power System—Average Grid Component Costs Report.”
[227] A. Q. Al-Shetwi and M. Z. Sujod, “Grid-connected photovoltaic power plants: A review of the recent integration requirements in modern grid codes,” *Int. J. Energy Res.*, vol. 42, no. 5, pp. 1849–1865, 2018, doi: 10.1002/er.3983.
[228] Y. K. Wu, S. M. Chang, and P. Mandal, “Grid-Connected Wind Power Plants: A Survey on the Integration Requirements in Modern Grid Codes,” *IEEE Trans. Ind. Appl.*, vol. 55, no. 6, pp. 5584–5593, 2019, doi: 10.1109/TIA.2019.2934081.
[229] Cigre, “Planning Criteria for Future Transmission Networks in the Presence of a Greater Variability of Power Exchange with Dis-tribution Systems”, [Online]. Available: https://e-cigre.org/publication/681-planning-criteria-for-future-transmission-networks-in-the-presence-of-a-greater-variability-of-power-exchange-with-distribution-systems
[230] Med-TSO, “Deliverable 2.1.1 Guidelines for Coordinated Planning: B) Survey and Tools for supporting the Harmonized Planning Process”, [Online]. Available: https://www.med-tso.com/publications/Deliverable_2.1.1_Guidelines_for_Coordinated_Planning__b)_Survey_and_Tools.pdf
[231] ACER, “Report on Unit Investment Cost Indicators and Corresponding Reference Values for Electricity and Gas Infrastruc-ture—Electricity Infrastructure Ref: 15-Infrastructure Unit Investment Costs-ELEC-2015,” 2015. [Online]. Available: http://www.acer.europa.eu
[232] J. A. Alonso and M. T. Lamata, “Estimation of the random index in the analytic hierarchy process,” *Proc. Inf. Process. Manag. Uncertain. knowledge-based Syst.*, pp. 317–322, 2004, [Online]. Available: http://scholar.google.es/scholar?start=20%5C&q=author:%22MT+lamata%22%5C&hl=es%5C&as%5C_sdt=0,5%5C#14
[233] J. Franek and A. Kresta, “Judgment Scales and Consistency Measure in AHP,” *Procedia Econ. Financ.*, vol. 12, no. March, pp. 164–173, 2014, doi: 10.1016/s2212-5671(14)00332-3.
[234] A. J. Wood and B. F. Wollenberg, *Power Generation, Operation, and Control*, 2nd ed. New York: J. Wiley & Sons, 1996.
[235] ENTSO-E, “TYNDP dataset.” [Online]. Available: https://tyndp.entsoe.eu/maps-data
[236] Terna, “Tyrrhenian Link.” [Online]. Available: https://www.terna.it/en/projects/public-engagement/Tyrrhenian-link
[237] Region Sicily, “Enviromental Energetic Plan of Sicily Region, 2030.” [Online]. Available: https://pti.regione.sicilia.it/portal/page/portal/PIR_PORTALE/PIR_LaStrutturaRegionale/PIR_AssEnergia/PIR_DipEnergia/PIR_Areetematiche/PIR_Altricontenuti/PIR_PianoEnergeticoAmbientaledellaRegioneSicilianaPEARS/Documento di Sintesi del PEARS_5_6_19_rev.pdf
[238] GME, “Public Bids.” [Online]. Available: https://www.mercatoelettrico.org/en/download/DownloadDati.aspx?val=OfferteFree_Pubbliche.5
[239] LeighFisher Ltd, “Electricity Generation Costs and Hurdle Rates, Lot 3: Non-Renewable Technologies.” [Online]. Available: https://assets.publishing.service.gov.uk/government/uploads/system/uploads/attachment_data/file/566803/Leigh_Fisher_Non-renewable_Generation_Cost.pdf
[240] ENTSO-E, “P1 – Policy 1: Load-Frequency Control and Performanc,” 2009. [Online]. Available: https://eepublicdownloads.entsoe.eu/clean-documents/pre2015/publications/ce/oh/Policy1_final.pdf
[241] Terna, “Annex A.22 – Method for the resources selection in the planning stage of ASM,” 2018. [Online]. Available: https://download.terna.it/terna/20211004 Allegato_A.22_8d987427a7fc012.pdf
[242] A. Gómez Expósito, J. L. Martínez Ramos, and J. Riquelme Santos, “Slack bus selection to minimize the system power imbalance in load-flow studies,” *IEEE Trans. Power Syst.*, vol. 19, no. 2, pp. 987–995, 2004, doi: 10.1109/TPWRS.2004.825871.
[243] D. Comanescu, G. Grigoras, G. Cartina, and F. Rotaru, “Determination of typical load profiles in hydro-power plant by clustering techniques,” in *Proceedings of the International Conference on Optimisation of Electrical and Electronic Equipment, OPTIM*, 2010, pp. 1294–1297. doi: 10.1109/OPTIM.2010.5510523.
[244] Terna, “Transparency Report Download Center.” [Online]. Available: https://www.terna.it/en/electric-system/transparency-report/download-center
[245] Terna, “Secondary and Tertiaries Reserves Reserve Requirements.” [Online]. Available:

https://www.terna.it/it/sistema-elettrico/dispacciamento/stima-domanda-oraria-energia-riserva-secondaria-terziaria
[246] Terna, “Market Zones.” [Online]. Available: https://www.terna.it/it/sistema-elettrico/mercato-elettrico/zone-mercato
[247] M. Alla, A. Guzmán, D. Finney, and N. Fischer, “Adaptive Loss-of-Field Protection Tailored to the Generator Capability Curve,” in *15th International Conference on Developments in Power System Protection*, 2020, pp. 1–6.
[248] M. Elsamahy, “Impact of Generator Distance Phase Backup Protection on Generator Overexcitation Thermal Capability during System Disturbances,” in *2014 IEEE Electrical Power and Energy Conference*, 2014, pp. 30–34. doi: 10.1109/EPEC.2014.28.
[249] B. Gellert, “8 - Turbogenerators in gas turbine systems,” in *Modern Gas Turbine Systems*, P. Jansohn, Ed. Woodhead Publishing, 2013, pp. 247–326. doi: https://doi.org/10.1533/9780857096067.2.247.
[250] Terna, “Renewable Resources.” [Online]. Available: https://www.terna.it/it/sistema-elettrico/dispacciamento/fonti-rinnovabili
[251] Terna, “Regional Statistics.” [Online]. Available: https://www.terna.it/it/sistema-elettrico/statistiche/pubblicazioni-statistiche
[252] Terna, “Transmission Evolution Planning.” [Online]. Available: https://www.terna.it/it/sistema-elettrico/rete/piano-sviluppo-rete
[253] Terna, “The National Electricity Transmission Grid Development Plan.” [Online]. Available: https://www.terna.it/en/electric-system/grid/national-electricity-transmission-grid-development-plan